Control of Vein Pattern Formation by the *GNOM* gene of Arabidopsis

by

Linh Manh Nguyen

A thesis submitted in partial fulfillment of the requirements for the degree of

Doctor of Philosophy

in

Plant Biology

Department of Biological Sciences
University of Alberta

Abstract

To form tissue networks, animal cells migrate and interact through proteins protruding from their plasma membranes. Plant cells can do neither, yet plants form vein networks. How plants do so is unclear, but the prevailing hypothesis proposes that GNOM — a regulator of vesicle formation in membrane trafficking — positions transporters of the plant hormone auxin to the correct side of the plasma membrane. The resulting cell-to-cell, polar transport of auxin would then induce vein formation. I tested that hypothesis and — contrary to its predictions — found that vein formation occurs in the absence of polar auxin transport and that the residual auxin-transport-independent vein-patterning activity relies on auxin signaling. My results suggest that a *GNOM*-dependent signal acts upstream of both auxin transport and signaling in vein patterning. However, plants inhibited in both auxin transport and signaling still formed veins. Patterning of vascular cells into veins was instead prevented in *gnom* mutants, suggesting the existence of at least one more *GNOM*-dependent vein-patterning pathway. I showed that such a pathway depends on the movement of auxin or an auxin-dependent signal through plasmodesmata intercellular channels. Plasmodesma permeability was high where veins were forming, lowered between veins and nonvascular tissues, but remained high between vein cells. Impaired ability to regulate plasmodesma aperture led to defects in auxin transport and signaling, ultimately leading to vein patterning defects that were enhanced by inhibition of auxin transport or signaling. *GNOM* controlled plasmodesma aperture regulation, and simultaneous inhibition of auxin signaling, polar auxin transport, and regulated plasmodesma aperture phenocopied *gnom* mutants. Therefore, veins are patterned by the coordinated action of three *GNOM*-dependent pathways: auxin signaling, polar auxin transport, and movement of auxin or an auxin-dependent signal through plasmodesmata. I next addressed the question whether — and if so, where and when in leaf development — *GNOM* controlled the production, the movement, or the interpretation of a vein patterning signal. My results suggest that *GNOM*

controls the production, propagation, or interpretation of a vein patterning signal in the leaf inner tissues. For that function, *GNOM* expression was required in all the inner tissues of the leaf throughout leaf development, but stronger *GNOM* expression seemed to be required where new veins were forming. By contrast, if a signal with vein patterning function were produced in the leaf epidermis, the production of such a signal would be independent of *GNOM*. I finally addressed the question whether *GNOM*-dependent, high plasmodesma permeability were required for vein patterning in all or only some of the tissues of the developing leaf. I found that wide plasmodesma aperture is required in newly formed veins and in all the inner cells in areas of the leaf where new veins are forming. By contrast, wide plasmodesma aperture was dispensable in the epidermis and in the nonvascular inner tissue surrounding newly formed veins. My results suggest that the epidermis is a sink for signals that are produced in inner cells and move there through plasmodesmata to promote vein formation. Therefore — contrary to widespread belief — the epidermis is not a source of auxin signals that diffuse or are transported into the inner tissues to induce vein formation. In conclusion, my results suggest an unprecedented mechanism of tissue network formation in multicellular organisms.

Preface

Chapter 1 was adapted from three published papers:

(i) Linh, N. M., Verna, C. and Scarpella, E. (2018). Coordination of cell polarity and the patterning of leaf vein networks. Current Opinion in Plant Biology 41, 116–124. I was a co-first-author, and my contribution included conceptualization, visualization, writing — original draft, writing — review and editing.

(ii) Ravichandran, S. J., Linh, N. M. and Scarpella, E. (2020). The canalization hypothesis - challenges and alternatives. New Phytologist 227, 1051–1059. I was a co-first-author, and my contribution included conceptualization, visualization, writing — original draft, writing — review and editing.

(iii) Lavania, D., Linh, N. M. and Scarpella, E. (2021). Of Cells, Strands, and Networks: Auxin and the Patterned Formation of the Vascular System. Cold Spring Harb Perspect Biol 13, a039958. I was a co-first-author and my contribution included conceptualization, visualization, writing — original draft, writing — review and editing.

Chapter 2 was published as Linh, N. M. and Scarpella, E. (2022). Confocal Imaging of Developing Leaves. Curr Protoc 2, e349. I was a first author, and my contribution included conceptualization, formal analysis, investigation, methodology, validation, visualization, writing — original draft, writing — review and editing.

Chapter 3 was adapted from Verna, C., Ravichandran, S. J., Sawchuk, M. G., Linh, N. M. and Scarpella, E. (2019). Coordination of Tissue Cell Polarity by Auxin Transport and Signaling. Elife 8, e51061. I was a co-author, and my contribution included formal analysis, investigation, methodology, validation, and visualization.

Chapter 4 was published as Amalraj, B., Govindaraju, P., Krishna, A., Lavania, D., Linh, N. M., Ravichandran, S. J. and Scarpella, E. (2020). GAL4/GFP enhancer-trap lines for identification and manipulation of cells and tissues in developing Arabidopsis leaves.

Developmental Dynamics 249, 1127–1146. I was a co-first-author, and my contribution included conceptualization, formal analysis, investigation, methodology, validation, visualization, writing — original draft, writing — review and editing.

Chapter 5 was published as Linh, N.M. and Scarpella, E. (2022). Leaf vein patterning is regulated by the aperture of plasmodesmata intercellular channels. PLoS Biol 20, e3001781. I was first author, and my contribution included conceptualization, formal analysis, investigation, methodology, validation, visualization, writing — original draft, writing — review and editing.

All the authors and publishers have given their permission for the inclusion of these publications in this thesis.

Acknowledgments

Back in 2010, a one-month misplacement of supporting documents for my application to the University of Alberta resulted in my entrance to the undergraduate program being delayed. Consequently, my visa application was approved late, causing my academic life to be postponed by an entire semester. Though being disappointed in this series of events, I was fortunately put in contact with Dr. Shelagh Campbell, who initially helped me remotely and eventually became my academic mentor. It was Dr. Shelagh Campbell who listened to my passion for plant genetics and decidedly introduced me to the Scarpella lab where I was welcomed to not just pursue undergraduate research but transition into a graduate program. Without Dr. Shelagh Campbell, my graduate journey in the Scarpella lab would not have happened; thus, I am greatly thankful for her support.

Every journey has a beginning, and my embarkation on this graduate program is not an exception. Since 2013, I started doing research projects as an undergraduate in the Scarpella lab. Then, with an ASPB 2014 Summer Undergraduate Research Fellowship from the American Society of Plant Biologists, I continued another research project the results of which became the inspiring factors for my pursuit of a graduate program in the Scarpella lab that eventually resulted in the work presented in this Ph.D. thesis. Undoubtedly, this journey was possible thanks to Dr. Enrico Scarpella who accepted me into the lab and has continuously supervised me since 2013. Thanks to his dedicated supervision, I have gained lots of experiences and continued to improve academic skillsets — both practically and intellectually — during my graduate time. More important, Enrico's supervision has gone beyond the academic setting: his continued constructive criticism and heartfelt encouragement have helped to keep me on the right track of life amid the chaos of COVID-19 crisis. I will always appreciate Enrico's support during my time as a member of the Scarpella lab.

Table of Contents

Chapter 3: Coordination of Tissue Cell Polarity by Auxin Transport and Signaling   97

Chapter 4: GAL4/GFP Enhancer-Trap Lines for Identification and Manipulation of Cells and Tissues in Developing Arabidopsis Leaves 120

Chapter 5: Leaf Vein Patterning is Regulated by the Aperture of Plasmodesmata Intercellular Channels 157

Chapter 6: Vein Patterning by Tissue-Specific *GNOM*

Expression 221

Chapter 7: Control of Vein Patterning by Tissue-Specific Regulation of Plasmodesmata Aperture   239

Chapter 8: General Discussion   253

Works Cited   265

List of Tables

List of Figures

List of Abbreviations

Å	Angstrom unit
Ab	Abaxial
ABCB	ATP-BINDING CASSETTE B
ABRC	ARABIDOPSIS BIOLOGICAL RESOURCE CENTER
ARF	AUXIN RESPONSE FACTOR
Ad	Adaxial
ADP	ADENOSINE DIPHOSPHATE
AFB2	AUXIN SIGNALING F-BOX2
a.k.a.	Also known as
Ap	Apical
ATML1	ARABIDOPSIS THALIANA MERISTEM LAYER 1
AU	Airy unit
Ar	Argon
Ba	Basal
BP	Band pass
CALS3	CALLOSE SYNTHASE 3
cals3-d	callose synthase 3 - dominant
cals3m	Mutated CALLOSE SYNTHASE 3
cas	CAS number
cat	Catalogue
cm	Centimeter

Col-0	Columbia-0
CVP2	COTYLEDON VASCULAR PATTERN 2
CV	Closed vein
DAG	Days after germination
dex	Dexamethasone
DNA	DEOXYRIBONUCLEIC ACID
DR5rev	REVERSE DIRECT REPEAT 5
e.g.	For example
ER	Endoplasmic reticulum
erGFP	Endoplasmic-reticulum-localized GREEN FLUORESCENT PROTEIN
EP	Exit point
ET	Enhancer-trap
Fig.	Figure
FT	Color splitter (Farb teiler)
FWHM	Minimum optical slice thickness
GAL4	GALACTOSE 4
GFP	GREEN FLUORESCENT PROTEIN
GSL8	GLUCAN-SYNTHASE-LIKE 8 / CHORUS / ENLARGED TETRAD 2 / MASSUE / ECTOPIC EXPRESSION OF SEED STORAGE PROTEINS 8
GSL8-CHOR	GSL8 - CHORUS
GSL8-ET2	GSL8 - ENLARGED TETRAD 2

GN	GNOM
GOI	GENE OF INTEREST
GR	GLUCOCORTICOID RECEPTOR
GTPase	GUANINE TRIPHOSPHATASE
GUS	B-GLUCURONIDASE
He/Ne	Helium/Neon
HFT	Main dichroic beam splitter (Haupt farb teiler)
HV or Hv or hv or MV	Minor vein
hy	Hydathode
IAA	Indole-3-acetic acid
i.e.	In other words
IR	Infrared
KOH	Potassium hydroxide
KP	Break point
l	Liter
La	Lateral
la or Lm	Lamina
LexO	LexA operator
LUT	Look-up table
L1,L2,L3 or l1,l2,l3	Loop 1, loop 2, loop 3
LV	Lateral vein
M or MV or Mv or mv	Midvein

Md	Median
Me	Marginal epidermis
MES	2-(N-Morpholino)ethanesulfonic Acid
mg	Milligram
min	Minute
ml	Milliliter
mm	Millimeter
M_{Obj}	Objective magnification
MP	MONOPTEROS
MS	Murashige & Skoog
M_{Sys}	System magnification
m^{-2}	Per meter
n	Refractive index
NA	Numerical aperture
NFT	Secondary dichroic beam splitter (Neben farb teiler)
nm	Nanometer
no	Number
NPA	N-1-naphthylphthalamic acid
nYFP	Nuclear YELLOW FLUORESCENT PROTEIN
OV	Open vein
P	Primordium
PBA	Phenylboronic acid

Pe	Petiole
PED	PIN1- expression domain
PD	Plasmodesma
PH	Pinhole
pH	Power of hydrogen
PH$_{(nm)}$	Pinhole diameter in nanometer
PIN	PIN-FORMED
PM	Plasma membrane
PMT	Photomultiplier tube
RNAi	Ribonucleic acid interference
SE	Standard error
sec	Second
SF	Shape factor
SHR	SHORT-ROOT
St	Stoma
s^{-1}	Per second
TIR1	TRANSPORT INHIBITOR RESPONSE1
TP	Touch point
Tr	Trichome
UAS	UPSTREAM ACTIVATING SEQUENCE
V	Volt
VP16	VIRAL PROTEIN 16

WT	Wild-type
XP	Exit point
XVE	LexA-viral protein 16-estrogen receptor
YFP	YELLOW FLUORESCENT PROTEIN
YUC	YUCCA
YUC_e	YUCCA genes with expression in epidermis
YUC_i	YUCCA genes with expression in inner tissues
YUC_l	YUCCA genes with expression in both epidermis and inner tissues
Z	Zoom factor
WD	Working distance
17βE	17-β-estradiol
º	Degree
°C	Degree Celsius
μl	Microliter
μm	Micrometer
μmol	Micromole
μs	Microsecond
$λ_{Em}$	Average emission wavelength
$λ_{Ex}$	Excitation wavelength
×	Times
%	Percent
<	Less than

≤	Less than or equal to
>	Greater than
≥	Greater than or equal to
~	Approximately

Gene and Protein Notation

WT gene	Uppercase, italics (e.g., *GNOM*)
Mutant gene	Lowercase, italics (e.g., *gnom*)
WT protein	Uppercase (e.g., GNOM)
Multiple Mutant of Gene *A* and *B*	*a;b* (e.g., *gnom*;*cals3-2d*)
Transactivation of gene *B* by enhancer A	A>>B (e.g., E100>>XVE)

Gene Fusion Notation

Transcriptional Fusion of Gene *A* to Gene *B* (Fusion of promoter *A* to gene *B*)	A::B (e.g., PIN1::GFP)
Translational Fusion of Gene *A* to Gene *B* (Fusion of gene *A* to gene *B*)	A:B (e.g., GN:YFP)

Gene Coordinates

All gene coordinates are relative to the adenine (position +1) of the start codon

Chapter 1: General Introduction[1]

1.1 THE PLANT HORMONE AUXIN, PLANT CELL POLARITY, AND THE PLANT VASCULAR SYSTEM

In most multicellular organisms, water, nutrients, and signals are transported by tissue networks. In animals, this essential transport function is distributed over separate tissue networks — for example, the nervous, circulatory, and respiratory systems. By contrast, in plants, all transport functions are performed by the only tissue network: the vascular system.

The plant vascular system is a network of vascular strands that connect the different parts of an organ and the different organs of a plant (Fig. 1.1, *left*) (Esau, 1965). Vascular strands are bundles of files of vascular cells that are elongated along the files and connected at their ends (Fig. 1.1, *right*). Vascular strands are named differently in different organs: veins in flat organs like leaves, petals, sepals, and cotyledons; vascular bundles in the stem; and vascular cylinder or stele in the root.

During development, cell behaviors such as expansion and division are coordinated between cells along preferential or exclusive orientations or directions (Wolpert, 2016). In plants, for example, cells in epidermal files of the root form hairs by locally expanding at their basal outer side (Fischer et al., 2006; Masucci and Schiefelbein, 1994), and cells in epidermal

---

[1] Adapted from (i) Lavania, D., Linh, N. M. and Scarpella, E. (2021). Of Cells, Strands, and Networks: Auxin and the Patterned Formation of the Vascular System. Cold Spring Harb Perspect Biol 13, a039958; (ii) Linh, N. M., Verna, C. and Scarpella, E. (2018). Coordination of cell polarity and the patterning of leaf vein networks. Current Opinion in Plant Biology 41, 116–124; and (iii) Ravichandran, S. J., Linh, N. M. and Scarpella, E. (2020). The canalization hypothesis - challenges and alternatives. New Phytologist 227, 1051–1059.
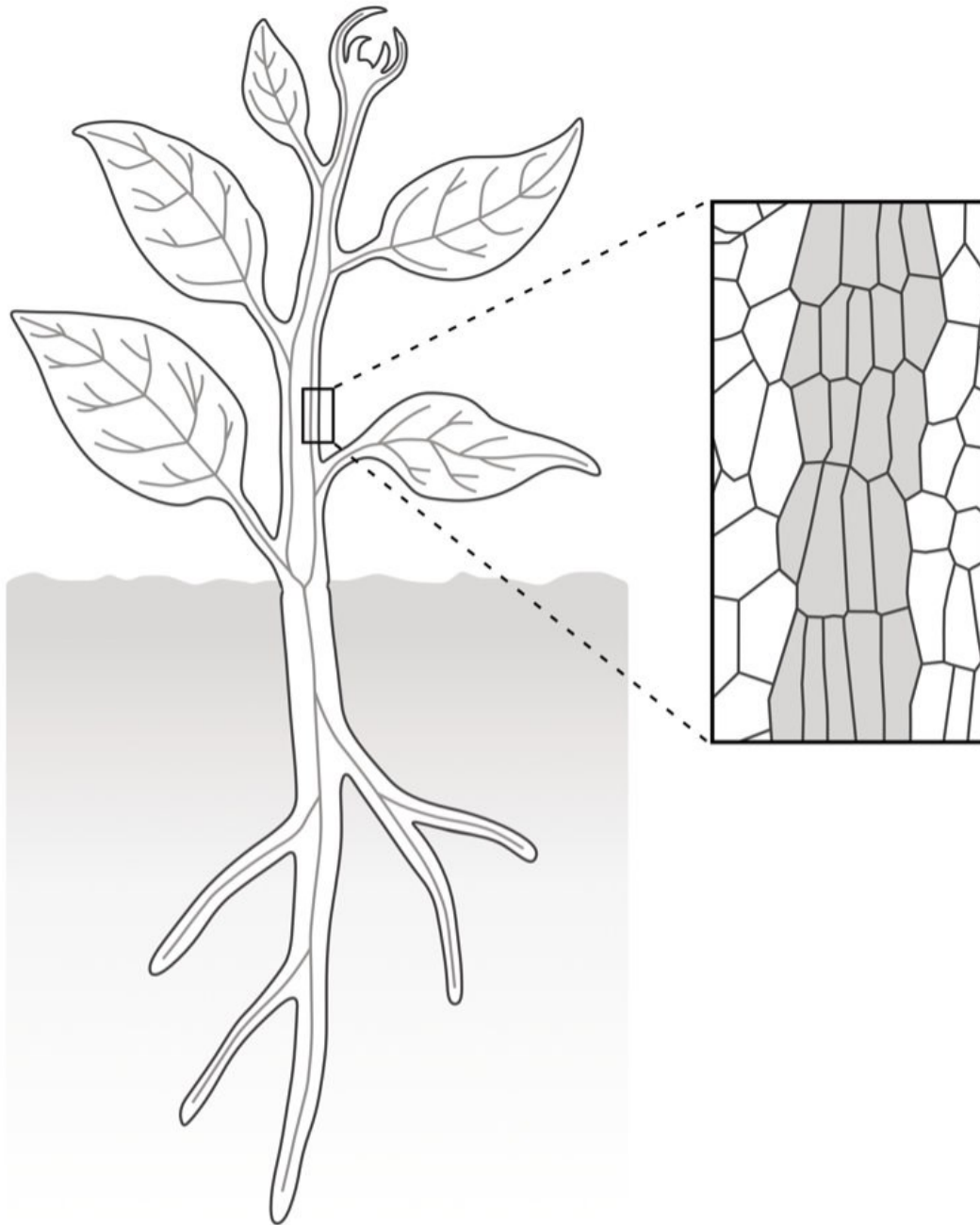
Figure 1.1. The Plant Vascular System

(*Left*) The plant vascular system is a network of vascular strands (gray lines) that connect the different parts of an organ and the different organs of a plant. (*Right*) Vascular strands are bundles of files of vascular cells (gray fill) that are elongated along the file and connected at their ends.

sheets of shoot organ primordia expand and divide along the proximodistal orientation (Kuchen et al., 2012; Reddy et al., 2004). How are these orientations and directions specified within cells and coordinated between cells?

In animals, where this question has been addressed extensively, the anisotropic localization of cellular components such as proteins provides cells with an internal compass that points in a specific direction (Goodrich and Strutt, 2011). These cell anisotropies, or cell polarities, are then coordinated between cells, often by mechanisms that rely on direct interaction between proteins bridging the plasma membranes of neighboring cells. These types of mechanisms are precluded in plants by a wall that separates the cells' plasma membranes. How then is cell polarity coordinated in plants?

In this chapter, I will review evidence that the patterning of leaf vein networks is an expression of coordination of cell polarity and that regulators of leaf vein patterning encode regulators of such coordination. Therefore, available evidence suggests that understanding how leaf vein networks are patterned will help understand how cell polarity is coordinated in plants. Furthermore, in this chapter I will discuss evidence that suggests that the plant hormone auxin controls the patterned formation of the vascular system at all the system's organization levels: the cells', the strands', and the network's.

1.2 AUXIN SIGNALING AND THE FORMATION OF THE FIRST VASCULAR CELLS

Much of a seedling can be seen as a cylinder with a vascular strand in its center (Fig. 1.2A). The formation of this cylinder coincides with the formation of the first vascular cells in the Arabidopsis globular embryo (Fig. 1.2B, *bottom*) (de Rybel et al., 2014; Gooh et al., 2015; Scheres et al., 1994; Yoshida et al., 2014). However, expression of vascular-specific markers
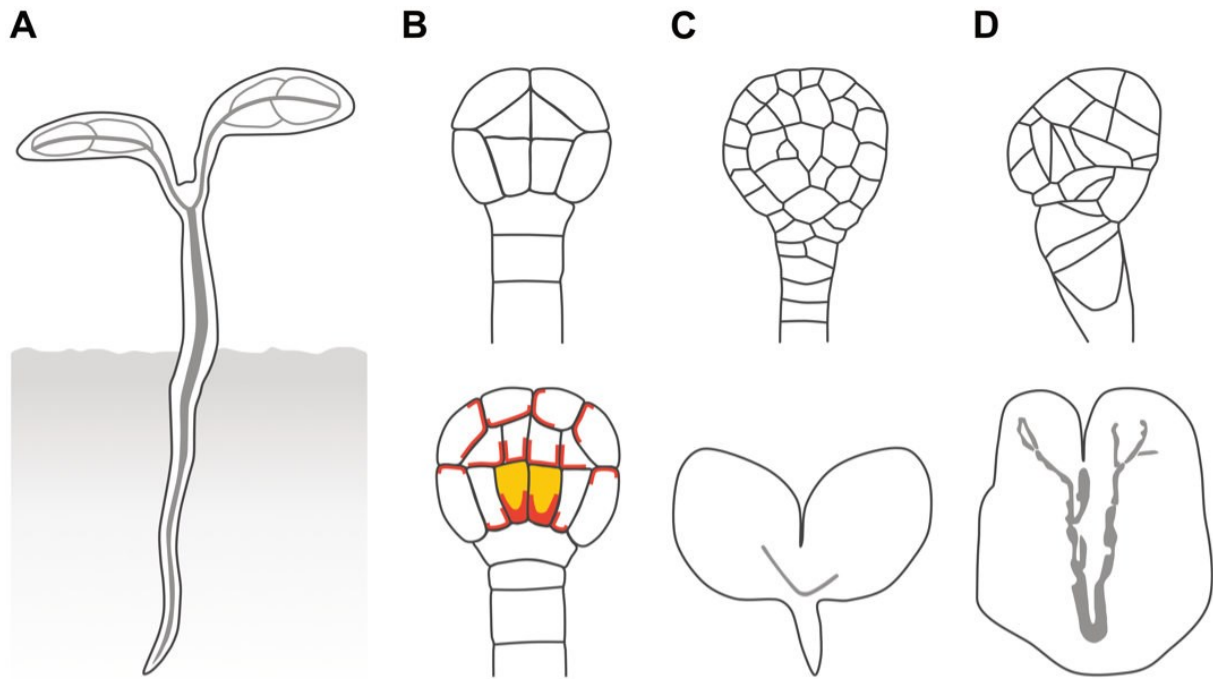
Figure 1.2. Auxin Signaling and the Formation of the First Vascular Cells

(A) Much of the seedling is a cylinder with a vascular strand (gray line) in its center. (B) The localization of PIN1 (red) is polarized in the first vascular cells (yellow fill) of the globular embryo (*bottom*), which originate from the periclinal, asymmetric division of the lower inner cells in the dermatogen embryo (*top*). (C) The lower inner cells in the dermatogen embryos of auxin signaling mutants fail to divide periclinally and asymmetrically, leading to vascularless globular embryos (*top*) and seedlings in which the vascularized cylinder is replaced by a vascularless cone (*bottom*). (D) Auxin-signaling-unrelated mutants whose cells divide along random planes (*top*) form vascular strands nonetheless (*bottom*).

suggests that the identity of these first vascular cells had been specified earlier, at the dermatogen stage (Fig. 1.2B, *top*) (Smit et al., 2020).

The Arabidopsis dermatogen embryo is composed of 16 cells: eight outer cells, which are the precursors of the epidermis, and eight inner cells, which are the precursors of all the other tissue types (Fig. 1.2B, *top*) (de Rybel et al., 2014; Gooh et al., 2015; Mansfield and Briarty, 1991; Yoshida et al., 2014). These eight inner cells will divide periclinally and asymmetrically, and the resulting four larger, innermost cells in the basal half of the globular embryo will become the first vascular cells (Fig. 1.2B, *bottom*) (Esau, 1965).

Available evidence suggests that the formation of the seedling cylinder and the vascular strand in its center depend on auxin signaling. Indeed, dermatogen embryos of auxin signaling mutants express vascular-specific markers abnormally — if at all — and the eight inner cells in these mutant embryos fail to divide periclinally and asymmetrically and to form the first vascular cells in globular embryos (Fig. 1.2C, *top*) (Berleth and Jurgens, 1993; Dharmasiri et al., 2005; Hamann et al., 1999; Hamann et al., 2002; Hardtke and Berleth, 1998; Hellmann et al., 2003; Hobbie et al., 2000; Smit et al., 2020; Yoshida et al., 2014). Most of these mutant embryos develop into seedlings in which the vascularized cylinder is replaced by a vascularless cone (Fig. 1.2C, *bottom*). This defect characterizes mutants in auxin perception or response but also mutants in auxin production and embryos developed in the presence of auxin antagonists (Cheng et al., 2007; Dharmasiri et al., 2003; Dharmasiri et al., 2007; Hadfi et al., 1998; Stepanova et al., 2008; Thomas et al., 2009).

Among such mutants, defects are most severe in mutants lacking the function of the *MONOPTEROS / AUXIN RESPONSE FACTOR5* (*MP* hereafter) gene of Arabidopsis, which encodes a transcription factor that regulates auxin-responsive gene expression (Berleth and Jurgens, 1993; Hardtke and Berleth, 1998; Mattsson et al., 2003; Ulmasov et al., 1997; Ulmasov et al., 1999), and in mutants with a stabilized variant of the otherwise short-lived MP- inhibitor INDOLE-3-ACETIC-ACID-INDUCIBLE12 / BODENLOS (Dharmasiri et al., 2005; Garrett et al.,

2012; Hamann et al., 1999; Hardtke et al., 2004; Krogan et al., 2012; Lau et al., 2011; Scarpella, 2017; Schlereth et al., 2010; Weijers et al., 2005; Weijers et al., 2006). Similar defects also characterize mutants in the *EMBRYO DEFECTIVE30 / GNOM* (*GN* hereafter) gene of Arabidopsis (Busch et al., 1996; Mayer et al., 1993; Shevell et al., 1994; Yoshida et al., 2014), which encodes a regulator of membrane trafficking that controls auxin signaling through unknown pathways (Mayer et al., 1993; Verna et al., 2019; Wolters et al., 2011) (Chapter 3).

That these mutants fail to form the first vascular cells seems to result from the inability of the lower inner cells of the dermatogen embryo to divide periclinally and asymmetrically, suggesting that auxin signaling promotes such asymmetric cell division (Hamann et al., 1999; Scarpella, 2017; Yoshida et al., 2014). However, vascular cells — although abnormally shaped — still form in mutant embryos in which cells divide along random planes (Fig. 1.2D) (Torres-Ruiz and Jurgens, 1994; Yoshida et al., 2014), random planes that presumably include those which in auxin signaling mutants are correlated with failure to form vascular cells. Furthermore, auxin application to various tissues induces the formation of vascular strands even in the absence of cell division (Fig. 1.3A,C) (see, e.g., (Sachs, 1969; Sinnott and Bloch, 1944)). Therefore, the vascular-differentiation-promoting influence of auxin does not seem to necessarily depend on its cell-division-orienting activity (Scarpella, 2017).

1.3 AUXIN TRANSPORT, COORDINATION OF CELL POLARITY, AND AUXIN-INDUCED VASCULAR STRAND FORMATION

The functional unit of the vascular system is the vascular strand, whose formation seems to be an expression of auxin transport and coordination of cell polarity. This conclusion is suggested by the result of experiments in which auxin is applied to mature plant tissues or in which plant tissues are wounded. Auxin application to a mature stem or root of a plant from which the immature leaves above the auxin application site have been removed leads to the formation of vascular strands that connect the applied auxin to the pre-existing vascular strands basally to
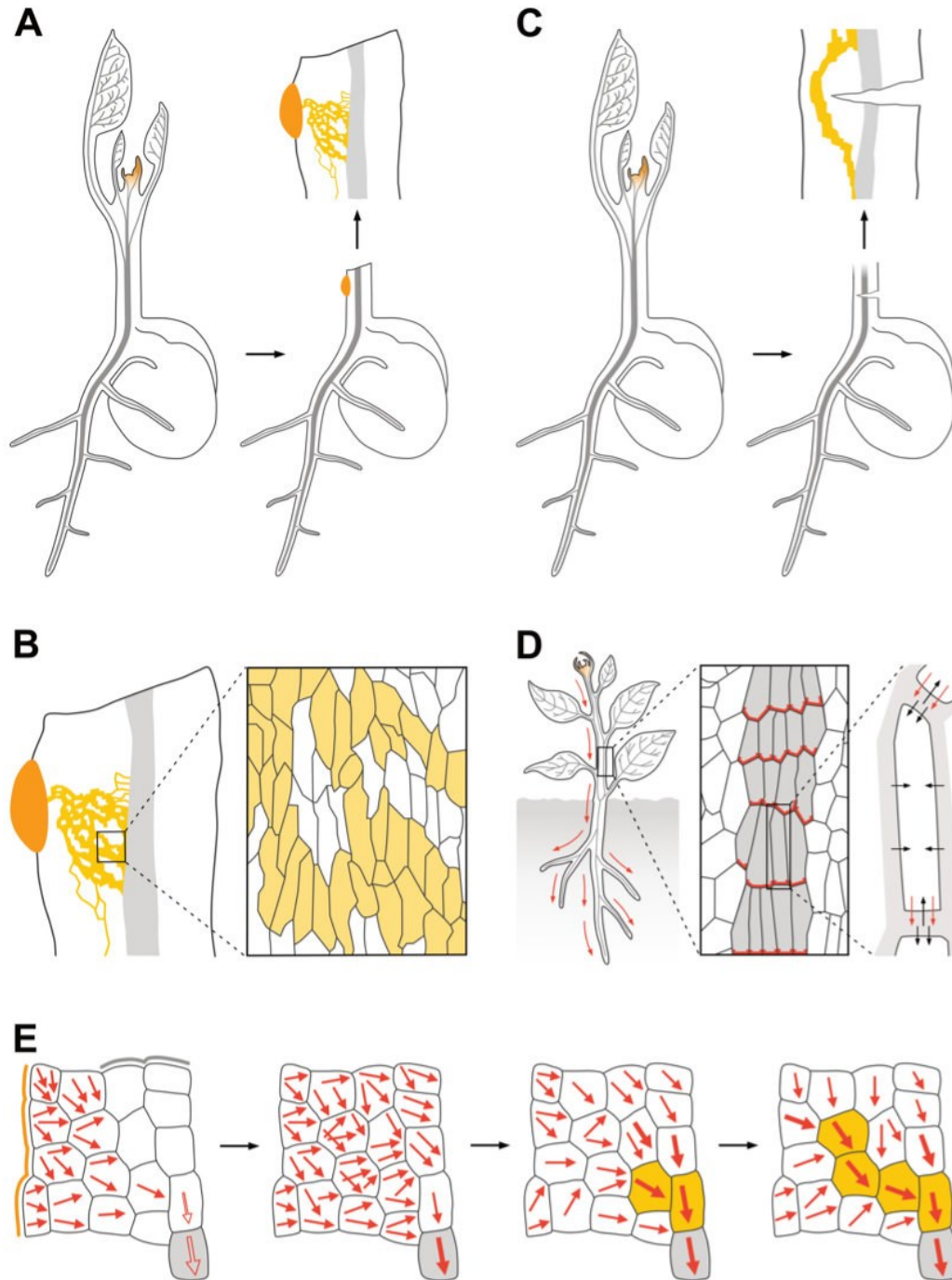
Figure 1.3. Auxin Transport, Coordination of Cell Polarity, and Vascular Strand Formation

(A) The application of auxin (orange) to a mature stem or root of a plant from which the immature leaves above the auxin application site have been removed induces the differentiation

of vascular cells in continuous files to form vascular strands (yellow lines) that connect the applied auxin to the pre-existing vascular strands (gray fill) basal to the application site. Inspired by work by (Sachs, 1968a). (B) Interruption of the supply of auxin that originates from the immature leaves by wounding a vascular strand (gray fill) in a mature stem or root induces the differentiation of vascular cells in continuous files to form vascular strands (yellow fill) connecting the pre-existing vascular strand above and below the wound. Inspired by work by (Benayoun et al., 1975; Thompson and Jacobs, 1966). (C) In the vascular strands formed in response to auxin application, vascular cells (yellow fill) are not aligned along the file like in Fig. 1.1, but along the axis of the tissue. (D) (*Left*) Auxin (orange) is mainly produced in immature shoot organs and transported (red arrows) toward the roots through vascular strands (gray lines). (*Middle*) Apico-basal, polar auxin transport results from the localization of auxin efflux carriers of the PIN family (red) at the basal plasma membrane of vascular cells (gray fill). (*Right*) Auxin efflux carriers are required for auxin to leave the cell (red arrows) because auxin is mostly negatively charged inside the cell; by contrast, in the extracellular space auxin is to a larger extent uncharged and can thus diffuse into the cell (black arrows). (E) Successive stages (connected by black arrows) of vascular strand formation in response to wounding or auxin application as accounted for by the canalization hypothesis. The auxin canalization hypothesis assumes that auxin or an auxin-dependent signal that is experimentally indistinguishable from auxin diffuses from the auxin application site (orange line) or from the tissue above the wounding site (gray line) toward the pre-existing vascular strands in the organ (gray fill). The positive feedback between auxin movement (red arrows) and localization of auxin efflux carriers to the site where auxin leaves the cell would gradually polarize auxin transport (thicker arrows). This would occur first in the cells connected to the pre-existing vasculature (gray fill), which are still polarized along the original, apico-basal polarity of the tissue (empty red arrows) and thus orient auxin movement toward themselves. Increased auxin transport polarity, capacity, or velocity in the selected cells would lead to vascular differentiation (yellow fill) and drain auxin

from neighboring cells, thus inhibiting their differentiation. The process would continue until a vascular strand formed that connected the applied auxin to the pre-existing vascular strands basal to the auxin application site. Inspired by work by (Sachs, 1991).

the site of auxin application (Fig. 1.3A,C) (Jacobs, 1952; Jost, 1942; Kraus et al., 1936; Sachs, 1968a). Likewise, interruption of the vascular connection with the immature leaves by wounding leads to the formation of vascular strands that connect the strands above the wound with those below it, thereby re-establishing the vascular connection with the immature leaves (Fig. 1.3B) (Benayoun et al., 1975). The vascular differentiation response of the tissue to auxin application or wounding seems to be blocked by inhibitors of polar auxin transport (Roberts, 1960; Thompson and Jacobs, 1966), suggesting that it depends on the ability of the responding tissue to transport auxin polarly.

Indeed, although auxin is mainly produced in immature shoot organs such as leaf and flower primordia (Avery Jr., 1935; Thimann and Skoog, 1934), it is transported toward the roots through vascular strands (Fig. 1.3D, *left*) (Wangermann, 1974; Went, 1928). This apico-basal, polar auxin transport is thought to result from the localization of auxin efflux carriers at the basal end of auxin-transporting cells (Fig. 1.3D, *middle*) (Raven, 1975; Ravichandran et al., 2020; Rubery and Sheldrake, 1974). Indeed, the weak acid indole-3-acetic acid (IAA) — the most abundant natural auxin — is mostly negatively charged inside the cell and can thus efficiently leave the cell only through plasma-membrane-localized auxin efflux carriers (Fig. 1.3D, *right*). Although the mechanism of action is still unclear (for review, see (Barbosa et al., 2018)), available evidence suggests that these auxin efflux carriers are encoded by *PIN-FORMED* (*PIN*) genes (for review, see (Adamowski and Friml, 2015)). Computational simulations of this model suggest that it can account for both polar auxin transport (Mitchison, 1980a) and the polar formation of vascular strands in response to auxin application, provided that auxin movement through a cell positively feeds back on the localization of auxin efflux carriers to the site where auxin leaves the cell, as proposed by the auxin canalization hypothesis (Sachs, 1981; Sachs, 1984; Sachs, 1991; Sachs, 2000). But how does the canalization hypothesis intend to account for the unique properties of the auxin-induced vascular-differentiation response?

The auxin canalization hypothesis assumes that when auxin is applied to a stem or root of plant from which the immature leaves above the auxin application site have been removed, an auxin-dependent signal that is experimentally indistinguishable from auxin slowly diffuses from the auxin application site toward the pre-existing vascular strands in the organ (Fig. 1.3E) (Sachs, 1981; Sachs, 1991; Sachs, 2000). In the cells between the application site and the pre-existing vascular strands, auxin efflux carriers would initially be localized to all the different sections of the plasma membrane (i.e. non-polarly). By contrast, in the pre-existing vascular strands, auxin efflux carriers would be localized along the original apico-basal, auxin transport polarity of the tissue. Though their supply of auxin would be low, the pre-existing vascular strands basal to the auxin application site would still be highly efficient and polarized auxin transporters because the continuous flow of auxin that would be maintaining their transport polarity would only recently have been interrupted. As such, the pre-existing vascular strands basal to the auxin application site would efficiently remove any auxin that reached them by diffusion from the auxin application site, thereby acting as auxin sinks that orient toward themselves auxin movement in the neighboring cells and polarize the localization of auxin efflux carriers in those same cells (Fig. 1.3E). The resulting induction of polar auxin transport in the cells neighboring the pre-existing vascular strands would be gradually enhanced by the positive feedback between auxin movement and localization of auxin efflux carriers proposed by the auxin canalization hypothesis. By draining auxin increasingly more efficiently and polarly, the cells neighboring the pre-existing vascular strands would behave as auxin sinks that in turn induce polar localization of auxin efflux carriers and polar auxin transport in the cells above them and inhibit the same processes in the lateral neighbors (Fig. 1.3E). The repetition of these steps would eventually lead to preferential auxin transport through single-cell files — the "canals" the hypothesis refers to — that would connect the applied auxin to the pre-existing vascular strands basal to the auxin application site and that would differentiate into vascular strands (Fig. 1.3A,C,E). During this process, any random polarization in the localization of auxin

efflux carriers would be stabilized by the positive feedback between auxin movement and localization of auxin efflux carriers proposed by the auxin canalization hypothesis and lead to random deviations in the course of the selected cell files and from the shortest route for auxin transport.

Likewise, when the supply of auxin that originates from the immature leaves is interrupted by wounding vascular strands, auxin would accumulate above the wound (Fig. 1.3E) (Sachs, 1991). Depleted of auxin supply, the vascular strands below the wounding site would become polarized sinks for auxin, which would slowly diffuse toward the vascular strands below the wounding site. These auxin-depleted vascular strands would thus polarize auxin movement toward themselves and, through the same process described above, would lead to the formation of vascular strands connecting the pre-existing vascular strands above and below the wound (Fig. 1.3B,E).

The plasma membrane localization of PIN1 auxin efflux carriers of Arabidopsis marks the presumed auxin efflux side of cells (Petrasek et al., 2006; Wisniewska et al., 2006). Therefore, the polarity of auxin transport can be inferred from the localization of PIN1 to the plasma membrane. Auxin application to mature plant tissues induces the formation of broad expression domains of non-polarly localized PIN1 that connect the applied auxin to the pre-existing vascular strands (Mazur et al., 2016; Sauer et al., 2006). Over time, the broad PIN1-expression domains (PEDs hereafter) become restricted to sites of auxin-induced vascular-strand formation, and PIN1 localization becomes polarized. In the cells along the PEDs' midline, PIN1 localization becomes polarized toward the pre-existing vascular strands basal to the site of auxin application; in the cells flanking the PEDs' midline, PIN1 localization becomes polarized toward the domain's midline. Eventually, narrow PEDs mark the sites of auxin-induced vascular strand formation, and polar PIN1 localization in the vascular strands formed in response to auxin application suggests auxin transport away from the applied auxin and toward the pre-existing vascular strands basal to the auxin application site. Both the restriction of broad PEDs

and the polarization of PIN1 localization during auxin- induced vascular-strand formation initiate and proceed away from the pre-existing vascular strands and are consistent with predictions of the auxin canalization hypothesis.

Consistent with predictions of the auxin canalization hypothesis is also the observation that auxin application fails to induce vascular strand formation in *pin1* mutants or plants treated with auxin transport inhibitors (Mazur et al., 2020). This observation is, however, unexpected because auxin application to shoot tips of *pin1* mutants or wild-type plants grown in the presence of auxin transport inhibitors leads to the formation of whole leaves, including their veins (Reinhardt et al., 2000; Reinhardt et al., 2003). This finding is not the only apparent inconsistency between assumptions or predictions of the auxin canalization hypothesis and experimental observations (Bennett et al., 2014; Runions et al., 2014). For example, the auxin canalization hypothesis assumes that auxin readily diffuses out of the cells (Sachs, 1981), but auxin diffusion out of the cell is unfavored over diffusion into the cell by nearly two orders of magnitude (Runions et al., 2014).

The auxin canalization hypothesis also assumes that cells can measure net auxin transport across their plasma membranes (Sachs, 1969). No biological mechanism is known that allows cells to measure net auxin transport directly (Cieslak et al., 2015; Kramer, 2009; Mitchison, 1980b; Mitchison, 1981). However, cells could use the concentration of auxin, of auxin-bound auxin carriers, or of substances produced or consumed during auxin transport to measure auxin influx and efflux separately, which would indirectly provide a measure of net auxin transport (Cieslak et al., 2015; Coen et al., 2004; Mitchison, 1980b). Alternatively, cells could measure intracellular auxin gradients, which depend on auxin transport: auxin concentration would be higher where auxin enters the cell and lower near auxin efflux carriers, where auxin leaves the cell (Kramer, 2009; Mitchison, 1981). Even though these mechanisms await experimental testing, they are both plausible; instead, that auxin controls polarization of PIN1 localization by inhibiting PIN1 deallocation from the section of the plasma membrane from

which auxin leaves the cell can be ruled out (Jásik et al., 2016; Narasimhan et al., 2021; Paponov et al., 2019).

Finally, the auxin canalization hypothesis assumes that developing vascular strands effortlessly connect to pre-existing vascular strands, an assumption that seems to be justified by experimental observations (Sachs, 1968a) but that cannot be easily reproduced by computational simulations (Bayer et al., 2009; Smith and Bayer, 2009). This limitation is overcome in plants that have two PIN1 proteins: one that broadly polarizes auxin transport toward pre-existing vascular strands, and the other that restricts the broad auxin transport domains to narrow sites of vascular strand formation (O'Connor et al., 2014; O'Connor et al., 2017). In plants like Arabidopsis that have only one PIN1 protein, instead, a hypothetical substance has been proposed to diffuse from pre-existing vascular strands and polarize PIN1 localization in developing vascular strands toward pre-existing vascular strands (Bayer et al., 2009; Smith and Bayer, 2009).

Despite the apparent limitations, vascular strand formation in response to auxin application seems to be an expression of auxin transport and coordination of cell polarity whose essence is captured by the auxin canalization hypothesis; can we say the same of the vascular strands that form during normal development?

1.4 AUXIN TRANSPORT, COORDINATION OF CELL POLARITY, AND VEIN FORMATION

Just like auxin application to mature plant tissues, auxin application to developing leaves leads to the formation of continuous files of vascular cells that connect the applied auxin to the pre-existing veins basal to the auxin application site (Scarpella et al. 2006; Sawchuk et al. 2007; Verna et al. 2019). During both auxin-induced and normally occurring vein formation, PIN1 expression is initiated in broad domains of leaf inner cells connected to pre-existing veins (Fig. 1.4A) (Marcos and Berleth, 2014; Scarpella et al., 2006; Wenzel et al., 2007). In the cells of
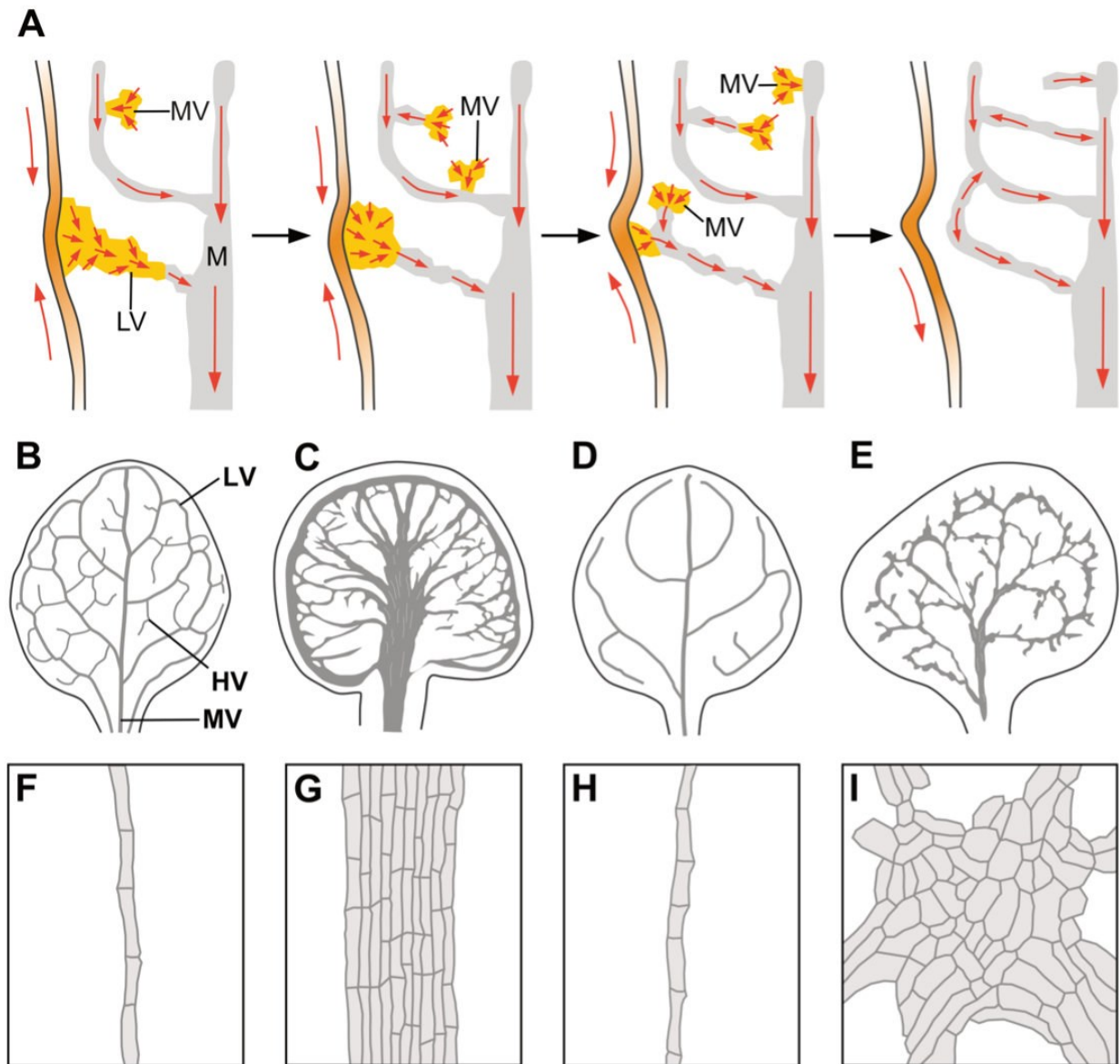
Figure 1.4. Auxin, Coordination of Cell Polarity, and Vein Formation

(A) In rounded leaves, PIN1 localization in epidermal cells of the leaf margin (red arrows) becomes polarized toward sites of leaf lateral growth (orange). Epidermal convergence points of PIN1 polarity are associated with sites of leaf lateral growth and broad PEDs in the inner tissue that become restricted to sites of lateral vein (LV) formation (yellow). Over time, PIN1 localization becomes polarized (red arrows) in the cells of these broad domains. In the cells

along the PEDs' midline, PIN1 localization becomes polarized toward pre-existing veins (gray); in the cells flanking PEDs' midline, PIN1 localization becomes polarized toward the domains' midline. Both the restriction of broad PEDs and the polarization of PIN1 localization initiate and proceed away from pre-existing veins (gray), in which PIN1 localization is polarized (red arrows). Broad PEDs in the inner tissue that become restricted to sites of minor vein (MV) formation (yellow) branch from pre-existing veins (gray). Over time, PIN1 localization becomes polarized (red arrows) in the cells of these broad domains. In the cells along the PEDs' midline, PIN1 localization becomes polarized toward pre-existing veins (gray); in the cells flanking PEDs' midline, PIN1 localization becomes polarized toward the domains' midline. Both the restriction of broad PEDs and the polarization of PIN1 localization initiate and proceed away from pre-existing veins, in which PIN1 localization is polarized (red arrows). Broad, MV-associated PEDs can gradually disappear instead of becoming restricted and polarized. Initially, MV-associated PEDs connect to pre-existing veins at one end only ("open" PEDs), but they can extend to connect to pre-existing veins at both ends ("closed" PEDs). Open PEDs have a single polarity; closed PEDs have two opposite polarities, which are connected by a "bipolar" cell, a cell in which PIN1 localization is polarized at both ends (see also Fig. 1.6F). Each vein loop forms from the fusion of LV-associated PEDs and MV-associated closed PEDs. Black arrows connect successive stages of leaf development. (B) Wild-type (WT) Arabidopsis grown under normal conditions forms leaves whose vein networks are defined by at least four reproducible features: a narrow I-shaped midvein (MV) that runs the length of the leaf; lateral veins (LV) that branch from the midvein and join distal veins to form closed loops; minor veins (HV) that branch from midvein and loops, and either end freely or join other veins; and minor veins and loops that curve near the leaf margin, lending a scalloped outline to the vein network. (C) Auxin-transport-inhibited leaves, either because of mutation in six of the eight *PIN* genes or because of growth in the presence of auxin transport inhibitors, form vein networks that differ from those of normally grown WT leaves in four respects: the vein networks are comprised of more lateral veins; lateral

veins fail to join the midvein but run parallel to it to form a wide midvein; lateral veins end in a marginal vein that closely paralleled the leaf margin, lending a smooth outline to the vein network; and veins are thicker. (D) Auxin-signaling-inhibited leaves, either because of mutation in auxin signaling components or because of growth in the presence of an auxin signaling inhibitor, form networks of fewer veins in which closed loops are often replaced by open loops (i.e. loops that contact the midvein or other loops at only one of their two ends). (E) Leaves in which both auxin transport and auxin signaling are inhibited, either because of mutation or because of growth in the presence of inhibitors, form vein networks whose outline is jagged because of narrow clusters of vascular elements that are oriented perpendicular to the leaf margin and that are laterally connected by veins. (F–I) In WT (F), auxin-transport-inhibited (G), and auxin-signaling-inhibited (H) leaves, vascular elements are connected end-to-end and aligned along the vein. By contrast, in leaves in which both auxin transport and auxin signaling are inhibited (I), veins are often replaced by clusters of vascular cells that are randomly oriented.

those broad PEDs, PIN1 is initially non-polarly localized (Carraro et al., 2006; Johnston et al., 2015; Lee et al., 2009; Marcos and Berleth, 2014; Scarpella et al., 2006; Wenzel et al., 2007). Over time, however, the broad PEDs become restricted to sites of vein formation, and PIN1 localization becomes polarized. In the cells along the PEDs' midline, PIN1 localization becomes polarized toward pre-existing veins; in the cells flanking the PEDs' midline, PIN1 localization becomes polarized toward the domain's midline (Fig. 1.4A). Both the restriction of broad PEDs and the polarization of PIN1 localization initiate and proceed away from pre-existing veins and are delayed by auxin transport inhibition. And both auxin transport inhibition and higher auxin levels lead to the formation of broader PEDs and delay coordination of cell polarity; however, given time even these broader PEDs eventually become restricted to sites of vein formation in which cell polarity is coordinated (Aloni et al., 2003; Hay et al., 2006; Mattsson et al., 2003; Scarpella et al., 2006; Wenzel et al., 2007)

Many of these observations can be accounted for by the positive feedback between auxin movement and localization of auxin efflux carriers proposed by the auxin canalization hypothesis (Mitchison, 1980a; Mitchison, 1981; Rolland-Lagan and Prusinkiewicz, 2005; Sachs, 1981; Sachs, 1991; Sachs, 2000). But if the auxin canalization hypothesis were truly to account for vein formation in response to auxin, leaves of *pin* mutant plants or wild-type plants grown in the presence of auxin transport inhibitors or lacking PIN proteins should form no veins (Rolland-Lagan and Prusinkiewicz, 2005). And indeed leaves of plants grown in the presence of high concentrations of auxin transport inhibitors seem to lack veins nearly completely (Mattsson et al., 1999); however, vascular differentiation occurs more slowly in auxin-transport-inhibited plants (Scarpella et al., 2006), raising the possibility that the apparent lack of veins in auxin-transport-inhibited plants had in fact been the result of incomplete vascular differentiation. This indeed turned out to be the case: when allowed to reach maturity, leaves that had developed in the presence of high concentrations of auxin transport inhibitors do form veins; and as in normally grown plants, the veins of auxin-transport-inhibited plants are

oriented along the apico-basal axis of the leaf, and their vascular cells are elongated along the vein and connected at their ends (Fig. 1.4B,C,F,G) (Sieburth, 1999; Verna et al., 2019). The veins of auxin-transport-inhibited plants are arranged in an abnormal pattern, but this pattern is reproducible. Moreover, veins with these same features also form in leaves of Arabidopsis plants that lack the function of the six *PIN* genes with vascular function (*pin* sextuple mutants hereafter) (Fig. 1.4C) (Verna et al., 2019). Therefore, that auxin-induced vascular-strand formation depends on auxin transport (i.e. the core prediction of the auxin canalization hypothesis) seems to be unsupported by experimental evidence.

It is of course possible that in *pin* sextuple mutants the two remaining PIN proteins, PIN2 and PIN5, supply all the auxin transport activity required for vein formation. However, mutation of *PIN2* fails to enhance the vein pattern defects of a mutant that lacks the function of four other *PIN* genes, suggesting that *PIN2* has no function in vein patterning (Verna et al., 2019). And mutation of *PIN5* partially suppresses the vein pattern defects of a mutant that lacks the function of three other *PIN* genes, suggesting that *PIN5* has functions in vein patterning that are opposite to those of other *PIN* genes (Sawchuk et al., 2013; Verna et al., 2015). Furthermore, the auxin-transport and vein-patterning activity of PIN2 and PIN5 would have to be insensitive to auxin transport inhibition because the vein pattern of *pin* sextuple mutants is phenocopied by treatment with chemically unrelated auxin transport inhibitors that are predicted to act through different mechanisms (Mattsson et al., 1999; Sieburth, 1999; Verna et al., 2019), and growth in the presence of an auxin transport inhibitor fails to induce additional defects in *pin* sextuple mutants (Verna et al., 2019). Though it is possible that PIN2 and PIN5 are insensitive to known auxin transport inhibitors, this possibility is difficult to reconcile with the observation that such inhibitors completely inhibit auxin transport in tissue segments (e.g. (Okada et al., 1991)). And yet leaves of *pin* sextuple mutants — unlike *pin1* mature stems but like *pin1* shoot apices — can still respond to auxin application by forming veins that connect to pre-existing veins basal to the auxin application site (Verna et al., 2019). This observation seems to suggest that vein formation

in *pin* mutants still depends on auxin and that auxin still moves polarly in *pin* mutant leaves, but how would auxin move in those plants in the absence of the six PIN proteins with vascular function?

Available evidence suggests that auxin movement in *pin* sextuple mutants, if at all existing, does not depend on known intercellular transporters (Verna et al., 2019). It is of course possible that it depends on known intracellular transporters or other unknown transporters. However, if so, such transporters would have to be insensitive to all known classes of auxin transport inhibitors because treatment with these inhibitors phenocopies the vein pattern of *pin* sextuple mutants (Mattsson et al., 1999; Sieburth, 1999; Verna et al., 2019). Furthermore, such transporters would have to be specific to leaves or lateral organs or transport auxin inefficiently because auxin movement in auxin-transport-inhibited stem and root segments is indistinguishable from diffusion (e.g. (Okada et al., 1991)). Finally, auxin movement through such transporters would have to be autocatalytic to account for the formation of veins, as opposed to that of broad zones of vascular differentiation (Sachs, 1969). All these requirements make the existence of such transporters, though possible, less likely. But if not through auxin transporters, how would oriented veins form in *pin* sextuple mutants?

1.5 AUXIN SIGNALING AND VEIN FORMATION

The residual vein-formation activity in auxin-transport-inhibited leaves turns out to depend, at least in part, on auxin signaling. That auxin signaling controls vein formation has long been known. Indeed, in auxin-signaling-inhibited leaves, fewer veins form, and veins are often incompletely differentiated; yet in those veins, vascular cells are still elongated along the vein and connected at their ends (Fig. 1.4D,H) (Alonso-Peral et al., 2006; Candela et al., 1999; Esteve-Bruna et al., 2013; Hardtke and Berleth, 1998; Mazur et al., 2020; Przemeck et al., 1996; Strader et al., 2008; Verna et al., 2019). Instead, inhibition of auxin signaling, either because of growth in the presence of auxin signaling inhibitors or because of mutation in auxin receptors or

their regulators, leads to entirely new vein defects in auxin-transport-inhibited leaves (Fig. 1.4E,I) (Ravichandran et al., 2020; Verna et al., 2019).

In the leaves of plants in which both auxin transport and signaling are inhibited, the end-to-end alignment of vascular cells oriented along the vein is replaced by the formation of clusters of randomly oriented vascular cells (Fig. 1.4I) (Verna et al., 2019) (Chapter 3). But how would auxin signaling, which takes place in the nucleus and is thus inherently non-polar (for review, see (Leyser, 2018)), would control the polar propagation of the auxin signal in the absence of polar auxin transport?

One possibility is that auxin signaling promotes auxin movement by passive diffusion, whose direction is determined by gradients generated by localized auxin production and consumption. However, auxin signaling promotes the acidification of the cell wall and consequent increase in cytoplasmic pH (Fendrych et al., 2016). Because IAA is already mostly negatively charged at the neutral pH of the cytoplasm (Raven, 1975; Rubery and Sheldrake, 1974; Runions et al., 2014), an even higher cytoplasmic pH would further decrease the proportion of intracellular auxin that is uncharged and that can thus diffuse out of the cell. As such, it is difficult to conceive how auxin signaling could promote auxin movement by passive diffusion.

Alternatively, auxin signaling could promote auxin movement by facilitated diffusion — for example, through the plasmodesmata intercellular channels — whose direction would still be determined by auxin gradients. Auxin movement through plasmodesmata had been hypothesized by Graeme Mitchison (Mitchison, 1980b) and has recently received some experimental support (Han et al., 2014). There is also evidence that the size of plasmodesmata aperture is controlled by auxin signaling (Han et al., 2014; Sager et al., 2020), so it is possible to conceive how auxin movement through plasmodesmata could positively feedback on itself. Moreover, it is possible to imagine how auxin could be drained away from flanking cells — for example, if auxin movement through plasmodesmata in transverse walls reduced movement

through plasmodesmata in lateral walls, by reducing either their number or their aperture. However, there is currently no evidence of such a mechanism or that plasmodesmata number or aperture controls vein patterning.

Finally, auxin may not be the mobile signal in *pin* sextuple mutants, but auxin may be activating one. However, in order to be consistent with all the evidence discussed above, the production, propagation, and perception of this hypothetical mobile signal would have to be distinct from, but functionally redundant with, auxin transport; at least the production of the signal would have to depend on auxin signaling; the signal would have to propagate along the apical-basal axis of the leaf; and perception of the signal would have to lead to vein formation. A signal with all these properties has yet to be identified; therefore, the existence of such a signal — whether of physical or chemical nature — remains speculative.

1.6 AUXIN, COORDINATION OF CELL POLARITY, AND THE FORMATION OF CONTINUOUS VASCULAR STRANDS

If vascular strand formation depended on the cell-to-cell transport of an auxin-dependent signal, vascular strands would always be "continuous" (i.e. they would connect to other vascular strands at least at one of their two ends). Yet vascular strands that fail to satisfy this requirement — vascular "fragments" — have been observed in leaves of wild types and mutants (e.g., (Berleth and Jurgens, 1993; Carland et al., 1999; Deyholos et al., 2000; Herbst, 1971; Koizumi et al., 2000; Lersten, 1965; Pray, 1955; Sawa et al., 2005; Scarpella, 2017; Steynen and Schultz, 2003)). Such vascular fragments are of two types.

Vascular fragments of the first type, including those observed in auxin signaling mutants, are composed of files of mature vascular cells that are connected by files of immature vascular cells (Fig. 1.5A) (Hardtke and Berleth, 1998; Herbst, 1972; Lersten, 1965; Mähönen et al., 2006; Pray, 1955; Przemeck et al., 1996; Ruiz Sola et al., 2017; Scacchi et al., 2010; Truernit et al., 2012). Because the identification of immature vascular cells can be problematic (Esau, 1943),
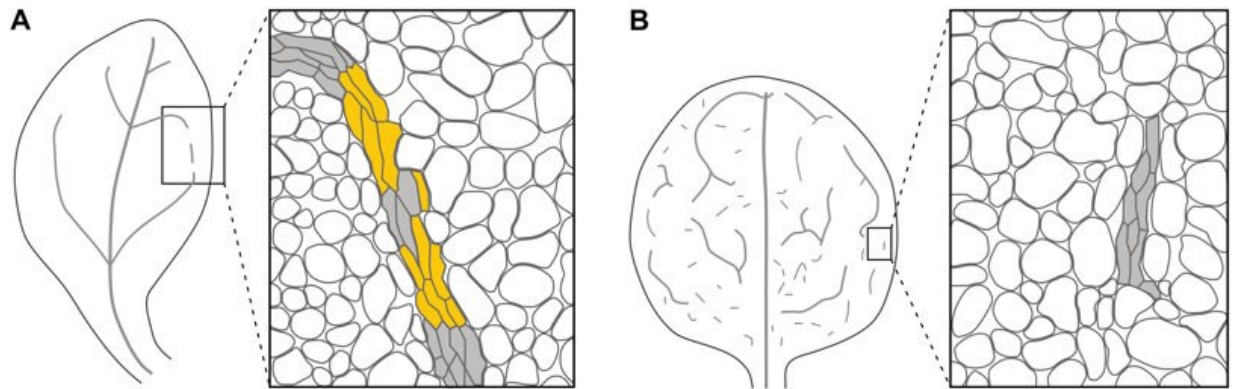
Figure 1.5. Formation of Discontinuous Veins

(A) Vein fragments of the first type are composed of files of mature vascular cells (gray fill) that are connected by files of immature vascular cells (yellow fill). (B) Vein fragments of the second type are composed of files of vascular cells (gray fill) that are separated by nonvascular cells (white fill). Vein fragments of this type originate from continuous PEDs within which some cells terminate PIN1 expression and differentiate into nonvascular cells.

vascular strands of this type have often been interpreted as fragmented when they are instead incompletely differentiated.

Vascular fragments of the second type are composed of files of vascular cells that are separated by nonvascular cells (Fig. 1.5B) (Carland et al., 1999; Deyholos et al., 2000; Herbst, 1972; Koizumi et al., 2000; Scarpella, 2017). Vascular fragments of this type originate from continuous PEDs within which some cells terminate PIN1 expression and differentiate into nonvascular cells (Naramoto et al., 2009; Scarpella et al., 2006). Therefore, both types of vascular fragments are continuous, at least at formative stages, and thus compatible with a vein formation mechanism that depends on the cell-to-cell transport of an auxin-dependent signal.

Vascular fragments of the first type have been observed in the leaf and the seedling cylinder (Herbst, 1972; Lersten, 1965; Mähönen et al., 2006; Marhava et al., 2018; Pray, 1955; Przemeck et al., 1996; Rodriguez-Villalon et al., 2014; Rodriguez-Villalon et al., 2015; Ruiz Sola et al., 2017; Scacchi et al., 2010; Truernit et al., 2012). However, no vascular fragments of the second type have ever been observed in the seedling cylinder, even in those mutants with such vascular fragments in their leaves. This observation suggests that the function of the genes that control the formation of continuous veins in the leaf is not required for the continuity of the vascular strand in the seedling cylinder. But how could that be?

PIN1 localization is already polarized in the first vascular cells that form in the globular embryo (Steinmann et al., 1999). These first vascular cells are stem cells, and as such they continually divide into cells with unequal fates: one cell will maintain the stem cell population; the other will extend the vascular strand in the cylinder of the embryo during embryogenesis and of the seedling root upon gemination (Aida et al., 2004; Scheres et al., 1994; van den Berg et al., 1997; Yoshida et al., 2014). Unlike in the embryo, in the leaf PIN1 localization is initially non-polar, and PIN1-expressing cells do not behave like vascular stem cells. In developing leaves of both wild-type and mutants with vascular fragments of the second type, PEDs are initially continuous. In wild-type, over time PIN1 localization becomes polarized (Marcos and Berleth,

2014; Scarpella et al., 2006; Wenzel et al., 2007). By contrast, in mutants with vascular fragments of the second type PIN1 expression is terminated in some of the cells in a PED before PIN1 localization becomes polarized in any of the cells in the domain (Naramoto et al., 2009; Scarpella et al., 2006; Verna et al., 2019). Therefore, it is possible that the function of the genes that control the formation of continuous veins in the leaf is required for the polarization of PIN1 localization, and that it is the lack of such polarization that leads to PED fragmentation. If so, the function of the genes that control the continuity of the veins in the leaf would not be required during the extension of the vascular strand in the embryo and seedling cylinder because polar PIN1 localization would only need to be maintained and propagated during such extension and not established anew as in leaf vein formation. In support of this interpretation, available evidence suggests that distinct mechanisms control the polarization of PIN1 localization and the maintenance of such polar localization (Kleine-Vehn et al., 2011).

1.7 AUXIN, COORDINATION OF CELL POLARITY, AND VASCULAR NETWORK FORMATION

1.7.1 Leaf Vein Networks

Just like a seedling can be seen as a vascularized cylinder, early, leafless plants can be seen as two systems of branched vascularized cylinders: one above ground and one below ground (Fig. 1.6A) (Fairon-Demaret and Li, 1993). And even flat organs such as leaves can be seen, at least at early stages of their development, as vascularized cylinders (Kang and Dengler, 2004; Mattsson et al., 1999; Scarpella et al., 2004). However, during their development, flat-organ primordia soon lose their cylindrical shape by expanding laterally to acquire their distinctive flattened shape, a process that coincides with the formation of branched systems of veins that largely mirror the shape of the leaf (Ash et al., 1999; Dengler and Kang, 2001; von Ettinghausen, 1861). These vein networks are said to be "open" if all the veins connect to other veins at only one end
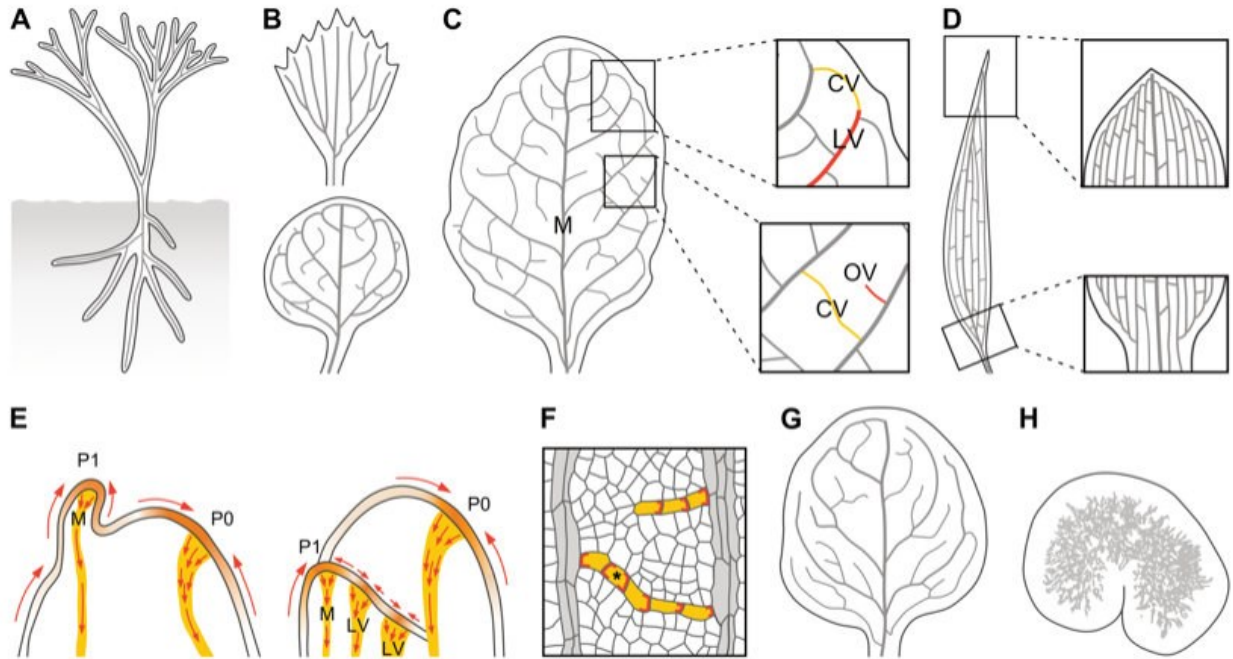
Figure 1.6. Auxin, Coordination of Cell Polarity, and Vein Network Formation

(A) Early, leafless plants are systems of branched cylinders with a vascular strand (gray line) in their center. (B) Leaves of extant plants have "open" (*top*) or "closed" (*bottom*) vein networks. (C) In rounded leaves, lateral veins (LVs) branch from a single midvein (M); minor veins branch from M and LVs, and either end freely ("open" veins [OVs]; red) or connect to other veins ("closed" veins [CVs]; yellow); and vein loops form from the fusion of LVs (red) and closed minor veins (yellow) (E). (D) In elongated leaves, vein loops are compressed laterally and stretched along the leaf, such that M and LVs seem to run parallel to one another; and M and LVs are connected laterally by minor veins. (E) In epidermal cells at the shoot tip of plants with either rounded (*left*) or elongated (*right*) leaves, PIN1 localization becomes polarized (red arrows) toward sites of leaf primordium formation (orange). These epidermal convergence points of PIN1 polarity are associated with broad PEDs in the inner tissue that become restricted to sites of M formation (yellow). Over time, PIN1 localization becomes polarized (red arrows) in the cells of these broad domains. In the cells along the PEDs' midline, PIN1 localization becomes

polarized toward pre-existing veins; in the cells flanking PEDs' midline, PIN1 localization becomes polarized toward the domains' midline. Both the restriction of broad PEDs and the polarization of PIN1 localization initiate and proceed away from pre-existing veins, in which PIN1 localization is polarized. P0 and P1 are successive stages of leaf primordium development. (F) The localization of PIN1 (red) in files of vascular cells (yellow) is polarized toward pre-existing veins (gray; for simplicity, PIN1 expression in pre-existing veins is not shown). In OVs, a single PIN1 localization polarity exists; in CVs, the two opposite PIN1 localization polarities are connected by a bipolar cell (asterisk): a cell with PIN1 at both ends. (G,H) Progressive reduction in the ability to polarize PIN1 localization during vein network formation leads to mutant vein networks with very few CVs (G); mutant vein networks in which vein fragments form along paths defined by initially continuous PEDs (Fig. 1.5B); or clusters of randomly oriented vascular cells, as in *gn* mutant leaves (H).

or "closed" if at least some veins connect to other veins at both ends (Fig. 1.6B) (Roth-Nebelsick et al., 2001; Verna et al., 2015).

In rounded leaves like those of Arabidopsis, lateral veins branch from a central midvein and connect to distal veins to form vein loops; minor veins branch from midvein and loops, and either end freely or connect to other veins to form a mesh; and loops and minor veins bend near the leaf edge to give the vein network a scalloped outline (Fig. 1.6C) (Gifford and Foster, 1989; Nelson and Dengler, 1997; Troll, 1937). In elongated leaves of grasses like maize, vein loops are compressed laterally and stretched along the leaf, such that midvein and lateral veins seem to run parallel to one another (Fig. 1.6D) (Gifford and Foster, 1989; Linh et al., 2018; Nelson and Dengler, 1997; Troll, 1937).

1.7.2 Auxin, Coordination of Cell Polarity, and the Formation of Open Vein Networks

In both rounded and elongated leaves, localization of PIN1 proteins at the plasma membrane of epidermal cells at the shoot tip becomes polarized toward sites of leaf primordium formation (Fig. 1.6E) (Bayer et al., 2009; Benkova et al., 2003; Carraro et al., 2006; Johnston et al., 2015; Lee et al., 2009; Reinhardt et al., 2003; Scarpella et al., 2006). The resulting epidermal "convergence points" of PIN1 polarity are associated with the appearance of broad PEDs in the inner tissue that will become restricted to sites of midvein formation. Likewise, epidermal convergence points of PIN1 polarity at the leaf edge are associated with both sites of leaf lateral growth and positions of broad PEDs in the inner tissue that become restricted to sites of lateral vein formation (Fig. 1.4A) (Hay et al., 2006; Scarpella et al., 2006; Wenzel et al., 2007). Both auxin transport inhibition or higher auxin levels reduces the distance between successive epidermal convergence points of PIN1 polarity and leaf primordia and between midvein and lateral veins (Bennett et al., 1995; Guenot et al., 2012; Mattsson et al., 1999; Okada et al., 1991; Reinhardt et al., 2000; Sawchuk et al., 2013; Scarpella et al., 2006; Sieburth, 1999; Verna et al.,

2019). These observations seem to suggest that a single mechanism controls positioning of leaf primordia at the shoot apex and of midvein and lateral veins in the leaf. This mechanism seems to depend on the positioning of epidermal convergence points of PIN1 polarity, which in turn seems to depend on auxin levels and transport, and is consistent with the hypothesis that broad leaves evolved from branched systems of cylindrical organs with a vein in their center (Alvarez et al., 2016; Beerling and Fleming, 2007). However, the relation between convergence points of epidermal PIN1 polarity and positioning of midvein and lateral veins seems to be correlative, rather than causal. Indeed, mutants that lack such convergence points form normal vein networks (Bilsborough et al., 2011), and epidermal expression of PIN1 is neither required nor sufficient for auxin-transport-dependent vein positioning (Govindaraju et al., 2020). These observations suggest that the mechanism that controls the positioning of midvein and lateral veins, and possibly of leaf primordia at the shoot apex, depends on auxin levels and transport but is independent of epidermal convergence points of PIN1 polarity.

1.7.3 Auxin, Coordination of Cell Polarity, and the Formation of Closed Vein Networks

Unlike the broad PEDs that become restricted to sites of formation of midvein and lateral veins, those that become restricted to sites of minor vein formation in rounded leaves are not associated with epidermal convergence points of PIN1 polarity; instead, the broad PEDs that become restricted to sites of minor vein formation branch from pre-existing veins (Fig. 1.4A) (Marcos and Berleth, 2014; Scarpella et al., 2006; Wenzel et al., 2007). Nevertheless, in all broad inner PEDs PIN1 is initially localized isotropically, or nearly so, to the plasma membrane of the cells in broad inner domains (Carraro et al., 2006; Johnston et al., 2015; Lee et al., 2008; Marcos and Berleth, 2014; Scarpella et al., 2006; Wenzel et al., 2007) (Fig. 1.4A; Fig. 1.6E). Over time, PIN1 localization becomes polarized: toward pre-existing PEDs, in the cells along the broad domains' midline; and toward the broad domains' midline, in the cells flanking it.

Furthermore, over time broad PEDs narrow to sites of vein formation. Both the narrowing of broad PEDs and the polarization of PIN1 localization initiate and proceed away from pre-existing PEDs and are delayed by auxin transport inhibition. Inhibition of polar auxin transport or higher auxin levels, occurring naturally at leaf margin outgrowths or induced experimentally by local direct auxin application, lead to the formation of broader inner PEDs (Aloni et al., 2003; Hay et al., 2006; Mattsson et al., 2003; Scarpella et al., 2006; Wenzel et al., 2007). Nevertheless, even these broader PEDs eventually narrow to sites of vein position, and also this narrowing is delayed by auxin transport inhibition.

Initially, the broad PEDs that become restricted to sites of minor vein formation connect to pre-existing veins at only one of their two ends ("open" PEDs), but they can extend to connect to other veins at both their ends ("closed" PEDs) (Fig. 1.4A) (Marcos and Berleth, 2014; Scarpella et al., 2006; Wenzel et al., 2007). The formation of such closed PEDs is promoted by auxin transport inhibition (Mattsson et al., 1999; Sieburth, 1999; Verna et al., 2015). Because auxin transport inhibition delays restriction of broad PEDs and polarization of PIN1 localization, only PEDs that have yet to differentiate into highly efficient auxin transport paths can connect to pre-existing veins at both ends.

But not all broad PEDs become restricted and polarized; some gradually disappear (Fig. 1.4A) (Marcos and Berleth, 2014), suggesting that PEDs compete for a limiting amount of auxin (Sachs, 2003). As such, how many PEDs will form at any given stage of leaf tissue development, where exactly they will form, how broad they will be, what shape they will have, and which ones will become restricted and polarized and which ones will instead gradually disappear will not only depend on positive feedback between polarization of PIN1 localization and polar auxin transport but on random variations in the local production of auxin and on the number, shape, size, position, and polarization of pre-existing PEDs. Therefore, the formation of new PEDs continuously builds upon that of previous ones.

Within narrow PEDs — whether open or closed — PIN1 localization is polarized toward pre-existing veins (Marcos and Berleth, 2014; Scarpella et al., 2006; Wenzel et al., 2007). Therefore, open PEDs have a single PIN1 localization polarity (Fig. 1.6F). By contrast, closed PEDs are composed of two segments, each with a single PIN1 localization polarity, opposite to that of the other (Fig. 1.6F). The two opposite polarities are coordinated by a "bipolar" cell, a cell in which PIN1 localization is polarized at both ends (Fig. 1.6F).

In rounded leaves, each loop forms from the fusion of a lateral-vein-associated PED and a minor-vein-associated closed PED (Fig. 1.4A) (Scarpella et al. 2006; Wenzel et al. 2007). Whether in elongated leaves PIN1 is expressed and localized during the formation of minor veins and loops as it is in rounded leaves is currently unknown; however, computational simulations suggest that the same vein-formation mechanism embedded in different leaf growth patterns can account for the different vein networks of elongated and rounded leaves (Fujita and Mochizuki, 2006a; Runions et al., 2005).

Therefore, available evidence suggests that like vascular strand formation in response to auxin application and vein formation during normal leaf development, vein network formation is an expression of auxin transport and coordination of cell polarity, many aspects of which are consistent with the auxin canalization hypothesis (Abley et al., 2016; Alim and Frey, 2010; Bayer et al., 2009; Cieslak et al., 2015; Feugier and Iwasa, 2006; Feugier et al., 2005; Fujita and Mochizuki, 2006b; Lee et al., 2014; Mitchison, 1980b; Mitchison, 1981; Rolland-Lagan and Prusinkiewicz, 2005; Sachs, 1991; Sachs, 2000; Smith and Bayer, 2009; Stoma et al., 2008; Wabnik et al., 2010; Walker et al., 2013).

Nevertheless, the auxin canalization hypothesis predicts the formation of networks of "open" veins (i.e. veins that connect to veins at only one of their two ends) (Mitchison, 1980b; Mitchison, 1981; Rolland-Lagan and Prusinkiewicz, 2005; Sachs, 1975). The formation of "closed" veins (i.e. veins that connect to other veins at both their ends) has thus been proposed to result from the diffusion of a hypothetical substance from pre-existing veins that allows

approaching veins to connect to pre-existing veins (Feugier and Iwasa, 2006). This hypothesis predicts that in closed PEDs, PIN1 will be polarized away from the pre-existing veins to which the closed PEDs connect, when in fact in closed PEDs, PIN1 is polarized toward the pre-existing veins to which the closed PEDs connect (Fig. 1.6F) (Marcos and Berleth, 2014; Scarpella et al., 2006; Wenzel et al., 2007). Therefore, this hypothesis seems to be unsupported by experimental evidence.

Alternatively, closed veins could form from veins meeting at points of peak auxin levels (Dimitrov and Zucker, 2006) or from localized auxin production at precisely defined times and places (Aloni et al., 2003; Mitchison, 1980b; Rolland-Lagan and Prusinkiewicz, 2005; Runions et al., 2005; Sachs, 1975; Sachs, 1989). Both hypotheses are consistent with the observation of bipolar cells and predict peak auxin levels in these cells; however, this prediction remains to be tested experimentally.

The formation of bipolar cells seems to be very sensitive to even the partial loss-of-function of the auxin-signaling- and auxin-transport-dependent pathway that controls the formation of continuous veins: mutants partially lacking the function of this pathway, such as mutants in *FORKED1/VASCULAR-NETWORK3-BINDING PROTEIN*, often fail to form bipolar cells and thus to polarize PIN1 localization along closed PEDs (Hou et al., 2010; Naramoto et al., 2009; Steynen and Schultz, 2003). This reduced ability to coordinate cell polarity along closed PEDs often leads to their "opening" and thus to vein networks with very few closed veins (Fig. 1.6G) (Naramoto et al., 2009; Steynen and Schultz, 2003). Nevertheless, these mutants are still able to coordinate cell polarity along open PEDs, which have a single polarity (Hou et al., 2010; Naramoto et al., 2009).

More severe loss-of-function of the pathway that controls the formation of continuous veins, such as in the *vascular network3/scarface* single mutant or in the *cotyledon vascular pattern2* (*cvp2*) ; *cvp2-like1* double mutant, leads to the inability to polarize PIN1 localization even along open PEDs (Carland and Nelson, 2004; Carland and Nelson, 2009; Carland et al.,

1999; Deyholos et al., 2000; Koizumi et al., 2000; Koizumi et al., 2005; Naramoto et al., 2009; Scarpella et al., 2006; Sieburth et al., 2006; Willemsen et al., 2003). The inability of these mutants to coordinate cell polarity along PEDs leads to termination of PIN1 expression in some of the cells in a PED before any of the cells in the domain become coordinately polarized (Naramoto et al., 2009; Scarpella et al., 2006). The cells that terminate PIN1 expression differentiate into nonvascular cells, while the remaining PED fragments differentiate into vascular fragments of the second type (Fig. 1.5B) (Carland and Nelson, 2004; Carland and Nelson, 2009; Carland et al., 1999; Deyholos et al., 2000; Koizumi et al., 2000; Koizumi et al., 2005; Naramoto et al., 2009; Scarpella et al., 2006; Sieburth et al., 2006; Tan et al., 2020; Willemsen et al., 2003; Xiao and Offringa, 2020). Nevertheless, these vascular fragments still form along the paths where continuous veins would form in wild type, a vestige of fragments that were once connected.

Defects in vein network formation are most severe in *gn* mutants. In *gn* cotyledons and leaves, individual cells can still localize PIN1 polarly — though to a lesser extent — but they seem to have almost entirely lost the ability to coordinate between them the polarity of PIN1 localization (Steinmann et al., 1999; Verna et al., 2019) (Chapter 3). The result of this inability is the formation of clusters of randomly oriented vascular cells (Fig. 1.6H) (Amalraj et al., 2020; Geldner et al., 2004; Mayer et al., 1993; Steinmann et al., 1999; Verna et al., 2019) (Chapters 4 and 5).

Based on their biochemical function and cellular localization, proteins in the pathway that controls the formation of continuous veins have been proposed to localize PIN1 to or retain it in the plasma membrane, polarize PIN1 localization, or maintain such polar localization (e.g., (Carland and Nelson, 2009; Geldner et al., 2004; Kleine-Vehn et al., 2008; Koizumi et al., 2005; Naramoto et al., 2009; Naramoto et al., 2010; Prabhakaran Mariyamma et al., 2018; Sieburth et al., 2006). However, the function of these proteins seems to entail more than the control of auxin transport and to include at least the control of auxin signaling. Indeed, defects in mutants

in the pathway that controls the formation of continuous veins cannot be phenocopied by mutation in *PIN* genes or growth in the presence of auxin transport inhibitors; instead, those defects are reproduced in plants in which both auxin transport and signaling are compromised (Verna et al., 2019) (Chapter 3). Though it is currently unclear how proteins in the pathway that control the formation of continuous veins control auxin signaling, the most parsimonious account is that such proteins control the polar localization of proteins with vein formation functions that are produced in response to auxin signaling.

1.8 CONCLUDING REMARKS

The past 20 years have witnessed unprecedented advances in our understanding of the role of auxin in the patterned formation of the vascular system; however, the very same research that has led to such advancement has also exposed unexpected gaps in our current knowledge. For example, a role for auxin signaling in vein positioning had been unsuspected because the fewer and incompletely differentiated veins of auxin signaling mutants still form in the same positions as they would in wild-type. It now turns out that functions of auxin signaling in vein positioning had been obscured by nonhomologous redundancy with auxin transport. Furthermore, it also turns out that auxin signaling and auxin transport had been eclipsing each other's functions in the end-to-end alignment of vascular cells oriented along the vein. However, how precisely auxin transport and signaling control all those processes remains unclear. These and other questions will have to be addressed in future research, and as past research has taught us, even more surprises are awaiting ahead.

1.9 SCOPE AND OUTLINE OF THE THESIS

The evidence discussed above suggests that auxin controls coordination of cell polarity and the formation of veins that derives from such coordination. How auxin coordinates cell polarity to

induce vein formation is poorly understood, and the goal of my Ph.D. thesis is to address that limitation.

For nearly 25 years the GN guanine-nucleotide exchange factor for ADP-ribosylation-factor GTPases has been thought to coordinate the cellular localization of PIN1 and possibly other PIN proteins; the resulting cell-to-cell, polar transport of auxin would propagate cell polarity across tissues and control developmental processes such as vein formation (reviewed above and, for example, in (Berleth et al., 2000; Lavania et al., 2021; Linh et al., 2018; Nakamura et al., 2012; Ravichandran et al., 2020; Richter et al., 2010)). In Chapter 3 — most of which was published in (Verna et al., 2019) — I test that hypothesis by a combination of molecular genetics, chemical interference, and cellular imaging, whose protocols I detail in Chapter 2 (Linh and Scarpella, 2022a) and use throughout my thesis.

Contrary to predictions of the hypothesis, in Chapter 3 — and in (Verna et al., 2019) — I find that auxin-induced vein formation occurs in the absence of polar auxin transport, that the residual auxin-transport-independent vein-patterning activity relies on auxin signaling, and that a *GN*-dependent cell polarizing signal acts upstream of both auxin signaling and polar auxin transport in vein patterning. However, interference with both auxin signaling and polar auxin transport only phenocopies intermediate *gn* mutants, suggesting that additional *GN*-dependent pathways are involved in vein patterning. Because experimental evidence suggests that auxin can move through plasmodesmata (recently reviewed in (Band, 2021; Paterlini, 2020)), in Chapter 5 I ask whether movement of auxin or an auxin-dependent signal through plasmodesmata is one of the missing *GN*-dependent vein-patterning pathways. To image plasmodesma permeability, I leverage the ability of a cytoplasmic, untargeted YFP to diffuse through plasmodesmata whose aperture is greater than the size of YFP. To transactivate YFP expression and to image vascular systems in the different genetic backgrounds and upon the different chemical treatments in Chapter 5, I use a vascular GAL4/GFP line I contribute to characterize in Chapter 4 — which was published as (Amalraj et al., 2020) (Chapter 4).

Chapter 5 shows that simultaneous interference with auxin signaling, polar auxin transport, and movement of an auxin signal through plasmodesmata recapitulates vein patterning defects of strong *gn* mutants. Therefore, my results suggest that veins are patterned by the coordinated action of three *GN*-dependent pathways: auxin signaling, polar auxin transport, and movement of auxin or an auxin-dependent signal through plasmodesmata. However, it was still unknown whether — and if so, where and when in leaf development — *GN* controls the production, the movement, or the interpretation of an auxin signal with vein patterning function. In Chapter 6, I address that question by determining GN expression in leaf development, by restricting that expression to specific tissues in a strong *gn* mutant, and by analyzing the effects of such tissue-specific *GN* expression on vein patterning. To restrict *GN* expression to specific tissues I use a GAL4/*UAS* transactivation approach and tissue-specific GAL4:VP16 drivers I contribute to characterize in Chapter 4 — which was published as (Amalraj et al., 2020) (Chapter 4).

Chapter 6 shows that GN is expressed in all the cells of the leaf throughout leaf development, though expression is stronger where new veins are forming. Furthermore, my results suggest that *GN* controls the production, propagation, or interpretation of a vein patterning signal in the leaf inner tissues. For that function, *GN* expression is required in all the inner tissues of the leaf throughout leaf development, but stronger *GN* expression seems to be required where new veins are forming. By contrast, if a signal with vein patterning function is produced in the leaf epidermis, my results suggest that the production of such a signal is independent of *GN*.

Like GN expression (Chapter 6), plasmodesma permeability is high in all the cells at early stages of leaf tissue development (Chapter 5). Over time, the permeability of plasmodesmata between newly formed veins and surrounding nonvascular tissues lowers but that of plasmodesmata between vein cells remains high. Interference with regulation of plasmodesma aperture and derived permeability leads to vein patterning defects, suggesting

that the changes in plasmodesma permeability that occur during leaf development are relevant for vein patterning. However, it was still unclear whether for vein patterning high plasmodesma permeability is required in all or only some of the tissues of the developing leaf. In Chapter 7, I address that question by reducing plasmodesma aperture and derived permeability in specific tissues and by analyzing the effects of such tissue-specific reduction of plasmodesma aperture on vein patterning. To reduce plasmodesma aperture in specific tissues I use a GAL4/*UAS* transactivation approach and tissue-specific GAL4:VP16 drivers I contribute to characterize in Chapter 4 — which was published as (Amalraj et al., 2020) (Chapter 4).

Chapter 7 shows that for vein patterning wide plasmodesma aperture is required in newly formed veins and in all the inner cells in areas of the leaf where new veins are forming. By contrast, for vein patterning wide plasmodesma aperture is dispensable in the epidermis and in the nonvascular inner tissue surrounding newly formed veins. Furthermore, my results suggest that the epidermis is a sink for signals that are produced in inner cells and move there through plasmodesmata to promote vein formation. Therefore, available evidence (Govindaraju et al., 2020; Krishna et al., 2021) and my results in Chapter 7 together suggest that — contrary to widespread belief (reviewed above and, for example, in (Bennett et al., 2014; Cieslak et al., 2021; Lavania et al., 2021; Linh et al., 2018; Prusinkiewicz and Runions, 2012; Runions et al., 2014)) — the epidermis is not a source of auxin signals that diffuse or are transported into the inner tissues to induce vein formation. In Chapter 8, I therefore propose and discuss the hypothesis that auxin is not produced in the epidermis, or its production in the epidermis is inconsequential for vein patterning, and that it's instead auxin production in the inner tissues that's relevant for vein patterning.

Chapter 2: Confocal Imaging of Developing Leaves[1]

2.1 INTRODUCTION

Historically, advances in developmental biology methods have fueled progress in other fields, from the discovery of new reporters to that of new drugs (e.g., (Chalfie et al., 1994; Peterson et al., 2000)). Such advances have often stemmed from the developmental biologists' need to visualize cell states that cannot be recognized by overt changes in cell shape or size. To satisfy that need, for the past 25 years developmental biologists have been fusing promoters and genes to fluorescent proteins to visualize gene activation and protein expression.

In contrast to the study of animal development, the study of plant development is simplified by the inability of plant cells to move. But precisely because plant cells are unable to move, the study of how plants develop has revealed unsuspected mechanisms of multicellular organism development (reviewed in (Willemsen and Scheres, 2004)). In particular, leaves offer several advantages to plant developmental biologists: (1) in many plants, leaves form post-germination, providing the opportunity to perturb leaf development systemically by adding drugs directly to the growth medium on which seeds are sown (e.g., (Mattsson et al., 1999; Sieburth, 1999)); (2) most leaves form externally, providing the opportunity to perturb leaf development locally by applying drugs directly to the developing leaves (e.g., (Sawchuk et al., 2007)); (3) cells and tissues differentiate anew in each leaf that forms and several leaves form on each plant, providing multiple opportunities for visualization and perturbation of leaf development (e.g., (Scarpella et al., 2006)). In spite of all these advantages, a detailed procedure for the perturbation, dissection, mounting, and imaging of developing leaves has not been described.

---

[1] Adapted from Linh, N. M. and Scarpella, E. (2022). Confocal Imaging of Developing Leaves. Curr Protoc 2, e349.

Here we address this limitation by providing a procedure for the imaging of leaves and leaf primordia by confocal microscopy. We first describe protocols to prepare plant growth medium and growth medium plates (Support Protocols 1 and 2). We next provide a protocol to sterilize, sow, and germinate seeds of transgenic lines expressing fluorescent proteins in their developing leaves, and to grow the derived seedlings on growth medium plates (Basic Protocol 1). We further provide protocols to prepare and locally apply to developing leaves a lanolin paste containing the plant hormone auxin (Support Protocol 3 and Basic Protocol 2), which is known to induce vein formation (Sachs, 1989). We then provide protocols to dissect and mount leaves and leaf primordia at relevant stages of leaf development (Basic Protocols 3–5 and Support Protocol 4). And finally, we provide practical guidelines to image mounted leaves and leaf primordia by confocal microscopy (Basic Protocol 6). We describe the methods for the first leaves of Arabidopsis, but the protocols can be easily adapted to other leaves of Arabidopsis or to leaves of other plants. The protocols described here require basic wet laboratory skills — including the use of autoclaves — knowledge of how to work aseptically in laminar flow cabinets, and basic training in confocal and fluorescence microscopy.

2.2 STRATEGIC PLANNING

Confocal time is expensive; the limiting step to acquiring informative confocal images is the quality of sample dissection and mounting; and dissecting and mounting first leaves and leaf primordia 6-, 4-, 2-, 1-, and 3-days-after-germination (DAG) is progressively more difficult. Therefore, we recommend that users start by dissecting (Basic Protocols 3 and 4) and mounting (Basic Protocol 5) 6-DAG leaves; proceed to assess the quality of their skills in dissecting and mounting of 6-DAG leaves by fluorescence microscopy (Support Protocol 4); and only when those skills are of sufficient quality, end by dissecting and mounting 6-DAG leaves and optimizing their imaging by confocal microscopy (Basic Protocol 6). Only when users have become proficient at dissecting, mounting, and confocal imaging of 6-DAG leaves, do we advise

them to repeat the sequence with leaves and leaf primordia at progressively more difficult stages of development (Fig. 2.1).

2.3 SUPPORT PROTOCOL 1

2.3.1 Support Protocol Title

Preparation of plant growth medium

2.3.2 Introductory Paragraph

Here we describe how to prepare plant growth medium for growth medium plates (whose preparation is described in Support Protocol 2) on which sterilized Arabidopsis seeds will be sown, sown seeds will germinate, and derived seedlings will grow (described in Basic Protocol 1). The protocol described here requires basic wet laboratory skills, including the use of autoclaves.

2.3.3 Materials

Demineralized water

Sucrose, ≥99% (e.g., BioShop Canada, cat. no. SUC600, cas no. 57-50-1)

Murashige & Skoog (MS) Basal Salts (e.g., Caisson Labs, cat. no. MSP01)

2-(N-Morpholino)Ethanesulfonic Acid (MES), Free Acid, Monohydrate, ≥99.5% (e.g., BioShop Canada, cat. no. MES503, cas no. 145224-94-8)

0.5 M KOH (see recipe in Reagents and Solutions)

Agar, Bacteriological Grade (e.g., BioShop Canada, cat. no. AGR001, cas no. 9002-18-0)

4-l beaker (e.g., Nalgene, cat. no. 12014000)

Magnetic stirrer (e.g., Fisherbrand, cat. no. S192925)

Magnetic stir bar (e.g., Fisherbrand, cat. no. 800371119)

Spatula (e.g., Eisco, cat. no. CH0635A)
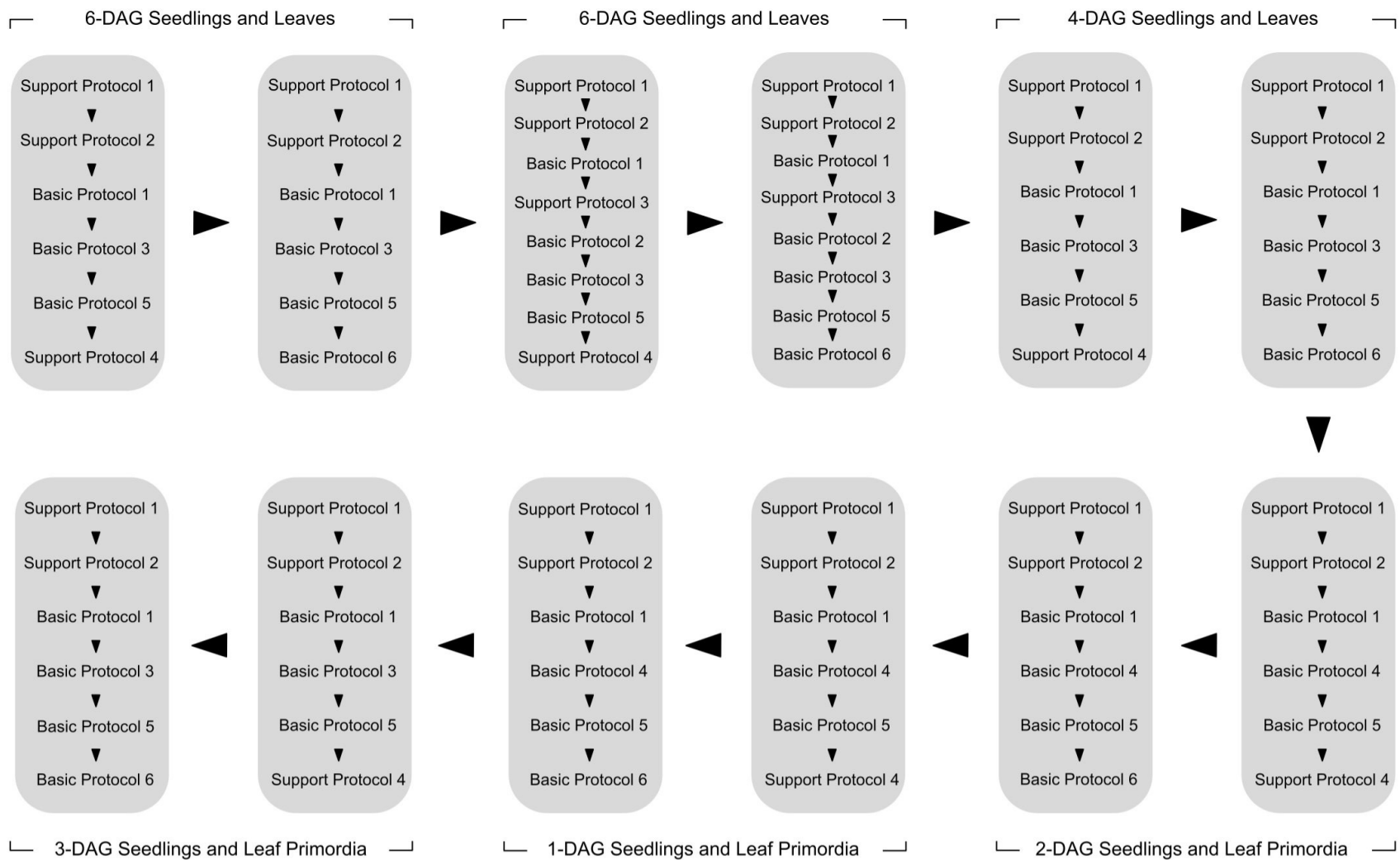
Figure 2.1: Order of Protocol Sequences

Suggested order of protocol sequences to become progressively more proficient in the methods.

Weighing dishes (e.g., Fisherbrand, cat. no. 02202102)

pH meter (e.g., Fisherbrand, cat. no. ORI13636AB150)

2-l graduated cylinder (e.g., Fisherbrand, cat. no. 08550J)

500-ml graduate cylinder (e.g., Fisherbrand, cat. no. 08550G)

500-ml bottles (e.g., Pyrex, cat. no. C1395500)

Autoclave (e.g., Steris Amsco Century SI-120 steam sterilizer or similar equipment)

Heat-resistant gloves (e.g., SP Bel-Art, cat. no. H13201-0000)

2.3.4 Protocol Steps with *Steps Annotations*

(1) To prepare 2 l of plant growth medium, add 1.5 l of demineralized water in a 4-l beaker. Place the beaker with water on a magnetic stirrer. Add a magnetic stir bar to the water in the beaker. Turn on the stirrer on low-to-medium stirring settings. Do not switch on heating on the stirrer.

MilliQ water is unnecessary.

(2) Weigh 30 g of sucrose and slowly add it to the stirring water.

Omitting sugar will delay seed germination and seedling growth by ~1 day. Furthermore, rate of seedling growth will vary more greatly and synchronization of seedling growth will be completely lost >5 days after germination (DAG; defined in Basic Protocol 1, step 10) on medium without sucrose. Increasing the concentration of sucrose from 1.5% to 2–3% will lengthen the lag phase when seedlings are transferred from growth medium to soil.

(3) Weigh 4.3 g of MS Basal Salts and slowly add it to the stirring sucrose solution once the sucrose has completely dissolved.

(4) Weigh 1 g of MES and slowly add it to the stirring sucrose-and-MS-salts solution once the MS salts have completely dissolved.

(5) Once the MES has completely dissolved, adjust the pH to 5.6–5.8 with 0.5 M KOH.

Remember to calibrate the pH meter before measuring the pH of the solution.

(6) Turn off the stirrer, remove the beaker from the stirrer, pour the pHed solution into a 2-l graduated cylinder, and add demineralized water to bring the volume to 2 l. Pour the solution back into the 4-l beaker containing the magnetic stir bar. Place the beaker with the solution back on the magnetic stirrer. Turn on the stirrer on low-to-medium stirring settings. Do not switch on heating on the stirrer. Stir until completely mixed.

(7) Weigh 3.2 g of agar and transfer it to a 500-ml bottle. Repeat four more times for each of the four additional 500-ml bottles.

(8) With a 500-ml graduated cylinder, aliquot 400 ml of solution in each of the five 500-ml bottles. Autoclave (121 °C, 20 min) on the same day. Store indefinitely at room temperature or proceed directly to Support Protocol 2.

Remember to unscrew slightly the bottles' caps before autoclaving. After autoclaving, remember to gently swirl each bottle to mix medium thoroughly and remember not to screw back the bottles' caps too tightly.

2.4 SUPPORT PROTOCOL 2

2.4.1 Support Protocol Title

Preparation of growth medium plates

2.4.2 Introductory Paragraph

Here we describe how to prepare plates of plant growth medium (whose preparation is described in Support Protocol 1) on which sterilized Arabidopsis seeds will be sown, sown seeds will germinate, and derived seedlings will grow (described in Basic Protocol 1). The protocol described here requires basic wet laboratory skills and knowledge of how to work aseptically in laminar flow cabinets.

2.4.3 Materials

Autoclaved growth medium (see Support Protocol 1)

Heat-resistant gloves (e.g., SP Bel-Art, cat. no. H13201-0000)

Laminar flow cabinet (e.g., Forma Laminar Airflow Workstation Class 100 Model 1828 or similar equipment)

Microwave oven (e.g., Kenmore, cat. no. A029066569)

60 °C incubator (e.g., Fisherbrand, cat. no. 51030513)

Water bath (e.g., Thermo Scientific, cat. no. 1523058)

Paper towels (e.g., Kimberly-Clark Professional, cat. no. KC01700)

Petri dishes (e.g., Fisherbrand, cat. no. 431761)

Parafilm (e.g., Bemis, cat. no. ACAPM996)

Refrigerator (e.g., Frigidaire, cat. no. FFRU17B2QW)

2.4.4 Protocol Steps with *Steps Annotations*

(1) If you are planning to pour plates within ~20 min, transfer — wearing heat-resistant gloves — a bottle of freshly autoclaved plant growth medium to a laminar flow cabinet. Alternatively, melt a bottle of previously autoclaved medium in a microwave oven and transfer the bottle of melted medium to the laminar flow cabinet. If you are instead planning to pour plates later in the day, transfer a bottle of freshly autoclaved or melted medium to a 60 °C incubator or water bath and transfer the bottle to the laminar flow cabinet only when ready to pour plates.

Add paper towels on the microwave plate to absorb medium spills. Remember to unscrew slightly the bottle cap before microwaving. At the highest microwave power level, it will take ~4 min to melt 400 ml of medium. Stop microwave often (e.g., every 10–30 sec) to

prevent the medium from boiling out of the bottle, and — wearing heat-resistant gloves — gently (otherwise the medium will boil out of the bottle) swirl the bottle to mix the medium.

(2) Wait until the medium has reached a temperature of ~60 °C.

It will take ~15 min at room temperature for freshly autoclaved or microwaved medium to cool to ~60 °C. It will take ~1.5 hours in a 60 °C incubator for freshly autoclaved or microwaved medium to cool to ~60 °C.

(3) Holding the bottle of medium through several (e.g., eight) layers of single-sheet paper towels, pour ~25 ml of medium in each Petri dish.

If you pour medium slowly and stop pouring as soon as a layer of medium covers the bottom of the dish, you will have poured ~25 ml of medium.

(4) Allow plates to dry and solidify by opening slightly the lid of the dishes toward the cabinet's air flow. Close the lid once the plate is solid and dry.

It will take ~15 min for plates to dry and solidify.

(5) Sow sterile seeds onto dried and solidified plates (see Basic Protocol 1) or seal the plates with Parafilm and store them in the refrigerator at 4 °C for up to a month.

Store plates upside down in the refrigerator to prevent condensation to accumulate on the medium surface.

2.5 BASIC PROTOCOL 1

2.5.1 Basic Protocol Title

Seed sterilization, sowing, and germination, and seedling growth

2.5.2 Introductory Paragraph

Here we describe how to sterilize, sow, and germinate Arabidopsis seeds, and how to grow the derived seedlings on plates of plant growth medium (whose preparation is described in Support

Protocols 1 and 2). The protocol described here requires basic wet laboratory skills and knowledge of how to work aseptically in laminar flow cabinets.

2.5.3 Materials

Growth medium plates (see Support Protocol 2)

Freshly, timely harvested and properly dried seeds of Arabidopsis (e.g., (Calhoun et al., 2021)) expressing a fluorescent protein (e.g., (Boulin et al., 2006; Rivero et al., 2014)) in developing leaves

70% ethanol (see recipe in Reagents and Solutions)

Sterilization solution (see recipe in Reagents and Solutions)

Autoclaved demineralized water

Laminar flow cabinet (e.g., Forma laminar airflow workstation model 1828 or similar equipment)

1.5-ml microtubes (e.g., Axygen, cat. no. MCT150LC)

Precision balance (e.g., Mettler Toledo, cat. no. 30029098)

Microtube rack (e.g., Heathrow Scientific, cat. no. HS29025C)

P1000 pipette (e.g., Gilson, cat. no. F123602)

P1000 pipette tips (e.g., Axygen, cat. no. T1000B)

Vortex mixer (e.g., Fisherbrand, cat. no. 9454FIALUS)

Mini-centrifuge (e.g., Fisherbrand, cat. no. HS120621)

Beaker (e.g., Fisherbrand, cat. no. FS14000250)

Parafilm (e.g., Bemis, cat. no. ACAPM996)

Aluminum foil (e.g., Fisherbrand, cat. no. 25SQFT)

Refrigerator (e.g., Frigidaire, cat. no. FFRU17B2QW)

Plant Growth Rack (e.g., Metro, Adjustable 5-Shelf Shelving Unit, 48-in L × 18-in W × 74-in H; GE Lighting, F40T12, 6500 K, 3050 lm, 48 in)

2.5.4 Protocol Steps with *Steps Annotations*

(1) If using plates that had been stored at 4 °C, dry them in a laminar flow cabinet by opening slightly the lid of the dishes toward the cabinet's air flow.

Drying plates in a laminar flow cabinet will take ~20 min.

(2) Aliquot in a 1.5-ml microtube up to ~20 µl, i.e. ~8 mg, of seeds of Arabidopsis expressing a fluorescent protein in developing leaves. Transfer the tube to a rack in a laminar flow cabinet.

We suggest using YFP as a reporter in leaves because YFP is ~50% brighter than GFP (Dobbie et al., 2008) and the wavelength used to excite YFP (514 nm) negligibly excites chlorophyll. To further increase the signal-to-background ratio, we also suggest multimerizing the fluorescent protein used by translationally fusing in tandem two or three copies of the fluorescent protein (e.g., (Gordon et al., 2007; Heisler et al., 2005; Weijers et al., 2006)). Twenty µl, i.e. ~8 mg, of Arabidopsis seeds correspond to ~400 seeds. If you need to sterilize more than that, scale up by aliquoting seeds in more 1.5-ml microtubes or in 2-, 15-, or 50-ml tubes. To ensure even exposure of all the seeds to the solutions, the volume of seeds in each tube should not be greater than 1/50th of the maximum volume of the tube.

(3) With a P1000 pipette, add 1 ml of 70% ethanol to the seeds, shake or vortex briefly (~1 sec) the tube to resuspend the seeds thoroughly, and put back the tube in the rack to let the seeds settle to the bottom of the tube or spin down the tube briefly (3–5 sec) in a mini-centrifuge to speed up the process. With a P1000 pipette, remove the 70% ethanol and discard it in a beaker.

Incubating the seeds in 70% ethanol >1 min will reduce seed germination and slow down seed germination and seedling growth. Therefore, do not sterilize seeds in a number of tubes greater than the one you are able to process in ≤1 min.

(4) With a P1000 pipette, add 1 ml of sterilization solution to the seeds, shake or vortex briefly (~1 sec) the tube to resuspend the seeds thoroughly, and position the tube horizontally on the tube rack or on the floor of the laminar flow cabinet. Incubate for 7 min.

Do not incubate >7 min or seedlings will be "bleached", i.e. they will be pale green.

(5) Put back the tube in the rack to let the seeds settle to the bottom of the tube or spin down the tube briefly (3–5 sec) in a mini-centrifuge to speed up the process. With a P1000 pipette, remove the sterilization solution and discard it in a beaker.

(6) With a P1000 pipette, add 1 ml of autoclaved demineralized water, shake or vortex briefly (~1 sec) the tube to resuspend the seeds thoroughly, and put back the tube in the rack to let the seeds settle to the bottom of the tube or spin down the tube briefly (3–5 sec) in a mini-centrifuge to speed up the process. With a P1000 pipette, remove the water and discard it in a beaker. Repeat at least four more times.

There is no limit to the number of washing steps or to their length, and more and longer washing steps will increase seed germination in older seeds.

(7) Resuspend the seeds in 1 ml of autoclaved demineralized water by pipetting up and down with a P1000 pipette. Pipette 500 µl of sterile seed suspension, let the seeds settle toward the pipette tip, and tap lightly the surface of the medium with the pipette tip. This action typically releases single seeds, but if necessary spread the seeds with the tip. If after a while seeds are no longer released, set the pipette to a lower volume by turning the volume adjusting knob by ~half-a-turn clockwise and try again. If this fails to solve the problem, empty the seed suspension back in the tube, resuspend by pipetting up and down, and start again. Sow the seeds ~1 cm apart, which will result in ~50 seeds per plate, except for IAA–lanolin paste application (Basic Protocol 2), in which case sow no more than ~10 seeds per plate.

(8) Allow the plates to dry by opening slightly the lid of the dishes toward the cabinet's air flow.

(9) Close the plates, seal them with Parafilm, wrap them in aluminum foil, and incubate them in

the refrigerator at 4 °C for 2–5 days (stratification).

A 2-day-long stratification — i.e. incubation of imbibed seeds at 4 °C in the dark — is

sufficient to induce synchronized seed germination and seedling growth in freshly

harvested and properly dried seeds. However, a longer stratification may be necessary for

older seeds. Stratifying >5 days will not synchronize germination and growth any further,

and seeds stratified for >7 days will germinate in the refrigerator and will lead to etiolated

seedlings. Furthermore, we found that seed stratification in water — i.e. immediately after

step 6 above — as opposed to on plate — as in step 9 here — will reduce and slow down seed

germination, and will slow down seedling growth. Therefore, seeds should be sterilized and

sown onto plates on the same day.

(10) Unwrap the plates and incubate them at 22 °C under continuous fluorescent light (~100

$\mu mol\ m^{-2}\ s^{-1}$). We refer to "days after germination" (DAG) as days after incubation of

sterilized, sown, and stratified seeds in light.

2.6 SUPPORT PROTOCOL 3

2.6.1 Support Protocol Title

Preparation of IAA–lanolin paste

2.6.2 Introductory Paragraph

Here we describe how to prepare a paste composed of lanolin and indole-3-acetic acid (IAA) —

the most active widespread form of the hormone auxin in plants (Cook, 2019; Jayasinghege et

al., 2019; Simon and Petrášek, 2011) — for local application to developing leaves (described in

Basic Protocol 2). A similar approach can be used to prepare pastes to apply other chemicals

directly to developing leaves for local perturbation of leaf development. The protocol described here requires basic wet laboratory skills.

2.6.3 Materials

Lanolin (e.g., Sigma-Aldrich, cat. no. L7387, cas no. 8006-54-0)

3-Indoleacetic acid (IAA) (e.g., Sigma-Aldrich, cat. no. I2886, cas no. 87-51-4)

Water bath (e.g., Thermo Scientific, cat. no. 1523058)

P1000 pipette (e.g., Gilson, cat. no. F123602)

P1000 pipette tips (e.g., Axygen, cat. no. T1000B)

P200 pipette tips (e.g., Axygen, cat. no. T200YR)

1.5-ml microtubes (e.g., Axygen, cat. no. MCT150)

Precision balance (e.g., Mettler Toledo, cat. no. 30029098)

Weighing dishes (e.g., Fisherbrand, cat. no. 02202102)

Spatula (e.g., Eisco, cat. no. CH0635A)

Aluminum foil (e.g., Fisherbrand, cat. no. 25SQFT)

Refrigerator (e.g., Frigidaire, cat. no. FFRU17B2QW)

2.6.4 Protocol Steps with *Steps Annotations*

(1) To prepare 1 ml of IAA–lanolin paste (1% IAA final concentration), incubate the lanolin bottle in a water bath at 55 °C for ~30 min.

It will take ~5 min for a water bath at room temperature to reach 55 °C.

(2) With a P1000 pipette and a P1000 pipette tip to which the tip had been cut off, quickly transfer 1 ml of melted lanolin from the bottle to a 1.5-ml microtube. Incubate the tube in the water bath at 55 °C.

Operate swiftly: lanolin will solidify quickly <55 °C. Do not incubate lanolin >55 °C, however, because the heat will decompose IAA.

(3) Weigh 0.01 g of IAA and quickly add it to the melted lanolin in the tube.

(4) With a P200 pipette tip, quickly mix the IAA–lanolin paste and return the tube to the water bath for ~5 min. Repeat at least three more times to make sure IAA is thoroughly dissolved in lanolin.

(5) Wrap the tube in aluminum foil and store at 4 °C for up to a week.

2.7 BASIC PROTOCOL 2

2.7.1 Basic Protocol Title

Application of IAA–lanolin paste to 3.5-DAG first leaves

2.7.2 Introductory Paragraph

Here we describe how to apply an IAA–lanolin paste (whose preparation is described in Support Protocol 3) to developing leaves of seedlings derived from the germination of sterilized seeds sown on plates of plant growth medium (described in Support Protocols 1 and 2, and Basic Protocol 1). Local application of the IAA–lanolin paste to developing leaves will lead to the formation of veins that will connect the site of paste application to pre-existing veins basally to the application site (Sawchuk et al., 2007; Scarpella et al., 2006; Verna et al., 2019) (Chapter 5). A similar approach can be used to apply other chemicals directly to developing leaves for local perturbation of leaf development. The protocol described here requires knowledge of how to work aseptically in laminar flow cabinets.

2.7.3 Materials

70% ethanol (see recipe in Reagents and Solutions)

3.5-DAG seedlings of Arabidopsis expressing in the developing veins an endoplasmic-reticulum (ER) - localized fluorescent protein — e.g., enhancer-trap lines Q0990, J1721, and E2331

(Amalraj et al., 2020; Sawchuk et al., 2007) (Chapter 4), which are available from the American (Arabidopsis Biological Resource Center, https://abrc.osu.edu) and Eurasian (Nottingham Arabidopsis Stock Centre, http://arabidopsis.info) stock centers with stock numbers CS9217/N9217, CS9105/N9105, and CS65892/N65892, respectively — grown at a density of no more than ~10 seedlings per plate (see Basic Protocol 1)

IAA-lanolin paste (see Support Protocol 3)

Stereomicroscope (e.g., Leica Zoom 2000 Stereo Microscope or similar equipment)

Laminar flow cabinet (e.g., Forma Laminar Airflow Workstation Class 100 Model 1828 or similar equipment)

Paper towels (e.g., Kimberly-Clark Professional, cat. no. KC01700)

Tweezers (e.g., Fisherbrand, cat. no. PL35)

Pin holder (Fine Science Tools, cat. no. 26016-12)

Pins, 0.1-mm diameter (Fine Science Tools, cat. no. 26002-10)

Microscissors (e.g., Fisherbrand, cat. no. SDI13550)

Plant growth rack (e.g., Metro, Adjustable 5-Shelf Shelving Unit, 48-in L × 18-in W × 74-in H; GE Lighting F40T12, 6500 K, 3050 lm, 48 in)

2.7.4 Protocol Steps with S*teps Annotations*

(1) Transfer a stereomicroscope to a laminar flow cabinet. Wipe the stereomicroscope with 70% ethanol.

(2) In the laminar flow cabinet, flame-sterilize a pair of tweezers and of microscissors.

(3) Transfer the pin holder to the laminar flow cabinet and wipe the holder with 70% ethanol. Loosen the pin holder jaws, insert a pin into the holder with the sterilized tweezers, and tighten the pin holder jaws.

(4) Transfer to the laminar flow cabinet a plate of plant growth medium with no more than ~10 3.5-DAG Arabidopsis seedlings expressing in the developing veins an ER-localized fluorescent protein. Remove the parafilm from the plate and open the plate.

IAA application will induce the formation of veins only in immature leaf tissues (Scarpella et al., 2006), and 3.5-DAG first leaves are the largest first leaves almost entirely composed of immature tissues.

(5) Under the stereomicroscope, gently hold one cotyledon with the sterilized tweezers, and with the sterilized microscissors remove the cotyledon right where its petiole joins the hypocotyl (Fig. 2.2A,B). Close the plate to prevent seedling wilting.

Removing one cotyledon provides easier access to one side of the first leaves.

(6) Dip the pin inserted into the holder into the tube with the IAA–lanolin paste to gather a drop of paste ~3 mm in diameter. Remove excess paste by running the pin across the rim of the tube.

(7) Open the plate. Under the stereomicroscope, gently apply the drop of paste to the bottom half of both first leaves on the side of the removed cotyledon (Fig. 2.2C).

Avoid applying the paste to the leaf petioles because IAA will promote their thickening, thereby making mounting of the dissected leaves (Basic Protocol 5) more difficult.

(8) Repeat steps 5–7 for the remaining seedlings.

If the seedlings start showing signs of wilting — e.g., they become flaccid and start shriveling — proceed immediately to step 9.

(9) Close the plate, seal it back with Parafilm, and return it to 22 °C under continuous fluorescent light (~100 µmol m^{-2} s^{-1}). Dissect, mount, and image the leaves 2.5 days later (6 DAG) (see Basic Protocols 3 and 5, Support Protocol 4, and Basic Protocol 6).

Approximately 90% of the leaves will respond to the IAA application by forming veins that connect the site of paste application to pre-existing veins basally to the application site (Fig. 2.2D) (Sawchuk et al., 2007; Scarpella et al., 2006; Verna et al., 2019) (Chapter 5).
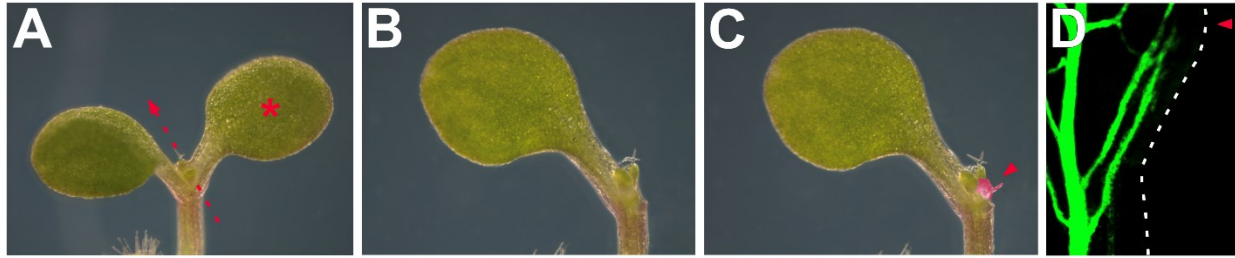
Figure 2.2: IAA–Lanolin Paste Application

(A–C) 3.5-DAG seedlings. (A,B) Remove one of the cotyledons. (C) Apply a ~3-mm drop of IAA–lanolin paste to the bottom half of both leaves on the side of the removed cotyledon. For clarity, the paste has been false-colored in red. (D) ER-localized GFP (erGFP) driven by the E2331 enhancer (Amalraj et al., 2020) (Chapter 4); first leaves 6 DAG; front view, median plane. Dissect, mount, and image the leaves 2.5 days after paste application — i.e. 6 DAG. Approximately 90% of the leaves will have responded to the IAA application by forming veins that connect the site of paste application to pre-existing veins basally to the application site (Sawchuk et al., 2007; Scarpella et al., 2006; Verna et al., 2019) (Chapter 5). Star, position of tweezer tips. Dashed-line arrow, direction of microscissor cut; dashed line, leaf outline; arrowhead, applied IAA–lanolin paste (C) or side of IAA–lanolin paste application (D).

2.8 BASIC PROTOCOL 3

2.8.1 Basic Protocol Title

Dissection of 3−6-DAG first leaves and leaf primordia

2.8.2 Introductory Paragraph

Here we describe how to dissect the first leaves and leaf primordia of Arabidopsis seedlings 3−6 DAG, derived from the germination of sterilized seeds sown on plates of plant growth medium (described in Support Protocols 1 and 2, and Basic Protocol 1). The protocol described here requires basic wet laboratory skills.

2.8.3 Materials

Demineralized water

3−6-DAG Arabidopsis seedlings expressing a fluorescent protein in developing leaves (see Basic Protocol 1)

P200 pipette (e.g., Gilson, cat. no. F123601)

P200 pipette tips (e.g., Axygen, cat. no. T200C)

Microscope slides (e.g., Bio Nuclear Diagnostics, cat. no. LAB-033)

Straight and slender fine-pointed tweezer (e.g., Fisherbrand, cat. no. PL35)

Stereomicroscope (e.g., Leica Zoom 2000 Stereo Microscope or similar equipment)

Syringes (e.g., Thermo Scientific, cat. no. S75101)

Needles (e.g., BD, cat. no. 305106)

2.8.4 Protocol Steps with *Steps Annotations*

 (1) With a P200 pipette, place ~50 μl of demineralized water on a microscope slide ~2/3 of the length of the slide from its left edge.

We illustrate steps for left-handed people, as we both are. Users should adapt instructions to their handedness.

(2) With a pair of tweezers, gently transfer a 3–6-DAG Arabidopsis seedling from a plate of plant growth medium to the left side of the water drop on the slide.

Place the tweezers below the cotyledons, around the seedling's cotyledonary node; close slightly the tweezer jaws — do not close them all the way or you will crush the hypocotyl; and lift the seedling from the plate. Do not use tweezers with serrated jaws.

(3) Under a stereomicroscope and with a syringe and a sharp needle in your right hand, hold down the seedling by the right cotyledon (Fig. 2.3A). With another syringe and a sharp needle in your left hand, slice off with a distal-to-proximal movement the left cotyledon right where its petiole joins the hypocotyl (Fig. 2.3B,C). Discard the cotyledon.

Orient the "slicing" needle with the beveled side of its tip — i.e. the side of the needle tip with the hole — away from the leaves.

(4) Under a stereomicroscope and with a syringe and a sharp needle in your left hand, slice off with a distal-to-proximal movement the first leaves (4- and 6-DAG seedlings) or leaf primordia (3-DAG seedlings) right where they join the hypocotyl (Fig. 2.3D,E). Discard the rest of the seedling.

(5) If the leaves or leaf primordia have been separated from each other as a result of the previous step, proceed to the next step. If not, under a stereomicroscope and with a syringe and a sharp needle in your left hand, with a distal-to-proximal movement slice through the tissue that is keeping the leaves or leaf primordia together (Fig. 2.3F).

(6) Under a stereomicroscope and with a syringe and a needle, gently push the leaves or leaf primordia toward the left edge of the water drop.

Always use the non-beveled side of the needle to handle the leaves and leaf primordia. The water is shallower at the edge of the drop; therefore, the leaves or leaf primordia will remain in position. However, positioning the leaves or leaf primordia at the edge of the
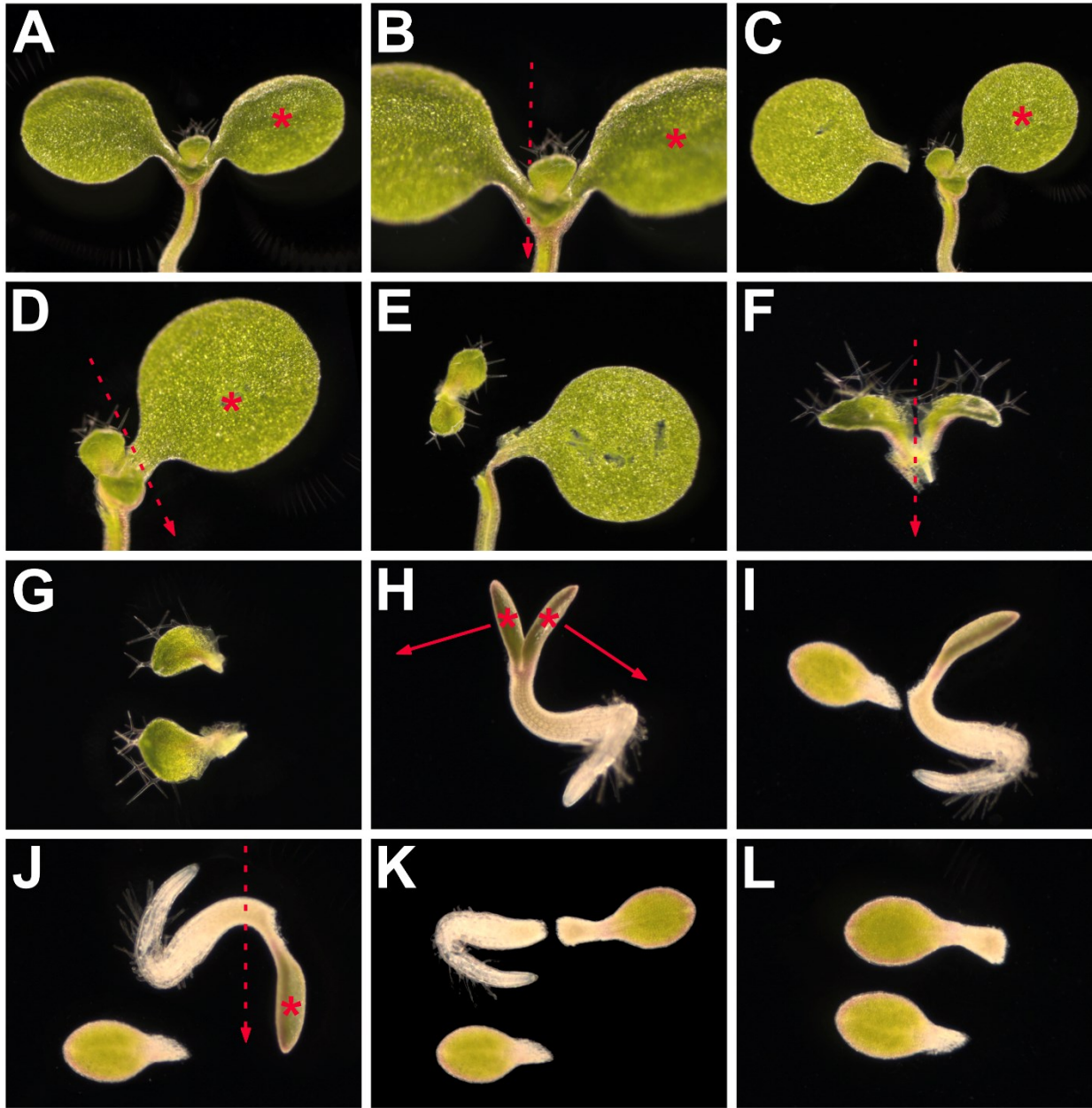
Figure 2.3: Leaf and Leaf Primordium Dissection

(A–G) 6-DAG seedlings and first leaves. (A–C) Slice off one of the cotyledons and discard it. (D,E) Slice off the first leaves and discard the rest of the seedling. (F) Slice through the tissue that is keeping the leaves together. (G) Orient the leaves with their long side parallel to the long side of the microscope slide. (H–L) 2-DAG seedlings. (H,I) Pull the cotyledons apart. Typically,

one cotyledon will detach. (J,K) Orient the dissected seedling with the hypocotyl–root axis parallel to the long side of the slide. Slice across the hypocotyl half-way its length and discard the root and half hypocotyl. (L) Orient the detached cotyledon and the dissected seedling with their long axis parallel to the long side of the slide. Star, position of needle tip; dashed-line arrow, direction of needle slicing; solid-line arrow, direction of needle pull.

water drop increases the risk that they will dry; therefore, as you proceed with the

protocol, regularly monitor the positioned leaves or leaf primordia to make sure they never

dry. Should they start to do so, with a syringe and a needle gently drag a bit of water from

the center of the drop to its edge, toward the leaves or leaf primordia.

(7) If the desired side of the leaves or leaf primordia faces up, proceed to the next step. If not, under a stereomicroscope and with a syringe and a needle, gently turn the leaves or leaf primordia upside down such that the desired side faces up.

Orient the leaves and leaf primordia with their abaxial (i.e. lower, or ventral) side up to

image the abaxial epidermis, including the stomata; the spongy mesophyll; and the veins.

Orient the leaves and leaf primordia with their adaxial (i.e. upper, or dorsal) side up to

image the adaxial epidermis, including trichomes, and the palisade mesophyll.

(8) Orient the leaves or leaf primordia with their long side parallel to the long side of the microscope slide (Fig. 2.3G).

Orienting the leaf or leaf primordium with its long side parallel to the long side of the

microscope slide reduces the chances that the leaf or leaf primordium will roll on itself as

the coverslip is lowered (see Basic Protocol 5).

(9) Proceed immediately to Basic Protocol 5.

2.9 BASIC PROTOCOL 4

2.9.1 Basic Protocol Title

Dissection of 1- and 2-DAG first-leaf primordia

2.9.2 Introductory Paragraph

Here we describe how to dissect the first-leaf primordia of Arabidopsis seedlings 1 and 2 DAG, derived from the germination of sterilized seeds sown on plates of plant growth medium

(described in Support Protocols 1 and 2, and Basic Protocol 1). The protocol described here requires basic wet laboratory skills.

2.9.3 Materials

Demineralized water

1- or 2-DAG Arabidopsis seedlings expressing a fluorescent protein in developing leaves (see Basic Protocol 1)

P200 pipette (e.g., Gilson, cat. no. F123601)

P200 pipette tips (e.g., Axygen, cat. no. T200C)

Microscope slides (e.g., Bio Nuclear Diagnostics, cat. no. LAB-033)

Straight and slender fine-pointed tweezer (e.g., Fisherbrand, cat. no. PL35)

Stereomicroscope (e.g., Leica Zoom 2000 Stereo Microscope or similar equipment)

Syringes (e.g., Thermo Scientific, cat. no. S75101)

Needles (e.g., BD, cat. no. 305106)

2.9.4 Protocol Steps with *Steps Annotations*

(1) With a P200 pipette, place ~50 μl of demineralized water on a microscope slide ~2/3 of the length of the slide from its left edge.
We illustrate steps for left-handed people, as we both are. Users should adapt instructions to their handedness.

(2) With a pair of tweezers, gently transfer a 1 or 2-DAG Arabidopsis seedling from a plate of plant growth medium to the left side of the water drop on the slide.
If the cotyledons have fully emerged from the seed coat, place the tweezers below them, around the seedling's cotyledonary node; close slightly the tweezer jaws — do not close them all the way or you will crush the hypocotyl; and lift the seedling from the plate. If the cotyledons are still, at least in part, inside the seed coat — which may be the case for 1-DAG

seedlings — place the tweezers around it; close slightly the tweezer jaws — do not close them all the way or you will crush the cotyledons; and lift the seedling from the plate. Do not use tweezers with serrated jaws.

(3) If the cotyledons have fully emerged from the seed coat, proceed to the next step. If the cotyledons are still, at least in part, inside the seed coat — which may be the case for 1-DAG seedlings — gently remove the seed coat with syringes and sharp needles under a stereomicroscope.

(4) Under a stereomicroscope, hold down the cotyledons with syringes and needles, and gently pull the cotyledons apart (Fig. 2.3H). Typically, one cotyledon will detach, leaving the other cotyledon — together with the two first-leaf primordia — attached to the hypocotyl (Fig. 2.3I). If so, discard the detached cotyledon and orient the dissected seedling with the leaf primordia facing up. Occasionally, one of the two leaf primordia will remain attached to the detached cotyledon; therefore, check carefully under the stereomicroscope whether that is the case before discarding the detached cotyledon. If indeed one of the two leaf primordia has remained attached to the detached cotyledon, keep both the detached cotyledon and the dissected seedling, and orient both of them with the leaf primordia facing up.

(5) Under a stereomicroscope and with syringes and needles, orient the dissected seedling with the hypocotyl–root axis parallel to the long side of the slide and with the remaining cotyledon toward the right (Fig. 2.3J). With a syringe and needle in your right hand, hold down the dissected seedling by the remaining cotyledon (Fig. 2.3J). With another syringe and a sharp needle in your left hand, slice across the hypocotyl half-way its length with a distal-to-proximal movement (Fig. 2.3J,K). Discard the root and half hypocotyl.
Removing the root and half of the hypocotyl will reduce the thickness of the sample.

(6) Under a stereomicroscope and with a syringe and a needle, gently push the dissected seedling and, if not discarded, the detached cotyledon toward the left edge of the water drop.

Always use the non-beveled side of the needle to handle the detached cotyledon and dissected seedling. The water is shallower at the edge of the drop; therefore, the detached cotyledon and dissected seedling will remain in position. However, positioning the detached cotyledon and dissected seedling at the edge of the water drop increases the risk that they will dry; therefore, as you proceed with the protocol, regularly monitor the positioned detached cotyledon and dissected seedling to make sure they never dry. Should they start to do so, with a syringe and a needle gently drag a bit of water from the center of the drop to its edge, toward the detached cotyledon and dissected seedling.

(7) Under a stereomicroscope and with syringes and needles, orient the detached cotyledon — if not discarded — with its main axis parallel to the long side of the microscope slide and with the cotyledon tip toward the left (Fig. 2.3L). Orient the dissected seedling with the hypocotyl–root axis parallel to the long side of the slide and with the remaining cotyledon toward the left (Fig. 2.3L).

(8) Proceed immediately to Basic Protocol 5.

2.10 BASIC PROTOCOL 5

2.10.1 Basic Protocol Title

Mounting of dissected leaves and leaf primordia

2.10.2 Introductory Paragraph

Here we describe how to place a coverslip (a.k.a. coverglass) onto dissected leaves and leaf primordia (see Basic Protocols 3 and 4). The protocol described here requires basic wet laboratory skills.

2.10.3 Materials

Dissected leaves or leaf primordia in water on microscope slide (see Basic Protocols 3 and 4)

Demineralized water

Coverslips, 18 mm × 18 mm, no. 1.5 (e.g., Fisherbrand, cat. no. 18X1815602811G)

P1000 pipette (e.g., Gilson, cat. no. F123602)

P1000 pipette tips (e.g., Axygen, cat. no. T1000B)

Syringes (e.g., Thermo Scientific, cat. no. S75101)

Needles (e.g., BD, cat. no. 305106)

Kimwipes (e.g., Kimberly-Clark Professional, cat. no. KC34120)

2.10.4 Protocol Steps with *Steps Annotations*

(1) Position the microscope slide with the dissected leaves or leaf primordia such that the edge of the water drop containing the sample is pointing left.

We illustrate steps for left-handed people, as we both are. Users should adapt instructions to their handedness.

(2) Take one coverslip out of the box by holding the coverslip by two opposite edges with the thumb and index finger of your left hand.

Most microscope objective lenses are corrected for the spherical aberration generated by coverslips 0.17-mm thick (a.k.a. no. 1.5). For optimal resolution, it is important to use this type of coverslip, especially for thick samples such as leaves and leaf primordia mounted in water. Handle coverslips only by their edges to avoid fingerprints.

(3) By keeping the coverslip perpendicular to the microscope slide, place the lower edge of the coverslip in contact with the edge of the water drop that is opposite to the edge of the water drop containing the sample (Fig. 2.4A).
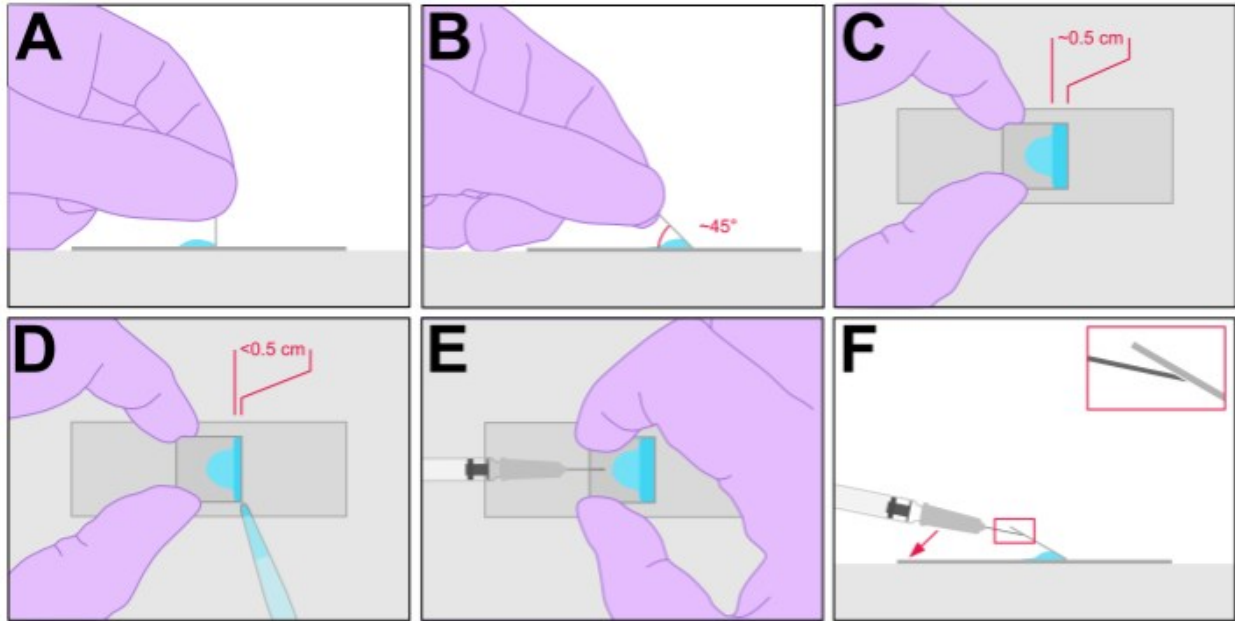
Figure 2.4: Mounting of Dissected Leaves and Leaf Primordia

(A) Keep the coverslip perpendicular to the microscope slide and place the lower edge of the coverslip in contact with the edge of the water drop that is opposite to the edge of the water drop containing the sample. (B) Lower the coverslip over the water drop containing the sample as though the coverslip were hinged at the edge that is in contact with the water. Stop when the angle between the coverslip and the slide is ~45°. (C,D) If the water strip between the hinged side of the coverslip and the slide is less than ~0.5-cm wide — i.e. ~1/4 of the coverslip size — slowly add more water until the water strip is ~0.5-cm wide. (E,F) Lower the coverslip to an ~30° angle and insert the needle of a syringe between the unhinged edge of the coverslip and the water drop containing the sample. Make sure the beveled side of the needle tip — i.e. the side of the needle tip with the hole — faces up (see high-magnification inset in F). Release the coverslip, and lower and slide the needle until it is free. Arrow, direction of needle movement.

(4) By slowly rotating your wrist, gently lower the coverslip over the water drop containing the sample as though the coverslip were hinged at the edge that is in contact with the water. Stop when the angle between the coverslip and the slide is ~45° (Fig. 2.4B). If the water strip between the hinged side of the coverslip and the slide is less than ~0.5-cm wide — i.e. less than ~1/4 of the coverslip size — slowly add more water with a P1000 pipette until the water strip is ~0.5-cm wide (Fig. 2.4C,D).

(5) Once the coverslip has been lowered to an ~30° angle between the coverslip and the slide, hold the coverslip in position with your right hand, and with your left hand insert the needle of a syringe between the unhinged edge of the coverslip and the water drop containing the sample (Fig. 2.4E,F). Make sure the beveled side of the needle tip — i.e. the side of the needle tip with the hole — faces up (Fig. 2.4E,F).

(6) Gently release the coverslip with your right hand, and with your left hand slowly lower and slide the needle toward the left until the needle is free (Fig. 2.4F).

(7) With a Kimwipe, gently remove excess water from around the coverslip without touching the coverslip.

(8) Proceed immediately to Support Protocol 4 or Basic Protocol 6.

Leaves and leaf primordia must be imaged immediately after mounting. Mounted leaves and leaf primordia cannot be stored for any amount of time.

2.11 SUPPORT PROTOCOL 4

2.11.1 Support Protocol Title

Quality check of mounted leaves and leaf primordia by fluorescence microscopy.

2.11.2 Introductory Paragraph

Confocal time is expensive, and the limiting step to acquiring informative confocal images is that samples are as flat and as close to the coverslip as possible without being damaged. Therefore, it is critical that users become proficient in dissection and mounting of leaves and leaf primordia before proceeding to confocal imaging. Here we describe a protocol to assess whether the user's skills in dissection and mounting of leaves and leaf primordia are of sufficient quality for confocal imaging. The protocol described here requires basic training in fluorescence microscopy.

2.11.3 Materials

Dissected and mounted leaves (see Basic Protocols 3–5) of Arabidopsis expressing in the developing veins an ER-localized fluorescent protein — e.g., enhancer-trap lines Q0990, J1721, and E2331 (Amalraj et al., 2020; Sawchuk et al., 2007) (Chapter 4), which are available at the American (Arabidopsis Biological Resource Center, https://abrc.osu.edu) and Eurasian (Nottingham Arabidopsis Stock Centre, http://arabidopsis.info) Arabidopsis stock centers with stock numbers CS9217/N9217, CS9105/N9105, and CS65892/N65892, respectively
Demineralized water for water-immersion objectives
Immersion oil for oil-immersion objectives (e.g., Carl Zeiss, cat. no. 000000-1111-806)
Fluorescence microscope (e.g., Zeiss Axio Imager 2 or Leica DM4/6 B)
Lens paper (e.g., Fisherbrand, 20205115)
Paper towels (e.g., Kimberly-Clark Professional, cat. no. KC01700)

2.11.4 Protocol Steps with *Steps Annotations*

 (1) View the dissected and mounted leaves or leaf primordia with a fluorescence microscope with the proper filter set.

(2) In a perfectly dissected and mounted leaf or leaf primordium, the whole vein network will be in focus in either a single plane (first leaves and leaf primordia ≤4 DAG) or in two planes (first leaves 4<DAG≤6) — one plane for the veins in the top half of the leaf and one plane for the veins in the bottom half of the leaf (Fig. 2.5A,B). If that is so, proceed to step 4; if more focal planes are instead necessary to view the whole vein network, proceed to the next step.

(3) More focal planes than necessary are required to view the whole vein network because of too much water between the microscope slide and coverslip. Remove the excess water by juxtaposing the edge of a strip of lens paper or paper towel to one of the edges of the coverslip while viewing the sample through the eyepieces or a live camera. The paper will absorb by capillary action some of the water, thereby flattening the sample. Stop as soon as the whole vein network of the leaf or leaf primordium is completely in focus either in a single plane (first leaves and leaf primordia ≤4 DAG) or in two planes (first leaves 4<DAG≤6) (Fig. 2.5C).

(4) Inspect the sample for signs of conspicuous tissue damage such as linear cuts or circular wounds (Fig. 2.5D,E). Linear cuts result from using the beveled side of the needle to position leaves or leaf primordia during dissection. Circular wounds result from using the tip of the needle to position leaves or leaf primordia during dissection. If signs of conspicuous tissue damage are detected, discard the sample, and dissect and mount new leaves or leaf primordia, carefully avoiding the use of the beveled side or the tip of the needle while positioning leaves or leaf primordia during dissection. If no signs of conspicuous tissue damage are detected, proceed to step 5.

(5) Inspect the sample for signs of more-subtle tissue damage, visible in first leaves and leaf primordia ≥3 DAG as vein loops disconnected from the midvein at their basal end (Fig. 2.5F) and resulting from too little water between the microscope slide and the coverslip. First-leaf primordia <3 DAG are usually protected from such more-subtle tissue damage by the presence of residual seedling tissue. If signs of more-subtle tissue damage are detected,
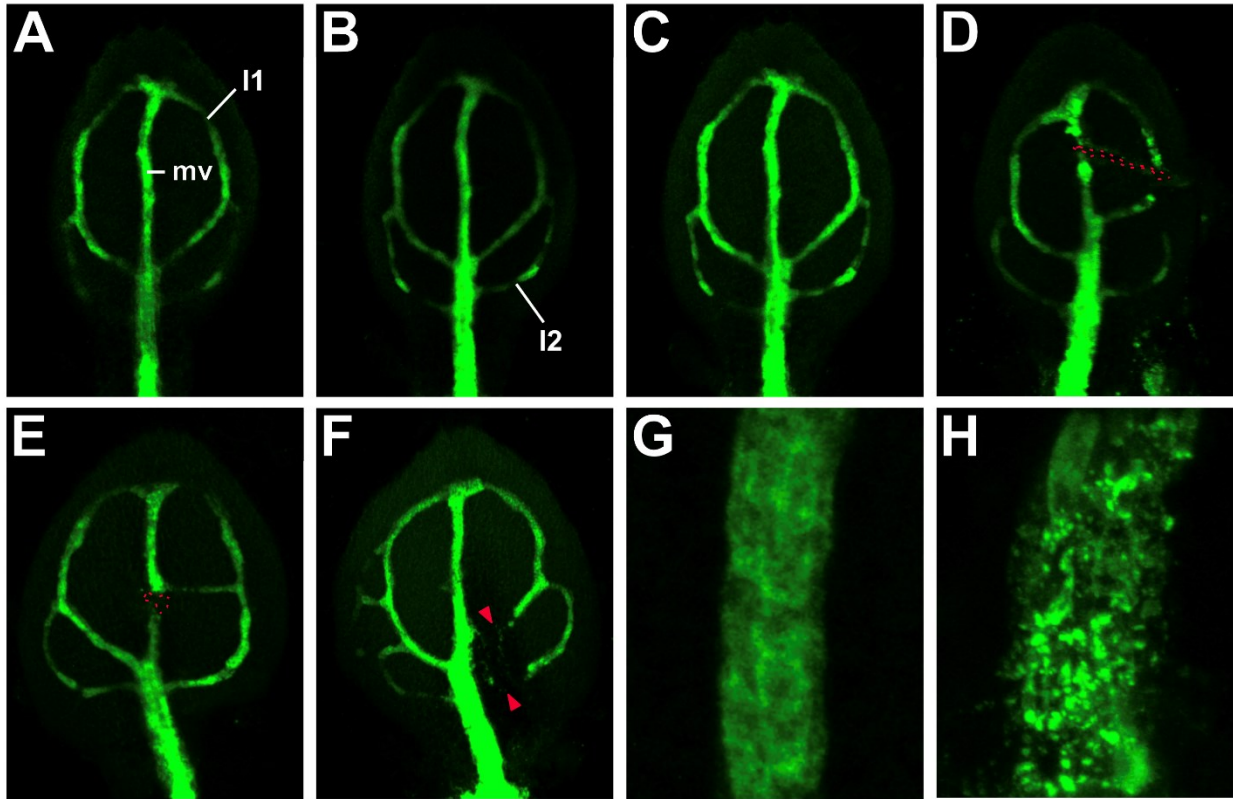
Figure 2.5: Assessing Proficiency in Leaf Dissection and Mounting

(A–H) erGFP driven by the E2331 enhancer (Amalraj et al., 2020) (Chapter 4); first leaves 4 DAG; front view, median plane. (A,B) Too much water between the microscope slide and the coverslip results in a thicker preparation; therefore, two planes are necessary for the whole vein network to be in focus: one plane for the veins in the top half of the leaf, i.e. the top part of the midvein (mv) and the first loops (l1) (A), and one plane for the veins in the bottom half of the leaf, i.e. the bottom half of the midvein and the second loops (l2) (B). (C) After the excess water has been removed by juxtaposing the edge of a strip of lens paper or paper towel to one of the edges of the coverslip, the whole vein network is in focus in a single plane. (D) Linear cut (dashed line) resulting from using the beveled side of the needle to position the leaf during dissection. (E) Circular wound (dashed line) resulting from using the tip of the needle to position the leaf during dissection. (F) Too little water between the microscope slide and the

coverslip results in vein loops disconnected from the midvein at their basal end (arrowheads). (G) In the absence of cellular damage, signal emitted by erGFP is stronger along the cell and nucleus outlines, and weaker but nearly homogeneously distributed in the cytoplasm. (H) In the presence of cellular damage, signal emitted by erGFP coalesces in vesicles.

discard the sample, and dissect and mount new leaves or leaf primordia using more water. If no signs of more-subtle tissue damage are detected, proceed to step 6.

(6) Inspect the sample for signs of cellular damage. In the absence of cellular damage, signal emitted by an ER-localized fluorescent protein is stronger along the cell and nucleus outlines, and weaker but nearly homogeneously distributed in the cytoplasm (Fig. 2.5G). In the presence of cellular damage, signal emitted by an ER-localized fluorescent protein coalesces in vesicles (Fig. 2.5H). Cellular damage near the basalmost end of the leaf or leaf primordium is normal and acceptable as long as that area of the sample is uninformative to the user. Cellular damage results from wounding while positioning leaves or leaf primordia during dissection, too little water between microscope slide and coverslip, or too much time between mounting and imaging. If signs of cellular damage are detected, discard the sample; dissect and mount new leaves or leaf primordia using more water and carefully avoiding the use of the beveled side or the tip of the needle while positioning leaves or leaf primordia during dissection; and image immediately after mounting. If no signs of cellular damage are detected, dissection and mounting skills are of sufficient quality for confocal imaging.

2.12 BASIC PROTOCOL 6

2.12.1 Basic Protocol Title

Imaging of mounted leaves and leaf primordia by confocal microscopy

2.12.2 Introductory Paragraph

Here we provide practical guidelines to image mounted leaves and leaf primordia by confocal microscopy. The protocol described here requires basic training in confocal microscopy, is designed for single-fluorophore imaging, and assumes the user has already optimized the light

path for the excitation of the fluorescent protein in their sample and the detection of the fluorescence emitted by the excited fluorescent protein.

2.12.3 Materials

Dissected and mounted leaves (see Basic Protocols 3–5)

Demineralized water for water-immersion objectives.

Immersion oil for oil-immersion objectives (e.g., Carl Zeiss, cat. no. 000000-1111-806).

Confocal laser scanning microscope (e.g., Zeiss LSM 510 or later model, or Leica TCS SP2 or later model)

2.12.4 Protocol Steps with *Steps Annotations*

(1) Turn on the desired laser. If using an Argon multi-line laser, first set to standby until warmed up, and then to on. If using an Argon multi-line laser, set laser output to achieve a tube current of ~6.0 A.

This value is a compromise between laser noise, which is lower at a tube current of 8 A, and laser lifetime, which will be longer at a tube current of 4 A.

(2) If using an Argon multi-line laser, select the desired laser line. Select the desired light path (e.g., dichroic beam splitters and filters) for the excitation of the fluorescent protein in the sample and the detection of the fluorescence emitted by the excited fluorescent protein.

(3) Determine the microscope objective you will need to use, and note its numerical aperture (NA) and the size of the objective's field of view that is captured at the lowest zoom value by the confocal microscope. For example, to image a whole 4-DAG leaf you will need to use a 20× objective, which has — for the sake of example — an NA of 0.8 and a captured field of view at the lowest zoom value of 595 μm × 595 μm.

The NA is a property of the objective and can be usually found written on the objective itself (e.g., 20×/0.8); alternatively, it can be found on the manufacturer's website through the

name or cat. no. of the objective. The size of the objective's field of view that is captured at the lowest zoom value by the confocal microscope is equal to a microscope-specific constant divided by the magnification of the objective. For Zeiss confocal microscopes, the constant is 11,900 — from which we derive that the field of view of a 20× objective is 11,900/20 μm × 11,900/20 μm, i.e. 595 μm × 595 μm. For Leica confocal microscopes, the constant is 15,000. Alternatively, to determine the size of the objective's field of view that is captured at the lowest zoom value by the confocal microscope, scan a micrometer slide.

(4) Set the scan mode to frame.

(5) Determine the maximum size that pixels can be in your images. To do so, first determine how close along the X/Y dimension the smallest objects that you need to be able to tell apart from one another will be in your leaves. For example, consider you are imaging the expression of a fluorescent-protein-tagged transcription factor. If so, the smallest objects you may need to be able to tell apart from one another in your images are the smallest nuclei expressing your fluorescent-protein-tagged transcription factor, i.e. spheroids with a ~4-μm diameter. Because those nuclei are usually at the center of cuboid cells with a ~6 μm side, the centers of the smallest objects you may need to be able to tell apart from one another in your images are ~6 μm away from one another. And because the distance between the smallest objects you will need to be able to tell apart from one another should not be represented by fewer than 3 pixels — ideally by as many as 8 and on average by 6 pixels (Shaw, 2006) — in your images the pixel size cannot be greater than 2 μm, i.e. 6 μm divided by 3 pixels. *Note that objects cannot be close at will and still be told apart from one another: for pinholes >1 Airy unit — which is often the case when imaging developing leaves (see step 11 below) — the minimum distance is $\frac{0.51\lambda_{Ex}}{NA}$, where λ_{Ex} is the excitation wavelength in nm (e.g., 488 for GFP).*

(6) Determine the minimum size of your image in pixels — e.g., 512 pixels × 512 pixels or 1,024 pixels × 1,024 pixels — that allows the distance between the smallest objects you will need to

be able to tell apart from one another to be represented by at least 3 pixels. To do so, first calculate the pixel size if the image were to be 512 pixels × 512 pixels, i.e. 595 μm × 595 μm divided by 512 pixels × 512 pixels or 1.16 μm × 1.16 μm / pixel. Because a 1.16-μm-×-1.16-μm pixel is smaller than a 2-μm-×-2-μm pixel, if your image were to be 512 pixels × 512 pixels in size the distance between the smallest objects you need to be able to tell apart from one another (i.e. 6 μm) would be represented by at least 3 pixels (to be precise, it would be represented by at least 5 pixels, i.e. 6 μm divided by 1.16 μm/pixel). If the image were instead to be 1,024 pixels × 1,024 pixels in size, the distance between the smallest objects you need to be able to tell apart from one another would be represented by at least 10 pixels, each 0.58 μm × 0.58 μm in size. Therefore, the minimum image size that allows the distance between the smallest objects you will need to be able to tell apart from one another to be represented by at least 3 pixels is 512 pixels × 512 pixels. One could argue that — even though unnecessary — an image size of 1,024 pixels × 1,024 pixels would be better. All other things being equal, however, the amount of light each pixel in a 1,024-pixel-×-1,024-pixel image collects will be four times smaller than if the image were 512 pixels × 512 pixels in size. Therefore, whether your image can be 1,024 pixels × 1,024 pixels in size will depend on how strong the signal is in your sample. Irrespective of that, scanning a 1,024-pixel-×-1,024-pixel image will take four times longer than scanning a 512-pixel-×-512-pixel image. Because longer scanning times increase fluorophore photobleaching and background autofluorescence, the result will be a lower signal-to-background ratio. Therefore, we advise setting the size of your image in pixels to the minimum value that allows the distance between the smallest objects you will need to be able to tell apart from one another to be represented by no fewer than 3 pixels and no more than 8 pixels.

(7) Set the scanning speed and image averaging at ~1.61 μs/pixel and 4-frame averaging, respectively.

We found that a scanning speed of 1.61 μs/pixel and an averaging of 5 frames is optimal. However, the desired field of view to be captured by the confocal may be too large for the scanner speed, in which case set the scanning speed to the maximum value possible — usually ~2.56 μs/pixel. Furthermore, most confocal microscopes will only allow averaging 4 or 8 frames, in which case use 4 frames: we noticed no improvement in signal-to-noise ratio by averaging 8 frames instead of 5 that justifies the longer scanning time, which will increase fluorophore photobleaching and background autofluorescence, and will consequently reduce the signal-to-background ratio. If you expect fluorescent features to move during the scanning time, average by line as opposed to by frame.

(8) Set the dynamic range — a.k.a. pixel (well) depth — of the digitizer (or analog-to-digital converter) to 8 bits.

The pixel depth will determine the number of gray levels in your image. For example, an image with pixel depth of 8 will have 2^8, i.e. 256 gray levels — with level 0 assigned to black and level 255 to white — and an image with pixel depth of 12 will have 4,096 gray levels — with level 0 assigned to black and level 4,095 to white. Our eyes can only differentiate a few tens (~20–40) of gray levels and a few hundred colors (Russ and Neal, 2016). This means that our eyes will never be able to distinguish all the gray levels in an 8-bit image, let alone in a 12-bit one. In both cases, one will therefore have to apply to the images a look-up-table (LUT) to assign different colors to the different gray levels. However, LUTs are based on shades of at most 10 colors (black, violet, blue, cyan, green, yellow, orange, red, magenta, and white). Applying such an LUT to a 8-bit image will assign to the 256 gray levels ~26 shades of each of the 10 colors, whose distinction is within the capabilities of the human eye. However, applying the same LUT to a 12-bit image will assign to the 4,096 gray levels ~410 shades of each of the 10 colors, whose distinction is well above the upper limit of the human eye. If one additionally considers that the most commonly used LUTs are based on shades of only five, six, or seven colors — black, red, orange, yellow, and

74

white (Fig. 2.6A); black, blue, cyan, green, yellow, and white (Fig. 2.6B); or black, blue,

violet, red, orange, yellow, white (Fig. 2.6C) — applying such LUTs to a 12-bit image will

assign to the 4,096 gray levels 819, 683, or 585 shades of each of the five, six, or seven

colors, respectively. As such, the need to acquire 12-bit images for display is questionable.

The problem, however, is not only one of display because partitioning the dynamic range of

the digitizer into 4,096 buckets means that 16-fold fewer photoelectrons will be collected in

each of those buckets than if the dynamic range had been partitioned into 256 buckets.

Therefore, we advise setting the pixel depth to 8 bits for most purposes.

(9) Select unidirectional scanning (or turn off bidirectional scanning).

Bidirectional scanning is faster but leads to artifacts at the left and right edges of the

images, where consecutive scans do not exactly line up.

(10) Determine the minimum optical slice thickness (FWHM). To do so, first determine how
close along the Z dimension the smallest objects that you need to be able to tell apart from
one another will be in your leaves. As per the example above (step 5), the centers of the
smallest objects you may need to be able to tell apart from one another in your images (i.e.
the smallest nuclei expressing your fluorescent-protein-tagged transcription factor) are ~6
μm away from one another. Because the distance between the smallest objects you will need
to be able to tell apart from one another should not be represented by fewer than 3 sampling
points — ideally by as many as 8 and on average by 6 points (Shaw, 2006) — in your images
FWHM cannot be greater than 2 μm, i.e. 6 μm divided by 3.

(11) Calculate and set the pinhole diameter in μm:

$$\sqrt{FWHM^2 - (\frac{0.88 \times \lambda_{Em}}{n - \sqrt{n^2 - NA^2}})^2} \times \frac{NA \times M_{Sys} \times M_{Obj} \times Z}{n \times \sqrt{2}}$$

Where λ_{Em} is the average emission wavelength in μm (e.g., if using a BP 505–530 filter —

typically used for GFP detection — $\lambda_{Em} = \frac{0.505+0.530}{2}$), n is the refractive index of immersion

liquid (i.e. 1 for air, 1.33 for water, and 1.52 for oil), M_{Sys} is the system magnification
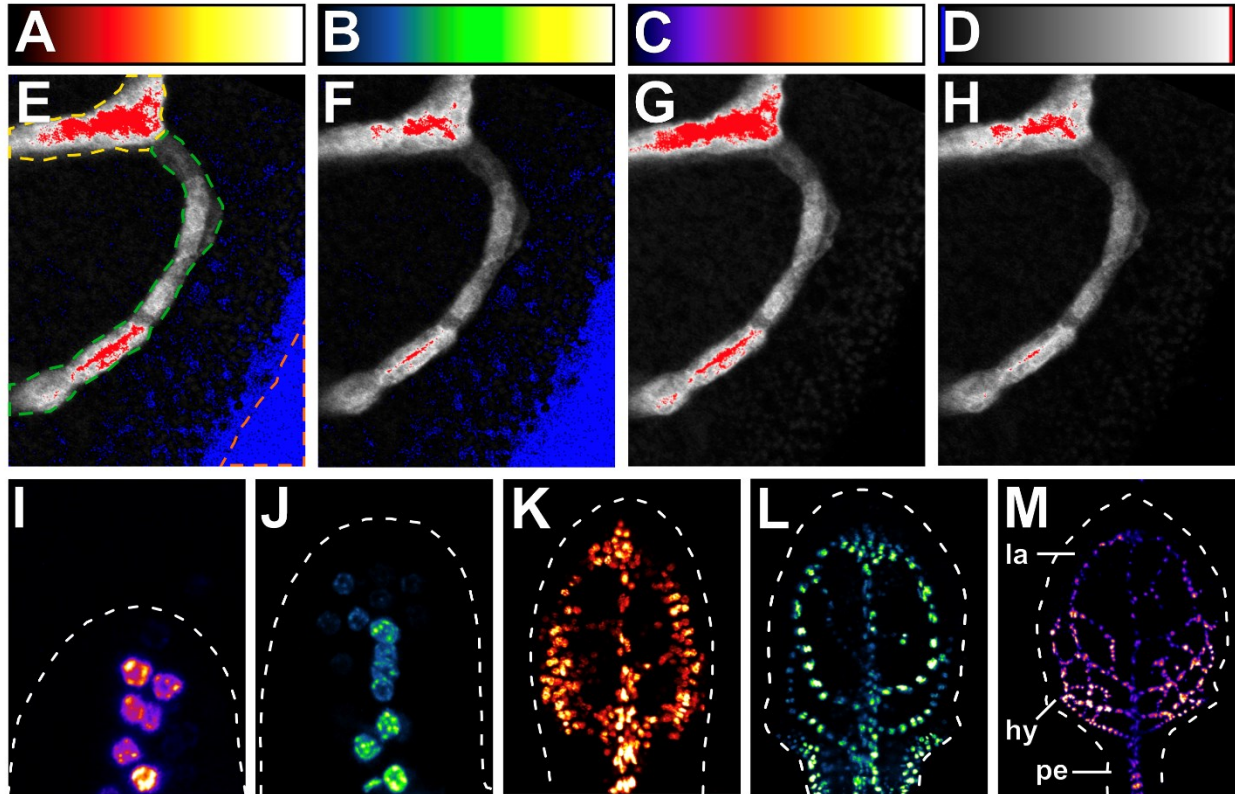
Figure 2.6: Imaging of Mounted Leaves and Leaf Primordia by Confocal Microscopy

(A–D) Most commonly used LUTs: Red Hot (A), Green Fire Blue (B), Fire (C), and HiLo (D) (Rueden et al., 2017; Schindelin et al., 2012; Schindelin et al., 2015; Schneider et al., 2012). (E–H) erGFP driven by the E2331 enhancer (Amalraj et al., 2020) (Chapter 4); first leaves 4 DAG; front view, median plane; HiLo LUT (ramp in D) visualizes GFP expression levels. (E) By adjusting laser transmission, saturated (i.e. red) pixels are ~5% of the total amount of pixels in the region of interest (dashed green line), but >5% of the total amount of pixels in the region of no interest (dashed yellow line). The featureless region (dashed orange line) mostly contains level-0 (i.e. blue) pixels. (F) By adjusting laser transmission, saturated pixels are ~1% of the total amount of pixels in the region of interest, but >1% of the total amount of pixels in the region of no interest. The featureless region mostly contains level-0 pixels. (G,H) Increasing detector

offset at laser-transmission settings in E and F, respectively, turns level-0 pixels into level-1 (i.e. black) pixels. (I–M) Nuclear YFP driven by the *ARABIDOPSIS THALIANA HOMEOBOX8* (I,M), *SHORT-ROOT* (J), *PIN-FORMED6* (K), or *CYCLIN A2;1* (L) promoter (Gardiner et al., 2011; Sawchuk et al., 2007; Sawchuk et al., 2013; Vanneste et al., 2011) in first-leaf primordia 1 (I), 2 (J), and 3 (K) DAG, and in first leaves 4 (L) and 6 (M) DAG. (I,J) Side view, median plane. Abaxial (ventral) side to the left; adaxial (dorsal) side to the right. (K–M) Front view, median plane. Fire LUT (ramp in C) visualizes YFP expression levels in I and M; Green Fire Blue LUT (ramp in B) visualizes YFP expression levels in J and L; Red Hot LUT (ramp in A) visualizes YFP expression levels in K. Dashed white line, leaf or leaf primordium outline. hy, hydathode; la, lamina; pe, petiole.

(see Table 2.1), M_{Obj} is the objective magnification (e.g., 20×), and Z is the zoom factor (e.g., 1×). For example, if the minimum FWHM were 2 μm — as in the example above (step 10) — and we were using a 20×/0.8 dry objective (see step 3) to detect GFP with a BP 505–530 filter at a zoom of 1×, the pinhole diameter would be ~62 μm.

The formula to calculate the pinhole diameter in μm assumes a circular pinhole; however, some confocal microscopes have pinholes with other shapes, in which case the pinhole size calculated through the formula above must be multiplied by a shape factor (shape factor 1, or SF1, in Table 2.1). For example, if λ_{Em} were 0.5175 μm, n were 1, NA were 0.8, M_{Obj} were 20×, and Z were 1× the pinhole size of an Olympus FV3000 confocal microscope corresponding to a minimum FWHM of 2 μm would be ~70 μm, i.e. 62 μm times SF1 for Olympus FV3000 confocal microscopes (i.e. 1.1284; see Table 2. 1). Calculations are a little more complex for Leica confocal microscopes because the size of their square pinholes is given by the manufacturer as the side length expressed in Airy units (AU) for the fixed wavelength of 580 nm. As such, if λ_{Em} were 517.5 nm, n were 1, NA were 0.8, M_{Obj} were 20×, and Z were 1× the pinhole size of a Leica TCS-SP8 confocal microscope corresponding to a minimum FWHM of 2 μm would be:

$$\frac{PH_{(nm)} \times SF2 \times NA}{0.61 \times \lambda_{Em} \times M_{Obj} \times M_{Sys}}$$

Or 1.19 AU — Where $PH_{(nm)}$ is the pinhole diameter in nm (i.e. 56,000 nm), SF2 is the shape factor 2 for Leica TCS-SP8 confocal microscopes (i.e. 0.5642; see Table 2.1), λ_{Em} is 580 nm, and M_{Sys} is the system magnification for Leica TCS-SP8 confocal microscopes (i.e. 3.0×; see Table 2.1).

(12) Set the digital gain to 1.

The digital gain proportionally increases signal, background, and noise of the same amount, so it is rarely helpful.

Table 2.1. System Magnification (M_{Sys}), Pinhole (PH) Shape and Size Given, and Shape Factors (SFs) for Different Confocal Microscopes

Manufacturer Model	M_{Sys}	PH Shape and Size Given	SF1	SF2
Leica TCS SP2	3.6×	The size of the square pinhole is given as the side length expressed in AU for the fixed wavelength of 580 nm.	1.1284	0.5642
Leica TCS SP5 and TCS SP8	3.0×			
Zeiss LSM510	3.33×	The size of the circular pinhole is given as diameter expressed in μm.	1	0.5
Zeiss LSM700	1.53×	The size of the square pinhole is given as the side length expressed in μm.	1.1284	0.5642
Zeiss LSM710 and LSM780	1.9048×			
Zeiss LSM800	1.53×			
Zeiss LSM880	1.9048×			
Olympus FV300	3.426×	The size of the circular pinhole is given as 1–5 integers, which correspond to diameters of 60, 100, 150, 200, and 300 μm, respectively.	1	0.5
Olympus FV500	3.796×	The size of the square pinhole is given as the side length expressed in μm and referred to as "C.A.".	1.1284	0.5642
Olympus FV1000	3.82×			
Olympus FV3000	7.6×			
Nikon TE2000 E C1	1×[1]	The size of the circular pinhole is given as diameter expressed in μm.	1	0.5

Manufacturer Model	M_{Sys}	PH Shape and Size Given	SF1	SF2
Nikon Ti-E Perfect Focus A1R (a.k.a. A1 Plus)	1×	The size of the hexagonal pinhole is given as the largest diameter expressed in μm. The pinhole covers ~83% of the area of a circle with the same diameter.	0.91	0.455

[1] An optional 1.5× M_{Sys} is available but rarely used.

(13) Set the detector gain (a.k.a. smart gain) to ~50% of the maximum gain value.

Most detector manufacturers claim the signal-to-noise ratio of their detectors will fall below 2.7, which is the minimum acceptable value (Colarusso and Spring, 2003), only when the detector gain is set >2/3 of the maximum gain value. For example, if the maximum gain value for a given detector is 1,250 V, the signal-to-noise ratio would be <2.7 at gain values >838 V. However, we find that for most detectors the best signal-to-noise ratio is achieved at ≤50% of the maximum gain value, i.e. ≤625 V for a detector whose maximum gain value is 1,250 V.

(14) Dissect and mount the leaves or leaf primordia of one seedling according to Basic Protocols 3–5 and Support Protocol 4.

(15) Start scanning the sample in preview (a.k.a. live) mode and select a range indicator (a.k.a. HiLo or quick) LUT. This LUT will typically highlight saturated (i.e. white) pixels in red or blue and level-0 (i.e. black) pixels in blue or green, respectively (e.g., Fig. 2.6D).

(16) Adjust laser transmission so that saturated (e.g., red) pixels are no more than ~5% of the total amount of pixels in the region of interest (Fig. 2.6E). This means that in regions of no interest the proportion of saturated pixels may be >5% (Fig. 2.6E). If fluorescence will need to be quantified, keep the proportion of saturated pixels in the region of interest to ≤1% (Fig. 2.6F). If even with 100% laser transmission, it is impossible to reach 1–5% of saturated pixels, increase the detector gain up to 2/3 of the maximum value (e.g., up to ~833 V for a detector whose maximum gain value is 1,250 V).

(17) Lower the detector offset (a.k.a. smart offset) until the global background (i.e. the featureless region of your image) turns into the color that the LUT assigns to level-0 (e.g., blue) pixels, and then increase the offset just enough so that no pixels in the featureless region of your image are highlighted in the color that the LUT assigns to level-0 pixels (e.g., until the featureless region switched in color from uniform blue to uniform black) (Fig. 2.6G,H).

(18) Acquire the image. Alternatively:

(19) If acquiring a Z-stack, set its upper position. Set detector gain, laser transmission, and detector offset for the upper position (steps 13 and 15–17), and save the parameters in the Auto Z Brightness Correction or Linear Z Compensation window. Set the lower position of the stack. Set detector gain, laser transmission, and detector offset for the lower position (steps 13 and 15–17), and save the parameters in the Auto Z Brightness Correction or Linear Z Compensation window. Set the Z-interval to half the minimum FWHM (step 10). Acquire the image stack. During the scan procedure, the values of detector gain, laser transmission, and detector offset for any optical slice in the Z-stack will be automatically linearly interpolated as a function of depth from the values of the parameters at the upper and lower positions.

2.13 REAGENTS AND SOLUTIONS

2.13.1 0.5 M KOH

- 2.81 g of potassium hydroxide (e.g., EMD, cat. no. PX1480, cas no. 1310-58-3). Potassium hydroxide is corrosive and hygroscopic: wear personal protection equipment (safety glasses, lab coat, long pants, closed-toe shoes, and gloves)
- Bring volume to 100 ml with demineralized water
- Autoclave (121 °C, 20 min)
- Store indefinitely at room temperature.

2.13.2 70% Ethanol

- 30 ml demineralized water
- 70 ml 95% ethanol (e.g., Sigma-Aldrich, cat. no. 793183, cas no. 64-17-5)
- Store indefinitely at room temperature.

2.13.3 Sterilization Solution

- 8 ml demineralized water

- 2 ml bleach at 5.25% sodium hypochlorite (final concentration of sodium hypochlorite: ~1%)

- 5 μl Tween-20 (e.g., Sigma-Aldrich, cat. no. P2287, cas no. 9005-64-5) (final concentration: ~0.05%)

- Store for up to a month at room temperature in the dark or wrapped in aluminum foil.

2.14 COMMENTARY

2.14.1 Background Information

For the past 25 years, confocal microscopy has routinely been used in both plants and animals to monitor gene activation and protein expression by fusing promoters and genes to fluorescent proteins (e.g., (Imlau et al., 1999; Wang and Hazelrigg, 1994)). In plant leaves, for example, confocal microscopy of fluorescently tagged genes and proteins has been invaluable to visualize processes — such as cell polarization and tissue patterning — that are not characterized by overt changes in cell shape or size (e.g., (Bayer et al., 2009; Bilsborough et al., 2011; Caggiano et al., 2017; Robinson et al., 2011; Scarpella et al., 2006; Wenzel et al., 2007)). And yet a detailed procedure for confocal imaging of developing leaves has not been described.

Here we have provided a procedure for confocal imaging of first leaves and leaf primordia of Arabidopsis during normal development and upon perturbation by local application of the plant hormone auxin. A similar method can be used to apply other chemicals for local perturbation of leaf development, and the imaging procedure can be easily adapted to other leaves of Arabidopsis or to leaves of other plants. However, the procedure does require basic knowledge of confocal microscopy; for those unfamiliar with the fundamentals of optics and with the principles and biological applications of fluorescence, fluorescent proteins, and

confocal microscopy, we suggest, for example, (Born and Wolf, 2019; Pawley, 1995; Sluder and Wolf, 2007; Sullivan, 2008; Wilson and Sheppard, 1984).

By reconstructing sequences of events from images of different samples taken at different time points, a limitation of the imaging approach described here is that it only allows inferring — as opposed to observing — sequences of events. To overcome this limitation, we suggest time-lapse imaging (e.g., (Caggiano et al., 2021; Kierzkowski et al., 2019; Kuchen et al., 2012; Marcos and Berleth, 2014; Sawchuk et al., 2007a)), which is, however, more time-consuming. Because of the variability inherent in self-organizing processes such as cell polarization and tissue patterning (see (Xavier da Silveira Dos Santos and Liberali, 2019) for a recent review), we find that assessing reproducibility of events in those processes from fewer than 10 observations is problematic, and often more than 50 samples need to be inspected to uncover underlying patterns (e.g., (Donner et al., 2009; Sawchuk et al., 2013; Verna et al., 2019) (Chapter 3)). However, in our experience (Sawchuk et al., 2007), acquiring one time point a day for only 25 first leaves of Arabidopsis from 1 to 4 DAG requires four nearly whole days of time-lapse imaging. By contrast, imaging the same number of leaves for each of those four time points can easily be achieved in just ten hours with the procedure described here. We therefore suggest that the procedure described here can be used for routine imaging of developing leaves by confocal microscopy.

2.14.2 Critical Parameters and Troubleshooting

The protocols described here require basic wet laboratory skills, including the use of autoclaves; knowledge of how to work aseptically in laminar flow cabinets; and basic training in confocal and fluorescence microscopy. Furthermore, the protocols are designed for single-fluorophore imaging and assume the user has already optimized the light path for the excitation of the fluorescent protein in their sample and the detection of the fluorescence emitted by the excited fluorescent protein. Because all that knowledge is a prerequisite for the protocols described

here, we will not discuss the critical parameters of that prerequisite knowledge, the problems that derive from ignoring those parameters, or the solutions to those problems. Instead, in Table 2.2 we identify the critical parameters specific to the protocols described here; we report the most common problems that arise from failure to take those parameters into full account; and we suggest solutions to those problems.

2.14.3 Understanding Results

The development of Arabidopsis first leaves has been described previously in detail (Amalraj et al., 2020; Candela et al., 1999; Donnelly et al., 1999; Kang and Dengler, 2002; Kang and Dengler, 2004; Kinsman and Pyke, 1998; Larkin et al., 1996; Mattsson et al., 1999; Mattsson et al., 2003; Pyke et al., 1991; Telfer and Poethig, 1994) (Chapter 4). Briefly, at 1 DAG the first leaf is recognizable as a semi-spherical primordium (Fig. 2.6I). By 2 DAG, the primordium has elongated along the proximo-distal axis, and by 3 DAG it has expanded laterally (Fig. 2.6J,K). By 4 DAG, a lamina and a petiole have become recognizable, and by 6 DAG lateral outgrowths (hydathodes) have become recognizable in the lower quarter of the lamina (Fig. 2.6L,M). Leaf hairs (trichomes) and pores (stomata) can be first recognized at the tip of 3-DAG primordia, and their formation spreads toward the base of the, respectively, adaxial (dorsal) or abaxial (ventral) side of the lamina during leaf development. The formation of the midvein is followed by the formation of the first loops of veins ("first loops"), which in turn is followed by the formation of second loops and minor veins. Loops and minor veins differentiate in a tip-to-base sequence during leaf development.

Fig. 2.6I–M illustrate typical results obtained by imaging in first leaves and leaf primordia 1–4 DAG and 6 DAG expression of nuclear YFP driven by promoters mainly active in veins (Gardiner et al., 2011; Sawchuk et al., 2007; Sawchuk et al., 2013; Vanneste et al., 2011). To visualize YFP expression levels, the most commonly used LUTs (Fig. 2.6A–C) were applied in

Table 2.2. Troubleshooting Most Common Problems Derived From Ignoring Critical Parameters

Problem	Possible cause	Solution
Seeds fail to germinate or germinate poorly; seedlings grow slowly or are pale green	pH of plant growth medium is too low	Make sure pH of plant growth medium is no higher than 5.8 (Support Protocol 1, step 5)
	Seeds are too old, were harvested too early, or were not properly dried	Use freshly, timely harvested and properly dried seeds (Basic Protocol 1, Materials)
	Seed incubation in 70% ethanol or in sterilization solution was too long	Limit seed incubation in 70% ethanol to 1 min and in sterilization solution to 7 min (Basic Protocol 1, steps 3 and 4)
Seedlings wilt after IAA–lanolin paste application	Plates were open for too long during cotyledon removal or IAA–paste application	Close plates between cotyledon removal and IAA–lanolin paste application (Basic Protocol 2, step 5)
		Watch for early signs of seedling wilting (Basic Protocol 2, step 8)
		Process fewer than ~10 seedlings at a time (Basic

Problem	Possible cause	Solution
		Protocol 1, step 7; Basic Protocol 2, Materials)
Fewer than ~90% of the leaves respond to IAA–lanolin paste application or leaves fail to respond altogether	IAA–lanolin paste was insufficiently mixed during preparation	Mix IAA–lanolin paste more than three times during preparation (Support Protocol 3, step 4)
	Lanolin or IAA–lanolin paste was incubated at temperatures higher than 55 °C	Incubate lanolin or IAA–lanolin paste at temperatures no higher than 55 °C (Support Protocol 3, step 2)
	IAA–lanolin paste is older than one week	Use IAA–lanolin paste no older than one week (Support Protocol 3, step 5)
	Insufficient amount of IAA–lanolin paste was applied to leaves	Increase amount of applied IAA–lanolin paste (Fig. 2.2C)
Dissected leaves or leaf primordia fail to remain in position after mounting	Too much water was placed on microscope slide	Place no more than ~50 µl of water on microscope slide (Basic Protocol 3, step 1; Basic Protocol 4, step 1)
	Dissected leaves or leaf primordia were not positioned at edge of water drop	Position dissected leaves or leaf primordia at edge of water drop (Basic Protocol 3,

Problem	Possible cause	Solution
		step 6; Basic Protocol 4, step 6)
More than one (leaves or leaf primordia 4 DAG or younger) or two (leaves older than 4 DAG) focal planes are required to view the whole vein network	Too much water between the microscope slide and coverslip	Remove excess water by juxtaposing edge of lens paper strip to edge of coverslip while viewing sample through eyepieces or live camera (Support Protocol 4, step 3).
Leaves or leaf primordia have linear cuts (Fig. 2.5D)	Beveled side of needle was used to position leaves or leaf primordia during dissection	Avoid using beveled side of needle while positioning leaves or leaf primordia during dissection (Basic Protocol 3, step 3 and 6; Basic Protocol 4, step 6; Support Protocol 4, step 4)
Leaves or leaf primordia have circular wounds (Fig. 2.5E)	Tip of needle was used to position leaves or leaf primordia during dissection	Avoid using tip of needle while positioning leaves or leaf primordia during dissection (Basic Protocol 3, step 3 and 6; Basic Protocol 4, step 6; Support Protocol 4, step 4)

Problem	Possible cause	Solution
Vein loops are disconnected from midvein at basal end (Fig. 2.5F)	Too little water between microscope slide and coverslip	Place no less than ~50 µl of water on microscope slide (Basic Protocol 3, step 1) Add more water during mounting of dissected leaves (Basic Protocol 5, step 4)
	Dissected leaves dried up during mounting	Regularly monitor dissected leaves to make sure they never dry up. Should they start to do so, with syringe and needle, gently drag water from center of drop to edge, toward leaves or leaf primordia (Basic Protocol 3, step 6)
Signal emitted by non-vesicle-localized fluorescent protein coalesces in vesicles (Fig. 2.5H)	Leaves or leaf primordia were wounded during dissection	Avoid using beveled side or tip of needle while positioning leaves or leaf primordia during dissection (Basic Protocol 3, step 3 and 6; Basic Protocol 4, step 6; Support Protocol 4, step 4)

Problem	Possible cause	Solution
	Too little water between microscope slide and the coverslip	Place no less than 50 μl of water on microscope slide (Basic Protocol 3, step 1; Basic Protocol 4, step 1) Add more water during mounting of dissected leaves or leaf primordia (Basic Protocol 5, step 4)
	Too much time between mounting and imaging	Image dissected leaves and leaf primordia immediately after mounting (Support Protocol 4, step 6)
Too few saturated (e.g., red) pixels in region of interest	Insufficient laser transmission at ~50% detector gain	Increase laser transmission so that proportion of saturated (e.g., red) pixels in region of interest is no more than ~5% (Fig. 2.6E,G). If fluorescence needs to be quantified, keep proportion of saturated pixels in region of interest to no more than ~1% (Fig. 2.6F,H) (Basic Protocol 6, step 16)

Problem	Possible cause	Solution
	Insufficient detector gain at 100% laser transmission	Increase detector gain up to 2/3 of maximum value, so that proportion of saturated (e.g., red) pixels in region of interest is no more than ~5% (Fig. 2.6E,G). If fluorescence needs to be quantified, keep proportion of saturated pixels in region of interest to no more than 1% (Fig. 2.6F,H) (Basic Protocol 6, step 16)
Too many saturated (e.g., red) pixels in region of interest	Laser transmission is too high at 50% detector gain	Lower laser transmission so that proportion of saturated (e.g., red) pixels in region of interest is no more than ~5% (Fig. 2.6E,G). If fluorescence needs to be quantified, keep proportion of saturated pixels in region of interest to no more than 1% (Fig. 2.6F,H) (Basic Protocol 6, step 16)
	Detector gain is too high at 0.2% laser transmission	Lower detector gain, so that proportion of saturated (e.g., red) pixels in region of

Problem	Possible cause	Solution
		interest is no more than ~5% (Fig. 2.6E,G). If fluorescence needs to be quantified, keep proportion of saturated pixels in region of interest to no more than 1% (Fig. 2.6F,H) (Basic Protocol 6, step 16)
Too many level-0 (e.g., blue) pixels in featureless regions of image (Fig. 2.6E,F)	Detector offset is too low	Increase detector offset just enough so that no pixels in featureless regions of image are highlighted in color LUT assigns to level-0 pixels (e.g., until featureless regions switch in color from uniform blue to uniform black) (Fig. 2.6G,H) (Basic Protocol 6, step 17)

Problem	Possible cause	Solution
No level-0 (e.g., blue) pixels in featureless regions of image	Detector offset is too high	Lower detector offset until featureless regions of image turn into color that LUT assigns to level-0 pixels (e.g., blue), and then increase offset just enough so that no pixels in featureless regions of image are highlighted in color that LUT assigns to level-0 pixels (e.g., until featureless regions switch in color from uniform blue to uniform black) (Fig. 2.6G,H) (Basic Protocol 6, step 17)

the Fiji distribution (Schindelin et al., 2012) of ImageJ (Rueden et al., 2017; Schindelin et al., 2015; Schneider et al., 2012).

Fig. 2.6C illustrates typical results obtained by imaging in a 4-DAG first leaf expression of ER-localized GFP (erGFP) driven by a vein-specific enhancer (Amalraj et al., 2020) (Chapter 4).

Fig. 2.2D illustrates typical results obtained by imaging expression of erGFP driven by a vein-specific enhancer (Amalraj et al., 2020) (Chapter 4) 2.5 days after local application of IAA–lanolin paste. Approximately 90% of the leaves respond to the application by forming veins that connect the site of paste application to pre-existing veins basally to the application site (Sawchuk et al., 2007; Scarpella et al., 2006; Verna et al., 2019) (Chapter 5).

Results of course depend on the strength and specificity of the promoter used to drive fluorescent protein expression, and on the fluorescent protein used and its cellular localization. In the Fiji distribution of ImageJ, maximum-intensity projection can be applied to image stacks before LUT application, and brightness and contrast can be adjusted by linear stretching of the histogram. For ethical image processing, see, for example, (Cromey, 2010; Martin and Blatt, 2013; North, 2006; Rossner and Yamada, 2004).

2.14.4 Time Considerations

It will take ~30 min to prepare plant growth medium according to Support Protocol 1, and it will take an additional ~30 min for medium sterilization. It will take ~15 min at room temperature for freshly autoclaved or microwaved medium (Support Protocol 2, step 1) to cool to ~60 °C, and it will take ~1.5 hours in a 60°C incubator for freshly autoclaved or microwaved medium to cool to ~60 °C.

It will take ~1 hour for an inexperienced user to sterilize four tubes of seeds, prepare medium plates, and sow sterilized seeds according to Support Protocol 2 and Basic Protocol 1. Medium can be microwaved during seed incubation in sterilization solution (Basic Protocol 1,

step 4), and plates can be prepared between washing steps (Basic Protocol 1, step 6). An experienced user will be able to process two or three times as many tubes of seeds in the same time. Seed stratification (Basic Protocol 1, step 9) will take 2–5 days, and seed germination and seedling growth will take an additional 1–6 days, depending on the time point of interest.

Preparation of the IAA–lanolin paste (Support Protocol 3) will take ~1 hour. It will take ~1 hour for an inexperienced user to apply the paste (Basic Protocol 2) to 10 seedlings. An experienced user will be able to process two or three times as many seedlings in the same time.

Confocal time is expensive; the limiting step to acquiring informative confocal images is the quality of sample dissection and mounting; and dissecting and mounting first leaves and leaf primordia 6-, 4-, 2-, 1-, and 3-DAG is progressively more difficult. Therefore, as mentioned in the Strategic Planning section and illustrated in detail in Fig. 2.1, we recommend that an inexperienced user starts by dissecting and mounting 6-DAG leaves (Basic Protocols 3 and 5) and by assessing their proficiency at dissecting and mounting those leaves (Support Protocol 4) before imaging same-stage leaves by confocal microscopy (Basic Protocol 6). In our experience, it will take at least three 2-hour sessions — but in some cases as many as 10 such sessions — for an inexperienced user to produce dissected and mounted 6-DAG leaves of sufficient quality for confocal imaging. In each of those 2-hour sessions, an inexperienced user will be able to dissect and mount, and will be able to assess the quality of dissection and mounting of, ~10–20 6-DAG leaves. Once the quality of dissection and mounting of 6-DAG leaves is deemed to be of sufficient quality, an inexperienced user will be able to image ~10 6-DAG leaves by confocal microscopy in ~2 hours. An experienced user will be able to image twice as many 6-DAG leaves in the same time.

Once a user has become proficient at confocal imaging of 6-DAG leaves, they will be able to move to confocal imaging of 4-DAG leaves by repeating for 4-DAG leaves the sequence of steps described above for 6-DAG leaves (Basic Protocols 3 and 5, and Support Protocol 4, followed by Basic Protocols 3, 5, and 6). Dissecting and mounting 4-DAG leaves is more difficult

— and therefore more time consuming — than dissecting and mounting 6-DAG leaves. However, by the time the user will start dissecting and mounting 4-DAG leaves, they will have become proficient at dissecting and mounting 6-DAG leaves. Therefore, to become proficient at dissecting and mounting 4-DAG leaves, it will take a user a number of 2-hour sessions similar to that which it took them to become proficient at dissecting and mounting 6-DAG leaves. Likewise, the user will be able to dissect and mount, and will be able to assess the quality of dissection and mounting of, ~10−20 4-DAG leaves in each of those 2-hour sessions. And as for confocal imaging of 6-DAG leaves, once the quality of dissection and mounting of 4-DAG leaves is deemed to be of sufficient quality, an inexperienced user will be able to image ~10 4-DAG leaves by confocal microscopy in ~2 hours; an experienced user will be able to image twice as many 4-DAG leaves in the same amount of time.

Finally, once a user has become proficient at confocal imaging of 4-DAG leaves, they will be able to progressively move to confocal imaging of 2-, 1-, and 3-DAG leaf primordia by repeating a sequence of steps similar to that described above for 6- and 4-DAG leaves — i.e. Basic Protocols 4 and 5, and Support Protocol 4, followed by Basic Protocols 4−6. To become proficient at confocal imaging of 2-, 1-, and 3-DAG leaf primordia, it will take a user an amount of time similar to that which it took them to become proficient at confocal imaging of 6- and 4-DAG leaves.

Chapter 3: Coordination of Tissue Cell Polarity by Auxin Transport and Signaling[1]

3.1 INTRODUCTION

How the polarity of cells in a tissue is coordinated is a central question in biology. In animals, the coordination of this tissue cell polarity requires direct cell–cell communication and often cell movements (Goodrich and Strutt, 2011), both of which are precluded in plants by a wall that holds cells apart and in place; therefore, tissue cell polarity is coordinated differently in plants.

The formation of plant veins is an expression of such coordination of tissue cell polarity; this is most evident in developing leaves. Consider, for example, the formation of the midvein at the center of the cylindrical leaf primordium. Initially, the plasma-membrane (PM)-localized PIN-FORMED1 (PIN1) protein of Arabidopsis (Galweiler et al., 1998), which catalyzes cellular efflux of the plant hormone auxin (Petrásek et al., 2009), is expressed in all the inner cells of the leaf primordium; over time, however, PIN1 expression becomes gradually restricted to the file of cells that will form the midvein (Bayer et al., 2009; Benkova et al., 2003; Heisler et al., 2005; Reinhardt et al., 2003; Scarpella et al., 2006; Verna et al., 2015; Wenzel et al., 2007). PIN1 localization at the PM of the inner cells is initially isotropic, but as PIN1 expression becomes restricted to the site of midvein formation, PIN1 localization becomes polarized: in the cells surrounding the developing midvein, PIN1 localization gradually changes from isotropic to medial — i.e. toward the developing midvein — to mediobasal; in the cells of the developing midvein, PIN1 becomes uniformly localized toward the base of the leaf primordium, where the midvein will connect to the pre-existing vasculature.

---

[1] Adapted from Verna, C., Ravichandran, S. J., Sawchuk, M. G., Linh, N. M. and Scarpella, E. (2019). Coordination of Tissue Cell Polarity by Auxin Transport and Signaling. Elife 8, e51061.

The correlation between coordination of tissue cell polarity, as expressed by the coordination of PIN1 polar localization between cells; polar auxin transport, as expressed by the auxin-transport-polarity-defining localization of PIN1 (Wisniewska et al., 2006); and vein formation does not seem to be coincidental. Auxin application to developing leaves induces the formation of broad expression domains of isotropically localized PIN1; such domains become restricted to the sites of auxin-induced vein formation, and PIN1 localization becomes polarized toward the pre-existing vasculature (Scarpella et al., 2006). Both the restriction of PIN1 expression domains and the polarization of PIN1 localization are delayed by chemical inhibition of auxin transport (Scarpella et al., 2006; Wenzel et al., 2007), which induces vein pattern defects similar to, though stronger than, those of *pin1* mutants (Mattsson et al., 1999; Sawchuk et al., 2013; Sieburth, 1999). Therefore, available evidence suggests that auxin coordinates tissue cell polarity to induce vein formation, and that the coordinative and inductive property of auxin depends on the function of *PIN1* and possibly other *PIN* genes.

How auxin coordinates tissue cell polarity to induce vein formation is unclear, but the current hypothesis is that the GNOM (GN) guanine-nucleotide exchange factor for ADP-ribosylation-factor GTPases, which regulates vesicle formation in membrane trafficking, controls the cellular localization of PIN1 and possibly other auxin transporters. The resulting cell-to-cell, polar transport of auxin would coordinate tissue cell polarity and control developmental processes such as vein formation (reviewed in, e.g., (Berleth et al., 2000; Linh et al., 2018; Nakamura et al., 2012; Richter et al., 2010); (Chapter 1)). Here I tested this hypothesis by a combination of cellular imaging, molecular genetic analysis, and chemical inhibition. Contrary to predictions of the hypothesis, I found that auxin-induced vein formation occurs in the absence of auxin transport and that the residual auxin-transport-independent vein-patterning activity relies on auxin signaling. I suggest that a *GN*-dependent tissue-cell-polarizing signal acts upstream of both auxin transport and signaling.

3.2 RESULTS

3.2.1 Testable Predictions of the Current Hypothesis of Coordination of Tissue Cell Polarity by Auxin

The current hypothesis of how auxin coordinates tissue cell polarity to induce vein formation proposes that GN controls the cellular localization of PIN1 and possibly other auxin transporters; the resulting cell-to-cell, polar transport of auxin would coordinate tissue cell polarity and control developmental processes such as vein formation (reviewed in, e.g., (Berleth et al., 2000; Linh et al., 2018; Nakamura et al., 2012; Richter et al., 2010); (Chapter 1)). The hypothesis makes three testable predictions:

(1) The restriction of PIN1 expression domains and coordination of PIN1 polar localization that normally occur during vein formation (Bayer et al., 2009; Benkova et al., 2003; Marcos and Berleth, 2014; Reinhardt et al., 2003; Sawchuk et al., 2013; Scarpella et al., 2006; Verna et al., 2015; Wenzel et al., 2007) will occur abnormally, or will fail to occur altogether, during *gn* leaf development;

(2) Were the defects in coordination of tissue cell polarity of *gn* the sole result of loss of polar auxin-transport, auxin transport inhibition would lead to defects in coordination of tissue cell polarity that approximate those of *gn*;

(3) Were the defects in coordination of tissue cell polarity of *gn* the result of abnormal polarity of auxin transport, they would depend on auxin transport; therefore, auxin transport inhibition should induce defects in *gn* that approximate those which it induces in WT.

Here I tested these predictions.

3.2.2 Testing Prediction 1: Restriction of PIN1 Expression Domains and Coordination of PIN1 Polar Localization Occur Abnormally, or Fail to Occur Altogether, During *gn* Leaf Development

I tested this prediction by imaging expression domains of PIN1::PIN1:YFP (PIN1:YFP fusion protein expressed by the *PIN1* promoter (Xu et al., 2006)) and cellular localization of expression of PIN1::PIN1:GFP (Benkova et al., 2003) during leaf development in WT and in the new strong allele *gn-13* (Table 3.1).

In Arabidopsis leaf development, the formation of the midvein precedes the formation of the first loops of veins ("first loops"), which in turn precedes the formation of the second loops (Fig. 3.1A–C) (Kang and Dengler, 2004; Mattsson et al., 1999; Sawchuk et al., 2007; Scarpella et al., 2004; Sieburth, 1999). The formation of second loops precedes the formation of third loops and that of minor veins in the area delimited by the midvein and the first loops (Fig. 3.1C,D). Loops and minor veins form first near the top of the leaf and then progressively closer to its bottom, and minor veins form after loops in the same area of the leaf (Fig. 3.1B–E).

Consistent with previous reports (Bayer et al., 2009; Benkova et al., 2003; Heisler et al., 2005; Marcos and Berleth, 2014; Reinhardt et al., 2003; Sawchuk et al., 2013; Scarpella et al., 2006; Verna et al., 2015; Wenzel et al., 2007), in WT leaves PIN1::PIN1:YFP was expressed in all the cells at early stages of tissue development (Fig. 3.1F–J). Over time, epidermal expression became restricted to the basalmost cells, and inner tissue expression became restricted to developing veins (Fig. 3.1F–J).

In *gn* leaves too, PIN1::PIN1:YFP was expressed in all the cells at early stages of tissue development, and over time epidermal expression became restricted to the basalmost cells; however, inner tissue expression failed to become restricted to developing veins and remained nearly ubiquitous even at very late stages of leaf development (Fig. 3.1K–O).

Table 3.1. Origin and Nature of Lines

Line	Origin/Nature
PIN1::PIN1:YFP	(Xu et al., 2006)
gn-13	SALK_045424 (ABRC[1]); (Alonso et al., 2003); contains a T-DNA insertion after +2835[2] of GN (AT1G13980)
PIN1::PIN1:GFP	(Benkova et al., 2003)
van7/emb30-7 (gn[van7])	(Koizumi et al., 2000)
tir1-1;afb2-3	(Savaldi-Goldstein et al., 2008)

[1] Arabidopsis Biological Resource Center

[2] Gene coordinates are relative to the adenine (position +1) of the start codon
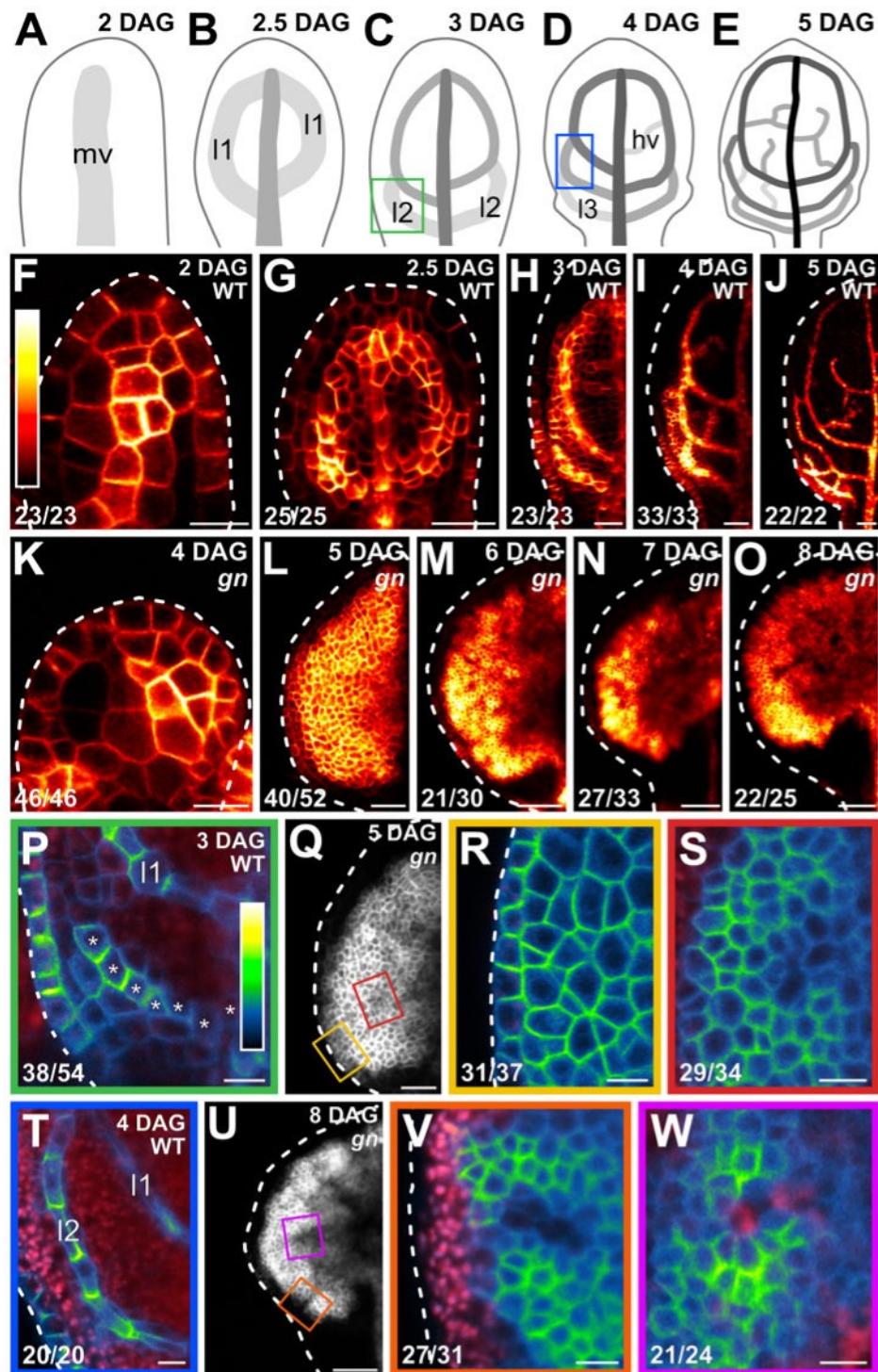
Figure 3.1. PIN1 Expression and Localization During *gn* Leaf Development

(A–Q,T,U) Top right: leaf age in days after germination (DAG). (A–E) Veins form sequentially during Arabidopsis leaf development: the formation of the midvein (mv) is followed by the

formation of the first loops of veins ("first loops"; l1), which in turn is followed by the formation of second loops (l2) and minor veins (hv) (Kang and Dengler, 2004; Mattsson et al., 1999; Scarpella et al., 2004; Sieburth, 1999). Loops and minor veins differentiate in a tip-to-base sequence during leaf development. Increasingly darker grays depict progressively later stages of vein development. Boxes in C and D illustrate positions of closeups in P and T. l3: third loop. (F–W) Confocal laser scanning microscopy. First leaves. For simplicity, only half-leaves are shown in H–J and L–O. Dashed white line in F–R and T–V delineates leaf outline. (F–Q,T,U) Top right: genotype. (F–P,R–T,V,W) Bottom left: reproducibility index. (F–O) PIN1::PIN1:YFP expression; look-up table (ramp in F) visualizes expression levels. (P,R–T,V,W) PIN1::PIN1:GFP expression; look-up table (ramp in P) visualizes expression levels. Red: autofluorescence. Stars in P label cells of the developing second loop. (Q,U) PIN1::PIN1:YFP expression. Boxes in Q and in U illustrate positions of closeups in R and S, and in V and W, respectively. Bars: (F,P,R–T,V,W) 10 µm; (G,I,L,Q) 30 µm; (H,K) 20 µm; (J,M–O,U) 60 µm.

Consistent with previous reports (Bayer et al., 2009; Benkova et al., 2003; Heisler et al., 2005; Marcos and Berleth, 2014; Reinhardt et al., 2003; Sawchuk et al., 2013; Scarpella et al., 2006; Verna et al., 2015; Wenzel et al., 2007), in the cells of the second loop at early stages of its development in WT leaves, PIN1::PIN1:GFP expression was mainly localized to the side of the plasma membrane (PM) facing the midvein; in the inner cells flanking the developing loop, PIN1::PIN1:GFP expression was mainly localized to the side of the PM facing the developing loop; and in the inner cells further away from the developing loop, PIN1::PIN1:GFP expression was localized isotropically at the PM (Fig. 3.1C,P). At later stages of second-loop development, by which time PIN1::PIN1:GFP expression had become restricted to the cells of the developing loop, PIN1::PIN1:GFP expression was localized to the side of the PM facing the midvein (Fig. 3.1D,T).

At early stages of development of the tissue that in *gn* leaves corresponds to that from which the second loop forms in WT leaves, PIN1::PIN1:GFP was expressed uniformly in the outermost inner tissue, and expression was localized isotropically at the PM (Fig. 3.1Q,R). PIN1::PIN1:GFP was expressed more heterogeneously in the innermost inner tissue, but expression remained localized isotropically at the PM, except in cells near the edge of higher-expression domains: in those cells, localization of PIN1::PIN1:GFP expression at the PM was weakly polar, but such weak cell polarities pointed in seemingly random directions (Fig. 3.1Q,S).

At late stages of *gn* leaf development, heterogeneity of PIN1::PIN1:GFP expression had spread to the outermost inner tissue, but expression remained localized isotropically at the PM, except in cells near the edge of higher-expression domains: in those cells, localization of PIN1::PIN1:GFP expression at the PM was weakly polar, but such weak cell polarities pointed in seemingly random directions (Fig. 3.1U,V). Heterogeneity of PIN1::PIN1:GFP expression in the innermost inner tissue had become more pronounced at late stages of *gn* leaf development, and the weakly polar localization of PIN1::PIN1:GFP expression at the PM had spread to the center

of the higher-expression domains (Fig. 3.1U,W); nevertheless, such weak cell polarities still pointed in seemingly random directions (Fig. 3.1U,W).

In conclusion, both restriction of PIN1 expression domains and coordination of PIN1 polar localization occur only to a very limited extent or fail to occur altogether during *gn* leaf development, which is consistent with the current hypothesis of how auxin coordinates tissue cell polarity to induce vein formation.

3.2.3 Testing Prediction 2: Auxin Transport Inhibition Leads to Defects in Coordination of Tissue Cell Polarity That Approximate Those of *gn*

To test this prediction, I imaged cellular localization of PIN1::PIN1:GFP expression during leaf development of WT, *gn-13*, and WT grown in the presence of N-1-naphthylphthalamic acid (NPA), which inhibits cellular auxin efflux (Cande and Ray, 1976; Katekar and Geissler, 1980; Sussman and Goldsmith, 1981).

Consistent with previous reports (Bayer et al., 2009; Benkova et al., 2003; Heisler et al., 2005; Marcos and Berleth, 2014; Reinhardt et al., 2003; Sawchuk et al., 2013; Scarpella et al., 2006; Verna et al., 2015; Wenzel et al., 2007), and as shown above (Fig. 3.1P,T), in the cells of the second loop at early stages of its development in WT leaves, PIN1::PIN1:GFP expression was mainly localized to the side of the PM facing the midvein; in the inner cells flanking the developing loop, PIN1::PIN1:GFP expression was mainly localized to the side of the PM facing the developing loop; and in the inner cells further away from the developing loop, PIN1::PIN1:GFP expression was localized isotropically at the PM (Fig. 3.2B). At later stages of second-loop development, by which time PIN1::PIN1:GFP expression had become restricted to the cells of the developing loop, PIN1::PIN1:GFP expression was localized to the side of the PM facing the midvein (Fig. 3.2F).

As shown above (Fig. 3.1Q,R), at early stages of development of the outermost inner tissue in the bottom half of *gn* leaves, PIN1::PIN1:GFP was expressed uniformly, and expression
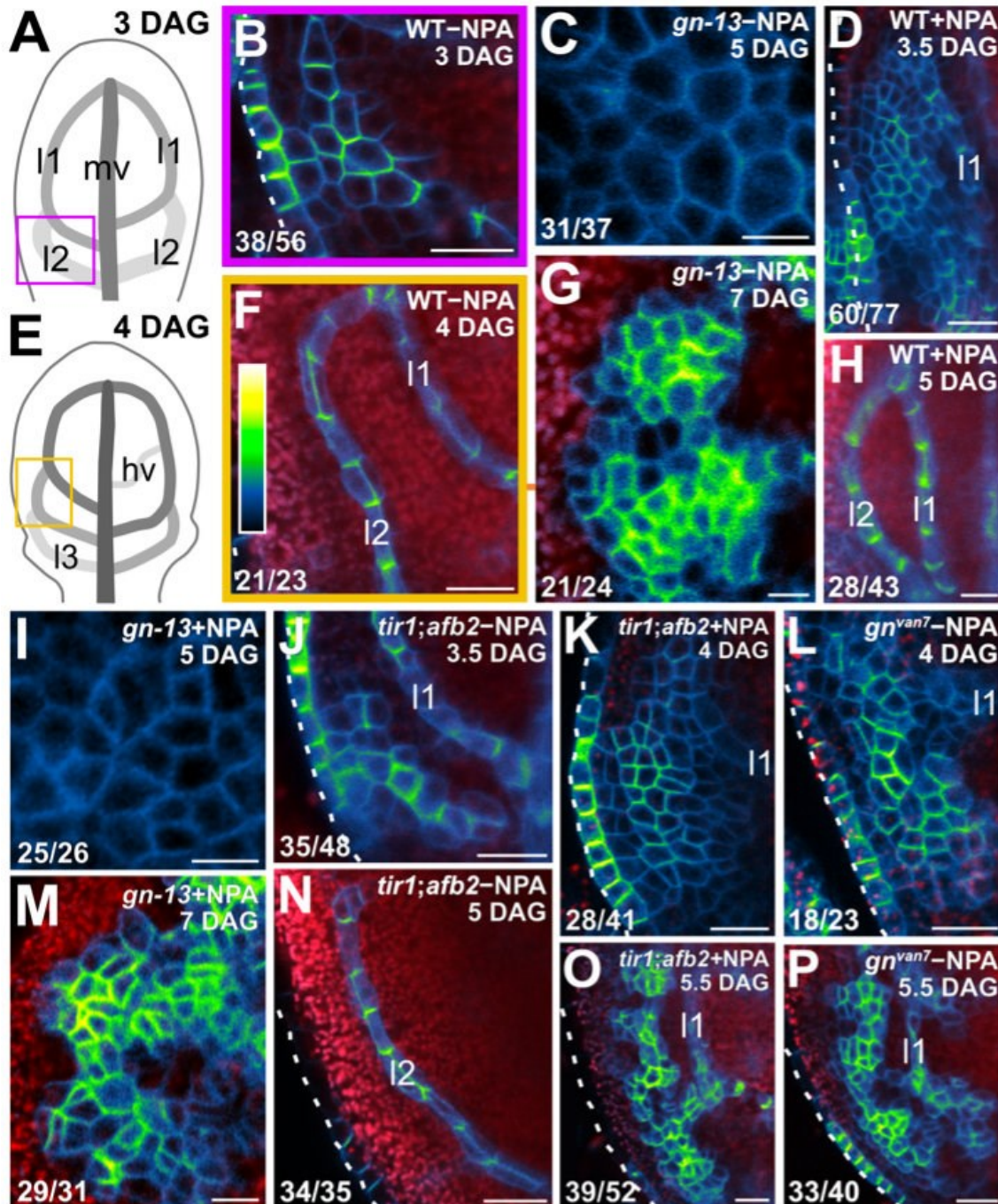
Figure 3.2. Auxin-Transport- and Auxin-Signaling-Dependent Coordination of PIN1 Localization in *gn* Developing Leaves

(A,E) Increasingly darker grays depict progressively later stages of vein development. Boxes illustrate positions of closeups in B and F, respectively. hv: minor vein; l1, l2 and l3: first, second

and third loops; mv: midvein. (B−D,F−P) Confocal laser scanning microscopy. First leaves. Top right: genotype, treatment and leaf age in days after germination (DAG). Dashed white line delineates leaf outline. Bottom left: reproducibility index. PIN1::PIN1:GFP expression; look-up table (ramp in F) visualizes expression levels. Red: autofluorescence. (N) 24/35 of second loops failed to connect to the first loop. Bars: (B,D,F,H,J−L,N−P) 20 μm; (C,G,I,M) 10 μm.

was localized isotropically at the PM (Fig. 3.2C). As also shown above (Fig. 3.1U,W), at late stages development of the innermost inner tissue in the bottom half of *gn* leaves, PIN1::PIN1:GFP was expressed heterogeneously; localization of expression at the PM was weakly polar, but such weak cell polarities pointed in seemingly random directions (Fig. 3.2G).

Consistent with previous reports (Scarpella et al., 2006; Wenzel et al., 2007), and as in *gn* (Fig. 3.1Q–S; Fig 3.2C,G), PIN1::PIN1:GFP expression domains were broader at early stages of development of the tissue that in NPA-grown WT corresponds to that from which the second loop forms in WT; PIN1::PIN1:GFP expression was localized isotropically at the PM in the outermost inner cells but was mainly localized to the basal side of the PM in the innermost inner cells (Fig. 3.2D). At later stages of second-loop development in NPA-grown WT, by which time PIN1::PIN1:GFP expression had become restricted to the cells of the developing loop, PIN1::PIN1:GFP expression was localized to the basal side of the PM (Fig. 3.2H).

In conclusion, auxin transport inhibition leads to defects in coordination of tissue cell polarity that are qualitatively different and quantitatively weaker than those of *gn*. As such, my results fail to support Prediction 2 of the current hypothesis of how auxin coordinates tissue cell polarity, a conclusion that is also independently suggested by the finding that auxin transport inhibition fails to lead to defects that fall within the vein phenotype spectrum of *gn* (Verna et al., 2019).

3.2.4 Testing Prediction 3: Auxin Transport Inhibition Induces in *gn* Defects in Coordination of Tissue Cell Polarity That Approximate Those Which Auxin Transport Inhibition Induces in WT

To test this prediction, I imaged cellular localization of PIN1::PIN1:GFP expression during leaf development of NPA-grown *gn-13* and compared it with that of NPA-grown WT and of *gn-13* grown under normal conditions.

Consistent with previous observations (Verna et al., 2019), and as in normally grown *gn* (Fig. 3.1Q,R; Fig. 3.2C) and NPA-grown WT (Fig. 3.1D), at early stages of development of the outermost inner tissue in the bottom half of NPA-grown *gn* leaves, PIN1::PIN1:GFP was expressed uniformly, and expression was localized isotropically at the PM (Fig. 3.2I). As also in normally grown *gn* (Fig. 3.1U,W; Fig. 3.2G) — but unlike NPA-grown WT (Fig. 3.1H) — at late stages development of the innermost inner tissue in the bottom half of NPA-grown *gn* leaves, PIN1::PIN1:GFP was expressed heterogeneously; localization of expression at the PM was weakly polar, but such weak cell polarities pointed in seemingly random directions (Fig. 3.2M).

In conclusion, auxin transport inhibition fails to induce in *gn* defects in coordination of tissue cell polarity that approximate those which auxin transport inhibition induces in WT. Therefore, my results also fail to support Prediction 3 of the current hypothesis of how auxin coordinates tissue cell polarity to induce vein formation, a conclusion that is also independently suggested by the finding that auxin transport inhibition fails to induce in *gn* vascular defects that approximate those which auxin transport inhibition induces in WT (Verna et al., 2019). Consequently, the hypothesis must be revised.

3.2.5 Revising the Current Hypothesis of Coordination of Tissue Cell Polarity and Vein Formation by Auxin

Auxin-transport-inhibited leaves respond to vein-formation-inducing auxin signals (Verna et al., 2019), suggesting that the residual vein-patterning activity in those leaves may be supplied by an auxin-dependent mechanism. Because vein formation is an expression of coordination of tissue cell polarity (reviewed in (Linh et al., 2018); (Chapter 1)), the residual tissue-cell polarizing activity in auxin-transport-inhibited leaves may also be supplied by an auxin-dependent mechanism. To test this possibility, I asked what the contribution of auxin signaling were to coordination of tissue cell polarity in the absence of auxin transport. To address this question, I used double mutants in *TRANSPORT INHIBITOR RESPONSE1* (*TIR1*) and *AUXIN*

SIGNALING F-BOX2 (*AFB2*), which lack the two auxin receptors that most contribute to auxin signaling (Dharmasiri et al., 2005).

As in WT (Fig. 3.1P; Fig. 3.2B), in the cells of the second loop at early stages of its development in *tir1*;*afb2* leaves, PIN1::PIN1:GFP expression was mainly localized to the side of the PM facing the midvein; in the inner cells flanking the developing loop, PIN1::PIN1:GFP expression was mainly localized to the side of the PM facing the developing loop; and in the inner cells further away from the developing loop, PIN1::PIN1:GFP expression was localized isotropically at the PM (Fig. 3.2J).

As also in WT (Fig. 3.1T; Fig. 3.2F), at later stages of second-loop development in *tir1*;*afb2* leaves, by which time PIN1::PIN1:GFP expression had become restricted to the cells of the developing loop, PIN1::PIN1:GFP expression was localized to the side of the PM facing the midvein (Fig. 3.2N). However, in *tir1*;*afb2* stages of second-loop development comparable to those in WT appeared at later stages of leaf development, and most of the second loops failed to connect to the first loop (Fig. 3.2J,N).

As in NPA-grown WT (Fig. 3.2D), in NPA-grown *tir1*;*afb2* PIN1::PIN1:GFP expression domains were broader at early stages of development of the tissue that corresponds to that from which the second loop forms in WT, but PIN1::PIN1:GFP was expressed more heterogeneously in NPA-grown *tir1*;*afb2* than in NPA-grown WT (Fig. 3.2D,K). Nevertheless, as in NPA-grown WT (Fig. 3.2D), in NPA-grown *tir1*;*afb2* PIN1::PIN1:GFP expression remained localized isotropically at the PM, except in cells near the edge of higher-expression domains: in those cells, localization of PIN1::PIN1:GFP expression at the PM was weakly polar, but such weak cell polarities pointed in seemingly random directions (Fig. 3.2K).

Unlike in NPA-grown WT (Fig. 3.2H), at later stages of second-loop development of NPA-grown *tir1*;*afb2*, heterogeneity of PIN1::PIN1:GFP expression had become more pronounced, and PIN1::PIN1:GFP expression had become restricted to narrow clusters of cells;

in those cells, localization of PIN1::PIN1:GFP expression at the PM was weakly polar, but such weak cell polarities still pointed in seemingly random directions (Fig. 3.2O).

In conclusion, as in vein patterning (Verna et al., 2019), the residual tissue-cell polarizing activity in auxin-transport-inhibited leaves is supplied by auxin signaling.

I finally asked whether simultaneous defects in auxin transport and signaling recapitulated *gn* defects in coordination of tissue cell polarity. To address this question, I imaged cellular localization of PIN1::PIN1:GFP expression during leaf development in the intermediate allele *gn^{van7}* (Koizumi et al., 2000) and compared it with that in NPA-grown *tir1*;*afb2*.

As in NPA-grown *tir1*;*afb2* (Fig. 3.2K), in *gn* PIN1::PIN1:GFP expression domains were broader and PIN1::PIN1:GFP was expressed more heterogeneously at early stages of development of the tissue that corresponds to that from which the second loop forms in WT (Fig. 3.2L). Furthermore, as in NPA-grown *tir1*;*afb2* (Fig. 3.2K), in *gn* PIN1::PIN1:GFP expression remained localized isotropically at the PM, except in cells near the edge of higher-expression domains: in those cells, localization of PIN1::PIN1:GFP expression at the PM was weakly polar, but such weak cell polarities pointed in seemingly random directions (Fig. 3.2L).

As also in NPA-grown *tir1*;*afb2* (Fig. 3.2O), at later stages of second-loop development of *gn*, heterogeneity of PIN1::PIN1:GFP expression had become more pronounced, and PIN1::PIN1:GFP expression had become restricted to narrow clusters of cells; in those cells, localization of PIN1::PIN1:GFP expression at the PM was weakly polar, but such weak cell polarities still pointed in seemingly random directions (Fig. 3.2P).

In conclusion, simultaneous defects in auxin transport and signaling recapitulate *gn* defects in coordination of PIN1 polar localization, suggesting that the defects in coordination of tissue cell polarity of *gn* are caused by simultaneous defects in auxin transport and signaling. This conclusion is consistent with the finding that the vein pattern defects of *gn* are caused by simultaneous defects in auxin transport and signaling (Verna et al., 2019).

3.3 DISCUSSION

The current hypothesis of how auxin coordinates tissue cell polarity to induce vein formation proposes that GN controls the cellular localization of PIN1 and other PIN proteins; the resulting cell-to-cell, polar transport of auxin would coordinate tissue cell polarity and control developmental processes such as vein formation (reviewed in, e.g., (Berleth et al., 2000; Linh et al., 2018; Nakamura et al., 2012; Richter et al., 2010)).

Contrary to predictions of the hypothesis, I found that tissue cell polarity is coordinated in the absence of auxin transport and that the residual auxin-transport-independent tissue-cell polarizing activity relies on auxin signaling. The defects in coordination of tissue cell polarity of leaves in which both auxin transport and signaling are compromised are never observed in leaves in which either process is; yet those defects are not unprecedented: they are observed, though in more extreme form, in leaves of *gn* mutants, suggesting that a *GN*-dependent signal coordinates tissue cell polarity upstream of both auxin transport and signaling (Fig. 3.3).

That *GN* controls auxin transport during vein patterning is also suggested by the very limited or altogether missing restriction of PIN1 expression domains and coordination of PIN1 polar localization during *gn* leaf development, which is consistent with observations in embryos and roots (Kleine-Vehn et al., 2008; Steinmann et al., 1999). However, if failure to coordinate the polar localization of PIN1, and possibly other PIN proteins, were the sole cause of the vein pattern defects of *gn*, these defects would depend on *PIN* function and would therefore be masked by those of *pin1,3,6;4;7;8*, which lacks the function of all the *PIN* genes with vein patterning function (Verna et al., 2019), in the *gn*;*pin1,3,6;4;7;8* mutant. The epistasis of the vein pattern defects of *gn* to those of *pin1,3,6;4;7;8* and the inability of NPA, which phenocopies the vein pattern defects of *pin1,3,6;4;7;8* (Verna et al., 2019), to induce additional defects in *gn* instead suggest that the vein pattern defects of *gn* are independent of all the *PIN* genes with vein patterning function, that *GN* acts upstream of all the *PIN* genes in vein patterning, and that the

Figure 3.3. Interpretation Summary
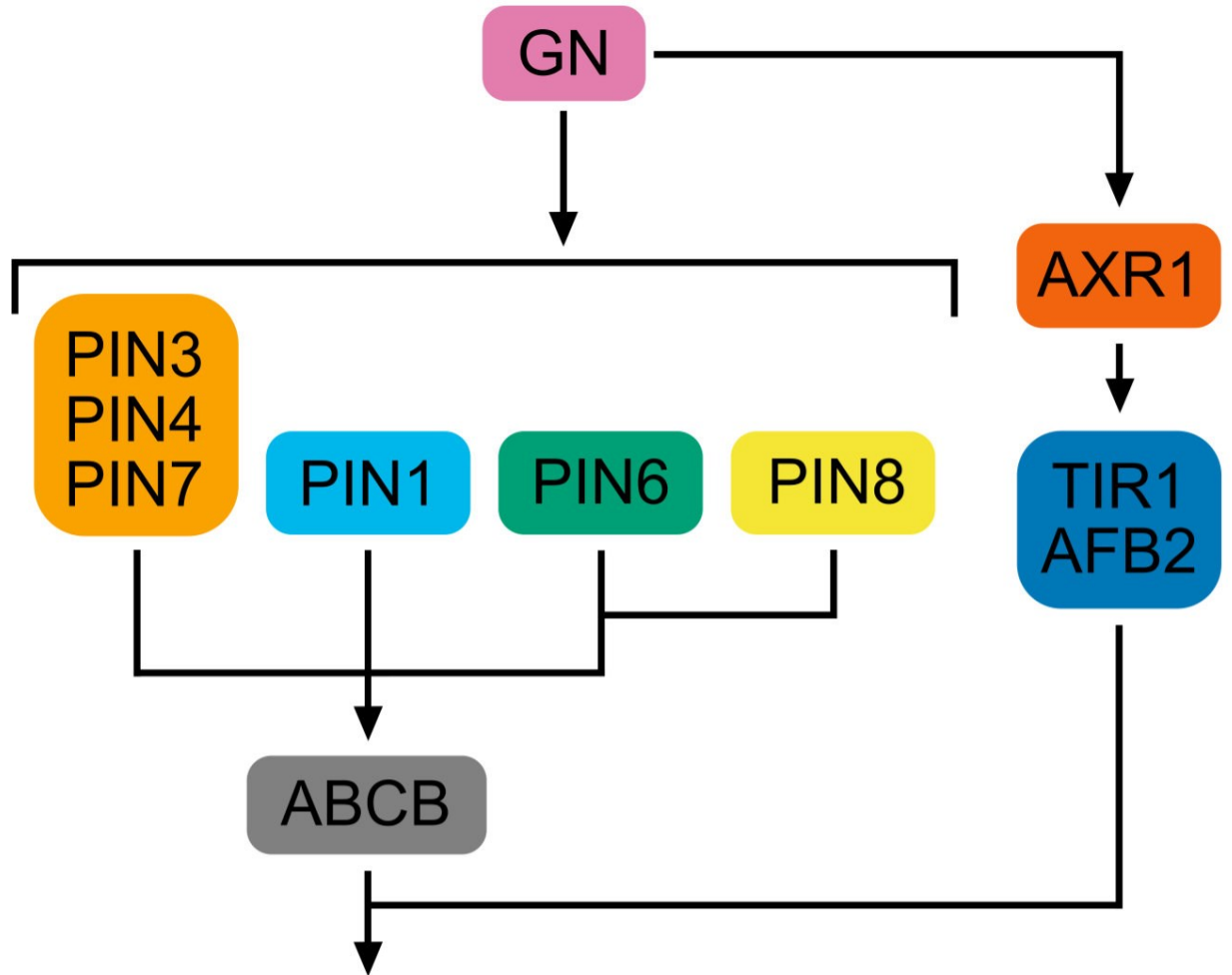
Genetic interaction network controlling tissue cell polarization and vein patterning. Arrows indicate positive effects.

vein pattern defects of *gn* are not the sole result of loss or abnormal polarity of PIN-mediated auxin transport (Verna et al., 2019).

The conclusion that the function of *GN* in coordination of tissue cell polarity and vein patterning entails more than control of PIN-mediated auxin transport is consistent with functions of *GN* that seem to be unrelated to auxin transport or independent of *PIN* function (Fischer et al., 2006; Irani et al., 2012; Moriwaki et al., 2014; Nielsen et al., 2012; Shevell et al., 2000).

The auxin-transport-, *PIN*-independent functions of *GN* in coordination of tissue cell polarity and vein patterning are, at least in part, mediated by TIR1/AFB2-mediated auxin signaling. This conclusion is suggested by the ability of simultaneous reduction in auxin transport and signaling to phenocopy *gn* defects in coordination of tissue cell polarity. The conclusion is also suggested by the ability of simultaneous reduction in auxin transport and signaling to phenocopy *gn* defects in auxin response and vein patterning (Verna et al., 2019); it is also supported by the epistasis of the defects of *gn* in vein and embryo patterning to those of auxin signaling mutants (Mayer et al., 1993; Verna et al., 2019).

How auxin signaling, inherently non-directional (Leyser, 2018), could contribute to the polar propagation of the inductive auxin signal in the absence of polar auxin transport is unclear. One possibility is that auxin signaling promotes the passive diffusion of auxin through the tissue by controlling, for example, the proton gradient across the PM (Fendrych et al., 2016). However, it is difficult to conceive how auxin diffusion through a specific side of the PM could positively feed back on the ability of auxin to diffuse through that specific side of the PM, a positive feedback that would be required to drain neighboring cells from auxin and thereby form veins, i.e. channels of preferential auxin movement (Sachs, 1969).

One other possibility is that auxin signaling promotes the facilitated diffusion of auxin through the plasmodesmata intercellular channels, a possibility that had previously been suggested (Mitchison, 1980b) and that has received some experimental support (Han et al.,

2014). Here, it is conceivable how auxin movement through a specific side of the PM could positively feed back on the ability of the cell to move auxin through that specific side of the PM (e.g., (Cieslak et al., 2015)), but no experimental evidence exists of such feedback or that auxin movement through plasmodesmata controls vein patterning.

Yet another possibility is that auxin signaling activates an unknown mobile signal. Such signal need not be chemical: alternatives, for example a mechanical signal, have been suggested (Corson et al., 2009; Couder et al., 2002; Laguna et al., 2008; Lee et al., 2014) and have been implicated in other auxin-driven processes (e.g., (Braybrook and Peaucelle, 2013; Hamant et al., 2008; Heisler et al., 2010; Nakayama et al., 2012; Peaucelle et al., 2011)). However, whether a mechanical signal controls vein patterning remains to be tested.

Though it is unclear how *GN* controls auxin signaling during vein patterning, the most parsimonious account is that GN controls the coordinated localization of proteins produced in response to auxin signaling. Auxin signaling indeed controls the production of proteins that are polarly localized at the plasma membrane of root cells (e.g., (Scacchi et al., 2009; Scacchi et al., 2010; Yoshida et al., 2019)), and at least some of these proteins act synergistically with PIN-mediated auxin transport in the root (e.g., (Marhava et al., 2018)); however, it remains to be tested whether such proteins have vein patterning activity, whether their localization is controlled by GN, and whether they mediate *GN* function in auxin signaling during vein patterning.

Alternatively, because cell wall composition and properties are abnormal in *gn* (Shevell et al., 2000), *GN* may control the production, propagation, or interpretation of a mechanical signal that has been proposed to be upstream of both auxin signaling and transport in the shoot apical meristem (Heisler et al., 2010; Nakayama et al., 2012); however, whether a mechanical signal controls vein patterning and whether such signal acts downstream of *GN* remain to be tested.

Irrespective of the mechanism of action, my results reveal synergism between auxin transport and signaling, and their unsuspected control by *GN* in the coordination of tissue cell polarity during vein patterning, a control whose logic is unprecedented in multicellular organisms.

3.4 MATERIALS & METHODS

3.4.1 Plants

Origin and nature of lines, genotyping strategies, and oligonucleotide sequences are in Tables 3.1–3.3. Seeds were sterilized and sown as in (Linh and Scarpella, 2022a) (Chapter 2). Stratified seeds were germinated and seedlings were grown at 22 °C under continuous fluorescent light (~80 µmol m^{-2} s^{-1}). Plants were grown at 25 °C under fluorescent light (~110 µmol m^{-2} s^{-1}) in a 16-h-light/8-h-dark cycle. Plants were transformed and representative lines were selected as in (Sawchuk et al., 2008).

3.4.2 Chemicals

NPA was dissolved in dimethyl sulfoxide and added ($25 - gn\text{-}13 -$ or $100 - tir1;afb2 - $ µM final concentration) to growth medium just before sowing.

3.4.3 Imaging

Developing leaves were mounted and imaged as in (Linh and Scarpella, 2022a) (Chapter 2), except that emission was collected from ~2.5-µm-thick optical slices. Light paths are in Table 3.4. Grayscaled RGB color images were turned into 8-bit images, look-up-tables were applied, and brightness and contrast were adjusted by linear stretching of the histogram in the Fiji distribution (Schindelin et al., 2012) of ImageJ (Rueden et al., 2017; Schindelin et al., 2015; Schneider et al., 2012).

Table 3.2. Genotyping Strategies

Line	Strategy
gn-13	*GN*: "SALK_045424 gn LP" and "SALK_045424 gn RP"; *gn*: "SALK_045424 gn RP" and "LBb1.3"
van7/emb30-7 (*gn*^*van7*)	"van7 Hpa1 FP" and "van7 Hpa1 RP"; *Hpa*I
tir1-1	"tir1-1F2" and "tir1-1R2"; *Bsa*I
afb2-3	*AFB2*: "AFB2+F" and "AFB2-TR"; *afb2*: "pROK-LB" and "AFB2-TR"

Table 3.3. Oligonucleotide Sequences

Name	Sequence (5' to 3')
SALK_045424 gn LP	TGATCCAAATCACTGGGTTTC
SALK_045424 gn RP	AGCTGAAGATAGGGAATTCGC
LBb1.3	ATTTTGCCGATTTCGGAAC
van7 Hpa1 FP	ATCCGTGCCCTTGATCTAATGGGAG
van7 Hpa1 RP	CACTTTTCTTAGTCCTTGAACAAGCGTTAA
tir1-1F2	AGCGACGGTGATTAGGAGG
tir1-1R2	CAGGAACAACGCAGCAAAA
AFB2+F	TTCTCCTTCGATCATTGTCAAC
AFB2-TR	TAGCGGCAATAGAGGCAAGA
pROK-LB	GGAACCACCATCAAACAGGA

Table 3.4. Confocal Light Paths

Fluorophore	Laser	Wavelength (nm)	Main dichroic beam splitter	First secondary dichroic beam splitter	Second secondary dichroic beam splitter	Emission filter (detector)
YFP	Ar	514	HFT 405/514/594	NFT 595	NFT 515	BP 520–555 IR (PMT3)
GFP; Autofluorescence	Ar	488	HFT 405/488/594	NFT 545	NFT 490 (PMT3); Plate (META)	BP 505–530 (PMT3); 550–574 (META)
GFP	Ar	488	HFT 405/488/594	NFT 545	NFT 490	BP 505–530 (PMT3)
Lignin	Diode	405	HFT 405/514/594	Mirror	NFT 490	BP 420–480 (PMT2)

Chapter 4: GAL4/GFP Enhancer-Trap Lines for Identification and Manipulation of Cells and Tissues in Developing Arabidopsis Leaves[1]

4.1 INTRODUCTION

The unambiguous identification of cell and tissue types and the selective manipulation of their properties is key to our understanding of developmental processes. Both the unambiguous identification and the selective manipulation can most efficiently be achieved by the GAL4 system (Brand and Perrimon, 1993). In such a system, a minimal promoter in a construct randomly inserted in a genome responds to neighboring regulatory elements and activates the expression of a gene, included in the same construct, encoding a variant of the GAL4 transcription factor of yeast; the same construct also includes a GAL4-responsive, *UAS*-driven lacZ, GUS, or GFP, which reports GAL4 expression. Independent, phenotypically normal lines, in which the construct is inserted in different genomic locations, are selected because they reproducibly express the GAL4-responsive reporter in cell- or tissue-specific patterns. Lines with cell- or tissue-specific GAL4-driven reporter expression can then be used to characterize the behavior of the labeled cells or tissues (Yang et al., 1995), to identify mutations that interfere with that behavior (Guitton et al., 2004), or to identify genes expressed in the labeled cells or tissues by cloning the DNA flanking the insertion site of the enhancer-trap construct (Calleja et al., 1996). Furthermore, lines with cell- or tissue-specific GAL4 expression can be crossed to lines containing *UAS*-driven RNAi constructs to trigger cell or tissue-specific gene silencing

---

[1] Adapted from Amalraj, B., Govindaraju, P., Krishna, A., Lavania, D., Linh, N. M., Ravichandran, S. J. and Scarpella, E. (2020). GAL4/GFP enhancer-trap lines for identification and manipulation of cells and tissues in developing Arabidopsis leaves. Developmental Dynamics 249, 1127–1146.

(Nagel et al., 2002), dominant-negative alleles to interfere with the WT gene function in specific cells or tissues (Elefant and Palter, 1999), toxic genes to induce cell- or tissue-specific ablation (Reddy et al., 1997), or genes of interest to investigate necessary or sufficient functions in specific cells or tissues (Gunthorpe et al., 1999). Though the GAL4 system does not allow to restrict the expression of *UAS*-driven transgenes to a temporal window that is narrower than that in which GAL4 is expressed, the system allows exquisite spatial control of transgene expression (McGuire et al., 2004).

One of the first implementations of the GAL4 system in Arabidopsis was the Haseloff collection of GAL4/GFP enhancer-trap lines, in which an endoplasmic-reticulum-localized GFP (erGFP) responds to the activity of a fusion between the GAL4 DNA-binding domain and the activating domain of VP16 of *Herpes simplex* (Berger et al., 1998; Haseloff, 1999). The Haseloff collection is the most extensively used GAL4 system in Arabidopsis (e.g., (Gardner et al., 2009; Laplaze et al., 2005; Sabatini et al., 1999; Sawchuk et al., 2007; Weijers et al., 2003; Wenzel et al., 2012)), even though it is in the C24 background. This is problematic because the phenotype of hybrids between C24 and Col-0, generally considered the reference genotype in Arabidopsis (Koornneef and Meinke, 2010), is different from that of either parent (e.g., (Groszmann et al., 2014; Kawanabe et al., 2016; Radoeva et al., 2016; Zhang et al., 2016)). The use of GAL4/GFP enhancer-trap lines in the C24 background to investigate processes in the Col-0 background thus imposes the burden of laborious generation of ad-hoc control backgrounds. Therefore, most desirable is the generation and characterization of GAL4/GFP enhancer-trap collections in the Col-0 background. Two such collections have been reported: the Berleth collection, which has been used to identify lines that express GAL4/GFP in vascular tissues (Ckurshumova et al., 2009); and the Poethig collection, which has been used to identify lines that express GAL4/GFP in stomata (Gardner et al., 2009).

Here we screened the Poethig collection. We provide a set of lines for the specific labelling of cells and tissues during early leaf development, and we show that these lines can be used to address key questions in plant developmental biology.

4.2 RESULTS & DISCUSSION

To identify enhancer-trap lines in the Col-0 background of Arabidopsis with reproducible GAL4-driven GFP expression during early leaf development, we screened the collection that Scott Poethig had generated with Jim Haseloff's GAL4/GFP enhancer-trap construct (Fig. 4.1A) and had donated to the Arabidopsis Biological Resource Center. We screened 312 lines for GFP expression in first leaves 4 and 5 DAG by fluorescence stereomicroscopy (see Materials & Methods); 29 lines satisfied this criterion (Table 4.1). In 10 of these 29 lines, we detected GFP in specific cells or tissues in first leaves 4 and 5 DAG by epifluorescence microscopy (see Materials & Methods); nine of these 10 lines were phenotypically normal (Table 4.1). We imaged GFP expression in first leaves of these nine lines from 2 to 5 DAG by confocal laser scanning microscopy.

The development of Arabidopsis leaves has been described previously (Candela et al., 1999; Donnelly et al., 1999; Kang and Dengler, 2002; Kang and Dengler, 2004; Kinsman and Pyke, 1998; Larkin et al., 1996; Mattsson et al., 1999; Mattsson et al., 2003; Pyke et al., 1991; Scarpella et al., 2004; Telfer and Poethig, 1994). Briefly, at 2 DAG the first leaf is recognizable as a cylindrical primordium with a midvein at its center (Fig. 4.1B). By 2.5 DAG, the primordium has elongated and expanded (Fig. 4.1C). By 3 DAG, the primordium has continued to expand and the first loops of veins ("first loops") have formed (Fig. 4.1D). By 4 DAG, a lamina and a petiole have become recognizable, second loops have formed, and minor veins have started to form the top half of the lamina (Fig. 4.1E). By 5 DAG, lateral outgrowths (hydathodes) have
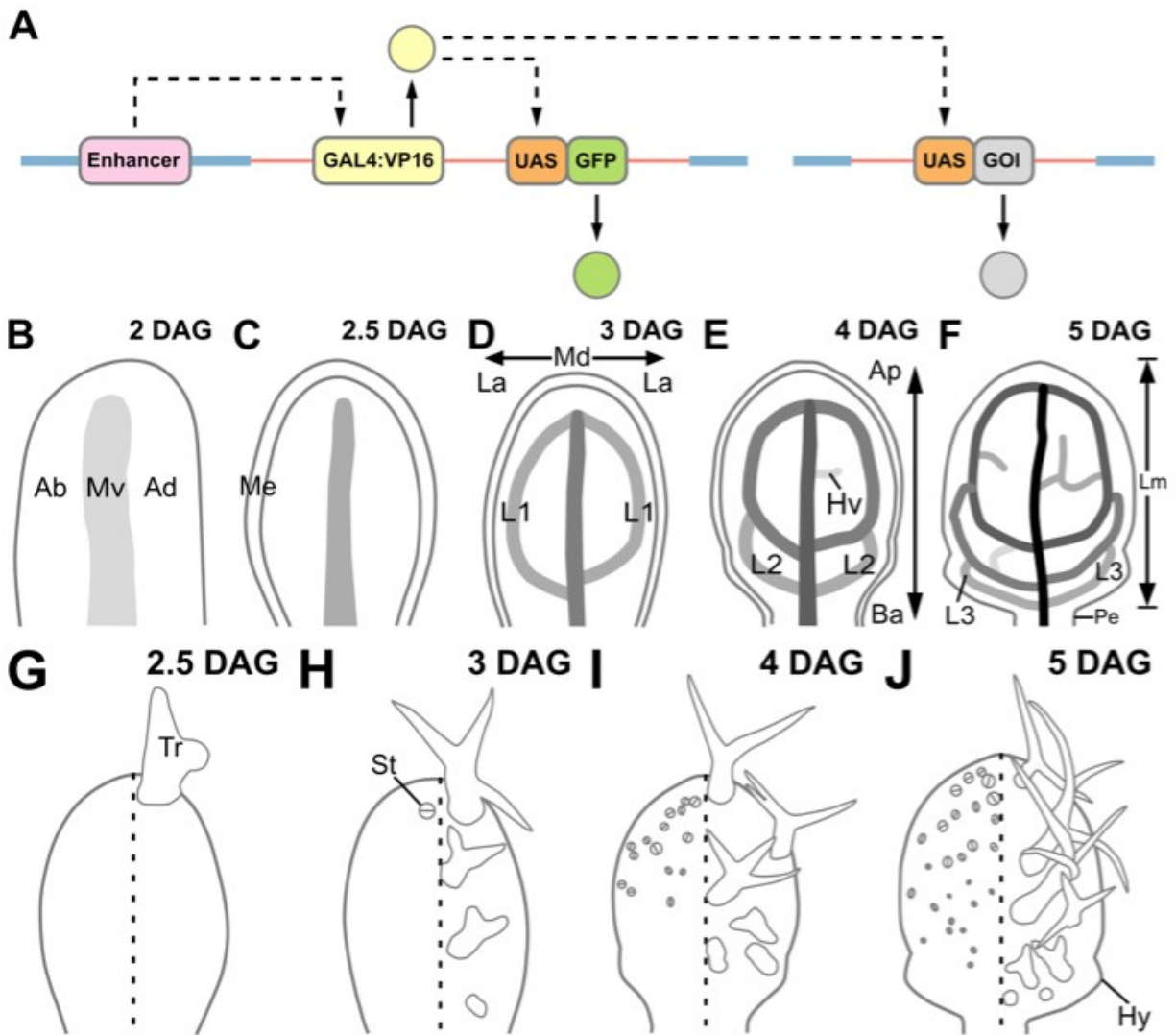
Figure 4.1. Poethig GAL4/GFP Enhancer-Trap Lines and Arabidopsis Leaf Development

(A) Cell- or tissue-specific enhancers in the Arabidopsis genome (blue line) activate transcription (dashed arrow) of a codon-usage-optimized translational fusion between the sequence encoding the GAL4 DNA-binding domain and the sequence encoding the activating domain of the Viral Protein 16 of *Herpes simplex* (GAL4:VP16) in a T-DNA construct (red line) that is randomly inserted in the Arabidopsis genome. Translation of the *GAL4:VP16* fusion transcript (solid arrow) leads to cell- or tissue-specific activation of transcription of a *UAS-*

driven gene encoding an endoplasmic-reticulum-localized, improved GFP (mGFP5) (Haseloff et al., 1997; Siemering et al., 1996). Crosses between lines with cell- or tissue-specific expression of GAL4:VP16 and lines with *UAS*-driven genes of interest (GOIs) lead to activation of GOI transcription in specific cells or tissues. See text and (Berger et al., 1998; Haseloff, 1999) for details. (B–J) First leaves. Top right: leaf age in days after germination (DAG); see Materials & methods for definition. (B–F) Development of leaf and veins; increasingly darker grays depict progressively later stages of vein development. (B) Side view, median plane. Abaxial (ventral) side to the left; adaxial (dorsal) side to the right. (C–F) Front view, median plane. See text for details. (G–J) Development of stomata and trichomes in abaxial (left) or adaxial (right) epidermis. Front ventral (left) or dorsal (right) view, epidermal plane. See text for details. Ab: abaxial; Ad: adaxial; Ap: apical; Ba: basal; Hv: minor vein; Hy: hydathode; L1, L2 and L3: first, second and third loop; La: lateral; Lm: lamina; Md: median; Me: marginal epidermis; Mv: midvein; Pe: petiole; St: stoma; Tr: trichome.

Table 4.1 Origin and Nature of Lines

ABRC stock no.	Donor stock no.	Expression in developing leaves	Tissue- and/or stage-specific expression	Phenotypically normal
CS24240	E53	N[1]	…	…
CS24241	E306	N	…	…
CS24242	E337	N	…	…
CS24243	E362	N	…	…
CS24244	E456	N	…	…
CS24245	E513	N	…	…
CS24246	E652	N	…	…
CS24247	E751	N	…	…
CS24248	E788	N	…	…
CS24249	E829	N	…	…
CS24250	E1012	N	…	…
CS24251	E1075	N	…	…
CS24252	E1195	N	…	…
CS24253	E1247	N	…	…
CS24254	E1287	N	…	…
CS24255	E1324	N	…	…
CS24256	E1332	Y[2]	N	…
CS24257	E2042	N	…	…
CS24258	E2065	N	…	…
CS24259	E2072	N	…	…
CS24260	E2119	N	…	…
CS24262	E2168	N	…	…

ABRC stock no.	Donor stock no.	Expression in developing leaves	Tissue- and/or stage-specific expression	Phenotypically normal
CS24264	E2242	N	…	…
CS24265	E2263	N	…	…
CS24266	E2271	N	…	…
CS70072	E1092	N	…	…
CS70073	E1100	N	…	…
CS70074	E1127	N	…	…
CS70075	E1128	N	…	…
CS70076	E1130	N	…	…
CS70077	E1155	N	…	…
CS70078	E1161	N	…	…
CS70079	E1176	N	…	…
CS70080	E1222	N	…	…
CS70081	E1223	N	…	…
CS70082	E1237	N	…	…
CS70083	E1238	N	…	…
CS70084	E1250	N	…	…
CS70085	E1252	N	…	…
CS70086	E1271	N	…	…
CS70087	E1289	Y	N	…
CS70088	E1304	N	…	…
CS70089	E1322	N	…	…
CS70090	E1325	N	…	…
CS70091	E1331	N	…	…

ABRC stock no.	Donor stock no.	Expression in developing leaves	Tissue- and/or stage-specific expression	Phenotypically normal
CS70092	E1341	N	…	…
CS70093	E1344	N	…	…
CS70094	E1356	N	…	…
CS70095	E1361	N	…	…
CS70096	E1362	N	…	…
CS70097	E1370	N	…	…
CS70098	E1387	N	…	…
CS70099	E1388	N	…	…
CS70100	E1395	N	…	…
CS70102	E1405	N	…	…
CS70103	E1416	N	…	…
CS70104	E1439	N	…	…
CS70105	E1439m	N	…	…
CS70106	E1457	N	…	…
CS70107	E1567	N	…	…
CS70108	E1570	N	…	…
CS70109	E1607	N	…	…
CS70110	E1626	N	…	…
CS70111	E1627	N	…	…
CS70112	E1628	N	…	…
CS70113	E1638	N	…	…
CS70114	E1644	N	…	…
CS70115	E1662	N	…	…

ABRC stock no.	Donor stock no.	Expression in developing leaves	Tissue- and/or stage-specific expression	Phenotypically normal
CS70116	E1663	Y	N	…
CS70117	E1665	N	…	…
CS70118	E1678	N	…	…
CS70119	E1684	N	…	…
CS70120	E1689	N	…	…
CS70121	E1691	N	…	…
CS70122	E1701	N	…	…
CS70123	E1728	N	…	…
CS70125	E1751	N	…	…
CS70126	E1765	N	…	…
CS70127	E1767	N	…	…
CS70128	E1785	N	…	…
CS70129	E1786	N	…	…
CS70130	E1797	N	…	…
CS70131	E1801	N	…	…
CS70132	E1809	N	…	…
CS70133	E1815	N	…	…
CS70134	E1817	N	…	…
CS70135	E1818	N	…	…
CS70136	E1819	N	…	…
CS70137	E1825	N	…	…
CS70138	E1828	N	…	…
CS70139	E1832	N	…	…

ABRC stock no.	Donor stock no.	Expression in developing leaves	Tissue- and/or stage-specific expression	Phenotypically normal
CS70140	E1833	N	...	...
CS70141	E1853	N	...	...
CS70142	E1868	N	...	...
CS70143	E1950	N	...	...
CS70144	E1998	N	...	...
CS70145	E2034	N	...	...
CS70146	E217	N	...	...
CS70147	E562	N	...	...
CS70148	E1001	N	...	...
CS70149	E1368	N	...	...
CS70150	E1690	N	...	...
CS70151	E1704-1	N	...	...
CS70152	E1704-3	N	...	...
CS70153	E1715	N	...	...
CS70154	E1723	N	...	...
CS70155	E1735	N	...	...
CS70156	E1935	N	...	...
CS70157	E1967	N	...	...
CS70158	E2014	N	...	...
CS70159	E2057	N	...	...
CS70160	E2207	N	...	...
CS70161	E2406	N	...	...
CS70162	E2408	Y	Y	Y

ABRC stock no.	Donor stock no.	Expression in developing leaves	Tissue- and/or stage-specific expression	Phenotypically normal
CS70163	E2410	N	...	...
CS70164	E2415	N	...	...
CS70165	E2425	N	...	...
CS70166	E2425	N	...	...
CS70167	E2441	N	...	...
CS70168	E2443	N	...	...
CS70169	E2448	N	...	...
CS70170	E2491	N	...	...
CS70171	E2502	N	...	...
CS70172	E2513	N	...	...
CS70173	E2563	N	...	...
CS70174	E2609	N	...	...
CS70175	E2633	N	...	...
CS70176	E2676	N	...	...
CS70177	E2692	Y	N	...
CS70178	E2724	N	...	...
CS70179	E2763	N	...	...
CS70180	E2764	N	...	...
CS70181	E2779	N	...	...
CS70182	E2861	N	...	...
CS70183	E2862	N	...	...
CS70184	E2897	N	...	...
CS70185	E2904	N	...	...

ABRC stock no.	Donor stock no.	Expression in developing leaves	Tissue- and/or stage-specific expression	Phenotypically normal
CS70186	E2905	N	…	…
CS70187	E2947	N	…	…
CS70188	E2993	N	…	…
CS70189	E3004	N	…	…
CS70190	E3006	N	…	…
CS70191	E3017	N	…	…
CS70192	E3065	N	…	…
CS70193	E3134	N	…	…
CS70194	E3190	N	…	…
CS70195	E3198	N	…	…
CS70196	E3258	N	…	…
CS70197	E3267	N	…	…
CS70198	E3298	N	…	…
CS70199	E3313	N	…	…
CS70200	E3317	Y	Y	N
CS70201	E3430	N	…	…
CS70202	E3459	N	…	…
CS70203	E3462	N	…	…
CS70204	E3474	N	…	…
CS70205	E3478	N	…	…
CS70206	E3501	N	…	…
CS70207	E3505	N	…	…
CS70208	E3530	N	…	…

ABRC stock no.	Donor stock no.	Expression in developing leaves	Tissue- and/or stage-specific expression	Phenotypically normal
CS70209	E3531	N	...	...
CS70210	E3598-1	N	...	...
CS70211	E3598-2	N	...	...
CS70212	E3637	N	...	...
CS70213	E3642	N	...	...
CS70214	E3655	Y	N	...
CS70215	E3683	N	...	...
CS70216	E3700	N	...	...
CS70217	E3754	N	...	...
CS70218	E3756	N	...	...
CS70219	E3783	Y	N	...
CS70220	E3806	N	...	...
CS70221	E3816	N	...	...
CS70222	E3826	N	...	...
CS70223	E3876	N	...	...
CS70224	E3879	N	...	...
CS70225	E3880	N	...	...
CS70226	E3885	Y	N	...
CS70227	E3912	Y	Y	Y
CS70228	E3927	N	...	...
CS70229	E3930	Y	N	...
CS70230	E3963	N	...	...
CS70231	E3980	N	...	...

ABRC stock no.	Donor stock no.	Expression in developing leaves	Tissue- and/or stage-specific expression	Phenotypically normal
CS70232	E4009	N	…	…
CS70233	E4028	Y	N	…
CS70234	E4058	N	…	…
CS70235	E4096	N	…	…
CS70236	E4104	N	…	…
CS70237	E4105	N	…	…
CS70238	E4110	N	…	…
CS70239	E4118	Y	N	…
CS70240	E4129	N	…	…
CS70241	E4148	N	…	…
CS70242	E4150	N	…	…
CS70243	E4151	N	…	…
CS70244	E4162	N	…	…
CS70245	E4223	N	…	…
CS70246	E4247	N	…	…
CS70247	E4256	N	…	…
CS70248	E4272	N	…	…
CS70249	E4285	N	…	…
CS70250	E4295	Y	Y	Y
CS70251	E4350	N	…	…
CS70252	E4396	N	…	…
CS70253	E4411	N	…	…
CS70254	E4423	N	…	…

ABRC stock no.	Donor stock no.	Expression in developing leaves	Tissue- and/or stage-specific expression	Phenotypically normal
CS70255	E4491	N	...	...
CS70256	E4506	Y	N	...
CS70257	E4522	Y	N	...
CS70258	E4583	N	...	...
CS70259	E4589	N	...	...
CS70260	E4633	N	...	...
CS70261	E4680	N	...	...
CS70262	E4695	N	...	...
CS70263	E4715	N	...	...
CS70264	E4716	Y	Y	Y
CS70265	E4722	Y	Y	Y
CS70266	E4751	N	...	...
CS70267	E4791	N	...	...
CS70268	E4801	N	...	...
CS70269	E4811	N	...	...
CS70270	E4812	N	...	...
CS70271	E4820	N	...	...
CS70272	E4856	Y	N	...
CS70273	E4907	N	...	...
CS70274	E4930	N	...	...
CS70275	E4940	N	...	...
CS70276	E4970	N	...	...
CS70277	E5008	N	...	...

ABRC stock no.	Donor stock no.	Expression in developing leaves	Tissue- and/or stage-specific expression	Phenotypically normal
CS70278	E5025	N	...	...
CS70279	E5026	N	...	...
CS70280	E5085	N	...	...
CS70281	E5096	Y	N	...

[1] N, No

[2] Y, Yes

become recognizable in the lower quarter of the lamina, third loops have formed and minor vein formation has spread toward the base of the lamina (Fig. 4.1F). Leaf hairs (trichomes) and pores (stomata) can be first recognized at the tip of 2.5- and 3-DAG primordia, respectively and their formation spreads toward the base of the lamina during leaf development (Fig. 4.1G–J).

Consistent with previous observations (Huang et al., 2014), E100>>erGFP was expressed at varying levels in all the cells of 2-, 2.5-, 3- and 4-DAG leaf primordia (Fig. 4.2B–E).

Consistent with previous observations (Krogan and Berleth, 2012), E861>>erGFP was expressed in all the inner cells of the 2-DAG primordium, though more strongly in its innermost cells (Fig. 4.2F). At 2.5 DAG, expression had been activated in the lowermost epidermal cells of the primordium margin and persisted in all the inner cells of the bottom half of the primordium; in the top half of the primordium, weaker expression persisted in inner cells, except near the midvein, where by then it had been terminated (Fig. 4.2G). At 3 DAG, expression continued to persist in all the inner cells of the bottom half of the primordium, though expression was stronger in the areas where second loops were forming; in the top half of the primordium, weaker expression had become restricted to the midvein, first loops and minor veins (Fig. 4.2H). At 4 DAG, expression in the top half of the leaf remained restricted to the midvein, first loops and minor veins and in the bottom half of the leaf it had declined in inner cells between the first loops and the developing second loops (Fig. 4.2I). In summary, E861>>erGFP was expressed ubiquitously at early stages of inner-cell development; over time, however, expression became restricted to developing veins. As such, expression of E861>>erGFP resembles that of *MONOPTEROS* and *PIN-FORMED1*, which marks the gradual selection of vascular cells from within the leaf inner tissue (Scarpella et al., 2006; Wenzel et al., 2007).

E4295>>erGFP expression was restricted to inner cells in 2-, 2.5-, 3- and 4-DAG leaf primordia (Fig. 4.2J–M,O–Q). At 2 DAG, E4295>>erGFP was expressed almost exclusively in the inner cells of the abaxial side of the primordium (Fig. 4.2J), but by 2.5 DAG E4295>>erGFP
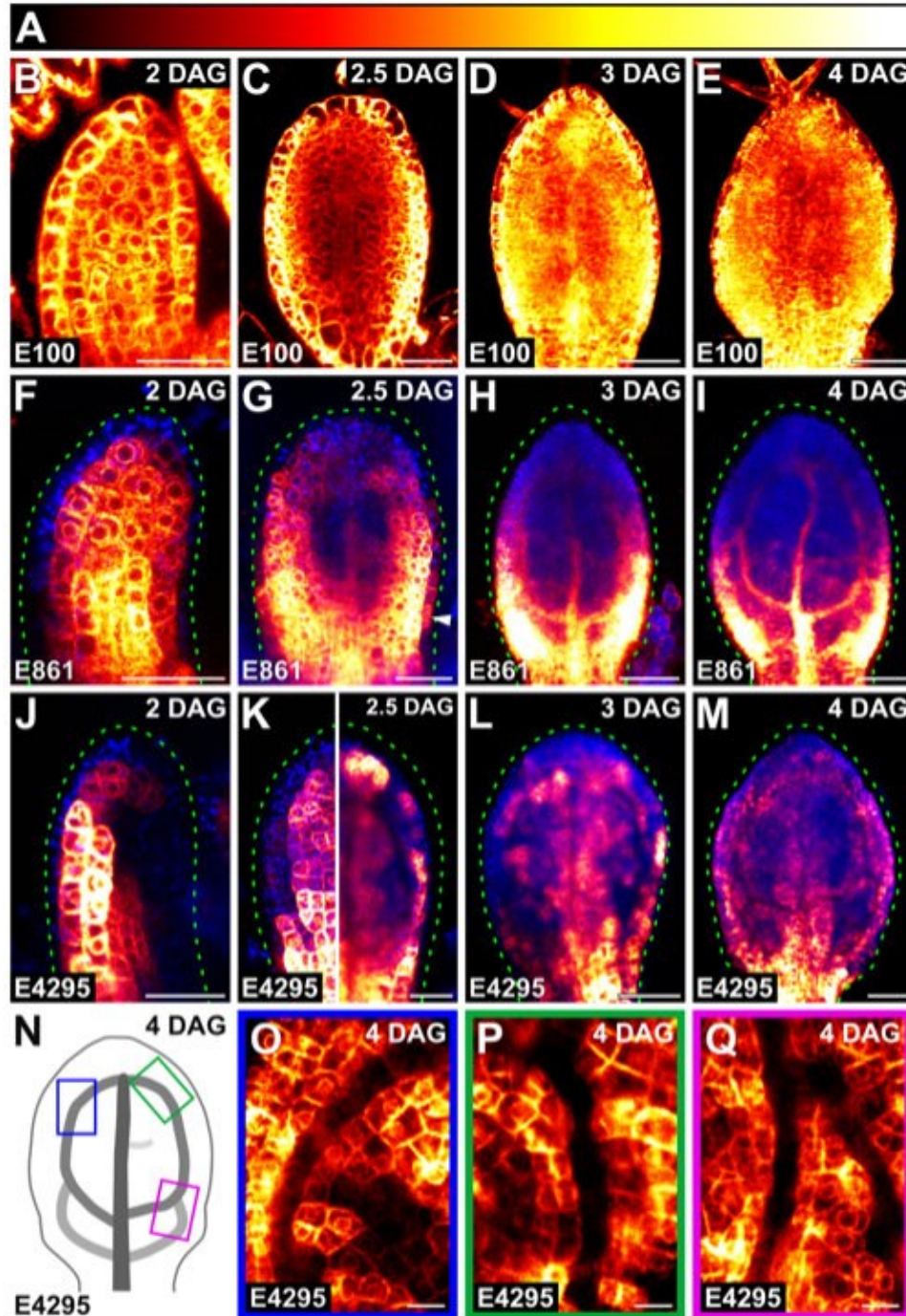
Figure 4.2. Expression of E100>>, E861>> and E4295>>erGFP in Leaf Development

(A) Look-up table visualizes global background (black) and erGFP expression levels (red to white through yellow). (B–Q) First leaves. Top right: leaf age in days after germination (DAG);

see Materials & methods for definition. (B–M,O–Q) Confocal laser scanning microscopy. Bottom left: genotype. Look-up table (ramp in A) visualizes erGFP expression levels (red to white through yellow). Blue: autofluorescence. Black: global background. Dashed green line delineates leaf outline. White arrowhead points to epidermal expression. (B,F,J) Side view, median plane. Abaxial (ventral) side to the left; adaxial (dorsal) side to the right. (C–E,G–I,L,M,O–Q) Front view, median plane. (K) Front ventral view, subepidermal plane (left); front view, median plane (right). (N) Increasingly darker grays depict progressively later stages of vein development. Boxes illustrate positions of closeups in O, P and Q. See Table 4.2 for reproducibility of expression features. Bars: (B,C,F,G,J,K) 30 µm; (D,E,H,I,L,M) 60 µm; (O–Q) 10 µm.

Table 4.2. Reproducibility of Expression and Pattern Features

Figure	Panel	No. leaves with displayed features / no. analyzed leaves	Assessed expression or pattern features
4.2	B	15/18	Ubiquitous
4.2	C	15/17	Ubiquitous
4.2	D	19/19	Ubiquitous
4.2	E	33/33	Ubiquitous
4.2	F	26/29	Inner cells
4.2	G	29/29	Vascular cells in top half of primordium, inner cells in basal half of primordium
4.2	H	31/31	Vascular cells in top half of primordium, inner cells in basal half of primordium
4.2	I	19/19	Vascular cells in top half of leaf, inner cells in basal half of leaf
4.2	J	16/19	Abaxial inner cells
4.2	K	34/36	Abaxial inner cells & middle tissue layer
4.2	L	24/25	Abaxial inner cells & middle tissue layer
4.2	M	34/34	Abaxial inner cells & middle tissue layer

Figure	Panel	No. leaves with displayed features / no. analyzed leaves	Assessed expression or pattern features
4.2	O	14/14	Inner, nonvascular cells
4.2	P	14/14	Inner, nonvascular cells
4.2	Q	14/14	Inner, nonvascular cells
4.3	A	26/28 (abaxial) 15/28 (adaxial)	Upper third of adaxial epidermis & whole abaxial epidermis
4.3	B (left)	30/30	Whole epidermis
4.3	B (right)	22/23	Top three-quarters of epidermis & trichomes
4.3	C (left)	15/15	Whole epidermis
4.3	C (right)	14/14	Top three-quarters of epidermis & trichomes
4.3	D (left)	18/18	Whole epidermis
4.3	D (right)	16/16	Epidermis of whole lamina and petiole midline & trichomes
4.3	E	16/16	Trichomes
4.3	F	17/18	Top three-quarters of marginal epidermis
4.3	G	14/14	Whole marginal epidermis
4.3	H	16/16	Whole marginal epidermis
4.3	I	59/59	Whole epidermis
4.3	J (left)	45/45	Whole epidermis

Figure	Panel	No. leaves with displayed features / no. analyzed leaves	Assessed expression or pattern features
4.3	J (right)	42/42	All cells of marginal epidermis, except few cells in top half of primordium
4.3	K (left)	21/21	Whole epidermis, including stomata
4.3	K (right)	33/38	Bottom quarter and few cells in top three-quarters of marginal epidermis
4.3	L (left)	21/21	Whole epidermis, including stomata
4.3	L (right)	31/31	Bottom quarter and few cells in top three-quarters of marginal epidermis
4.3	M	29/30	Absent
4.3	N	26/26	Top quarter of primordium
4.3	P	18/18	Whole leaf
4.3	Q	31/33	Absent
4.3	R	19/21	Top quarter of primordium
4.3	S	23/28	Top half of lamina
4.3	T	16/18	Top three-quarters of lamina
4.4	A	22/22	Midvein

Figure	Panel	No. leaves with displayed features / no. analyzed leaves	Assessed expression or pattern features
4.4	B	30/30	Midvein
4.4	C	16/17	Midvein & first loop
4.4	D	34/48	Midvein & first and second loop
4.4	E	25/25	Absent
4.4	F	20/20	Midvein
4.4	G	27/37	Midvein & first loop
4.4	H	24/28	Midvein & first and second loop
4.6	A	NDa	Narrow midvein & scalloped vein-network outline
4.6	B	19/20	Shapeless vascular cluster
4.6	C	32/46	Midvein & first and second loop
4.6	D	21/21	Shapeless vascular domain
4.6	E	16/23	Midvein & first and second loop
4.6	F	18/18	Broad vascular domain
4.6	G	21/21	Narrow midvein & scalloped vein-network outline
4.6	H	19/19	Broad vascular zone

was additionally expressed in the middle tissue layer (Fig. 4.2K), from which veins form (Stewart, 1978; Tilney-Bassett, 1986). Expression persisted in the inner cells of the abaxial side and of the middle tissue layer in 3- and 4-DAG primordia (Fig. 4.2L,M). High-resolution images of the middle tissue layer showed that expression was excluded from developing veins (Fig. 4.2O–Q), suggesting that it marks inner, non-vascular cells. Therefore, expression of E4295>>erGFP resembles that of *LIGHT HARVESTING COMPLEX A6* and *SCARECROW-LIKE32* (Gardiner et al., 2011; Sawchuk et al., 2008) and that of J0571>>erGFP in the C24 background (Wenzel et al., 2012).

As described below, expression of E4259>>erGFP and E4722>>erGFP was restricted to the epidermis at all analyzed stages (Fig. 4.3A–L).

At 2 DAG, E4259>>erGFP was expressed in the upper third of the adaxial epidermis and in the whole abaxial epidermis, though expression was stronger in the top half of the primordium (Fig. 4.3A). By 2.5 DAG, E4259>>erGFP was strongly expressed in the whole abaxial epidermis and the top three-quarters of the marginal epidermis; E4259>>erGFP was also expressed in the top three-quarters of the adaxial epidermis, but expression was stronger in the top half of the primordium (Fig. 4.3B,F). At 3 DAG, E4259>>erGFP was strongly expressed in the top three-quarters of the adaxial epidermis and in the whole marginal epidermis and strong expression persisted in the whole abaxial epidermis (Fig. 4.3C,G). At 4 DAG, strong expression persisted in the whole marginal epidermis, continued to persist in the whole abaxial epidermis and E4259>>erGFP was now strongly expressed also in the adaxial epidermis of the whole lamina and the petiole midline (Fig. 4.3D,H). At all analyzed stages, E4259>>erGFP was expressed in trichomes but was not expressed in mature stomata (Fig. 4.3B–H). In conclusion, expression of E4259>>erGFP resembles that of ARABIDOPSIS THALIANA MERISTEM LAYER1 (Lu et al., 1996; Sessions et al., 1999), which marks epidermal cells and whose
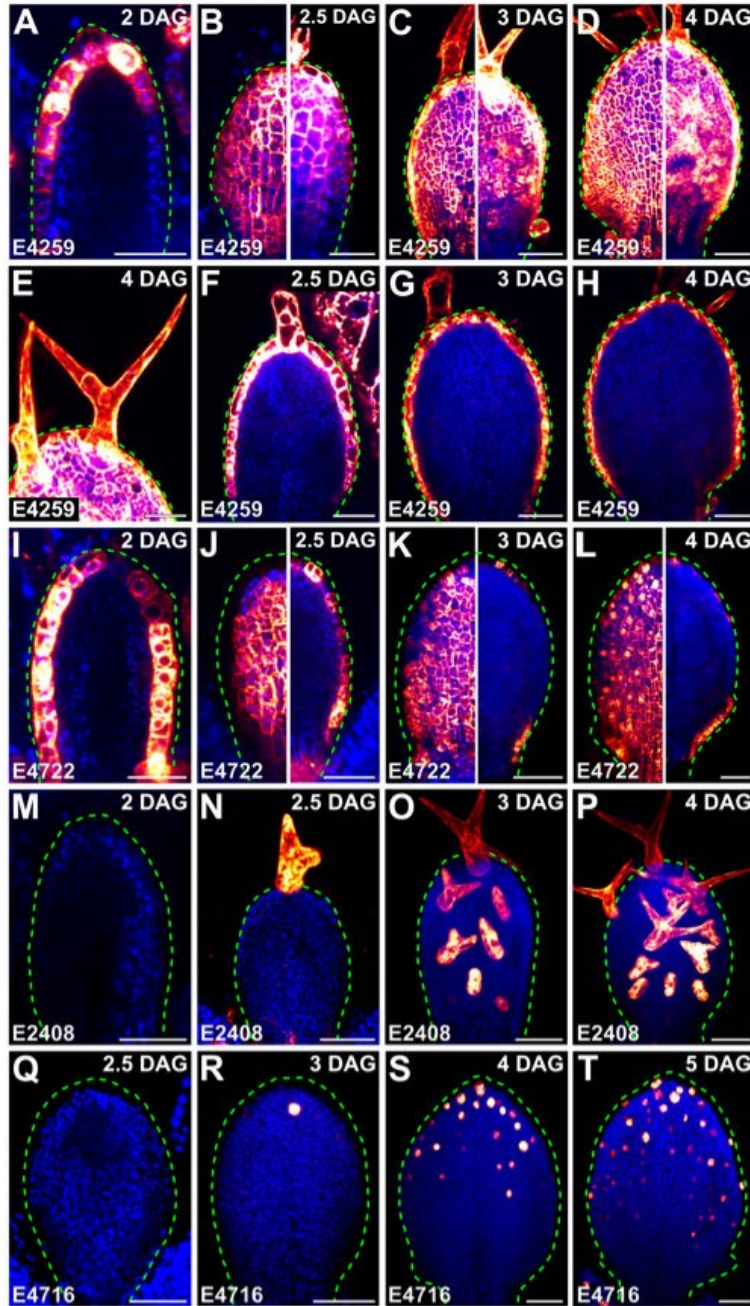
Figure 4.3. Expression of E4259>>, E4722>>, E2408>> and E4716>>erGFP in Leaf Development

(A–T) Confocal laser scanning microscopy. First leaves. Top right: leaf age in days after germination (DAG); see Materials & methods for definition. Bottom left: genotype. Look-up table (ramp in Fig. 4.2A) visualizes erGFP expression levels (red to white through yellow). Blue:

autofluorescence. Black: global background. Dashed green line delineates leaf outline. (A,I,M) Side view, median plane. Abaxial (ventral) side to the left; adaxial (dorsal) side to the right. (B–D) Front ventral (left) or dorsal (right) view, epidermal plane. (E) Closeup of trichome in D, right. (F–H) Front view, median plane. (J–L) Front ventral view, epidermal plane (left); front view, median plane (right). (N–P) Front dorsal view, epidermal plane. (Q–T) Front ventral view, epidermal plane. See Table 4.2 for reproducibility of expression features. Bars: (A,B,F,I,J,M,N,Q) 30 µm; (C,D,E,G,H,K,L,O,P,R,S,T) 60 µm.

promoter is used to drive epidermis-specific expression (e.g., (Bilsborough et al., 2011; Govindaraju et al., 2020; Kierzkowski et al., 2013; Takada and Jürgens, 2007)).

E4722>>erGFP was expressed in all the epidermal cells of the 2-DAG primordium, though more weakly at its tip (Fig. 4.3I). E4722>>erGFP was expressed in all the epidermal cells of the 2.5-DAG primordium too, except at its margin, where expression had been terminated in a few cells of its top half (Fig. 4.3J). At 3 DAG, expression persisted in all the epidermal cells, except at the primordium margin, where expression had been terminated in most of the cells of its top three-quarters (Fig. 4.3K). At 4 DAG, expression continued to persist in all the epidermal cells, except at the leaf margin, where expression had been terminated in nearly all the cells of its top three-quarters (Fig. 4.3L). Unlike E4259>>erGFP, E4722>>erGFP was expressed in stomata but was not expressed in trichomes (Fig. 4.3J–L).

At all analyzed stages, expression of E2408>>erGFP and E4716>>erGFP was restricted to trichomes and stomata, respectively (Fig. 4.3M–T). E2408>>erGFP was first expressed in developing trichomes at the tip of the 2.5-DAG primordium (Fig. 4.3M,N). By 3 DAG, E2408>>erGFP was expressed in the developing and mature trichomes of the top three-quarters of the primordium (Fig. 4.3O) and by 4 DAG in those of the whole lamina (Fig. 4.3P). E4716>>erGFP was first expressed in stomata at the tip of the 3-DAG primordium (Fig. 4.3Q,R). By 4 DAG, E4716>>erGFP was expressed in the stomata of the top half of the lamina (Fig. 4.3S) and by 5 DAG in those of its top three-quarters (Fig. 4.3T).

At all analyzed stages, expression of E2331>>erGFP and E3912>>erGFP was restricted to developing veins (Fig. 4.4). E2331>>erGFP was expressed in both isodiametric and elongated cells of the midvein in 2- and 2.5-DAG primordia (Fig. 4.4A,B). By 3 DAG, E2331>>erGFP was expressed in first loops and by 4 DAG in second loops and minor veins (Fig. 4.4C,D). E3912>>erGFP was first expressed in the midvein of the 3-DAG primordium (Fig. 4.4E,F). By 4 DAG, E3912>>erGFP was expressed in first loops and by 5 DAG in second loops and minor veins (Fig. 4.4G,H). These observations suggest that expression of E3912>>erGFP is

146
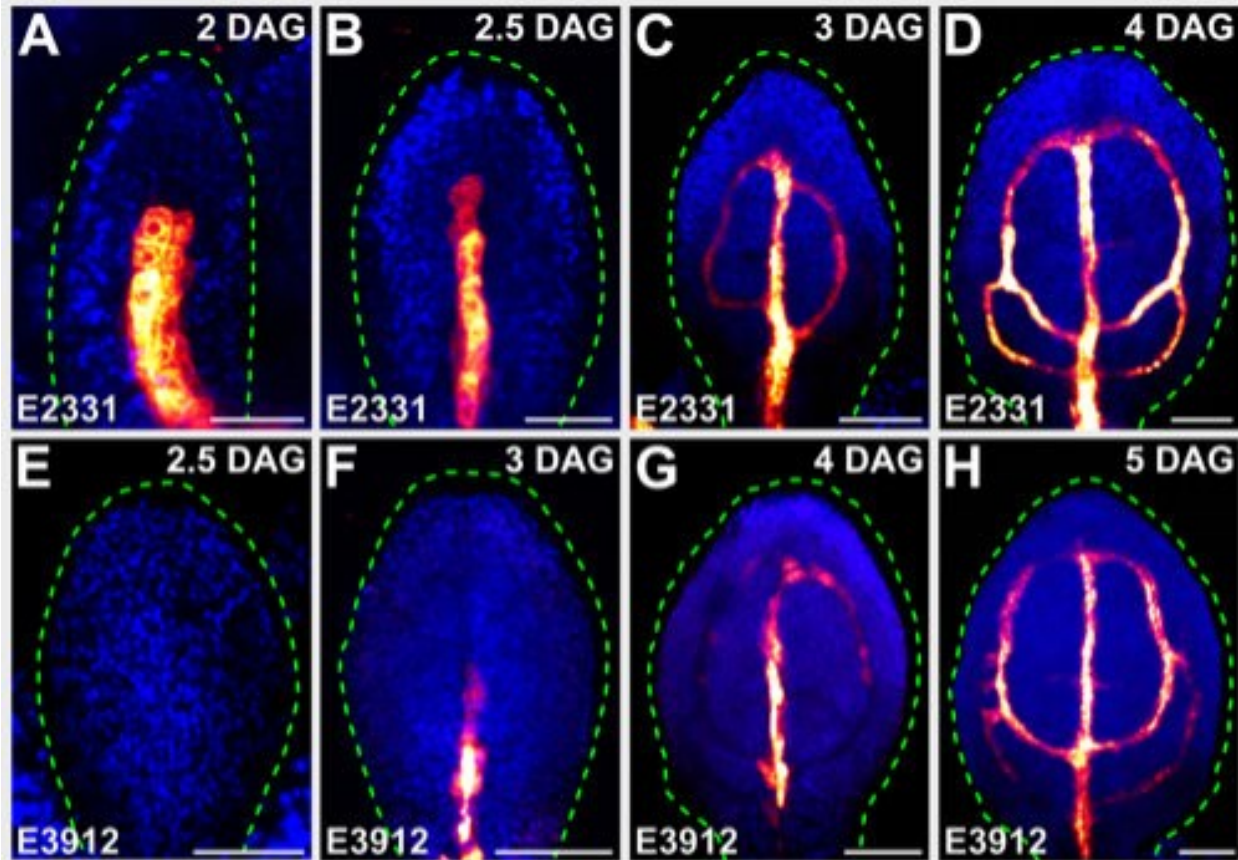
Figure 4.4. Expression of E2331>> and E3912>>erGFP in Leaf Development

(A–H) Confocal laser scanning microscopy. First leaves. Top right: leaf age in days after germination (DAG); see Materials & methods for definition. Bottom left: genotype. Look-up table (ramp in Fig. 4.2A) visualizes erGFP expression levels (red to white through yellow). Blue: autofluorescence. Black: global background. Dashed green line delineates leaf outline. (A) Side view, median plane. Abaxial (ventral) side to the left; adaxial (dorsal) side to the right. (B–H) Front view, median plane. See Table 4.2 for reproducibility of expression features. Bars: (A,B,E) 30 µm; (C,D,F–H) 60 µm.

initiated later than that of E2331>>erGFP in vein development. Furthermore, because the

expression of E2331>>erGFP resembles that of the preprocambial markers ATHB8::nYFP,

J1721>>erGFP and SHR::nYFP (Donner et al., 2009; Gardiner et al., 2011; Sawchuk et al.,

2007), we suggest that E2331>>erGFP expression marks preprocambial stages of vein

development, a conclusion that is consistent with E2331>>erGFP expression during

embryogenesis (Gillmor et al., 2010). Finally, because E3912>>erGFP expression resembles that

of the procambial marker Q0990>>erGFP in the C24 background (Sawchuk et al., 2007)), we

suggest that E3912>>erGFP expression marks procambial stages of vein development.

In the lines characterized above, GFP was expressed in specific cells and tissues during

early leaf development; however, as it is most frequently the case for other enhancer-trap lines

(e.g., (Ckurshumova et al., 2009; Gardiner et al., 2011; Gardner et al., 2009; Radoeva et al.,

2016; Wenzel et al., 2012)), in the lines reported here GFP was additionally expressed in other

organs (Fig. 4.5). To show the informative power for plant developmental biology of the lines

characterized above, we selected the E2331 line, which marks early stages of vein development

(Fig. 4.4A–D).

In WT leaves, the elongated vascular cells are connected to one another into continuous

veins (Fig. 4.6A) (Esau, 1965). By contrast, in mature leaves of the *gnom* (*gn*) mutant, putative

vascular cells fail to elongate and to connect to one another into continuous veins; instead, they

accumulate into shapeless clusters of seemingly disconnected and randomly oriented cells (Fig.

4.6B) (Shevell et al., 2000; Verna et al., 2019) (Chapter 5). Though the cells in these clusters

have some features of vascular cells (e.g., distinctive patterns of secondary cell-wall

thickenings), they lack others (e.g., elongated shape and end-to-end connection to form

continuous veins). Therefore, it is unclear whether the clustered cells in *gn* mature leaves are

abnormal vascular cells or nonvascular cells that have recruited a cellular differentiation

pathway that is normally, but not always (e.g., (Kubo et al., 2005; Solereder, 1908; Yamaguchi et

al., 2010)), associated with vascular development. To address this question, we imaged
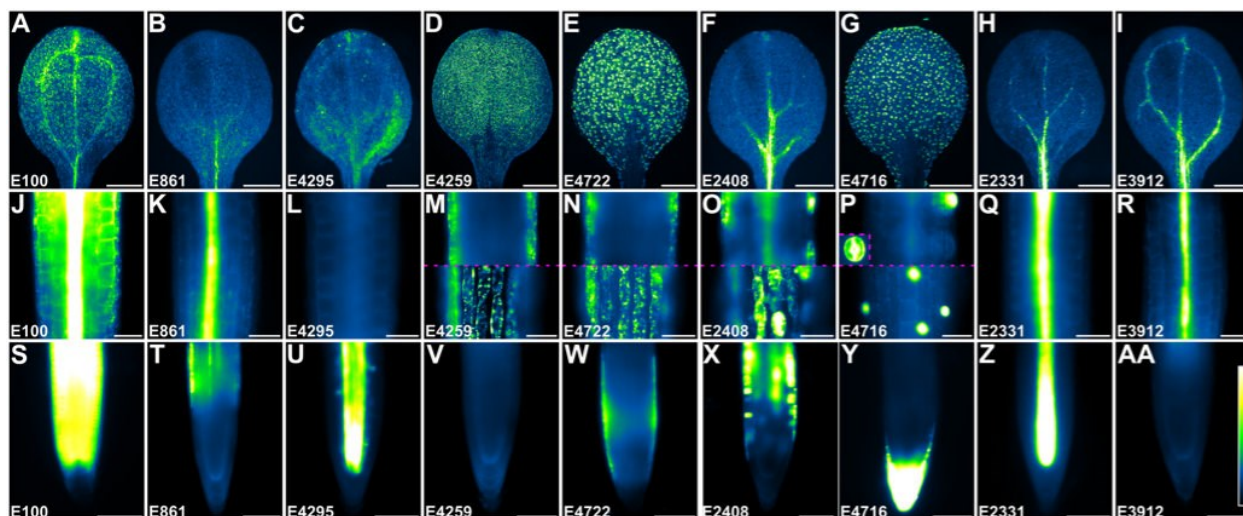
Figure 4.5. Expression of E100>>, E861>>, E4295>>, E4259>>, E4722>>, E2408>>, E4716>>, E2331>> and E3912>>erGFP in Seedling Organs

(A–AA) Epifluorescence microscopy. Seedlings 5 days after germination (see Materials & methods for definition). Bottom left: genotype. Look-up table (ramp in AA) visualizes global background (black) and levels of autofluorescence (blue to cyan) and erGFP expression (green to white through yellow). (A–I) Cotyledon. (J–R) Hypocotyl. (P) Inset: stoma. (S-AA) Root. (A–I) Front view, median plane. (J–L,Q–AA) Median plane. (M–P) Median (top) or tangential (bottom) plane. Bars: (A–I) 500 μm.; (J–AA) 100 μm.
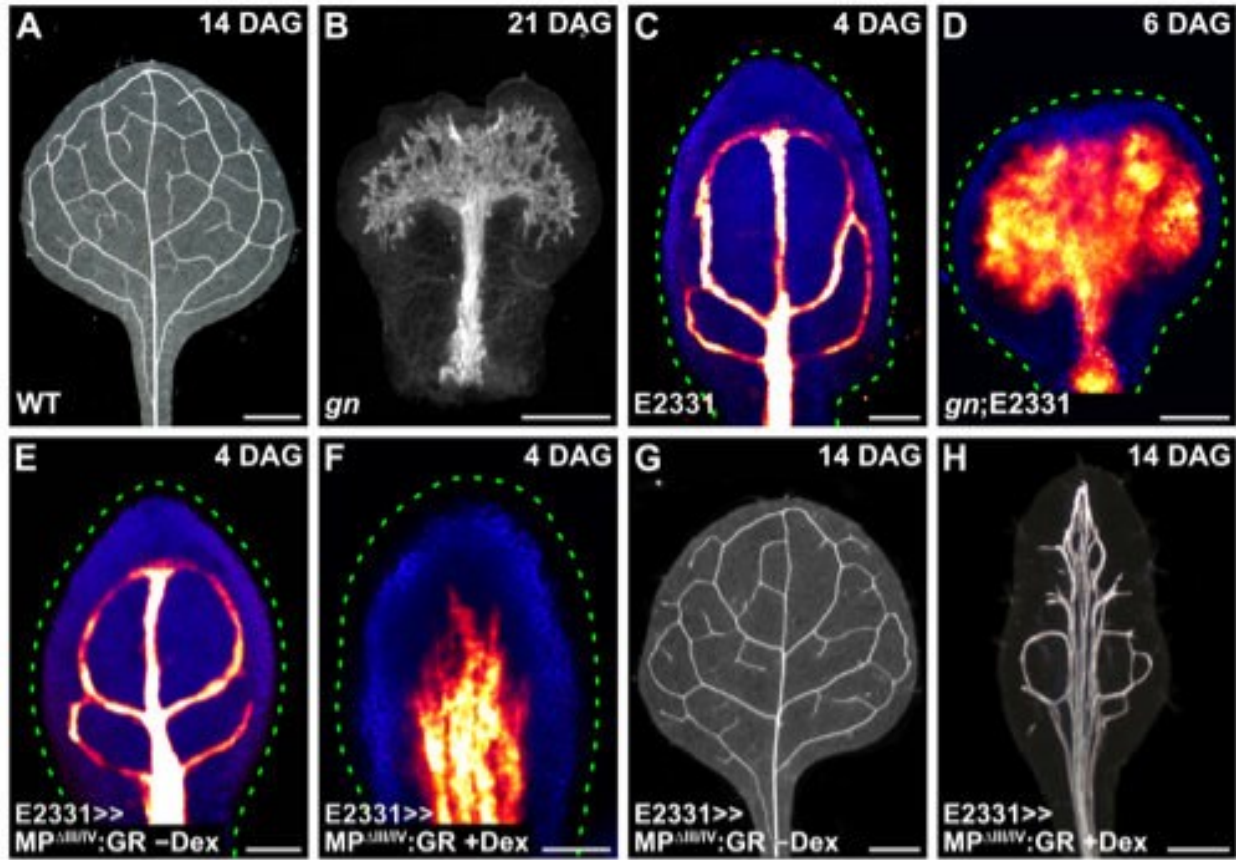
Figure 4.6. E2331-Mediated Visualization and Manipulation of Developing Veins

(A–H) First leaves. Top right: leaf age in days after germination (DAG); see Materials & methods for definition. Bottom left: genotype and treatment. (A,B,G,H) Dark-field microscopy of cleared leaves. (C–F) Confocal laser scanning microscopy. Look-up table (ramp in Fig. 4.2A) visualizes erGFP expression levels (red to white through yellow). Blue: autofluorescence. Black: global background. Dashed green line delineates leaf outline. Front view, median plane. See Table 4.2 for reproducibility of expression and pattern features. Bars: (A,B,G,H) 500 μm; (C–F) 60 μm.

E2331>>erGFP expression in developing leaves of WT and *gn*.

As shown above (Fig. 4.4D), E2331>>erGFP was expressed in midvein, first and second loops and minor veins in WT (Fig. 4.6C). In *gn*, the pattern of E2331>>erGFP expression in developing leaves recapitulated that of vascular differentiation in mature leaves (Fig. 4.6B,D), suggesting that the putative vascular cells in the shapeless clusters are indeed vascular cells, albeit abnormal ones.

Auxin signals are transduced by multiple pathways (reviewed in (Leyser, 2018) and (Gallei et al., 2020)); best characterized is the auxin signalling pathway that releases from repression activating transcription factors of the ARF family, thereby allowing them to induce transcription of auxin-responsive genes (reviewed in (Powers and Strader, 2019)). Auxin signalling is thought to be required for vein formation because mutations in genes involved in auxin signalling or treatment with inhibitors of auxin signalling leads to the formation of fewer, incompletely differentiated veins (Hardtke and Berleth, 1998; Mattsson et al., 2003; Przemeck et al., 1996; Verna et al., 2019). Increasing auxin signalling by means of broadly expressed mutations or transgenes leads to the formation of supernumerary veins, suggesting that auxin signalling is also sufficient for vein formation (Garrett et al., 2012; Krogan et al., 2012). This interpretation assumes that it is the increased auxin signalling in the cells that normally would not differentiate into vein elements that leads those cells to differentiate in fact into such elements. However, it is also possible that it is the increased auxin signalling in the cells that normally differentiate into vein elements that leads the flanking cells, which normally would not differentiate into such elements, to do in fact so. To discriminate between these possibilities, we increased auxin signalling in developing veins by expressing by the E2331 driver a dexamethasone (dex)-inducible, constitutively active variant of the MP protein — the only activating ARF with non-redundant functions in vein formation (Stamatiou, 2007). As previously reported (Krogan et al., 2012; Schena et al., 1991; Smetana et al., 2019), we constitutively activated MP by deleting domains III and IV, which are required for ARF

repression (Krogan et al., 2012; Tiwari et al., 2003; Wang et al., 2005) and fused the resulting MPΔIII/IV to a fragment of the rat glucocorticoid receptor (GR) (Picard et al., 1988) to confer dex-inducibility. We imaged E2331>>erGFP expression in developing leaves and vein patterns in mature leaves of E2331>>MPΔIII/IV:GR grown with or without dex.

Consistent with previous observations (Fig. 4.4D; Fig. 4.6C), in developing leaves of E2331>>MPΔIII/IV:GR grown without dex, E2331>>erGFP was expressed in narrow domains (Fig. 4.6E). By contrast, E2331>>erGFP was expressed in broad domains in developing leaves of dex-grown E2331>>MPΔIII/IV:GR (Fig. 4.6F). Whether with or without dex, the patterns of E2331>>erGFP expression in developing leaves of E2331>>MPΔIII/IV:GR presaged those of vein formation in mature leaves: narrow zones of vein formation in the absence of dex; broad areas of vascular differentiation in the presence of dex, often with multiple veins running parallel next to one another (Fig. 4.6G,H). Though the areas of vascular differentiation in dex-grown E2331>>MPΔIII/IV:GR are not as broad as those of leaves in which MPΔIII/IV is expressed in all the inner cells (Krogan et al., 2012), they are broader than those of E2331>>MPΔIII/IV:GR grown without dex. These observations suggest that, at least in part, it is the increased auxin signalling in the cells that normally differentiate into vein elements that leads the flanking cells, which normally would not differentiate into such elements, to do in fact so. Our conclusion is consistent with interpretations of similar findings in other plant organs (e.g., (Fukaki et al., 2005; Hay et al., 2003; Nakata et al., 2018; Pautot et al., 2001; Simon et al., 1996)) and, more in general, with organ-specific interpretations of genetic mosaics that span multiple organs in other organisms (e.g., (Morgan et al., 1919; Sturtevant 1920; Sturtevant 1932)). Nevertheless, we cannot rule out an effect on leaf vein patterning of increased auxin signalling in the vascular tissue of non-leaf organs, where E2331>>erGFP is also expressed (Fig. 4.5H,Q,Z); in the future, that possibility will have to be addressed by complementary approaches such as clonal analysis (e.g., (Burke and Basler, 1996; Posakony et al., 1991)).

In conclusion, we provide a set of GAL4/GFP enhancer-trap lines in the Col-0 background of Arabidopsis for the specific labeling of cells and tissues during early leaf development (Fig. 4.7) and we show that these lines can be used to address key questions in plant developmental biology.

4.3. MATERIALS & METHODS

4.3.1. Plants

Origin and nature of GAL4 enhancer-trap lines are in Table 4.1. *gn-13* (SALK_045424; ABRC) (Alonso et al., 2003; Verna et al., 2019) (Chapter 3) contains a T-DNA insertion after nucleotide +2835 of *GN* and was genotyped with the "SALK_045424 gn LP" (5'-TGATCCAAATCACTGGGTTTC-3') and "SALK_045424 gn RP" (5'-AGCTGAAGATAGGGAATTCGC-3') oligonucleotides (*GN*) and with the "SALK_045424 gn RP" and "LBb1.3" (5'-ATTTTGCCGATTTCGGAAC-3') oligonucleotides (*gn*). To generate the UAS::MPΔIII/IV:GR construct, the *UAS* promoter was amplified with the "UAS Promoter SalI Forward" (5'-ATAGTCGACCCAAGCGCGCAATTAACCCTCAC-3') and the "UAS Promoter XhoI Reverse" (5'-AGCCTCGAGCCTCTCCAAATGAAATGAACTTCC-3') oligonucleotides; MPΔIII/IV was amplified with the "MP Delta XhoI Forward" (5'-AAACTCGAGATGATGGCTTCATTGTCTTGTGTT-3') and the "MP EcoRI Reverse" (5'-ATTGAATTCGGTTCGGACGCGGGGTGTCGCAATT-3') oligonucleotides; and a fragment of the rat glucocorticoid (GR) receptor gene was amplified with the "SpeI GR Forward" (5'-GGGACTAGTGGAGAAGCTCGAAAAACAAAG-3') and the "GR ApaI Reverse" (5'-GCGGGGCCCTCATTTTTGATGAAACAG-3') oligonucleotides. Seeds were sterilized and sown as in (Linh and Scarpella, 2022a) (Chapter 2). Germination was synchronized as in (Scarpella et al., 2004).
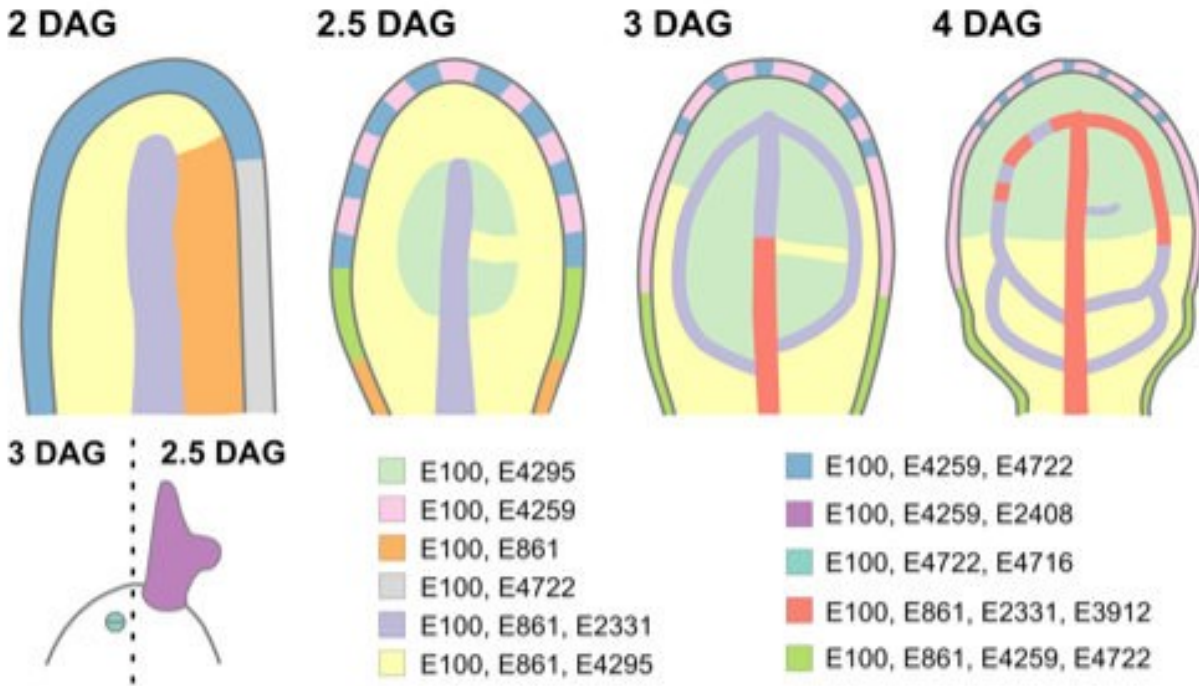
Figure 4.7. Expression Map of E100>>, E861>>, E4295>>, E4259>>, E4722>>, E2408>>, E4716>>, E2331>> and E3912>>erGFP in Leaf Development

First leaves. Top: leaf age in days after germination (DAG); see Materials & methods for definition. 2-DAG leaf primordium: side view, median plane; abaxial (ventral) side to the left, adaxial (dorsal) side to the right. Leaves 2.5–4 DAG: front view, median plane. 2.5-/3-DAG leaf composite: front ventral (left) or dorsal (right) view, epidermal plane. Map illustrates inferred overlap and exclusivity of expression. See text for details.

We refer to "days after germination" (DAG) as days after exposure of stratified seeds to light. Stratified seeds were germinated, and seedlings were grown at 22 °C under continuous fluorescent light (~80 $\mu mol\ m^{-2}\ s^{-1}$). Plants were grown at 24 °C under fluorescent light (~85 $\mu mol\ m^{-2}\ s^{-1}$) in a 16-h-light/8-h-dark cycle. Plants were transformed and representative lines were selected as in (Sawchuk et al., 2008).

4.3.2. Chemicals

Dexamethasone (Sigma-Aldrich, catalogue no. D4902) was dissolved in dimethyl sulfoxide and was added to growth medium just before sowing.

4.3.3. Imaging

Seedlings were imaged with a 1.0x Planapochromat (NA, 0.041; WD, 55 mm) objective of a Leica MZ 16FA stereomicroscope equipped with an HBO103 mercury vapor short-arc lamp and an Andor iXonEM+ camera. GFP was detected with a 480/40-nm excitation filter and a 510-nm emission filter, or with a 470/40-nm excitation filter and a 525/50-nm emission filter. Seedling organs were imaged with a 5x Fluar (NA, 0.25; WD, 12.5 mm) or a 20x Planapochromat (NA, 0.8; WD, 0.55 mm) objective of an Axio Imager.M1 microscope (Carl Zeiss) equipped with an HBO103 mercury vapor short-arc lamp and a Hamamatsu ORCA-AG camera. GFP was detected with a BP 470/40 excitation filter, an FT495 beam splitter and a BP 525/50 emission filter. Developing leaves were mounted and imaged as in (Sawchuk et al., 2013), except that emission was collected from ~1.5–5-μm-thick optical slices. Fluorophores were excited with the 488-nm line of a 30-mW Ar laser; GFP emission was collected with a BP 505–530 filter and autofluorescence was collected between 550 and 754 nm. Mature leaves were fixed in 3 : 1 or 6 : 1 ethanol : acetic acid, rehydrated in 70% ethanol and in water, cleared briefly (few seconds to few minutes) — when necessary — in 0.4 M sodium hydroxide, washed in water, mounted in 80% glycerol or in 1 : 2 : 8 or 1 : 3 : 8 water : glycerol : chloral hydrate and imaged as in (Odat et

al., 2014). In the Fiji distribution (Schindelin et al., 2012) of ImageJ (Rueden et al., 2017; Schindelin et al., 2015; Schneider et al., 2012), grayscaled RGB color images were turned into 8-bit images; when necessary, 8-bit images were combined into stacks and maximum-intensity projection was applied to stacks; look-up-tables (Sawchuk et al., 2007) were applied to images or stacks and brightness and contrast were adjusted by linear stretching of the histogram.

Chapter 5: Leaf Vein Patterning is Regulated by the Aperture of Plasmodesmata Intercellular Channels[1]

5.1 INTRODUCTION

Most multicellular organisms solve the problem of long-distance transport of water, nutrients, and signaling molecules by tissue networks such as the vascular system of vertebrate embryos and the vein network of plant leaves. How tissue networks form is therefore a key question in developmental biology. In vertebrates, for example, formation of the embryonic vascular system involves direct cell–cell interaction and cell migration (reviewed, for example, in (Betz et al., 2016; Hogan and Schulte-Merker, 2017)). Both those processes are precluded in plants by a cell wall that keeps plant cells apart and in place. Therefore, leaf veins and their networks form by a different mechanism.

How leaf veins form is poorly understood, but the cell-to-cell, polar transport of the plant signaling molecule auxin has long been thought to be both necessary and sufficient for vein formation (recently reviewed in (Cieslak et al., 2021; Lavania et al., 2021)). Inconsistent with that notion, however, veins still form in mutants lacking the function of PIN-FORMED (PIN) auxin exporters, whose polar localization at the plasma membrane determines the polarity of auxin transport (Petrasek et al., 2006; Verna et al., 2019; Wisniewska et al., 2006; Zourelidou et al., 2014). By contrast, patterning of vascular cells into veins is prevented in mutants lacking the function of the guanine exchange factor for ADP ribosylation factors GNOM (GN): the vascular system of null *gn* mutants is no more than a shapeless cluster of randomly oriented vascular cells (Amalraj et al., 2020; Geldner et al., 2004; Koizumi et al., 2000; Mayer et al., 1993; Steinmann et al., 1999; Verna et al., 2019) (Chapters 4 and 5).

---

[1] Adapted from Linh, N.M. and Scarpella, E. (2022). Leaf vein patterning is regulated by the aperture of plasmodesmata intercellular channels. *PLoS Biol* **20**, e3001781.

For over 20 years, the vesicle trafficking regulator GN has been thought to perform its essential vein-patterning function solely through its ability to control the polarity of PIN protein localization (recently reviewed in (Lavania et al., 2021)). However, two pieces of evidence argue against that notion. First, the vein patterning defects of *gn* mutants are quantitatively stronger than and qualitatively different from those of *pin* mutants (Verna et al., 2019). Second, *pin* mutations are inconsequential to the *gn* vascular phenotype (Verna et al., 2019). These observations suggest that other pathways besides polar auxin transport are involved in vein patterning and that *GN* controls such additional pathways too. Such pathways seem to rely on auxin-transporter-independent movement of auxin or an auxin-dependent signal because *pin* mutant leaves respond to auxin application by forming veins that extend away from the auxin application site (Verna et al., 2019). Because vein patterning defects of auxin-transport-inhibited leaves are enhanced by auxin signaling inhibition, the auxin-transporter-independent movement of auxin or an auxin-dependent signal with vein patterning function seems to rely, at least in part, on auxin signal transduction (Lavy and Estelle, 2016; Ramos Báez and Nemhauser, 2021; Verna et al., 2019). However, mutants impaired in both auxin signaling and polar auxin transport only phenocopy intermediate *gn* mutants (Verna et al., 2019), suggesting that additional *GN*-dependent pathways are involved in vein patterning.

Because experimental evidence suggests that auxin can move through plasmodesmata (PDs) intercellular channels (recently reviewed in (Band, 2021; Paterlini, 2020)), here we ask whether movement of auxin or an auxin-dependent signal through PDs is one of the missing *GN*-dependent vein-patterning pathways. We find veins are patterned by the coordinated action of three *GN*-dependent pathways: auxin signaling, polar auxin transport, and movement of auxin or an auxin-dependent signal through PDs

5.2 RESULTS

Available evidence suggests that auxin or an auxin-dependent signal (hereafter collectively referred to as "auxin signal") moves during leaf development, that such movement is not mediated by known auxin transporters, and that such auxin-transporter-independent movement controls vein patterning (Verna et al., 2019). Here we tested the hypothesis that the movement of an auxin signal that controls vein patterning and that is not mediated by auxin transporters is enabled by PDs.

5.2.1 Control of Vein Patterning by Regulated PD Aperture

Should the movement of an auxin signal that controls vein patterning be enabled by PDs, defects in PD aperture regulation would lead to vein pattern defects. Because severe defects in the ability to regulate PD aperture lead to embryo lethality (e.g., (Kim et al., 2002; Kobayashi et al., 2007; Patton et al., 1991; Stonebloom et al., 2009; Xu et al., 2012; Yamagishi et al., 2005)), to test the prediction that defects in PD aperture regulation will lead to vein pattern defects, we analyzed vein patterns in mature first leaves of the *callose synthase 3 - dominant* (*cals3-d*) and *glucan-synthase-like 8 / chorus / enlarged tetrad 2 / massue / ectopic expression of seed storage proteins 8* (*gsl8* hereafter) mutants of Arabidopsis, which have respectively near-constitutively narrow and near-constitutively wide PD aperture and can survive embryogenesis (Chen et al., 2009; de Storme et al., 2013; Guseman et al., 2010; Han et al., 2014; Saatian et al., 2018; Thiele et al., 2009; Vatén et al., 2011).

WT Arabidopsis forms broad leaves whose vein networks are defined by at least four reproducible features: (i) a narrow I-shaped midvein that runs the length of the leaf; (ii) lateral veins that branch from the midvein and join distal veins to form closed loops; (iii) minor veins that branch from midvein and loops and either end freely or join other veins; and (iv) minor veins and loops that curve near the leaf margin and give the vein network a scalloped outline

(Fig. 5.1A,B,F) (Candela et al., 1999; Kinsman and Pyke, 1998; Mattsson et al., 1999; Nelson and Dengler, 1997; Sawchuk et al., 2013; Sieburth, 1999; Steynen and Schultz, 2003; Telfer and Poethig, 1994; Verna et al., 2015; Verna et al., 2019). Within individual veins, vascular elements are connected end to end and are aligned along the length of the vein, and free vein ends are as narrow as the rest of the vein (Fig. 5.1G).

cals3-d mutants formed narrow leaves whose vein networks deviated from those of WT in at least four respects: (i) fewer veins were formed; (ii) closed loops were often replaced by open loops, i.e. loops that contact the midvein or other loops at only one of their two ends; (iii) veins were often replaced by "vein fragments", i.e. stretches of vascular elements that fail to contact other stretches of vascular elements at either of their two ends, or by "vascular clusters", i.e. isolated clusters of varied sizes and shapes, composed of improperly aligned and connected vascular elements; and (iv) free vein ends often terminated in vascular clusters (Fig. 5.1C,D,F,H,I; Fig. 5.2).

Like *cals3-d*, mutants in *GSL8* formed networks of fewer veins in which closed loops were often replaced by open loops; veins were often replaced by vein fragments or isolated vascular clusters; and free vein ends often terminated in vascular clusters (Fig. 5.1E,F,J,K; Fig. 5.2). However, the vein fragments of strong *gsl8* mutants, such as *gsl8-2* and *gsl8 - chorus* (*gsl8-chor* hereafter), were shorter, and the clusters were rounder and larger than those of *cals3-d* and weak *gsl8* mutants such as *gsl8 - enlarged tetrad 2* (*gsl8-et2* hereafter) (Fig. 5.1E,F,J,K; Fig. 5.2). Finally, the leaves of strong *gsl8* mutants were smaller than those of WT, *cals3-d*, and weak *gsl8* mutants; and in contrast to the entire leaf-margin of WT, *cals3-d*, and weak *gsl8* mutants, the leaf margin of strong *gsl8* mutants was lobed (Fig. 5.1E,F; Fig. 5.2).

That defects in PD aperture regulation led to defects in vein formation, vascular element alignment and connection, and vein continuity and connection is consistent with the hypothesis that movement of an auxin signal through PDs controls vein patterning.
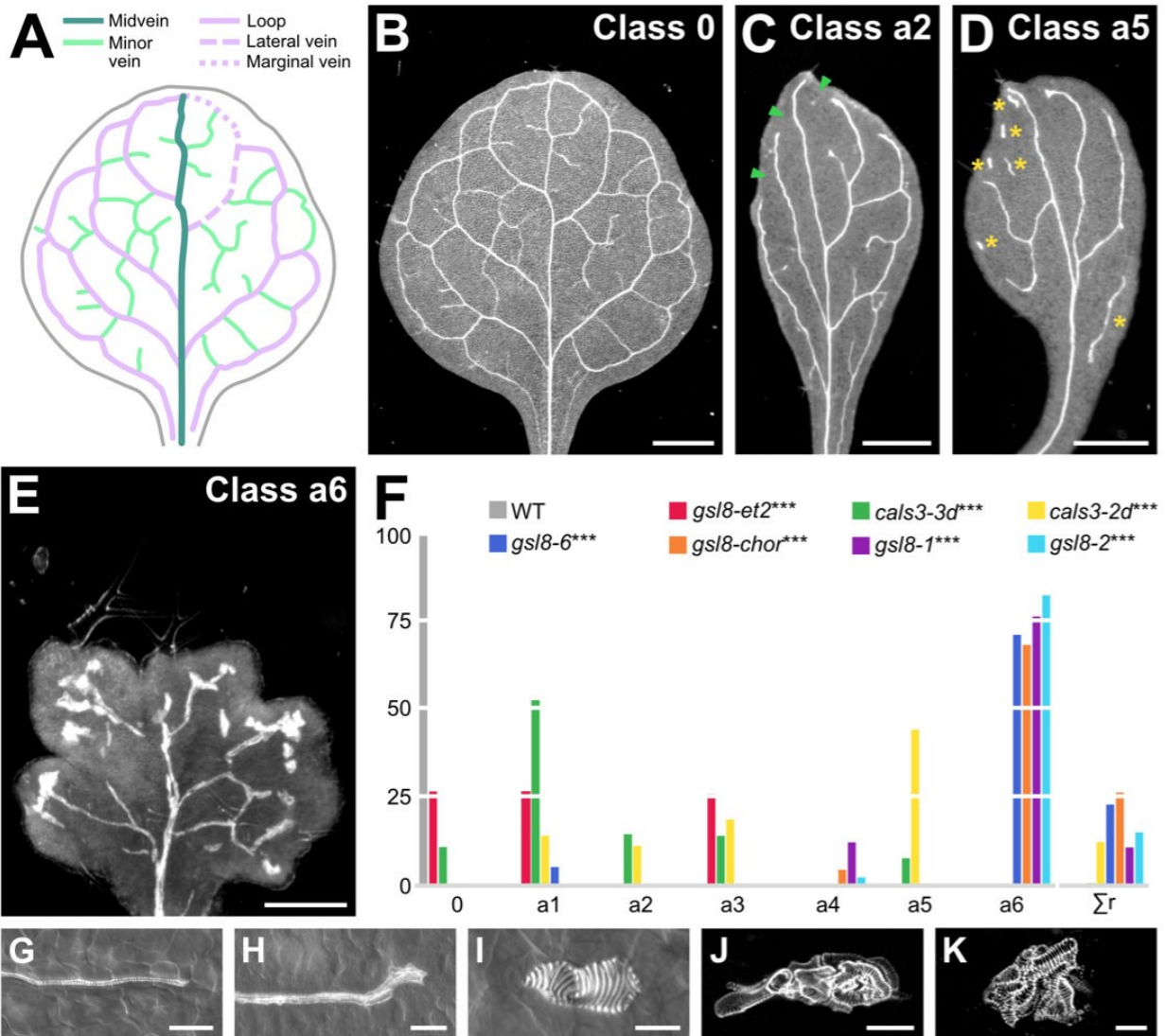
Figure 5.1. Control of Vein Patterning by PD Aperture

(A,B) Vein pattern of mature first leaf of WT Arabidopsis. In A: teal, midvein; lavender, loops; mint, minor veins. Each loop is formed by the combination of a lateral vein (dashed line) and a marginal vein (dotted line) (only shown, for simplicity, for the first loop on the right side of the leaf). (B–E) Dark-field illumination of mature first leaves illustrating phenotype classes (top right). Class 0: narrow I-shaped midvein and scalloped vein-network outline (B); class a2: narrow leaf and open vein-network outline (C); class a5: narrow leaf, open vein-network outline, and vein fragments and/or vascular clusters (D); class a6: lobed leaf, open vein-network outline,

and vein fragments and/or vascular clusters (E). Arrowheads: open loops; asterisks: vein fragments and vascular clusters. (F) Percentages of leaves in phenotype classes. Class a1: open vein-network outline (Fig. 5.2A); class a3: vein fragments and/or vascular clusters (Fig. 5.2B); class a4: lobed leaf and vein fragments and/or vascular clusters (Fig. 5.2C). Rare vein pattern defects were grouped in class Σr. Difference between *gsl8-et2* and WT, between *cals3-3d* and WT, between *cals3-2d* and WT, between *gsl8-6* and WT, between *gsl8-chor* and WT, between *gsl8-1* and WT, and between *gsl8-2* and WT was significant at $P<0.001$ (***) by Kruskal-Wallis and Mann-Whitney test with Bonferroni correction. Sample population sizes: WT, 30; *gsl8-et2*, 108; *cals3-3d*, 215; *cals3-2d*, 173; *gsl8-6*, 39; *gsl8-chor*, 45; *gsl8-1*, 65; *gsl8-2*, 47. (G–K) Details of veins and vein ends in WT (G) and *cals3-2d* (H) or of vascular clusters in *cals3-2d* (I) and *gsl8-2* (J,K). Differential-interference-contrast (G–I) or confocal-laser-scanning (J,K) microscopy. See also Table 5.1. Bars: (B–D) 1 mm; (E) 0.25 mm; (G,H,J) 50 μm; (I,K) 25 μm.
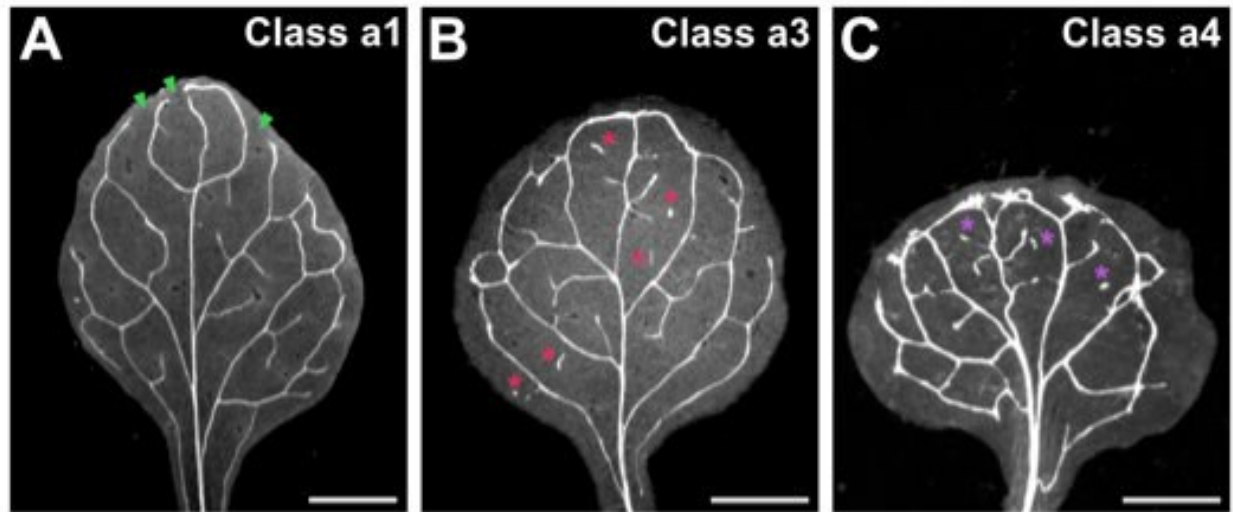
Figure 5.2. Phenotype Classes of Mature Vein Patterns

Dark-field illumination of mature first leaves illustrating phenotype classes (top right). Class a1: open vein-network outline (A); class a3: vein fragments and/or vascular clusters (B); class a4: lobed leaf and vein fragments, and/or vascular clusters (C). Arrowheads: open loops; asterisks: vein fragments and vascular clusters. Bars: 1 mm.

Table 5.1. Reproducibility of Expression and Pattern Features

Figure	Panel	No. Leaves With Displayed Features / No. Analyzed Leaves	Assessed Expression or Pattern Features
1	B	NA[1]	Narrow I-shaped midvein and scalloped vein-network outline
1	C	NA	Narrow leaf and open vein-network outline
1	D	NA	Narrow leaf, open vein-network outline, and vein fragments and/or vascular clusters
1	E	NA	Lobed leaf, open vein-network outline, and vein fragments and/or vascular clusters
1	G	NA	Free vein end as narrow as the rest of vein
1	H	NA	Free vein end terminating in vascular cluster
1	I	NA	Small vascular cluster
1	J	NA	Large, elongated vascular cluster
1	K	NA	Large, round vascular cluster
2	G	20/20	Absent (erGFP and YFP)
2	H	20/20	Midvein (erGFP). Whole primordium (YFP)

Figure	Panel	No. Leaves With Displayed Features / No. Analyzed Leaves	Assessed Expression or Pattern Features
2	I	19/19	Midvein and first loop (erGFP). Whole primordium but weaker at primordium tip (YFP)
2	J	21/21	Midvein and first and second loops (erGFP). Mainly restricted to veins in top half of leaf and nearly ubiquitous in bottom half of leaf (YFP)
2	K	16/16	Midvein; first, second, and third loops; and minor veins (erGFP). Mainly restricted to veins in upper three-quarters of leaf and nearly ubiquitous in lower quarter of leaf (YFP)
2	L	17/17	Midvein; first, second, and third loops; and minor veins (erGFP). Mainly restricted to veins in whole leaf except for lowermost part, where also in surrounding tissues (YFP)
2	M	28/28	Midvein (erGFP). Whole primordium (YFP)
2	N	16/20	Midvein (erGFP). Whole leaf but weaker at leaf tip (YFP)
2	O	15/19	Midvein and first loop (erGFP). Mainly restricted to veins in top half of leaf and nearly ubiquitous in bottom half of leaf (YFP)

Figure	Panel	No. Leaves With Displayed Features / No. Analyzed Leaves	Assessed Expression or Pattern Features
2	P	19/19	Midvein and first and second loops (erGFP). Mainly restricted to veins in whole leaf except for lowermost part, where also in surrounding tissues (YFP)
2	Q	19/19	Absent (erGFP and YFP)
2	R	35/37	Midvein (erGFP). Mainly restricted to midvein in top half of leaf and nearly ubiquitous in bottom half of leaf (YFP)
2	S	28/34	Midvein and first loop (erGFP). Mainly restricted to midvein and first loop (YFP)
2	T	37/44	Midvein, first and second loops, and minor veins (erGFP). Mainly restricted to midvein, first and second loops, and minor veins (YFP)
2	U	49/69	Segments of midvein and first loop (erGFP). Mainly restricted to whole midvein and first loop in top half of leaf (YFP)
2	V	49/53	Segments of midvein and first loop (erGFP). Mainly restricted to whole midvein and first loop (YFP)

Figure	Panel	No. Leaves With Displayed Features / No. Analyzed Leaves	Assessed Expression or Pattern Features
2	W	38/47	Segments of midvein and first and second loops (erGFP). Mainly restricted to whole midvein and first and second loops (YFP)
2	X	47/55	Segments of midvein and first, second, and third loops (erGFP). Mainly restricted to whole midvein; first, second, and third loops; and minor veins (YFP)
2	Y	27/31	Midvein (erGFP). Mainly restricted to midvein in whole primordium except for lowermost part, where also in surrounding tissues (YFP)
2	Z	38/42	Midvein, closed or open first and second loops, and vein fragments (erGFP). Mainly restricted to veins in whole leaf except for lowermost part, where also in surrounding tissues (YFP)
2	AA	50/61	Midvein (erGFP). Whole primordium (YFP)
2	AB	31/38	Midvein, closed or open loops, and vein fragments and/or vascular clusters (erGFP). Whole leaf but heterogeneous (YFP)
3	A	30/32	Midvein and closed first and open second loops

Figure	Panel	No. Leaves With Displayed Features / No. Analyzed Leaves	Assessed Expression or Pattern Features
3	B	28/34	Midvein and open first and second loops
3	C	63/79	Vein formed in response to IAA connects to midvein
3	D	27/44	Vein formed in response to IAA runs parallel to midvein
3	E	20/22	Midvein and closed first loop
3	F	24/24	Midvein
3	G	22/25	Vein formed in response to IAA connects to midvein
3	H	10/56	Vein formed in response to IAA connects to midvein by broad vascular zone
3	I	13/15	Restricted to veins in whole leaf (erGFP). Mainly restricted to veins in top half of leaf and nearly ubiquitous in bottom half of leaf (YFP)
3	J	20/22	Restricted to veins in whole leaf (erGFP). Mainly restricted to veins in whole leaf except for lowermost part, where also in surrounding tissues (YFP)

Figure	Panel	No. Leaves With Displayed Features / No. Analyzed Leaves	Assessed Expression or Pattern Features
3	K	24/27	Restricted to veins in whole leaf (erGFP). Mainly restricted to veins in middle of leaf and nearly ubiquitous on side of leaf where IAA was applied (YFP)
3	L	18/26	Restricted to veins in whole leaf (erGFP). Mainly restricted to veins in whole leaf except for lowermost part, where also in surrounding tissues (YFP)
4	A	24/26	Midvein, first and second loops, and minor veins
4	B	24/30	Midvein, closed or open first and second loops, and vein fragments
4	C	15/20	Midvein, open first loops, and vascular clusters
4	D	54/58	More lateral-veins, running parallel to one another in middle of leaf to form wide midvein and joining distal veins at margin of leaf to form smooth vein-network outline
4	E	38/38	More lateral-veins, running parallel to one another in middle of leaf to form wide midvein and joining distal veins at margin of

Figure	Panel	No. Leaves With Displayed Features / No. Analyzed Leaves	Assessed Expression or Pattern Features
			leaf to form scalloped vein-network outline or ending freely in the lamina
4	F	13/16	More lateral-veins, running parallel to one another in middle of leaf to form wide midvein and ending freely in the lamina
4	G	37/37	Midvein (erGFP). Whole primordium (YFP)
4	H	36/36	Midvein (erGFP). Whole primordium (YFP)
4	I	21/26	Midvein, first and second loops, and minor veins (erGFP). Mainly restricted to veins in top half of leaf and nearly ubiquitous in bottom half of leaf (YFP)
4	J	25/26	Restricted to veins (erGFP). Throughout leaf but weaker along margin in top half of leaf (YFP)
4	K	28/29	Restricted to veins (erGFP). Mainly restricted to veins in whole leaf except for lowermost part, where also in surrounding tissues (YFP)
4	L	27/27	Whole marginal epidermis; all inner cells but stronger in midvein

Figure	Panel	No. Leaves With Displayed Features / No. Analyzed Leaves	Assessed Expression or Pattern Features
4	M	21/21	Whole marginal epidermis; all inner cells but stronger in midvein and first loop
4	N	28/30	Whole marginal epidermis but weaker at leaf tip; in inner tissue, mainly restricted to midvein, first and second loops, and surrounding cells
4	O	28/32	Marginal epidermis in bottom half of leaf; in inner tissue, mainly restricted to midvein, loops, minor veins, and — in bottom half of leaf — surrounding cells
4	P	30/30	Whole marginal epidermis; all inner cells but stronger in midvein
4	Q	37/40	Whole marginal epidermis; all inner cells but stronger in midvein and continuous and connected first loop
4	R	24/39	Whole marginal epidermis; all inner cells but stronger, though heterogeneously so, in continuous and connected first loop
4	S	36/61	Marginal epidermis in bottom half of leaf; in inner tissue, mainly restricted to midvein, open first loop, and continuous and connected second loop and surrounding cells

Figure	Panel	No. Leaves With Displayed Features / No. Analyzed Leaves	Assessed Expression or Pattern Features
4	T	20/61	Marginal epidermis in bottom half of leaf; in inner tissue, mainly restricted to midvein, open first loop, vein fragments and/or vascular clusters, and continuous and connected second loop and surrounding cells
4	U	34/68	Marginal epidermis in lower third of leaf; in inner tissue, mainly restricted to midvein, open first loop, and minor veins
4	V	31/68	Marginal epidermis in lower third of leaf; in inner tissue, mainly restricted to midvein, open first loop, minor veins, and vein fragments and/or vascular clusters
4	W	39/61	All inner cells in bottom half of leaf but stronger, though heterogeneously so, in continuous and connected second loop
4	X	50/68	In bottom half of leaf, mainly restricted to open second loop and minor veins and surrounding cells
4	Y	19/20	Whole marginal epidermis; all inner cells but stronger in midvein
4	Z	18/22	Whole marginal epidermis; all inner cells but stronger in midvein and continuous and connected first loop

Figure	Panel	No. Leaves With Displayed Features / No. Analyzed Leaves	Assessed Expression or Pattern Features
4	AA	14/22	Whole marginal epidermis; most inner cells but stronger, though heterogeneously so, in continuous and connected first loop
4	AB	24/32	Whole marginal epidermis; in inner tissue, mainly restricted to continuous and connected first loop, though more heterogeneously so, and surrounding cells
4	AC	25/32	Marginal epidermis in bottom half of leaf; in inner tissue, mainly restricted to midvein, open loops, and vein fragments and/or vascular clusters
4	AD	25/25	Localized to plasma-membrane side facing veins to which second loop is connected
4	AE	17/20	Localized to plasma-membrane side facing contiguous cell in vein fragment
4	AF	11/12	Localized to plasma membrane side facing other cell in two-cell vascular clusters
4	AG	27/27	Localized to plasma membrane sides facing contiguous cells in larger vascular clusters

Figure	Panel	No. Leaves With Displayed Features / No. Analyzed Leaves	Assessed Expression or Pattern Features
5	A	21/23	Midvein, first and second loops, and minor veins
5	B	20/23	Midvein, first and second loops, and minor veins
5	C	22/25	Midvein and open first loop
5	D	20/20	Midvein, open or closed first loop, and vein fragments
5	E	27/30	Midvein, open first loop, vein fragments, and vascular clusters
5	F	20/26	Midvein and scattered vascular clusters
5	G	18/22	Midvein, open first loop, and vascular clusters
5	H	9/22	Midvein, vein fragments, and vascular clusters
5	I	9/22	Midvein
5	J	15/46	Midvein, vein fragments, and vascular clusters
5	K	27/46	Midvein
5	L	24/24	Midvein (erGFP). Whole primordium (YFP)
5	M	22/22	Midvein (erGFP). Whole primordium (YFP)
5	N	19/20	Midvein, first and second loops, and minor veins (erGFP). Mainly restricted to veins in top half of leaf and nearly ubiquitous in bottom half of leaf (YFP)

Figure	Panel	No. Leaves With Displayed Features / No. Analyzed Leaves	Assessed Expression or Pattern Features
5	O	18/21	Midvein and first loop (erGFP). Mainly restricted to veins in upper three-quarters and nearly ubiquitous in lower quarter of leaf (YFP)
5	P	40/42	Strong and mainly associated with veins
5	Q	58/58	Weak and broad
5	R	26/31	Strong and mainly associated with veins
5	S	31/44	Weak and broad
6	A	NA	Narrow I-shaped midvein and scalloped vein-network outline
6	B	NA	Open vein-network outline or narrow leaf and open vein-network outline
6	C	NA	Lobed leaf, open vein-network outline, and vein fragments and/or vascular clusters
6	D	NA	Wide midvein and shapeless vascular cluster
6	E	NA	Wide midvein and shapeless vascular cluster
6	F	NA	Wide midvein and shapeless vascular cluster

Figure	Panel	No. Leaves With Displayed Features / No. Analyzed Leaves	Assessed Expression or Pattern Features
6	H	21/23	Midvein, first and second loops, and minor veins
6	I	25/29	Wide midvein, dense network of thick veins, and thick vein-network outline
6	J	22/42	Wider midvein, denser network of thicker veins, and jagged vein-network outline
6	K	20/42	Even wider midvein, even denser network of even thicker veins, and pronouncedly jagged vein-network outline
6	L	13/15	Wide midvein and shapeless vascular cluster
6	M	27/27	Wide midvein and shapeless vascular cluster
6	N	21/22	Midvein (erGFP). Whole primordium (YFP)
6	O	22/22	Midvein, first and second loops, and minor veins (erGFP). Mainly restricted to veins in top half of leaf and nearly ubiquitous in bottom half of leaf (YFP)
6	P	36/36	Midvein (erGFP). Whole primordium but weaker in nonvascular tissues (YFP)

Figure	Panel	No. Leaves With Displayed Features / No. Analyzed Leaves	Assessed Expression or Pattern Features
6	Q	26/31	Wide midvein and shapeless vascular cluster (erGFP). Mainly restricted to the wide midvein in the bottom half of the leaf; nearly ubiquitous in the top half of the leaf but weaker in nonvascular tissues (YFP)

[1] Not applicable

5.2.2 PD Permeability Changes During Leaf Development

Because both near-constitutively wide and near-constitutively narrow PD aperture control vein patterning (Fig. 5.1; Fig. 5.2), we asked how PD permeability changed during leaf development. To address this question, we expressed an untargeted YFP, which diffuses through PDs (Imlau et al., 1999; Kim et al., 2005a; Kim et al., 2005b), by the *UAS* promoter, which is inactive in plants in the absence of a GAL4 driver (Fig. 5.3G). We activated YFP expression by tissue- and stage-specific GAL4/erGFP enhancer-trap (ET) drivers (Fig. 5.3F), and imaged erGFP expression and YFP signals in first leaves of the resulting ET>>erGFP/YFP plants 2.5 to 6 days after germination (DAG).

In ET>>erGFP/YFP plants, expression of a nondiffusible endoplasmic-reticulum-localized GFP (erGFP) (Oparka et al., 1999) reports expression of GAL4 (Gardner et al., 2009; Haseloff, 1999; Laplaze et al., 2005), which activates expression of the diffusible YFP. Should the aperture of the PDs in the cells in which YFP expression is activated be narrower than the size of YFP, erGFP and YFP would be detected in the same cells. By contrast, should the aperture be wider than the size of YFP, YFP would be detected in additional cells.

The development of Arabidopsis leaves has been described previously (Candela et al., 1999; Donnelly et al., 1999; Kang and Dengler, 2002; Kang and Dengler, 2004; Kinsman and Pyke, 1998; Mattsson et al., 1999; Mattsson et al., 2003; Pyke et al., 1991; Scarpella et al., 2004; Telfer and Poethig, 1994). Briefly, at 2 DAG the first leaf is recognizable as a cylindrical primordium with a midvein at its center (Fig. 5.3A). By 2.5 DAG the primordium has expanded (Fig. 5.3B), and by 3 DAG the first loops of veins ("first loops") have formed (Fig. 5.3C). By 4 DAG, a lamina and a petiole have become recognizable, and second loops have formed (Fig. 5.3D). By 5 DAG, lateral outgrowths have become recognizable in the lower quarter of the lamina; third loops have formed; and minor vein have formed in the upper three-quarters of the lamina (Fig. 5.3E). Finally, by 6 DAG minor vein formation has spread to the whole lamina.
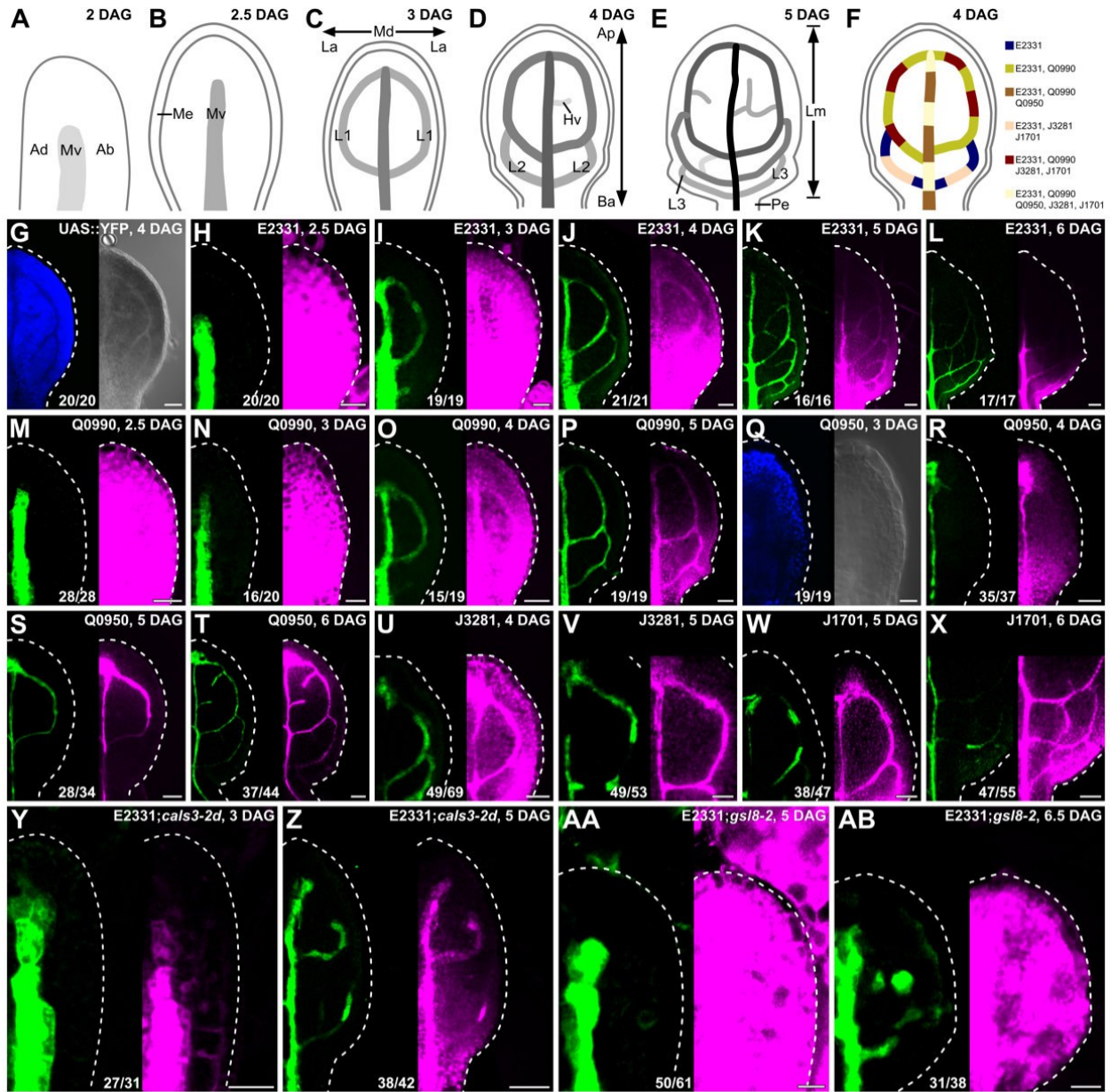
Figure 5.3. PD Permeability Changes During Leaf Development

(A–F) Top right: leaf age in days after germination (DAG). (A–E) Veins form sequentially during Arabidopsis leaf development: the formation of the midvein is followed by the formation of the first loops of veins ("first loops"); the formation of first loops is followed by that of second loops and minor veins; and the formation of second loops and minor veins is followed by that of third loops. Loops and minor veins form in a tip-to-base sequence during leaf development.

179

Increasingly darker grays depict progressively later stages of vein development. Ab, abaxial; Ad, adaxial; Ap, apical; Ba, basal; Hv, minor vein; L1, L2, and L3: first, second, and third loop; La, lateral; Lm, lamina; Md, median; Me, marginal epidermis; Mv, midvein; Pe, petiole. (F) Expression map of tissue- and stage-specific GAL4/erGFP enhancer-trap (ET) drivers in developing leaves illustrates inferred overlap and exclusivity of expression. (G–AB) Differential-interference-contrast (G, right; Q, right) or confocal-laser-scanning (all other panels) microscopy. First leaves (for simplicity, only half-leaves are shown). Blue, autofluorescence; green, GFP expression; magenta, YFP signals. Dashed white line delineates leaf outline. Top right: leaf age in DAG and genotype. Bottom center: reproducibility index (see Table 5.1). Bars: (H,I,M,N,Q,Y,AA) 20 μm; (G,J,O,R,U) 40 μm; (K,P,S,V,W,Z,AB) 60 μm; (L,T,X) 80 μm.

In 2.5-DAG primordia of E2331>>erGFP/YFP, in which GAL4 expression is activated at early stages of vein development (Amalraj et al., 2020) (Chapter 4), YFP was detected throughout the 2.5-DAG primordium, even though erGFP was only expressed in the midvein (Fig. 5.3H). At 3 DAG, erGFP was only expressed in the midvein and first loops; nevertheless, YFP was still detected throughout the primordium, even though YFP signals were weaker at the primordium tip (Fig. 5.3I). At 4 DAG, erGFP was only expressed in the midvein and first and second loops (Fig. 5.3J). YFP signals were mainly restricted to the veins in the top half of the 4-DAG leaf but were detected throughout the bottom half of the 4-DAG leaf (Fig. 5.3J). At 5 DAG, erGFP was only expressed in the midvein; first, second, and third loops; and minor veins (Fig. 5.3K). YFP signals were mainly restricted to the veins in the upper three-quarters of the 5-DAG leaf but were detected throughout the lower quarter of the 5-DAG leaf (Fig. 5.3K). At 6 DAG, erGFP continued to be only expressed in the midvein; first, second, and third loops; and minor veins (Fig. 5.3L). YFP signals were mainly restricted to the veins in the whole 6-DAG leaf except for its lowermost part, where YFP was additionally detected in surrounding tissues (Fig. 5.3L).

YFP signals behaved during Q0990>>erGFP/YFP leaf development as they did during E2331>>erGFP/YFP leaf development (Fig. 5.3M–P; compare with Fig. 5.3H–L), even though GAL4 expression is activated at intermediate stages of vein development in Q0990, i.e. later than in E2331 (Amalraj et al., 2020; Sawchuk et al., 2007) (Chapter 4).

In 3-DAG primordia of Q0950>>erGFP/YFP, in which GAL4 is activated at late stages of vein development, i.e. later than in Q0990 (Sawchuk et al., 2007), neither erGFP nor YFP was expressed (Fig. 5.3Q), further suggesting that the *UAS* promoter is not active in plants in the absence of GAL4. At 4 DAG, erGFP was only expressed in the midvein (Fig. 5.3R). YFP signals were mainly restricted to the midvein in the top half of the 4-DAG leaf but were detected throughout the bottom half of the 4-DAG leaf (Fig. 5.3R). At 5 and 6 DAG, expression of both erGFP and YFP was restricted to the veins (Fig. 5.3S,T).

Consistent with previous observations (Kim et al., 2005a), our results suggest that PD permeability is high throughout the leaf at early stages of tissue development. PD permeability remains high in areas of the leaf where veins are still forming, but PD permeability between veins and surrounding nonvascular tissues lowers in areas of the leaf where veins are no longer forming. Eventually, veins become symplastically isolated from surrounding nonvascular tissues. To test whether vein cells become isolated also from one another, we imaged J3281>> and J1701>>erGFP/YFP, in which GAL4 is activated in vein segments (Sawchuk et al., 2007).

In 4- and 5-DAG J3281>>erGFP/YFP leaves, erGFP was only expressed in segments of midvein and first loops, but YFP was detected in the whole midvein and first loops (Fig. 5.3U,V). Likewise, in 5- and 6-DAG J1701>>erGFP/YFP leaves, erGFP was only expressed in segments of midvein and first and second loops, but YFP was detected in whole midvein and loops (Fig. 5.3W,X). These results suggest that vein cells are not symplastically isolated from one another even when they are isolated from surrounding nonvascular tissues.

To test whether the reduction in PD permeability between veins and surrounding nonvascular tissues that occurs during normal leaf development were relevant for vein patterning, we imaged E2331>>erGFP/YFP in *cals3-2d* and *gsl8-2* developing leaves.

As in 2.5-DAG E2331>>erGFP/YFP (Fig. 5.3H), in 5-DAG E2331>>erGFP/YFP;*gsl8-2* erGFP was only expressed in the midvein, and YFP was detected throughout the primordia (Fig. 5.3AA). Also in 3-DAG E2331>>erGFP/YFP;*cals3-2d*, erGFP was only expressed in the midvein (Fig. 5.3Y). However, unlike in E2331>>erGFP/YFP and E2331>>erGFP/YFP;*gsl8-2*, in 3-DAG E2331>>erGFP/YFP;*cals3-2d* YFP signals too were mainly restricted to the midvein — except for its lowermost part, where weak YFP signals were additionally detected in surrounding nonvascular tissues (Fig. 5.3Y).

As in 4-DAG E2331>>erGFP/YFP (Fig. 5.3J), erGFP was only expressed in the vascular tissue of 5-DAG E2331>>erGFP/YFP;*cals3-2d* and 6.5-DAG E2331>>erGFP/YFP;*gsl8-2* (Fig. 5.3Z,AB). However, unlike in 4-DAG E2331>>erGFP/YFP (Fig. 5.3J), YFP was mainly restricted

to the vascular tissue of the whole 5-DAG E2331>>erGFP/YFP;*cals3-2d* leaf — except for its lowermost part, where weak YFP signals were additionally detected in surrounding nonvascular tissues (Fig. 5.3Z). And YFP signals failed to become restricted to the vascular tissue of 6.5-DAG E2331>>erGFP/YFP;*gsl8-2*, though signal intensity was heterogeneous across the leaf (Fig. 5.3AB).

We conclude that vein patterning defects in *gsl8* and *casl3-d* are respectively associated with near-constitutively high and near-constitutively low PD permeability between veins and surrounding nonvascular tissues

5.2.3 Auxin-Induced Vein Formation and PD Aperture Regulation

Auxin application induces vein formation (Aloni, 2001; Linh and Scarpella, 2022a; Sachs, 1989; Sawchuk et al., 2007; Scarpella et al., 2006; Verna et al., 2019) (Chapter 2). Therefore, should the movement of an auxin signal that controls vein patterning be enabled by PDs, defects in PD aperture regulation would lead to defects in auxin-induced vein formation. To test this prediction, we applied the natural auxin indole-3-acetic acid (IAA) to one side of developing first leaves of E2331;*cals3-2d* and Q0990;*gsl8-2* and their respective controls E2331 and Q0990 (Fig. 5.4A,B,E,F). Because *cals3-2d* and *gsl8* leaves develop more slowly than WT leaves (Fig. 5.5M−O,Q,S−X,Z,AC), we applied IAA to 3.5-DAG first leaves of E2331 and Q0990, and to 4.5-DAG first leaves of E2331;*cals3-2d* and Q0990;*gsl8-2*. We then assessed erGFP-expression-labeled, IAA-induced vein formation 2.5 days later.

Consistent with previous reports (Aloni, 2001; Linh and Scarpella, 2022a; Sachs, 1989; Sawchuk et al., 2007; Scarpella et al., 2006; Verna et al., 2019) (Chapter 2), IAA application induced the formation of veins in ~80% (63/79) of E2331 leaves and ~90% (22/25) of Q0990 leaves (Fig. 5.4C,G). Furthermore, in ~55% (34/63) of the E2331 leaves and ~65% (14/22) of the Q0990 leaves in which veins formed in response to IAA application, veins readily connected to the midvein (Fig.5.4C,G). By contrast, IAA application induced vein formation in only ~60%
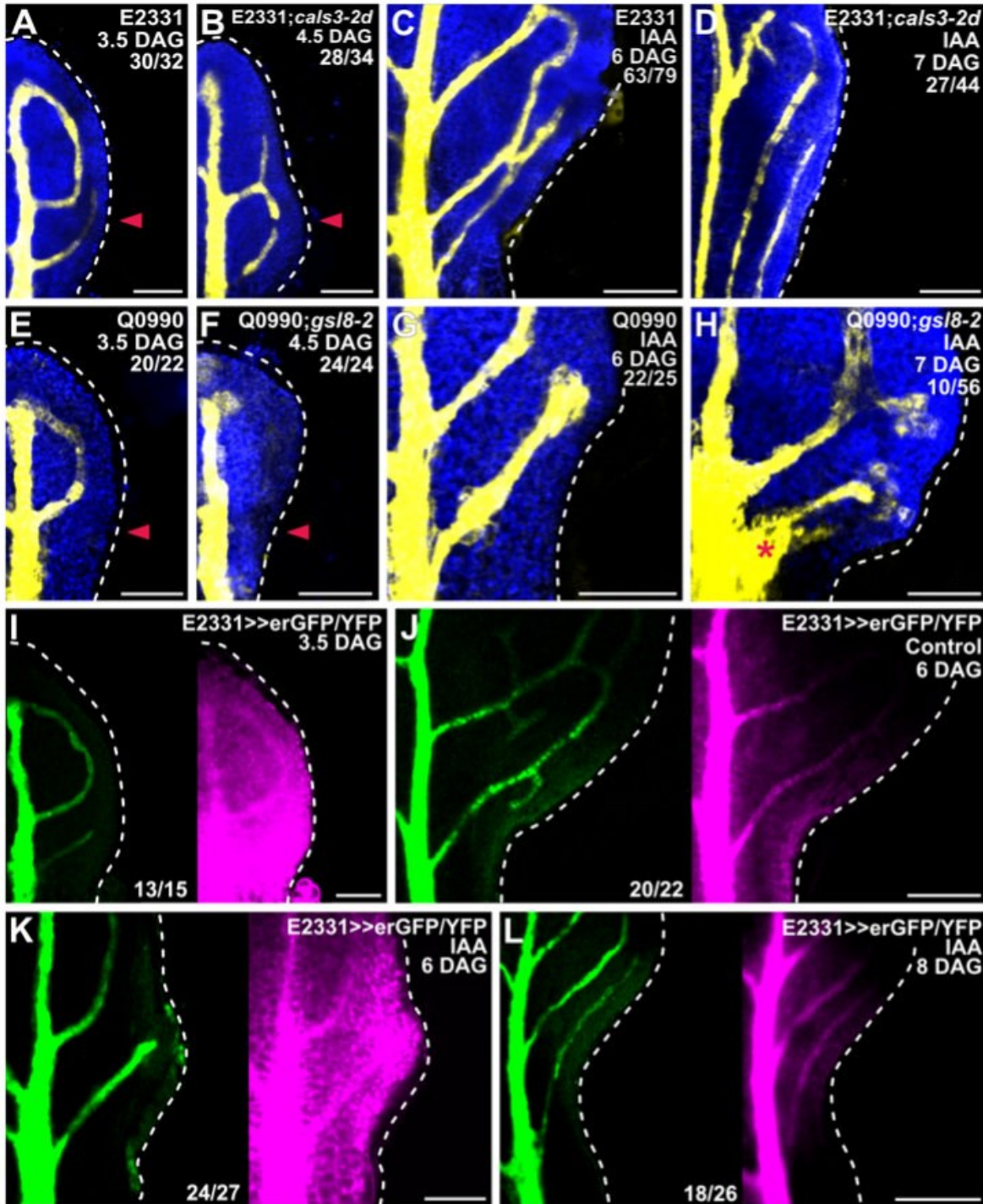
Figure 5.4. Auxin-Induced Vein Formation and PD Aperture Regulation

(A–L) Confocal laser scanning microscopy. First leaves (for simplicity, only half-leaves are

shown). Blue, autofluorescence; yellow (A–H) or green (I–L), GFP expression; magenta, YFP

signals. Dashed white line delineates leaf outline. Top right: leaf age in DAG, genotype, treatment, and — in A–H — reproducibility index (see Table 5.1). Bottom center (I-L): reproducibility index. Arrowhead in A,B,E,F indicates position of IAA application. Star in H indicates broad area of vascular differentiation connecting the midvein with the vein whose formation was induced by IAA application. Bars: (A,E,F,G–I,K) 80 μm; (B) 60 μm; (C,J,L) 120 μm; (D) 150 μm.
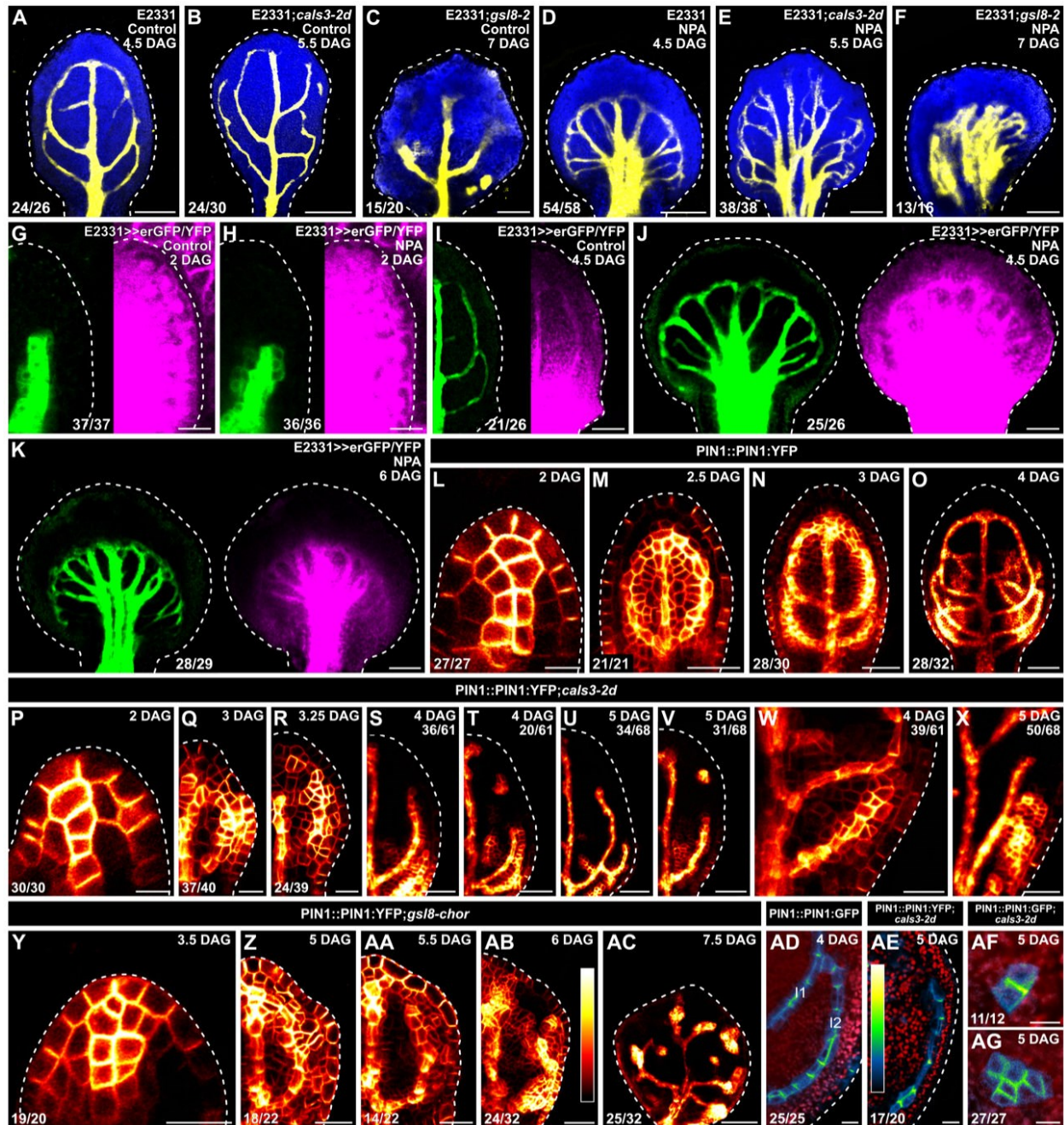
Figure 5.5. Auxin-Transport-Dependent Vein Patterning and Regulated PD Aperture

(A–AG) Confocal laser scanning microscopy. First leaves (for simplicity, only half-leaves are shown in G–I, Q–V, and Z–AB). Blue (A–F) or red (AD–AG), autofluorescence; yellow (A–F) or green (G–K), GFP expression; magenta, YFP signals. Dashed white line delineates leaf outline.

(G,H,L,P,Y) Side view, adaxial side to the left. (L–AC) PIN1::PIN1:YFP expression; look-up table (ramp in AB) visualizes expression levels. (AD–AG) PIN1::PIN1:GFP (AD,AF,AG) or PIN1::PIN1:YFP (AE) expression; look-up table (ramp in AE) visualizes expression levels. Top right: leaf age in DAG, genotype, and treatment (25 µM NPA), and — in S–V,X — reproducibility index. Bottom left (A–F,L–R,W,Y–AG) or center (G–K): reproducibility index (see Table 5.1). Bars: (A–F,I–K) 120 µm; (G,H,Q,R,W,X,Y) 20 µm; (L,P,AD–AG) 10 µm; (M,N,S,T,Z,AA,AB) 40 µm; (O,U,V,AC) 60 µm.

(27/44) of E2331;*cals3-2d* leaves and ~20% (10/56) of Q0990;*gsl8-2* leaves (Fig. 5.4D,H).

Moreover, only in ~30% (8/27) of the E2331;*cals3-2d* leaves in which veins did form in response

to IAA application did these veins connect to the midvein (Fig. 5.4D). In the remaining ~70% of

the responding E2331;*cals3-2d* leaves (19/27), the veins whose formation was induced by IAA

application ran parallel to the midvein through the leaf petiole (Fig. 5.4D). Conversely, in 90%

(9/10) of the Q0990;*gsl8-2* leaves in which IAA induced vein formation, not only did the veins

whose formation was induced by IAA application connect to the midvein, but they did so by

expanding into a broad vascular differentiation zone (Fig. 5.4H). Therefore, both near-

constitutively wide and near-constitutively narrow PD aperture inhibit auxin-induced vein

formation. Whenever the tissue escapes such an effect, near-constitutively narrow PD aperture

inhibits connection of newly formed veins to pre-existing ones, and near-constitutively wide PD

aperture accentuates that connection through excess vascular differentiation. These

observations suggest that auxin-induced vein formation depends on regulated PD aperture, that

restriction of auxin-induced vascular differentiation to limited cell files depends on narrow PD

aperture, and that connection of veins whose formation is induced by auxin depends on wide PD

aperture. Were that so, auxin application would impinge on the reduction in PD permeability

between veins and surrounding nonvascular tissues that occurs during normal leaf development

(Fig. 5.3). To test this prediction, we applied IAA to one side of 3.5-DAG first leaves of

E2331>>erGFP/YFP and assessed erGFP-expression-labeled, IAA-induced vein formation and

YFP-signal-inferred PD permeability 2.5 and 4.5 days later (i.e. 6 and 8 DAG, respectively).

Consistent with what is shown above (Fig. 5.3I,J; Fig. 5.4A), at 3.5 DAG erGFP was only

expressed in the midvein and in first and second loops (Fig. 5.4I). In the top half of 3.5-DAG

leaves, YFP signals were weaker in nonvascular tissues than in veins but were uniformly strong

in the bottom half of the leaves (Fig.5. 4I). As shown above (Fig. 5.3L), at 6 DAG erGFP

expression was restricted to the veins (Fig. 5.4J,K). In 6-DAG leaves to which IAA had not been

applied, YFP signals were mainly restricted to the veins in the whole leaf except for its

lowermost part, where YFP was additionally detected in surrounding tissues (Fig. 5.4J). By contrast, YFP signals were detected throughout the bottom half of the 6-DAG leaves to which IAA had been applied (Fig. 5.4K). By 8 DAG, however, both erGFP and YFP signals had become mainly restricted to the veins also in the leaves to which IAA had been applied (Fig. 5.4L).

In conclusion, our results suggest that auxin application delays the reduction in PD permeability between veins and surrounding nonvascular tissues that occurs during normal leaf development, and that auxin-induced vein formation and connection depends on the ability to regulate PD aperture. Such conclusions are consistent with the hypothesis that the movement of an auxin signal that controls vein patterning is enabled by PDs.

5.2.4 Auxin-Transport-Dependent Vein Patterning and Regulated PD Aperture

Should the movement of an auxin signal that controls vein patterning and is not mediated by auxin transporters be enabled by PDs, defects in PD aperture regulation would enhance vein patterning defects induced by auxin transport inhibition. To test this prediction, we grew E2331, E2331;*cals3-2d*, and E2331;*gsl8-2* in the presence or absence of the auxin transport inhibitor N-1-naphthylphthalamic acid (NPA) (Morgan and Söding, 1958), which binds PIN proteins and inhibits their activity (Abas et al., 2021; Teale et al., 2020) and which induces vein patterning defects that phenocopy the loss of that *PIN*-dependent auxin transport pathway that is relevant for vein patterning (Verna et al., 2019) (Chapter 3). We then imaged erGFP-expression-labeled vein networks 4.5 DAG in E2331. Because *cals3-2d* and *gsl8* leaves develop more slowly than WT leaves (Fig. 5.5M–O,Q,S–X,Z,AC), we imaged erGFP-expression-labeled vein networks 5.5 and 7 DAG in E2331;*cals3-2d* and E2331;*gsl8-2*, respectively.

Consistent with what is shown above (Fig. 5.3J,K), in the absence of NPA vein networks were composed of midvein, first and second loops, and minor veins in E2331, and of midvein, loops — whether open or closed — vein fragments, and vascular clusters in E2331;*cals3-2d* and E2331;*gsl8-2* (Fig. 5.5A–C).

Consistent with previous reports (Mattsson et al., 1999; Sieburth, 1999; Verna et al., 2019), NPA reproducibly induced characteristic vein pattern defects in E2331 leaves: (i) the vein network comprised more lateral-veins; (ii) lateral veins failed to join the midvein in the middle of the leaf and instead ran parallel to one another to form a wide midvein; and (iii) lateral veins joined distal veins in a marginal vein that closely paralleled the leaf margin and gave a smooth outline to the vein network (Fig. 5.5D).

As in E2331, in E2331;*cals3-2d* NPA induced the formation of more lateral-veins that failed to join the midvein in the middle of the leaf and instead ran parallel to one another to form a wide midvein (Fig. 5.5E). However, unlike in NPA-grown E2331, in NPA-grown E2331;*cals3-2d* lateral veins often failed to join distal veins in a marginal vein and instead ended freely in the lamina near the leaf margin (Fig. 5.5E).

As in both E2331 and E2331;*cals3-2d*, in E2331;*gsl8-2* NPA induced the formation of more veins, but these veins ran parallel to one another to give rise to a midvein that spanned almost the entire width of the leaf (Fig. 5.5F). And as in NPA-grown E2331;*cals3-2d* — but unlike in NPA-grown E2331 — in NPA-grown E2331;*gsl8-2* only rarely did veins join one another in a marginal vein; instead, they most often ended freely in the lamina near the leaf tip (Fig. 5.5F).

In conclusion, both near-constitutively wide and near-constitutively narrow PD aperture enhance vein patterning defects induced by auxin transport inhibition, a conclusion that is consistent with the hypothesis that the movement of an auxin signal that controls vein patterning and is not mediated by auxin transporters is enabled by PDs. Moreover, because auxin transport inhibition promotes vein connection (Verna et al., 2015), that NPA was unable to induce vein connection in E2331;*cals3-2d* and E2331;*gsl8-2* suggests that the promoting effect of auxin transport inhibition on vein connection depends on regulated PD aperture. Were that so, auxin transport inhibition would impinge on the reduction of PD permeability that occurs between veins and surrounding nonvascular tissues during normal leaf development. To

test this prediction, we grew E2331>>erGFP/YFP in the presence or absence of NPA, and assessed erGFP-expression-labeled vein network formation and YFP-signal-inferred PD aperture in first leaves 2, 4.5, and 6 DAG.

Consistent with what is shown above (Fig. 5.3H), at 2 DAG erGFP was only expressed in the midvein of both NPA- and normally grown E2331>>erGFP/YFP — though the erGFP expression domain was broader in NPA-grown than in normally grown primordia (Fig. 5.5G,H). Likewise, in both NPA- and normally grown E2331>>erGFP/YFP YFP was detected throughout the 2-DAG primordia (Fig. 5.5G,H).

Also consistent with what is shown above (Fig. 5.3J,K), at 4.5 DAG erGFP was only expressed in the midvein, first and second loops, and minor veins of normally grown E2331>>erGFP/YFP (Fig. 5.5I). YFP signals were mainly restricted to the veins in the top half of normally grown 4.5-DAG E2331>>erGFP/YFP leaves but were detected throughout the bottom half of the leaves (Fig. 5.5I). Also in NPA-grown 4.5-DAG E2331>>erGFP/YFP leaves, erGFP expression was restricted to the veins; however, YFP was detected throughout NPA-grown 4.5-DAG E2331>>erGFP/YFP leaves — though YFP signals were weaker along the margin in the top half of the leaves (Fig. 5.5J). Nevertheless, by 6 DAG both erGFP and YFP signals had become mainly restricted to the veins also in NPA-grown E2331>>erGFP/YFP (Fig. 5.5K).

We conclude that auxin transport inhibition delays the reduction in PD permeability between veins and surrounding nonvascular tissues that occurs during normal leaf development, and that such delay mediates the promoting effect of auxin transport inhibition on vein connection.

We next asked whether regulated PD aperture in turn controlled polar auxin transport during leaf development. Because *PIN1* is the only auxin-transporter-encoding gene in Arabidopsis with nonredundant functions in vein patterning (Sawchuk et al., 2013), to address that question we imaged domains and cellular localization of expression of PIN1::PIN1:YFP

(PIN1:YFP fusion protein expressed by the PIN1 promoter (Xu et al., 2006)) or PIN1::PIN1:GFP

(Benkova et al., 2003) during first-leaf development in WT, *cals3-2d*, and *gsl8-chor*.

Consistent with previous reports (Bayer et al., 2009; Benkova et al., 2003; Heisler et al.,

2005; Marcos and Berleth, 2014; Reinhardt et al., 2003; Sawchuk et al., 2013; Verna et al., 2015;

Verna et al., 2019; Wenzel et al., 2007) (Chapter 3), in WT PIN1::PIN1:YFP was expressed in all

the cells at early stages of tissue development, and inner tissue expression was stronger in

developing veins (Fig. 5.5L–O). Over time, epidermal expression became restricted to the

basalmost cells, and inner tissue expression became restricted to developing veins (Fig. 5.5L–O).

Also in *cals3-2d* and *gsl8-chor*, PIN1::PIN1:YFP was expressed in all the cells at early

stages of tissue development, and inner tissue expression was stronger in developing veins (Fig.

5.5P–AC). Furthermore, as in WT, in both *cals3-2d* and *gsl8-chor* PIN1::PIN1:YFP expression

domains associated with loop formation were initially connected on both ends to pre-existing

expression domains, and PIN1::PIN1:YFP was evenly expressed along those looped domains

(Fig. 5.5Q,Z). However, in *casl3-2d* and *gsl8-chor* PIN1::PIN1:YFP expression along looped

domains soon became heterogeneous, with domain segments with stronger expression

separated by segments with weaker expression (Fig. 5.5R,W,AA,AB). Such heterogeneity in

PIN1::PIN1:YFP expression at early stages of loop formation was associated with open or

fragmented looped domains of PIN1::PIN1:YFP expression at later stages (Fig. 5.5S–V,X,AC).

Finally, equivalent stages of vein development occurred at later time points in *casl3-2d* and

gsl8-chor than in WT (e.g., compare Fig. 5.5Q,Z with Fig. 5.5M, Fig. 5.5S,T,W with Fig. 5.5N,

and Fig. 5.5U,V,X,AC with Fig. 5.5O).

Consistent with previous reports (Bayer et al., 2009; Marcos and Berleth, 2014; Sawchuk

et al., 2013; Scarpella et al., 2006; Verna et al., 2015; Verna et al., 2019; Wenzel et al., 2007)

(Chapter 3), in cells at late stages of second loop development in WT leaves, by which time

PIN1::PIN1:GFP expression had become restricted to the cells of the developing loop,

PIN1::PIN1:GFP expression was polarly localized to the side of the plasma membrane facing the veins to which the second loop was connected (Fig. 5.5AD).

By contrast, in cells at late stages of development of vein fragments and isolated vascular clusters in *cals3-2d*, by which time expression domains of PIN1::PIN1:GFP or PIN1::PIN1:YFP (hereafter collectively referred to as PIN1::PIN1:FP) had become disconnected from other veins on both ends, PIN1::PIN1:FP expression was polarly localized to any of the plasma membrane sides facing a contiguous PIN1::PIN1:FP-expressing cell (Fig. 5.5AE–AG).

In conclusion, our results suggest that vein patterning is controlled by the coordinated action of polar auxin transport and movement of an auxin signal through PDs.

5.2.5 Auxin-Signaling-Dependent Vein Patterning and Regulated PD Aperture

The movement of an auxin signal that controls vein patterning and is not mediated by auxin transporters depends, in part, on auxin signaling (Verna et al., 2019). Should the residual, auxin-transporter- and auxin-signaling-independent movement of an auxin signal that controls vein patterning be enabled by PDs, defects in PD aperture regulation would enhance vein patterning defects induced by auxin signaling inhibition — just as defects in PD aperture enhance vein patterning defects induced by auxin transport inhibition (Fig. 5.5A–F). To test the prediction that defects in PD aperture will enhance vein patterning defects induced by auxin signaling inhibition, we grew E2331, E2331;*cals3-2d*, and E2331;*gsl8-2* in the presence or absence of the auxin signaling inhibitor phenylboronic acid (PBA) (Matthes and Torres-Ruiz, 2016), which induces vein patterning defects that phenocopy the loss of that *AUXIN RESISTANT 1* -, *TRANSPORT INHIBITOR RESPONSE 1 / AUXIN SIGNALING F-BOX 2* -, and *MONOPTEROS* - dependent auxin signaling pathway that is relevant for vein patterning (Matthes and Torres-Ruiz, 2016; Verna et al., 2019). We then imaged erGFP-expression-labeled vein networks 4.5 DAG in E2331. Because *cals3-2d* and *gsl8* leaves develop more slowly than

WT leaves (Fig. 5.5M–O,Q,S–X,Z,AC), we imaged erGFP-expression-labeled vein networks 5.5 and 6.5 DAG in E2331;*cals3-2d* and E2331;*gsl8-2*, respectively.

As shown above (Fig. 5.5A–C), in the absence of PBA vein networks were composed of midvein, first and second loops, and minor veins in E2331, and of midvein, loops — whether open or closed — vein fragments, and vascular clusters in E2331;*cals3-2d* and E2331;*gsl8-2* (Fig. 5.6A,D,G).

Ten μM PBA failed to induce vein network defects in E2331 but led to the formation of fewer veins and opening or fragmentation of all the loops in E2331;*cals3-2d* and E2331;*gsl8-2* (Fig. 5.6B,E,H,I). Formation of fewer veins and opening of all the loops — though not their fragmentation — were induced in E2331 by 50 μM PBA (Fig. 5.6C). At that concentration of PBA, the vascular systems of E2331;*cals3-2d* and E2331;*gsl8-2* were mainly composed of very few, scattered vascular clusters (Fig. 5.7F,J,K).

These observations suggest that defects in PD aperture enhance vein patterning defects induced by auxin signaling inhibition, a conclusion that is consistent with the hypothesis that the residual, auxin-transporter- and auxin-signaling-independent movement of an auxin signal that controls vein patterning is enabled by PDs. Moreover, these observations suggest that the vein patterning defects induced by auxin signaling inhibition may, at least in part, depend on regulated PD aperture. Were that so, auxin signaling inhibition would impinge on the reduction of PD permeability that occurs between veins and surrounding nonvascular tissues during normal leaf development. To test this prediction, we grew E2331>>erGFP/YFP in the presence or absence of PBA, and assessed erGFP-expression-labeled vein network formation and YFP-signal-inferred PD aperture in first leaves 2 and 4.5 DAG.

As shown above (Fig. 5.5G), at 2 DAG erGFP was only expressed in the midvein of both PBA- and normally grown E2331>>erGFP/YFP (Fig. 5.6L,M). Likewise, in both PBA- and normally grown E2331>>erGFP/YFP YFP was detected throughout the 2-DAG primordia (Fig. 5.6L,M).
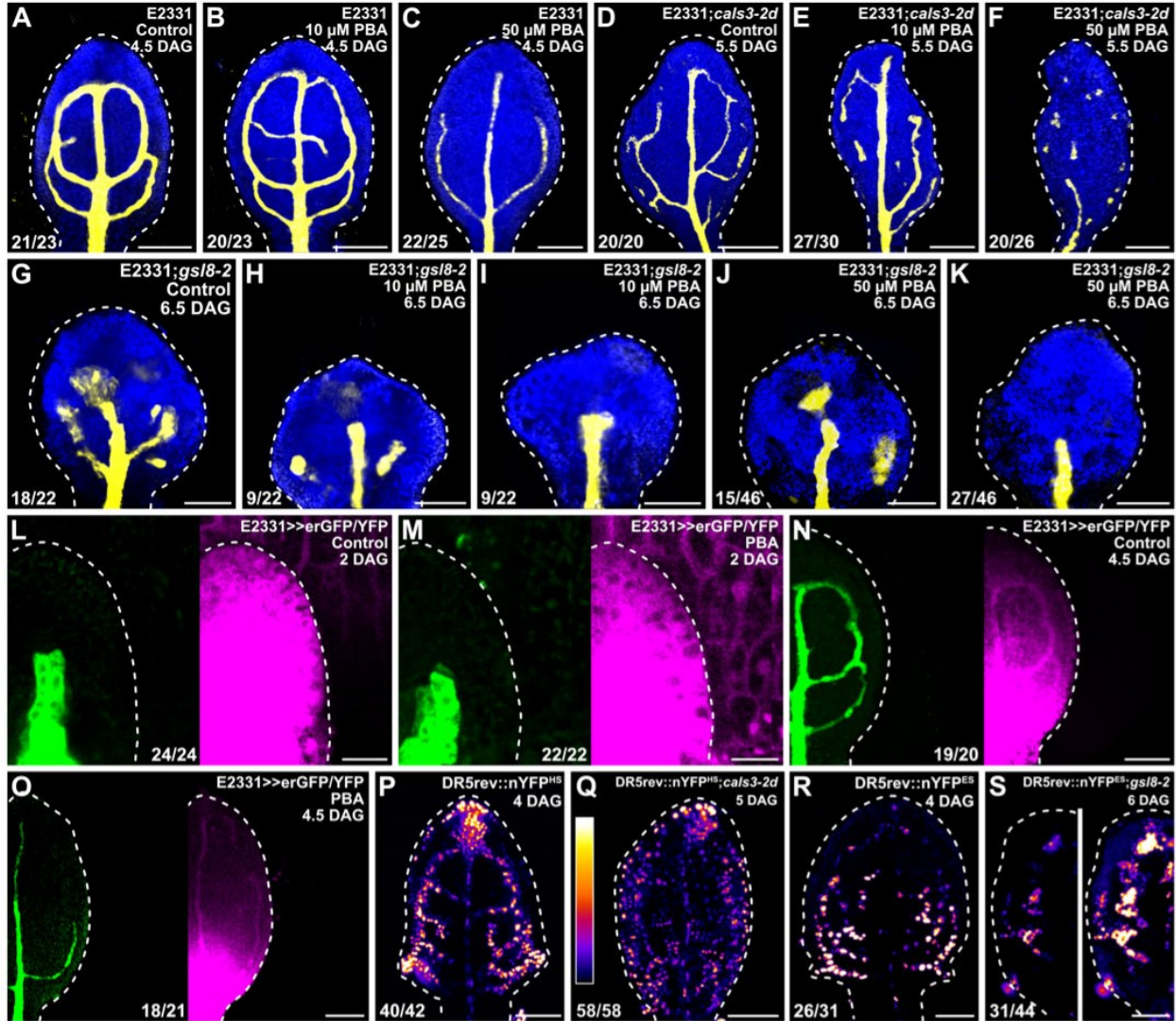
Figure 5.6. Auxin-Signaling-Dependent Vein Patterning and Regulated PD Aperture

(A–S) Confocal laser scanning microscopy. First leaves (for simplicity, only half-leaves are shown in L–O,S). Blue, autofluorescence; yellow (A–K) or green (L–O), GFP expression; magenta, YFP signals. Dashed white line delineates leaf outline. (L,M) Side view, adaxial side to the left. (P–S) DR5rev::nYFP^{HS} (P,Q) or DR5rev::nYFP^{ES} (R,S) expression; look-up table (ramp in Q) visualizes expression levels. Top right: leaf age in DAG, genotype, and treatment (10 or 50 μM PBA). Bottom left (A–K,P–S) or center (L–O): reproducibility index (see Table 5.1). Images

in P and R were acquired by matching signal intensity to detector's input range (~1% saturated pixels). Images in P and Q were acquired at identical settings and show weaker and broader DR5rev::nYFP[HS] expression in *cals3-2d*. Images in R and S (left) were acquired at identical settings and show weaker DR5rev::nYFP[ES] expression in *gsl8-2*. Image in S (right) was acquired by matching signal intensity to detector's input range (~1% saturated pixels), and show broader DR5rev::nYFP[ES] expression in *gsl8-2*. Bars: (A–K) 120 μm; (L,M) 20 μm; (N–S) 80 μm.

Figure 5.7. Control of PD-Aperture-Dependent Vein Patterning by *GNOM*

(A–F) Dark-field illumination of mature first leaves illustrating phenotype classes (top right) and genotypes (bottom left). Classes 0, a1, a2, and a6 defined in Fig. 1. Class a7: wide midvein and shapeless vascular cluster (D–F). (G) Percentages of leaves in phenotype classes. Classes 0, a1–a3, a5, and a6 defined in Fig. 1. Class a8, shapeless vascular cluster (not shown). Difference

between *cals3-3d* and WT, between *cals3-2d* and WT, and between *gn-13* and WT was significant at $P<0.001$ (***) by Kruskal-Wallis and Mann-Whitney test with Bonferroni correction. Sample population sizes: WT, 30; *cals3-3d*, 62; *cals3-2d*, 67; *gn-13*, 89; *gn-13*;*cals3-3d*, 100; *gn-13*;*cals3-2d*, 52. (H–Q) Confocal laser scanning microscopy. First leaves. Blue, autofluorescence; yellow (H–M) or green (N–Q), GFP expression; magenta, YFP signals. Dashed white line delineates leaf outline. Top right: leaf age in DAG, genotype, and treatment (25 µM NPA + 10 µM PBA). Bottom left: reproducibility index (see Table 5.1). Bars: (A,B) 1 mm; (C,D,F) 0.5 mm; (E) 0.25 mm; (H,J,K,O) 100 µm; (I,L,M,Q) 150 µm; (N,P) 25 µm

As also shown above (Fig. 5.5I), at 4.5 DAG erGFP was only expressed in the midvein, first and second loops, and minor veins of normally grown E2331>>erGFP/YFP (Fig. 5.6N). YFP signals were mainly restricted to the veins in the top half (49.83% ± 0.73, n=20) of normally grown 4.5-DAG E2331>>erGFP/YFP leaves but were detected throughout the bottom half of the leaves (Fig. 5.6N). Also in PBA-grown 4.5-DAG E2331>>erGFP/YFP leaves, erGFP expression was restricted to the veins; however, YFP signals were already restricted to the veins in the top two-thirds (66.78% ± 0.63, n=21, P<0.001) of PBA-grown 4.5-DAG E2331>>erGFP/YFP leaves (Fig. 5.6O), suggesting that auxin signaling inhibition leads to premature reduction in PD permeability.

We conclude that auxin signaling inhibition prematurely reduces PD permeability between veins and surrounding nonvascular tissues, and that such premature reduction mediates, at least in part, the effects of auxin signaling inhibition on vein patterning.

We next asked whether regulated PD aperture in turn controlled response to auxin signals in developing leaves. To address this question, we imaged expression of the auxin response reporter DR5rev::nYFP (Heisler et al., 2005; Sawchuk et al., 2013) (Table 5.2) 4 DAG in WT and — because *cals3-2d* and *gsl8* leaves develop more slowly than WT leaves (Fig. 5.5M–O,Q,S–X,Z,AC) — 5 and 6 DAG in *cals3-2d* and *gsl8-2*, respectively.

As previously shown (Sawchuk et al., 2013; Verna et al., 2015; Verna et al., 2019), in WT strong DR5rev::nYFP expression was mainly associated with developing veins (Fig. 5.5P,R). By contrast, DR5rev::nYFP expression was weaker and expression domains were broader in *cals3-2d* and *gsl8-2* (Fig. 5.6Q,S).

In conclusion, our results suggest that vein patterning is controlled by the mutually coordinated action of auxin signaling and movement of an auxin signal through PDs.

Table 5.2. Origin and Nature of Lines

Line	*Origin/Nature*
cals3-2d	(Vatén et al., 2011); introgressed into Col-0
cals3-3d	(Vatén et al., 2011)
gsl8-et2	(de Storme et al., 2013)
gsl8-6	SAIL_679_H10 (ABRC)[2]; (Chen et al., 2009; Sessions et al., 2002)
gsl8-chor	(Guseman et al., 2010)
gsl8-1	SALK_111094 (ABRC); (Alonso et al., 2003; Töller et al., 2008)
gsl8-2	GK_851C04 (ABRC); (Kleinboelting et al., 2012; Töller et al., 2008)
UAS::YFP	Transcriptional fusion of six copies of the *UAS* sequence (Giniger et al., 1985) upstream of the -46[3] Cauliflower Mosaic Virus 35S promoter (Odell et al., 1985) to a translationally enhanced Venus-encoding sequence (Gallie et al., 1988; Nagai et al., 2002) (primers: "TeVENUS Fwd XbaI" and "TeVENUS Rev SacI")
E2331	(Amalraj et al., 2020; Gardner et al., 2009); (Chapter 4)
Q0990	(Haseloff, 1999; Sawchuk et al., 2007)
Q0950	(Haseloff, 1999; Sawchuk et al., 2007)
J3281	(Haseloff, 1999; Sawchuk et al., 2007)
J1701	(Haseloff, 1999; Sawchuk et al., 2007)
PIN1::PIN1:YFP	(Xu et al., 2006)
PIN1::PIN1:GFP	(Benkova et al., 2003)

Line	Origin/Nature
DR5rev::nYFP[HS]	(Heisler et al., 2005; Sawchuk et al., 2013)
DR5rev::nYFP[ES]	Transcriptional fusion of nine copies of the DR5rev sequence (Ulmasov et al., 1997) upstream of the -46 Cauliflower Mosaic Virus 35S promoter (Odell et al., 1985) to EYFP-Nuc (Clontech)
gn-13	(Alonso et al., 2003; Verna et al., 2019); (Chapter 3)

[2] Arabidopsis Biological Resource Center

[3] Gene coordinates are relative to the adenine (position +1) of the start codon

5.2.6 Control of PD-Aperture-Dependent Vein Patterning by *GN*

Vein patterning is controlled by the mutually coordinated action of auxin signaling, polar auxin transport, and movement of an auxin signal through PDs (Fig. 5.1–5.6). Vein patterning activities of both auxin signaling and polar auxin transport depend on *GN* function (Verna et al., 2019) (Chapter 3). We asked whether *GN* also controlled PD-aperture-dependent vein patterning. To address this question, we compared the phenotypes of mature first leaves of the *gn-13*;*cals3-2d*, *gn-13*;*cals3-3d*, and *gn-13*;*gsl8-2* double mutants with those of their respective single mutants.

The phenotypes of *gn-13*;*cals3-2d* and *gn-13*;*cals3-3d* were no different from those of *gn-13* (Fig. 5.7A,B,D,E,G), suggesting that the effects of the *gn-13* mutation on vein patterning are epistatic to those of the *cals3-d* mutation. Furthermore, the gn phenotype segregated in approximately one quarter (559/2,353) of the progeny of plants heterozygous for both *gn-13* and *gsl8-2* — no different from the frequency expected by the Pearson's chi-squared ($\chi 2$) goodness-of-fit test for the hypothesis that the phenotype of *gn-13* is epistatic to that of *gsl8-2*. We confirmed by genotyping that some of the *gn*-looking seedlings are indeed *gn-13*;*gsl8-2* double homozygous mutants whose leaves are no different from those of *gn-13* (Fig. 5.7A,C,D,F), suggesting that the effects of the *gn-13* mutation on vein patterning are epistatic to those of the *gsl8-2* mutation. These observations suggest that *GN* controls PD-aperture-dependent vein patterning; were that so, *gn* leaves would have defects in regulation of PD permeability. To test this prediction, we imaged E2331>>erGFP/YFP in developing *gn-13* leaves.

In both E2331>>erGFP/YFP and E2331>>erGFP/YFP;*gn-13*, erGFP was only expressed in the vascular tissue (Fig. 5.7N–Q). Furthermore, in both 2.5-DAG E2331>>erGFP/YFP and 4.5-DAG E2331>>erGFP/YFP;*gn-13*, YFP was detected throughout the primordium; however, in 4.5-DAG E2331>>erGFP/YFP;*gn-13* YFP signals were weaker in nonvascular tissues than in the vascular tissue (Fig. 5.7N,P). Finally, and as shown above (Fig. 5.5I; Fig. 5.6N), YFP signals

were mainly restricted to the veins in the top half of 4.5-DAG E2331>>erGFP/YFP leaves and were detected throughout the bottom half of the leaves (Fig. 5.7O). By contrast, YFP signals were mainly restricted to the vascular tissue in the bottom half of 6.5-DAG E2331>>erGFP/YFP;*gn-13* leaves and were detected throughout the top half of the leaves — though YFP signals were still weaker in nonvascular tissues than in the vascular tissue (Fig. 5.7Q). We conclude that *GN* controls PD-aperture-dependent vein patterning.

Vein pattern defects of intermediate alleles of *gn* are phenocopied by growth of WT in the presence of both NPA and PBA (Fig. 5.7I) (Verna et al., 2019). Because *GN* controls PD-aperture-dependent vein patterning besides auxin-transport- and auxin-signaling-dependent vein patterning, we asked whether defects in PD aperture regulation shifted the defects induced by NPA and PBA toward more severe classes of the *gn* vein patterning phenotype. To address this question, we grew E2331, E2331;*cals3-2d*, and E2331;*gsl8-2* in the presence or absence of NPA and PBA. We then imaged erGFP-expression-labeled vein networks 5 DAG in E2331 and — because *cals3-2d* and *gsl8* leaves develop more slowly than WT leaves (Fig. 5.5M−O,Q,S−X,Z,AC) — 6 and 8 DAG in E2331;*cals3-2d* and E2331;*gsl8-2*, respectively.

Growth of *cals3-2d* in the presence of both NPA and PBA led to vein pattern defects similar to those of the strong *gn^van7* allele (Fig. 5.7J,K) (Koizumi et al., 2000; Verna et al., 2019), and growth of *gsl8-2* in the presence of both NPA and PBA even phenocopied vein patterning defects of the null *gn-13* allele (Fig. 5.7L,M).

We conclude that vein patterning is controlled by the *GN*-dependent, coordinated action of auxin signaling, polar auxin transport, and movement of an auxin signal through PDs.

5.3 DISCUSSION

Unlike the tissue networks of animals, the vein networks of plant leaves form in the absence of cell migration and direct cell−cell interaction. Therefore, leaf vein networks are patterned by a mechanism unrelated to that which patterns animal tissue networks. Here we show that leaf

veins are patterned by the coordinated action of three *GN*-dependent pathways: auxin signaling, polar auxin transport, and movement of an auxin signal through PDs (Fig. 5.8F).

5.3.1 Regulation of PD Permeability During Leaf Development

At early stages of leaf tissue development — stages at which veins are forming — PD permeability is high throughout the leaf (Fig. 5.8A). As leaf tissues develop, PD permeability between veins and surrounding nonvascular tissues becomes gradually lower but remains high between vein cells. These results suggest that at early stages of leaf tissue development all cells are symplastically connected. As veins develop, vein cells remain symplastically connected but become isolated from the surrounding nonvascular tissues.

The changes in PD permeability that occur during leaf development resemble those observed during the development of embryos (Godel-Jedrychowska et al., 2020; Kim et al., 2005a; Kim et al., 2005b; Stadler et al., 2005), lateral roots (Benitez-Alfonso et al., 2013; Sager et al., 2020), and stomata (Palevitz and Hepler, 1985; Wille and Lucas, 1984; Willmer and Sexton, 1979). By contrast, the changes in PD permeability that occur during leaf development are unlikely to be related to those observed during the transition of leaf tissues from sink to source of photosynthates as this transition begins when new veins are no longer forming and all existing veins have completely differentiated (e.g., (Imlau et al., 1999; Oparka et al., 1999; Roberts et al., 1997; Roberts et al., 2001; Wright et al., 2003)).

Consistent with the observation that vein formation is associated first with high and then with low PD permeability between veins and surrounding nonvascular tissues, defects in PD aperture regulation — whether leading to near-constitutively wide or narrow PD aperture — lead to similar vein patterning defects: fewer veins form, and those that do form become disconnected and discontinuous. In the most extreme cases, randomly oriented vascular elements differentiate in clusters, a phenotype that so far had only been observed in *gn* mutants
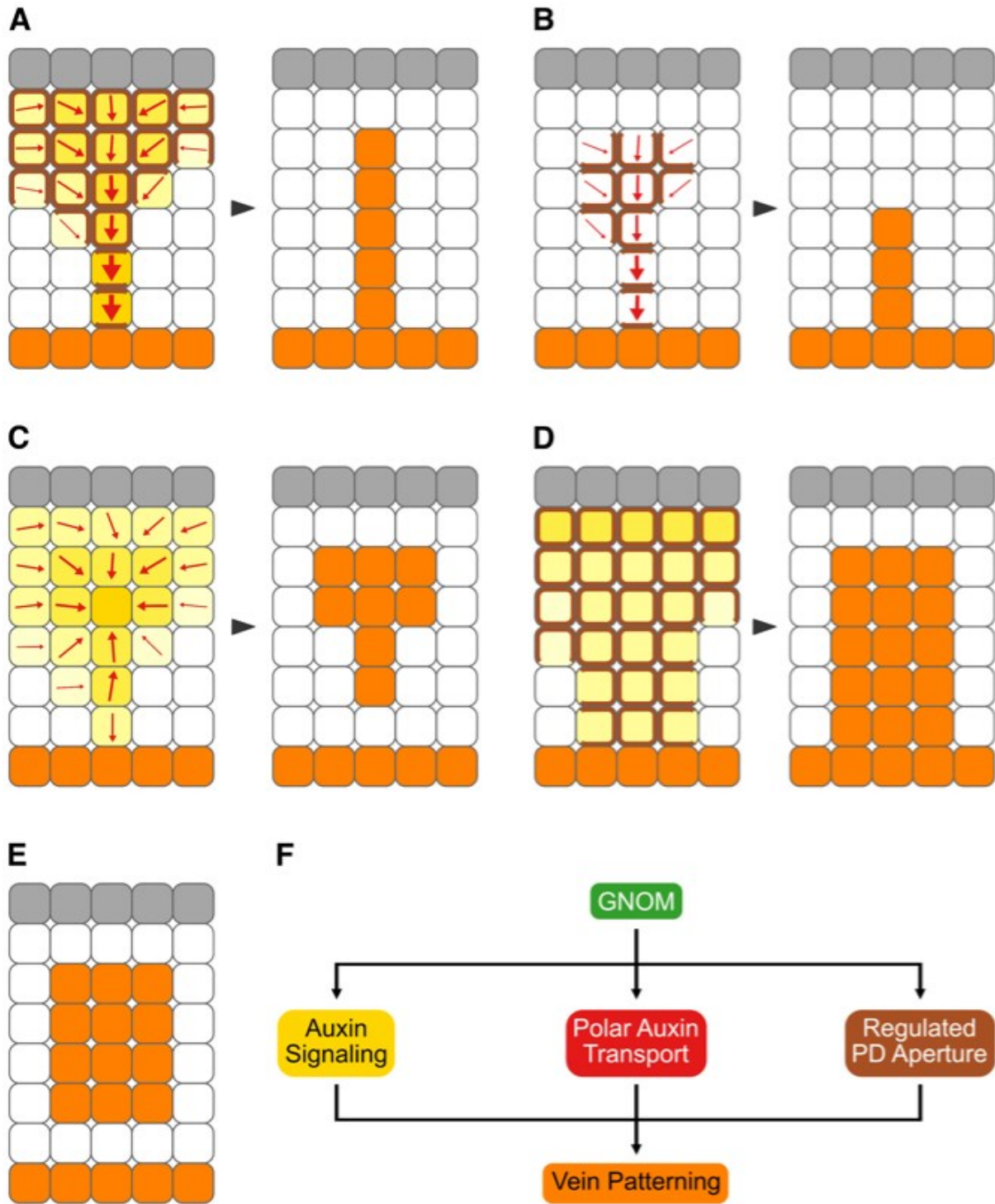
Figure 5.8. Summary and Interpretation

(A–F) Gray: epidermis, whose role in vein patterning — if any — remains unclear (Govindaraju et al., 2020). Increasingly darker yellow: progressively stronger auxin signaling. Increasingly

205

thicker arrows: progressively more polarized auxin transport. Brown: PD-mediated cell–cell connection. Orange: veins. Arrowheads temporally connect vein patterning stages with mature vein patterns. (A) In WT, veins are patterned by gradual restriction of auxin signaling domains (Donner et al., 2009; Esteve-Bruna et al., 2013; Krishna et al., 2021; Krogan et al., 2012; Marcos and Berleth, 2014; Wenzel et al., 2007), gradual restriction of auxin transport domains and polarization of auxin transport paths (Bayer et al., 2009; Esteve-Bruna et al., 2013; Krogan et al., 2012; Marcos and Berleth, 2014; Sawchuk et al., 2013; Scarpella et al., 2006; Verna et al., 2015; Verna et al., 2019; Wenzel et al., 2007) (Chapter 3), and gradual reduction of PD permeability between incipient veins and surrounding nonvascular tissues. (B) Inhibition of auxin signaling leads to narrower domains of auxin transport (Esteve-Bruna et al., 2013; Verna et al., 2019; Wenzel et al., 2007) (Chapter 3) and promotes reduction of PD permeability between incipient veins and surrounding nonvascular tissues. (C) Defects in the ability to regulate PD aperture lead to weaker and broader domains of auxin signaling, fragmentation of auxin transport domains, and abnormal polarization of auxin transport paths. (D) Inhibition of auxin transport leads to weaker and broader domains of auxin signaling (Esteve-Bruna et al., 2013; Mattsson et al., 2003; Verna et al., 2015; Verna et al., 2019) and delays reduction of PD permeability between incipient veins and surrounding nonvascular tissues. (E) Loss of *GN* function or simultaneous inhibition of auxin signaling, polar auxin transport, and ability to regulate PD aperture leads to clusters of vascular cells. (F) Veins are patterned by the coordinated activities of three *GN*-dependent pathways: auxin signaling, polar auxin transport, and regulated PD aperture.

or in plants impaired in both auxin signaling and polar auxin transport (Geldner et al., 2004; Koizumi et al., 2000; Mayer et al., 1993; Verna et al., 2019).

How symplastic connection between vein cells and their isolation from surrounding nonvascular tissues is brought about during vein development remains to be understood. One possibility is that, as in cells of the embryonic hypocotyl (Kim et al., 2005a), there are more PDs along the transverse walls of vein cells than along their longitudinal walls — perhaps because no new PDs form in the longitudinal walls of vein cells during their elongation, as it happens in elongating root cells (Gunning, 1978; Zhu et al., 1998). One other possibility is that, as it happens to elongating root cells (Seagull, 1983), during vein cell elongation simple PDs coalesce into branched PDs, which have narrower aperture (Oparka et al., 1999). Consistent with this possibility, there are more branched PDs along the longitudinal walls than along the transverse walls of epidermal cells underlying the midvein (Gao et al., 2020). Yet another possibility is that the aperture of PDs along the longitudinal walls of vein cells is narrower than that of PDs along their transverse walls — perhaps because the aperture of PDs along longitudinal walls is closed by the same turgor pressure that drives cell elongation (Oparka and Prior, 1992; Park et al., 2019; Ruan et al., 2001) or because more callose accumulates at PDs along the longitudinal walls than at PDs along the transverse walls, as it happens in epidermal cells underlying the midvein (Gao et al., 2020). In the future, it will be interesting to distinguish between these possibilities; however, the mechanism by which changes in PD permeability are brought about during leaf development is inconsequential to the conclusions we derive from such changes.

5.3.2 Auxin, Regulated PD Aperture, and Vein Patterning

Our results suggest that auxin controls PD permeability and that regulated PD aperture controls auxin-induced vein formation. Auxin application delays the reduction in PD permeability between veins and surrounding nonvascular tissues that occurs during normal leaf

development. And in the most severe cases, impaired ability to regulate PD aperture almost entirely prevents auxin-induced vein formation.

Our results suggest that also auxin signaling and regulated PD aperture control each other during vein patterning. Auxin signaling inhibition prematurely reduces PD permeability between veins and surrounding nonvascular tissues (Fig. 5.8B), suggesting that auxin signaling normally delays such reduction. In turn, defects in the ability to regulate PD aperture lead to defects in expression of auxin response reporters (Fig. 5.8C). Near-constitutively narrow PD aperture leads to lower levels and broader domains of expression of auxin response reporters, suggesting that an auxin signal is produced at low levels in all cells and reaches veins through PDs. Also near-constitutively wide PD aperture leads to lower levels and broader domains of expression of auxin response reporters, suggesting that high levels of an auxin signal are maintained at sites of vein formation by reducing its leakage through PDs toward surrounding nonvascular tissues.

Our findings are consistent with the inability of plants with impaired ability to regulate PD aperture to restrict expression domains and maintain high expression levels of auxin response reporters in hypocotyl and root (Han et al., 2014; Liu et al., 2017; Mellor et al., 2020). Our interpretation is consistent with high levels of auxin signaling at early stages of vein formation and low levels of auxin signaling at late stages of vein formation (Krishna et al., 2021; Mattsson et al., 2003). And mutual control of auxin signaling and PD aperture regulation is consistent with the finding that simultaneous inhibition of auxin signaling and of the ability to regulate PD aperture leads to vein patterning defects that are more severe than the addition of the defects induced by auxin signaling inhibition and those induced by impaired ability to regulate PD aperture. In the most severe cases, simultaneous inhibition of auxin signaling and of the ability to regulate PD aperture leads to vascular systems comprised of very few, scattered vascular clusters.

It is unclear how auxin and its signaling could delay the reduction in PD permeability between veins and surrounding nonvascular tissues that occurs during normal leaf development. One possibility is that such delay is brought about by the ability of auxin to rapidly induce the expression of PD beta glucanases (Benitez-Alfonso et al., 2013; Parizot et al., 2010), which degrade callose at PDs and thus prevent callose-mediated restriction of PD aperture (Benitez-Alfonso et al., 2013; Iglesias and Meins Jr, 2000; Levy et al., 2007; Rinne et al., 2011). Another possibility is that the delay derives from the induction by auxin of pectin methylesterase activity (Bryan and Newcomb, 1954), which localizes around PDs (Morvan et al., 1998) and can increase their permeability (Chen and Citovsky, 2003; Chen et al., 2000; Dorokhov et al., 2012; Lionetti et al., 2014). A further possibility rests on the ability of auxin to reduce levels of reactive oxygen species in plastids (George et al., 2010), which leads to increased PD permeability (Benitez-Alfonso et al., 2009; Stonebloom et al., 2012). In the future, it will be interesting to test these possibilities; nevertheless, the mechanism by which auxin and its signaling delay the reduction in PD permeability between veins and surrounding nonvascular tissues has no bearing on our interpretation of such delay.

Our results also suggest that polar auxin transport and regulated PD aperture control each other during vein patterning. Auxin transport inhibition delays the reduction in PD permeability that occurs between veins and surrounding nonvascular tissues during normal leaf development (Fig. 5.8D), suggesting that polar auxin transport normally promotes such reduction. In turn, defects in the ability to regulate PD aperture lead to defects in expression and polar localization of the PIN1 auxin exporter (Fig. 5.8C), whose function is nonredundantly required for vein patterning (Sawchuk et al., 2013). Impaired ability to regulate PD aperture leads first to heterogeneous PIN1 expression along continuous expression domains and then to disconnection of those expression domains from pre-existing veins and breakdown of expression domains into domain fragments, suggesting that connection and continuity of PIN1 expression domains depend on regulated PD aperture. These defects in *PIN1* expression

resemble those of mutants in pathways that counteract *GN* function (Koizumi et al., 2005; Naramoto et al., 2009; Scarpella et al., 2006; Sieburth et al., 2006). And as in those mutants, in mutants impaired in PD aperture regulation PIN1 polarity is directed away from the edge of vein fragments and vascular clusters. That defects in the ability to regulate PD aperture lead to defects in PIN1 expression and polar localization is consistent with reduced polar auxin transport and defective PIN2 expression and polar localization in mutants and transgenics that are impaired in PD aperture regulation (Gao et al., 2020; Wu et al., 2016).

How polar auxin transport and regulated PD aperture could control each other during vein patterning remains to be explored, but PDs are associated with receptor-like proteins (Faulkner et al., 2013; Stahl et al., 2013; Vaddepalli et al., 2014) and PIN proteins with leucin-rich-repeat receptor kinases (Hajný et al., 2020; Wang et al., 2013), suggesting possibilities for the two pathways to interact. The molecular details of such interaction will have to be addressed in future research; however, our conclusion that polar auxin transport promotes the reduction in PD permeability that occurs between veins and surrounding nonvascular tissues is consistent with lower expression levels of positive regulators of callose production in auxin-transport-inhibited lateral roots (Sager et al., 2020). Moreover, mutual control of polar auxin transport and PD aperture regulation is consistent with the finding that simultaneous inhibition of auxin transport and the ability to regulate PD aperture leads to vein patterning defects that are more severe than the addition of the defects induced by auxin transport inhibition and those induced by impaired ability to regulate PD aperture. In the most severe cases, simultaneous inhibition of auxin transport and of the ability to regulate PD aperture leads to a vascularization zone that spans almost the entire width of the leaf. However, in those leaves veins still form oriented along the longitudinal axis of the leaf, suggesting the presence of residual vein patterning activity. That such residual vein patterning activity is provided by auxin signaling is suggested by the finding that the vascular system of leaves in which auxin signaling, polar auxin transport, and the ability

to regulate PD aperture are simultaneously inhibited is no more than a shapeless cluster of vascular cells.

All these observations suggest that during normal leaf development auxin, through its signal transduction, induces high PD permeability and that absence of such induction, through auxin removal by polar transport, allows PD permeability to lower between veins and nonvascular tissues. This conclusion seems to be inconsistent with the observation that auxin promotes low PD permeability during development of lateral roots and bending of mature hypocotyls (Han et al., 2014; Sager and Lee, 2014) or that auxin has no effect on PD permeability in mature leaves and root tips (Gao et al., 2020; Rutschow et al., 2011). However, such seeming inconsistency may simply reflect organ (leaf vs. root and hypocotyl) or developmental stage (mature vs. developing) responses. Indeed, auxin application induces vein formation only in developing leaves and fails to do so in mature leaves or in hypocotyls and roots of Arabidopsis (Sauer et al., 2006; Scarpella et al., 2006).

5.3.3 Control of PD Aperture Regulation by *GN*

The vein pattern of leaves both lacking *GN* function and impaired in the ability to regulate PD aperture is no different from that of *gn* mutants. This suggests that *GN* controls PD aperture regulation, just as it controls auxin signaling and polar auxin transport (Verna et al., 2019) (Chapter 3). That *GN* controls PD aperture regulation is supported by the defects in regulation of PD permeability we observed in *gn* mutants. How *GN* controls PD aperture regulation is unclear, but the most parsimonious account is that *GN* controls the localization of proteins that regulate PD aperture. This hypothesis remains to be tested but is consistent with abnormal callose accumulation upon genetic or chemical inhibition of *GN* (Nielsen et al., 2012).

Irrespective of how *GN* precisely controls PD aperture regulation, simultaneous inhibition of auxin signaling, polar auxin transport, and the ability to regulate PD aperture phenocopies even the most severe vein patterning defects of *gn* mutants (Fig. 5.8E). Because

vein patterning is prevented in both the strongest *gn* mutants and in the most severe instances of inhibition of auxin signaling, polar auxin transport, and the ability to regulate PD aperture, we conclude that vein patterning result from the coordinated action of three *GN*-dependent pathways: auxin signaling, polar auxin transport, and regulated PD aperture (Fig. 5.8F).

5.3.4 A Diffusion–Transport-Based Vein-Patterning Mechanism

The Canalization Hypothesis was proposed over 50 years ago to account for the inductive effects of auxin on vein formation (Sachs, 1968b; Sachs, 1981). In its most recent formulation (Sachs, 2000), the hypothesis proposes positive feedback between cellular auxin efflux mediated by exporters polarly localized to a plasma membrane segment and polar localization of those auxin exporters to that membrane segment. The Canalization Hypothesis is supported by overwhelming experimental evidence and computational simulations; nevertheless, both experiments and simulations have brought to light inconsistencies between hypothesis and evidence (recently reviewed in (Cieslak et al., 2021; Ravichandran et al., 2020)). For example, the hypothesis assumes that at early stages of auxin-induced vein formation auxin diffuses from auxin sources (e.g., the applied auxin) toward auxin sinks (i.e. the pre-existing veins) (Sachs, 1981), but auxin diffusion out of the cell is unfavored over diffusion into the cell by almost two orders of magnitude (Runions et al., 2014). Furthermore, the hypothesis assumes that the veins whose formation is induced by auxin readily connect to pre-existing veins (i.e. auxin sinks) — an assumption that is supported by experimental evidence (Sachs, 1968a) but that simulations have been unable to reproduce without the addition of ad-hoc solutions (Bayer et al., 2009; Smith and Bayer, 2009) or the existence of multiple auxin exporters with distinct patterns of auxin-responsive expression and polarization (O'Connor et al., 2014). Finally, the hypothesis relies on the function of auxin exporters (Sachs, 1984) — a requirement that is unsupported by experimental evidence because genetic or chemical inhibition of all the *PIN* genes with vein

patterning function fails to prevent patterning of vascular cells into veins (Mattsson et al., 1999; Sieburth, 1999; Verna et al., 2019).

Our results suggest that those discrepancies between experiments and simulations, on the one hand, and the Canalization Hypothesis, on the other, could be resolved by supplementing the positive feedback between auxin and its polar transport postulated by the hypothesis with movement of an auxin signal through PDs according to its concentration gradient (Fig. 5.8A). At early stages of vein formation, movement through PDs would dominate; at later stages, polar transport would take over. Computational simulations suggest that our conclusion is justified (Cieslak et al., 2021).

A vein patterning mechanism that combines the positive feedback between auxin and its polar transport postulated by the Canalization Hypothesis with diffusion of an auxin signal through PDs requires at least two conditions to be met. First, auxin must promote the movement of an auxin signal through PDs such that gradual reduction in PD permeability between veins and surrounding nonvascular tissues as well as maintenance of symplastic connection between vein cells are accounted for by feedback between movement of the auxin signal through PDs and PD permeability. Our results support such requirement: auxin application delays the reduction in PD permeability that occurs during normal leaf development, thereby promoting movement of an auxin signal through PDs. Second, auxin signaling, polar auxin transport, and movement of an auxin signal through PDs must be coupled. Were they not — for example, if PD permeability between developing veins and surrounding nonvascular tissues remained high — the high levels of auxin signaling in early stage PIN1 expression domains (Bhatia et al., 2019; Marcos and Berleth, 2014), which inefficiently transport auxin because of PIN1 isotropic localization (Benkova et al., 2003; Marcos and Berleth, 2014; Sawchuk et al., 2013; Scarpella et al., 2006; Verna et al., 2015; Verna et al., 2019), would be dissipated by lateral diffusion of the auxin signal through PDs. And if, conversely, PD permeability in tissues where veins are forming was already low, the auxin signal would not be able to diffuse toward

pre-existing veins, which transport auxin efficiently because of PIN1 polar localization and have low levels of auxin signaling (Benkova et al., 2003; Marcos and Berleth, 2014; Mattsson et al., 2003; Sawchuk et al., 2013; Scarpella et al., 2006; Verna et al., 2015; Verna et al., 2019). That auxin signaling and polar auxin transport control each other during vein patterning is known (Fig. 5.8B,D) (Donner et al., 2009; Krogan et al., 2012; Mattsson et al., 2003; Verna et al., 2015; Verna et al., 2019; Wenzel et al., 2007). Our results support the additional requirement that polar auxin transport and movement of an auxin signal through PDs control each other and that movement of an auxin signal through PDs and auxin signaling control each other (Fig. 5.8B–D).

In this study, we derived patterns of PD permeability change during leaf development from movement of a soluble YFP through leaf tissues. We note that auxin, being smaller than YFP, could for example move from the veins to the surrounding nonvascular tissues when YFP no longer can. Nevertheless, the reduced permeability of the PDs along the longitudinal walls of vein cells suggests that less auxin moves laterally than longitudinally. Moreover, unlike YFP, auxin is the substrate of PIN exporters (Petrasek et al., 2006; Zourelidou et al., 2014). By the time YFP can no longer move out of the veins, PIN1 has become polarly localized to the basal plasma membrane of vein cells (Bayer et al., 2009; Benkova et al., 2003; Heisler et al., 2005; Marcos and Berleth, 2014; Reinhardt et al., 2003; Sawchuk et al., 2013; Scarpella et al., 2006; Verna et al., 2015; Verna et al., 2019; Wenzel et al., 2007) (Chapter 3). Such polarization drives removal of auxin — but not YFP — from vein cells (Wisniewska et al., 2006), thereby dissipating the gradient in auxin signaling between veins and surrounding nonvascular tissues (Donner et al., 2009; Krogan et al., 2012; Marcos and Berleth, 2014; Mattsson et al., 2003; Scarpella et al., 2006; Verna et al., 2015; Verna et al., 2019; Wenzel et al., 2007), and as such the driving force for auxin movement from the veins to the surrounding nonvascular tissues. These considerations notwithstanding, the most stringent piece of evidence in support of our conclusions would be provided by the direct visualization of auxin movement. Despite considerable advances in the visualization of auxin signals (Brunoud et al., 2012; Herud-Sikimić

et al., 2021; Liao et al., 2015), direct visualization of auxin movement remains to this day impossible. Should this change, it would also be possible to test whether it is auxin itself or an auxin-dependent signal that moves through PDs; nevertheless, the logic of the mechanism we report is unaffected by such limitation.

Our observations pertain to vein patterning, but they may be relevant for other processes too — for example, stoma patterning. Indeed, like vein patterning, stoma patterning depends on auxin signaling (Balcerowicz et al., 2014; Le et al., 2014; Zhang et al., 2014), polar auxin transport (Le et al., 2014), regulated PD aperture (Bundy et al., 2016; Guseman et al., 2010; Kong et al., 2012), and *GN* (Le et al., 2014; Mayer et al., 1993; Wang et al., 2022). And as in vein patterning, stoma patterning defects in plants lacking *GN* function are quantitatively stronger than and qualitatively different from those in plants impaired in auxin signaling, polar auxin transport, or the ability to regulate PD aperture (Balcerowicz et al., 2014; Bundy et al., 2016; Guseman et al., 2010; Kong et al., 2012; Le et al., 2014; Wang et al., 2022; Zhang et al., 2014). It will be interesting to understand whether the pathway network that patterns veins also patterns other plant cells and tissues.

Despite plants and animals gained multicellularity independently of each other, a mechanism similar to that which patterns plant veins and depends on the movement of an auxin signal through PDs also patterns animal tissues. At early stages of tissue development in animal embryos, cells are connected by open gap junctions such that the tissue is a syncytium (reviewed in (Levin, 2007; Mathews and Levin, 2017)). And at later stages of tissue development, tissue compartments become isolated by selective closure of gap junctions to prevent unrestricted movement of signaling molecules. However, whereas in plants regulated PD aperture interacts with the polar transport of auxin and its signal transduction, in animals gap junction gating interacts with the polar secretion of signaling molecules or the binding of polarly localized ligands and receptors protruding from the plasma membranes (reviewed in (Levin, 2021)). Therefore, control of vein patterning by *GN*-dependent auxin signaling, polar auxin transport,

and regulated PD aperture is an unprecedented mechanism of tissue network formation in multicellular organisms (van Peer et al., 2010).

5.4 MATERIALS & METHODS

5.4.1 Plants

Origin and nature of lines, genotyping strategies, and oligonucleotide sequences are in Table 5.2, Table 5.3, and Table 5.4, respectively. Seeds were sterilized and sowed as in (Sawchuk et al., 2008). Stratified seeds were germinated and seedlings were grown at 23 °C under continuous light (~100 μmol m^{-2} s^{-1}). Plants were grown at 24 °C under fluorescent light (~100 μmol m^{-2} s^{-1}) in a 16-h-light/8-h-dark cycle. Plants were transformed and representative lines were selected as in in (Sawchuk et al., 2008).

5.4.2 Chemicals

NPA and PBA were dissolved in dimethyl sulfoxide and stored at -20 °C indefinitely (NPA) or up to a week (PBA). Dissolved chemicals were added (25 μM final NPA concentration; 10 or 50 μM final PBA concentration) to growth medium just before sowing. IAA was dissolved in melted (55 °C) lanolin (1% final IAA concentration) and stored at 4 °C up to a week. Controls were treated with the sole chemical solvents.

5.4.3 Imaging

Developing leaves were mounted and imaged by confocal laser scanning microscopy as in (Linh and Scarpella, 2022a; Sawchuk et al., 2013) (Chapter 2). For each ET driver, acquisition parameters (i.e. laser transmission, detector gain, and detector offset) were first adjusted for the oldest ET>>erGFP/YFP leaves such that signals were saturated only in up to ~1% of the pixels in the acquired images. The same parameters were then used for younger leaves, which led to

Table 5.3. Genotyping Strategies

Line	Genotyping Strategy
cals3-2d	"CALS3 FWD 1" and "CALS3 m REV2"
cals3-3d	"cals3-3d F" and "cals3-3d R"; *Taq*I
gsl8-et2	"ET2dCAPS F" and "ET2dCAPS R2"; *Hin*dIII
gsl8-6	*GSL8*: "SAIL_679_H10LP" and "SAIL_679_H10RP"; *gsl8-6*: "SAIL_679_H10RP" and "LBb1.3"
gsl8-chor	"chorus dCAPS F" and "chorus dCAPS R"; *Nla*IV
gsl8-1	*GSL8*: "GSL8 FWD" and "GSL8 REV"; *gsl8-1*: "GSL8 FWD" and "LBb1.3"
gsl8-2	*GSL8*: "GK_851C04LP" and "GK_851C04RP"; *gsl8-2*: "GK_851C04RP" and "o8474"
gn-13	*GN*: "SALK_045424 gn LP" and "SALK_045424 gn RP"; *gn*: "SALK_045424 gn RP" and "LBb1.3"

Table 5.4. Oligonucleotide Sequences

Name	Sequence (5' to 3')
CALS3 FWD 1	ATCCCTTGTCAACTCAGG
CALS3 m REV2	GAGAGATCTGAAGAGCTT
cals3-3d F	CCATCTCTTGTGCAACTTTACAATG
cals3-3d R	TATCAGGATCGAGAGGTAGGATATTATCG
ET2dCAPS F	AAATTGTATTGGATCGTGACCTGTAATCTTTCATGC
ET2dCAPS R2	CTCCAATATCCTTCCTCTTAATGTTTGGATATAAGC
SAIL_679_H10LP	GCCCAGGTATACTAAGCTGGG
SAIL_679_H10RP	CTTTTTCTTCTAACGTGGGGG
LBb1.3	ATTTTGCCGATTTCGGAAC
chorus dCAPS F	TCATGTGGATGCTTAGTGAACTGCTTCTTACTAACT
chorus dCAPS R	AGCCAACTGACCCAGTCTTCAAAATCCTCGAGGGTC
GSL8 FWD	TCACATGCATATAGCTGTGGG
GSL8 REV	TAGTTCCGCAGACAAAGTTGC
GK_851C04LP	TTCAGAAGTTGCATCTGCATG
GK_851C04RP	ACACTCTGGAAGAAAGCGGAC
o8474	ATAATAACGCTGCGGACATCTACATTTT
TeVENUS Fwd XbaI	GCGCGCTCTAGAGTATTTTTACAACAATTACCAACAACAAC
TeVENUS Rev SacI	AAAGAGCTCTTACTCGTCCATGCCGAGAGTG
SALK_045424 gn LP	TGATCCAAATCACTGGGTTTC
SALK_045424 gn RP	AGCTGAAGATAGGGAATTCGC

images in which signals were saturated in >1% of the pixels in the acquired images but ensured that for each ET driver all the images of ET>>erGFP/YFP leaves could be compared to one another. Mature leaves were fixed in 6 : 1 ethanol : acetic acid, rehydrated in 70% ethanol and water, cleared briefly (few seconds to few minutes) — when necessary — in 0.4 M sodium hydroxide, washed in water, and either (i) mounted in 1 : 2 : 8 water : glycerol : chloral hydrate and imaged by differential-interference-contrast or dark-field-illumination microscopy as in (Odat et al., 2014) or (ii) stained for 6–16 h in 0.2% basic fuchsin in ClearSee (Kurihara et al., 2015), washed in ClearSee for 30 min, incubated in daily changed ClearSee for three days, and mounted in ClearSee for imaging by confocal laser scanning microscopy. Light paths for confocal laser scanning microscopy are in Table 5.5. In the Fiji distribution (Schindelin et al., 2012) of ImageJ (Rueden et al., 2017; Schindelin et al., 2015; Schneider et al., 2012), grayscaled RGB color images were turned into 8-bit images; when necessary, 8-bit images were combined into stacks, and stacks were projected at maximum intensity; look-up-tables were applied to images; and image brightness and contrast were adjusted by linear stretching of the histogram.

Table 5.5. Confocal Light Paths

Fluorophore	Laser	Wavelength (nm)	Main Dichroic Beam Splitter	First Secondary Dichroic Beam Splitter	Second Secondary Dichroic Beam Splitter	Emission Filter (Detector)
Lignin	HeNe	543	HFT 405/488/543	Mirror	NFT 515	BP 600–650 (PMT3)
YFP; Autofluorescence	Ar	514	HFT 405/514/594	NFT 595	NFT 515 (PMT3); Plate (META)	BP 520-555 IR (PMT3); 593–754 (META)
GFP; YFP	Ar	458; 514	HFT 458/514	NFT 595	NFT 545 (PMT2); NFT 545 (PMT3)	BP 475–525 (PMT2); BP 520-555 IR (PMT3)
GFP; YFP; Autofluorescence	Ar	458; 514	HFT 458/514	NFT 595	NFT 545 (PMT2); NFT 545 (PMT3); Plate (META)	BP 475–525 (PMT2); BP 520-555 IR (PMT3); 657–754 (META)
GFP; Autofluorescence	Ar	488	HFT 405/488/594	NFT 545	NFT 490 (PMT3); Plate (META)	BP 505–530 (PMT3); 550–754 (META)
YFP	Ar	514	HFT 405/514/594	NFT 595	NFT 515	BP 520-555 IR (PMT3)

Chapter 6: Vein Patterning by Tissue-Specific *GNOM* Expression

6.1 INTRODUCTION

Most multicellular organisms solve the problem of long-distance transport of water, signals, and nutrients by tissue networks such as the vascular system of vertebrate embryos and the vein networks of plant leaves. How vascular networks form is therefore a key question in biology. In vertebrates, for example, the formation of the embryonic vascular system relies on direct cell–cell interaction and at least in part on cell migration (e.g., (Betz et al., 2016; Hogan and Schulte-Merker, 2017)). Both direct cell–cell interaction and cell migration are instead precluded in plants by cell walls that keep plant cells apart and in place. Therefore, veins and their networks form by a different mechanism in plant leaves.

How leaf veins form is poorly understood, but genetic evidence suggests a key role for the guanine exchange factor for ADP ribosylation factors GNOM (GN) in vein patterning: the vascular system of strong *gn* mutants is no more than a shapeless cluster of randomly oriented vascular cells (Geldner et al., 2004; Koizumi et al., 2000; Mayer et al., 1993; Steinmann et al., 1999; Verna et al., 2019). However, it is unclear how the vesicle trafficking regulator GN performs its essential function in vein patterning. For nearly 25 years, GN has been thought to perform such function solely through its ability to control the polar localization at the plasma membrane of proteins members of the PIN-FORMED (PIN) family, which catalyze cellular efflux of the plant signaling molecule auxin and whose polar localization determines the polarity of the cell-to-cell transport of auxin (recently reviewed in (Lavania et al., 2021); (Chapter 1)). However, the vein patterning defects of strong *gn* mutants are quantitatively stronger than and qualitatively different from those of *pin* mutants (Verna et al., 2019). Moreover, *pin* mutations are inconsequential to the vascular phenotype of strong *gn* mutants (Verna et al., 2019). These observations suggest that other pathways besides polar auxin transport are involved in vein

patterning and that *GN* controls those pathways too. Two such pathways are auxin signal transduction and movement of auxin or an auxin-dependent signal through plasmodesmata intercellular channels (Verna et al., 2019) (Chapters 3 and 5). Indeed, simultaneous interference with auxin signaling, polar auxin transport, and movement of an auxin signal through plasmodesmata recapitulates vein patterning defects of strong *gn* mutants (Chapter 5). Mechanisms by which GN controls polar auxin transport have been suggested (e.g., (Luschnig and Vert, 2014; Naramoto et al., 2014; Richter et al., 2010)), but how GN controls auxin signaling and movement of an auxin signal through plasmodesmata remains to be clarified. Moreover, it is unknown whether — and if so, where and when in leaf development — GN controls the production, the movement, or the interpretation of an auxin signal with vein patterning function.

Here we address this question by determining GN expression in leaf development, by restricting that expression to specific tissues in a strong *gn* mutant, and by analyzing the effects of such tissue-specific *GN* expression on vein patterning. Our results suggest that *GN* controls the production, propagation, or interpretation of a vein patterning signal in the leaf inner tissues. For that function, *GN* expression is required in all the inner tissues of the leaf throughout leaf development, but stronger *GN* expression seems to be required where new veins are forming. By contrast, if a signal with vein patterning function is produced in the leaf epidermis, our results suggest that the production of such a signal is independent of *GN*.

6.2 RESULTS

6.2.1 *GNOM* Expression During Leaf Development

The development of Arabidopsis leaves has been described previously (Kang and Dengler, 2004; Kinsman and Pyke, 1998; Larkin et al., 1996; Mattsson et al., 2003; Pyke et al., 1991; Scarpella et al., 2004; Telfer and Poethig, 1994). Briefly, at 1.5 days after germination (DAG) the first leaf is

recognizable as a semispherical primordium (Fig. 6.1A). By 2 DAG, the primordium has elongated, and the midvein has formed in the primordium center (Fig. 6.1B). By 2.5 DAG, the primordium has expanded (Fig. 6.1C). By 3 DAG, the first loops of veins ("first loops") have formed (Fig. 6.1D). By 4 DAG, a lamina and a petiole have become recognizable, second loops have formed, and minor veins have started to form in the top half of the lamina (Fig. 6.1E).

How *GNOM* (*GN*) is expressed during leaf development is unknown. To address this limitation, we fused the sequence encoding YFP to the 3'-end of the *GN* gene and cloned the resulting GN:YFP between the ~2.1-kb sequence upstream of the *GN* start codon and the ~0.6-kb sequence downstream of the *GN* stop codon (Fig. 6.1F). We expressed the resulting GN::GN:YFP in the strong *gn-13* mutant background (Verna et al., 2019), whose defects were rescued by GN::GN:YFP expression, and imaged GN::GN:YFP;*gn-13* expression in first leaves 1.5, 2, 2.5, 3, and 4 DAG.

Like PIN1 (Bayer et al., 2009; Benkova et al., 2003; Heisler et al., 2005; Marcos and Berleth, 2014; Reinhardt et al., 2003; Sawchuk et al., 2013; Scarpella et al., 2006; Verna et al., 2015; Verna et al., 2019; Wenzel et al., 2007) (Chapters 3 and 5), GN::GN:YFP;*gn-13* was expressed in all the cells of the leaf at early stages of tissue development, though expression was stronger where new veins were forming (Fig. 6.1H−L). Unlike PIN1 (Bayer et al., 2009; Benkova et al., 2003; Heisler et al., 2005; Marcos and Berleth, 2014; Reinhardt et al., 2003; Sawchuk et al., 2013; Scarpella et al., 2006; Verna et al., 2015; Verna et al., 2019; Wenzel et al., 2007) (Chapters 3 and 5), however, over time epidermal expression of GN::GN:YFP;*gn-13* failed to become restricted to the basalmost cells, and inner-tissue expression of GN::GN:YFP;*gn-13* failed to became restricted to developing veins (Fig. 6.1H−L). Instead, GN::GN:YFP;*gn-13* was still expressed in all the cells of the leaf at late stages of tissue development, though expression was stronger where new veins were forming (Fig. 6.1H−L).
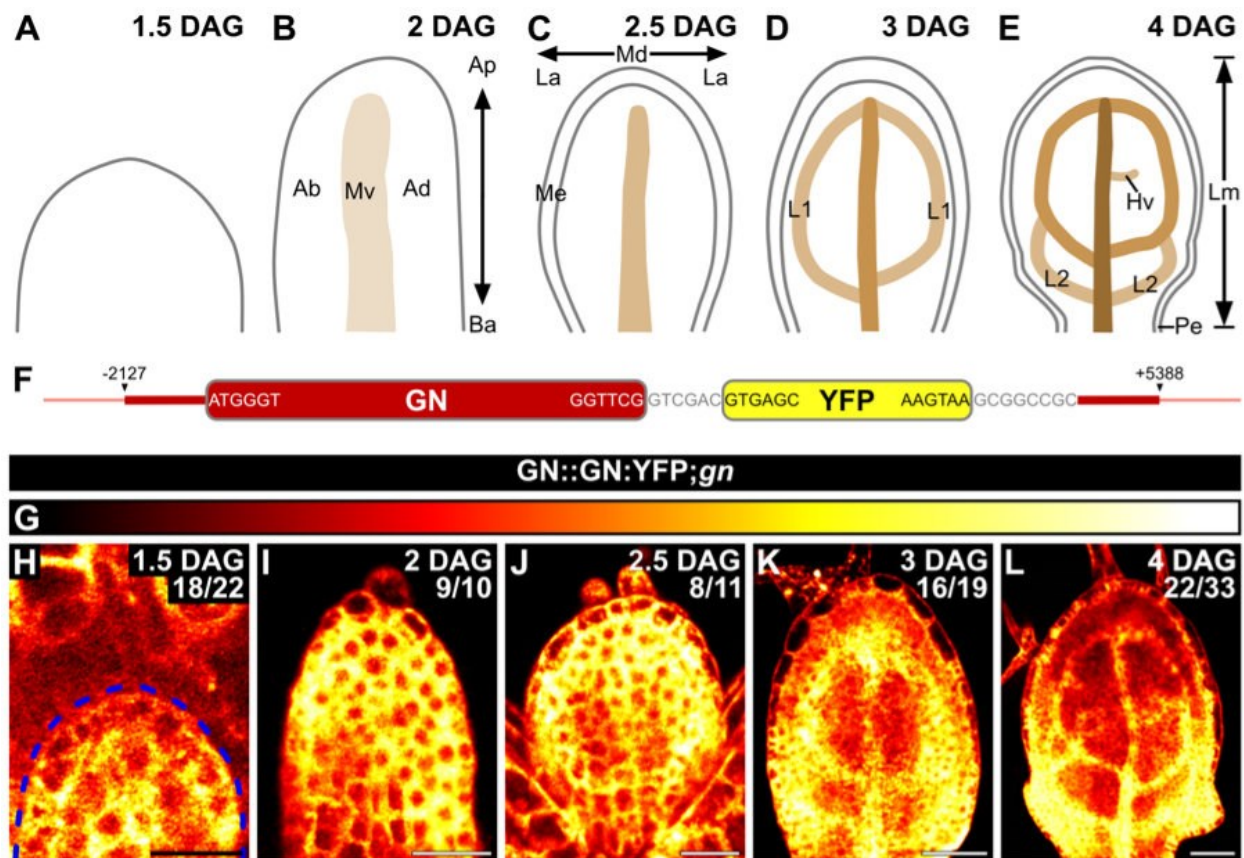
Figure 6.1. *GNOM* Expression During Leaf Development

(A–E,H–L) First leaves. Top right: leaf age in days after germination (DAG) and, in H–L,

reproducibility index (number of samples with the displayed features / number of analyzed

samples). (A,B,H,I) Side view, median plane. Abaxial (ventral) side to the left; adaxial (dorsal)

side to the right. (C-E,J–L) Front view, median plane. (A–E) Development of leaf and veins;

increasingly darker browns depict progressively later stages of vein development. See text for

details. Ab, abaxial; Ad, adaxial; Ap, apical; Ba, basal; Hv, minor vein; L1 and L2: first and

second loop; La, lateral; Lm, lamina; Md, median; Me, marginal epidermis; Mv, midvein; Pe,

petiole. (F) In the GN::GN:YFP construct, the sequence encoding YFP (yellow box) is fused to

the 3'-end of the *GN* gene (red box). The resulting GN:YFP is inserted between the ~2.1-kb

sequence upstream of the *GN* start codon and the ~0.6-kb sequence downstream of the *GN* stop

codon (thick red lines). Assembly of the GN::GN:YFP construct resulted in the addition of 6 bp

between the 3′-end of the *GN* gene and the 5'-end of the sequence encoding YFP and of 8 bp between 3'-end of the sequence encoding YFP and the 5'-end of the ~0.6-kb sequence downstream of the *GN* stop codon (gray). Coordinates are relative to the first nucleotide of the *GN* start codon (+1). (H−L) Top center: genotype. Confocal laser scanning microscopy. Look-up table (ramp in G) visualizes global background (black) and erGFP expression levels (red to white through yellow). Dashed blue line delineates leaf outline. Bars: (H−J) 25 μm; (K,L) 50 μm.

6.2.2 Marker Expression in *gn* Developing Leaves

gn leaves are defective in patterning of epidermis and inner tissues (Le et al., 2014; Mayer et al., 1993; Verna et al., 2019; Wang et al., 2022) (Chapters 3 and 5). We therefore asked whether tissue- and stage-specific drivers retained their tissue- and stage-specific activity in *gn* leaves. To address this question, we imaged expression of a transcriptional fusion of the *UAS* promoter to the sequence encoding an endoplasmic-reticulum localized GFP (erGFP) activated by the E100, E861, E4259, J0571, and E2331 tissue-specific GAL4:VP16 drivers (Amalraj et al., 2020; Wenzel et al., 2012) (Chapter 4) in developing first-leaves of WT and *gn-13*.

As in WT, in *gn-13* E100>>erGFP was expressed homogeneously in all the cells (Fig. 6.2A,B). In WT, E861>>erGFP expression was restricted to the midvein, first loops, and minor veins in the top half of the leaf and was expressed in nearly all the cells in the bottom half of the leaf, even though expression was stronger where new veins were forming (Fig. 6.2C). In *gn-13* too, E861>>erGFP expression was restricted to the vascular tissue in the top part of the leaf and was expressed in nearly all the cells in the bottom part of the leaf, even though expression was stronger where vascular tissue was forming (Fig. 6.2D). Finally, in both WT and *gn-13*, E4259>>erGFP was expressed in the epidermis, J0571>>erGFP in the nonvascular inner tissue, and E2331>>erGFP in the vascular tissue (Fig. 6.2E–J).

In conclusion, tissue-specific drivers retain their tissue-specific activity in *gn* leaves, despite the tissue patterning defects of those leaves (Fig. 6.2K,L).

6.2.3 Rescue of *gn* Defects in Vein Patterning by Tissue-Specific *GN* Expression

To understand whether — and if so, where and when in leaf development — GN controls the production, the movement, or the interpretation of a signal with vein patterning function, we expressed a transcriptional fusion of the *UAS* promoter (Sabatini et al., 2003) to the *GN* gene by
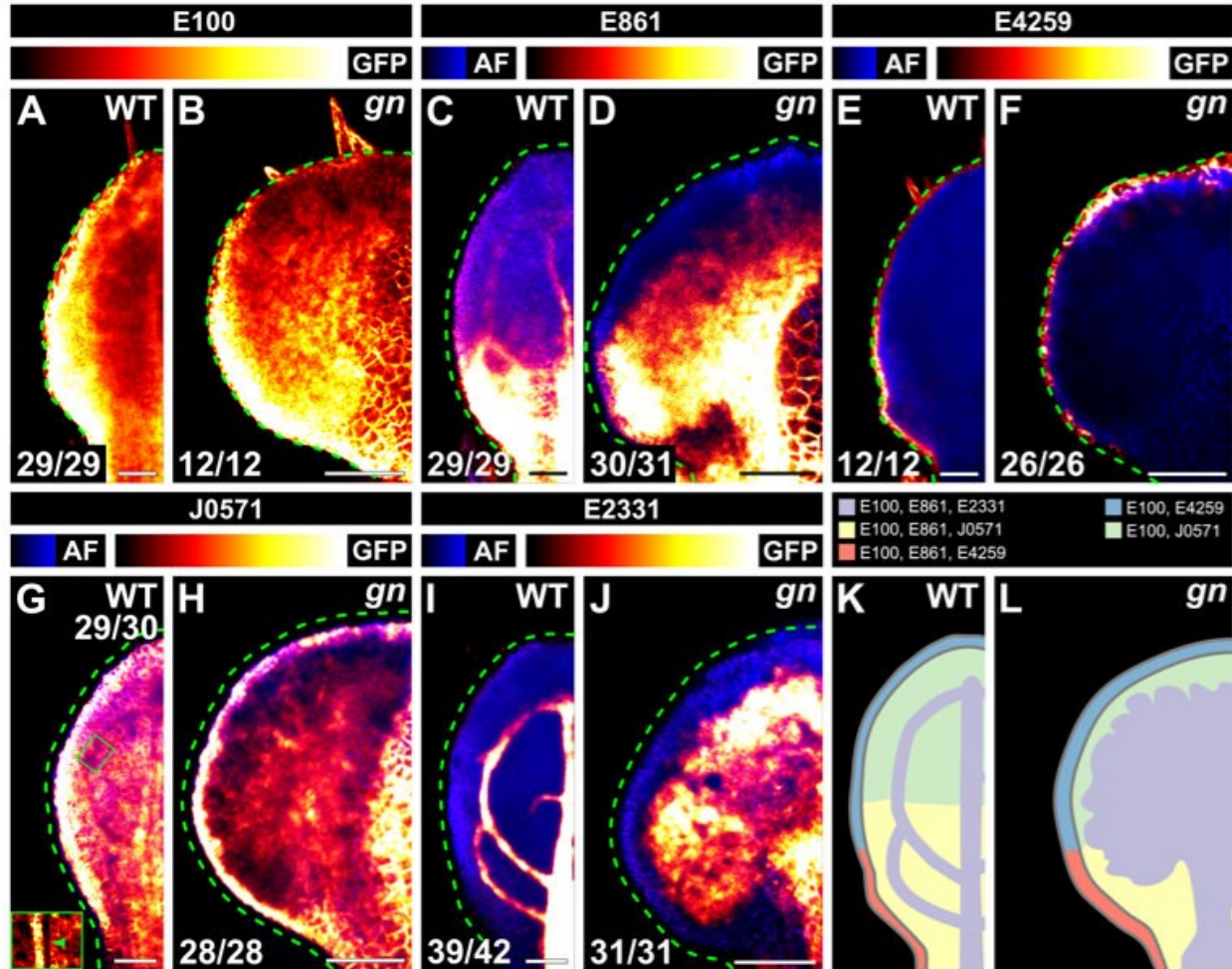
Figure 6.2. Marker Expression in *gn* Developing Leaves

(A–L) Top right: genotype. (A–J) Confocal laser scanning microscopy. First leaves 4 DAG (for simplicity, only half-leaves are shown). Front view, median plane. Look-up table (ramp above panels) visualizes global background (black) and erGFP expression levels (red to white through yellow). Driver identity above look-up table ramps. Dashed green line delineates leaf outline. Bottom left (A–F,H–J) or top right (G): reproducibility index (C–J) Look-up table (ramp above panels) visualizes global background (black) and autofluorescence levels (blue). Detail in G shows absence of expression in vein (indicated by green arrowhead). (K,L) Expression map of tissue- and stage-specific GAL4:VP16 drivers in developing leaves illustrates inferred overlap and exclusivity of expression. Bars: (A,C,E,G,I) 50 μm; (B,D,F,H,J) 100 μm.

the E100, E861, E4259, J0571, and E2331 tissue-specific GAL4:VP16 drivers (Fig. 6.2) (Amalraj et al., 2020; Wenzel et al., 2012) (Chapter 4) in the *gn-13* mutant background (Fig. 6.3A). We then imaged and compared vein patterning — as reported by expression of PIN1::PIN1:YFP (Xu et al., 2006) or PIN1::PIN1:GFP (Benkova et al., 2003) and by mature vascular systems — in first leaves of WT, *gn-13*, and ET>>GN;*gn-13* backgrounds.

As previously shown (Verna et al., 2019) (Chapters 3 and 5), in WT PIN1::PIN1:YFP epidermal expression was restricted to the basalmost cells and inner-tissue expression was mainly restricted to developing veins (Fig. 6.3G). As in WT, and as previously shown (Verna et al., 2019) (Chapter 3), in *gn-13* PIN1::PIN1:YFP epidermal expression was restricted to the basalmost cells; however, inner-tissue expression failed to become restricted to developing veins and instead remained nearly ubiquitous (Fig. 6.3K).

As previously shown (Scarpella et al., 2006; Verna et al., 2019; Wenzel et al., 2007) (Chapters 3 and 5), in cells at late stages of second loop development in WT leaves, PIN1::PIN1:GFP expression was localized to the side of the plasma membrane facing the veins to which the second loop was connected (Fig. 6.3L). By contrast, and consistent with previous observations (Verna et al., 2019) (Chapter 3), at late stages of development of the inner tissue in the bottom half of *gn-13* leaves, localization of PIN1::PIN1:GFP expression at the plasma membrane was only weakly polar, and such weak cell polarities pointed in seemingly random directions (Fig. 6.3P).

WT Arabidopsis forms leaves whose mature vein networks are defined by at least four reproducible features: (1) a narrow I-shaped midvein that runs the length of the leaf; (2) lateral veins that branch from the midvein and join distal veins to form closed loops; (3) minor veins that branch from midvein and loops, and either end freely or join other veins; (4) minor veins and loops that curve near the leaf margin, lending a scalloped outline to the vein network
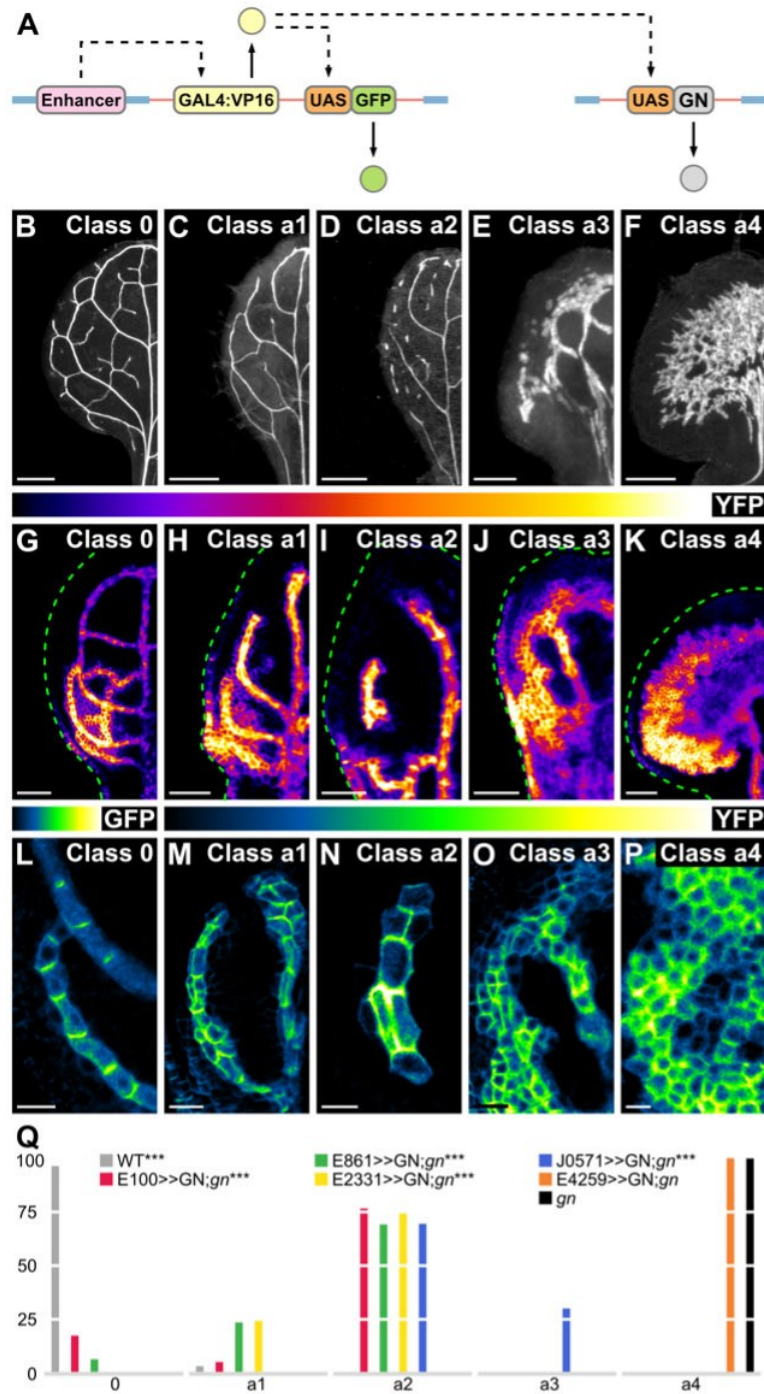
Figure 6.3. Rescue of *gn* Defects in Vein Patterning by Tissue-Specific *GN* Expression

(A) The GAL4/*UAS* transactivation system. Cell- or tissue-specific enhancers in the Arabidopsis genome (blue line) activate transcription (dashed arrow) of a codon-usage-optimized

translational fusion between the sequence encoding the GAL4 DNA-binding domain and the sequence encoding the activating domain of the *Herpes simplex* Viral Protein 16 (GAL4:VP16) in a T-DNA construct (red line) that is randomly inserted in the Arabidopsis genome (Berger et al., 1998; Haseloff, 1999). Translation of the *GAL4:VP16* fusion gene (solid arrow) leads to cell- or tissue-specific activation of transcription of a GAL4:VP16-responsive, *UAS*-driven, endoplasmic-reticulum-localized, improved *GFP* gene (*mGFP5*) (Haseloff et al., 1997; Siemering et al., 1996). Crosses between lines with cell- or tissue-specific expression of GAL4:VP16 and lines where the *GN* coding sequence is driven by the *UAS* promoter lead to activation of *GN* transcription in specific cells or tissues. (B–F) Dark-field illumination of mature first leaves illustrating phenotype classes (top right). For simplicity, only half-leaves are shown. Class 0: closed vein-network outline (B); class a1: open vein-network outline (C); class a2: fragmented vein network (D); class a3: distal vascular band and proximal vein netwI (E); class a4: wide midvein and shapeless vascular cluster (F). (G–P) Confocal laser scanning microscopy. First leaves (front view, median plane; for simplicity, only half-leaves are shown) 4–6 DAG showing cellular (G–K) or subcellular (L–P) localization of expression of PIN1::PIN1:YFP (G–K,M–P) or PIN1::PIN1:GFP (L) in phenotype classes (top-right) as defined above. Look-up tables (ramps above panels) visualize global background (black) and YFP or GFP expression levels. Dashed green line (G–K) delineates leaf outline. (Q) Percentages of leaves in phenotype classes. Difference between WT and *gn-13*, between E100>>GN;*gn-13* and *gn-13*, between E861>>GN;*gn-13* and *gn-13*, between E2331>>GN;*gn-13* and *gn-13*, and between J0571>>GN;*gn-13* and *gn-13* was significant at *P*<0.001 (***) by Kruskal-Wallis and Mann-Whitney test with Bonferroni correction. Sample population sizes: WT, 28; E100>>GN;*gn-13*, 56; E861>>GN;*gn-13*, 59; E2331>>GN;*gn-13*, 47; J0571>>GN;*gn-13*, 23; E4259>>GN;*gn-13*, 25; *gn-13*, 34. Bars: (B–D) 1 mm; (E,F) 0.25 mm; (G–H) 50 μm; (L–P) 10 μm.

(Fig. 6.3B) (Candela et al., 1999; Kinsman and Pyke, 1998; Mattsson et al., 1999; Nelson and Dengler, 1997; Sawchuk et al., 2013; Sieburth, 1999; Steynen and Schultz, 2003; Telfer and Poethig, 1994; Verna et al., 2015; Verna et al., 2019) (Chapter 5). By contrast, and as previously shown (Verna et al., 2019) (Chapter 5), the vascular system of mature *gn-13* leaves was composed of a shapeless cluster of seemingly randomly oriented vascular elements that was connected to a short and wide midvein (Fig. 6.3F).

The expression of PIN1::PIN1:YFP in developing leaves and the vascular system in mature leaves of E4259>>GN;*gn-13* were no different from those of *gn-13* (Fig. 6.3F,K,P,Q). By contrast, *gn-13* defects in PIN1::PIN1:YFP expression and vein network formation were partially rescued by J0571-driven *GN* expression (Fig. 6.3D,E,H,I,J,M,N,O,Q). The vein network of ~70% of J0571>>GN;*gn-13* leaves resembled that of weak *gn* mutants (Verna et al., 2019) and deviated from that of WT in two respects: closed loops were often replaced by open loops — i.e. loops that contact the midvein or other loops at only one of their two ends — and veins were often replaced by "vein fragments" — i.e. stretches of vascular elements that fail to contact other stretches of vascular elements at either one of their two ends (Fig. 6.3D,H,I,Q). In cells at late stages of open loop development, PIN1::PIN1:YFP expression was localized to the side of the plasma membrane facing the vein to which the open loop was connected (Fig. 6.3M,Q), as it also happens in free-ending veins of WT and mutants (Hou et al., 2010; Marcos and Berleth, 2014; Naramoto et al., 2009; Prabhakaran Mariyamma et al., 2018; Scarpella et al., 2006; Verna et al., 2019; Wenzel et al., 2007) (Chapter 3). And in cells at late stages of vein fragment development, PIN1::PIN1:YFP expression was localized to any of the plasma membrane sides facing a contiguous PIN1::PIN1:YFP-expressing cell (Fig. 6.3N,Q), as it also happens in vein fragments of other mutants (Naramoto et al., 2009; Scarpella et al., 2006) (Chapter 5).

The vascular system of the remaining ~30% of J0571>>GN;*gn-13* leaves deviated from that of *gn-13* in two respects: the shapeless cluster of seemingly randomly oriented vascular elements was restricted to a narrow band that ran parallel to the leaf margin, and the wide

midvein was replaced by individual veins that ran parallel to one another (Fig. 6.3E,J,Q). In cells at late stages of development of those veins, PIN1::PIN1:YFP expression was localized to the bottom side of the plasma membrane (Fig. 6.3O,Q), as it normally happens in the midvein (Bayer et al., 2009; Scarpella et al., 2006; Wenzel et al., 2007). And in cells of the narrow bands that ran parallel to the leaf margin, localization of PIN1::PIN1:GFP expression at the plasma membrane was only weakly polar, and such weak cell polarities pointed in seemingly random directions (Fig. 6.3O,Q), as it happens in strong *gn* mutants (Fig. 6.3O,Q) (Verna et al., 2019) (Chapter 3).

Defects in PIN1::PIN1:YFP expression and vein network formation of *gn-13* were further rescued by E2331-driven *GN* expression (Fig. 6.3C,D,H,I,M,N,Q). The vein networks of ~25% of E2331>>GN;*gn-13* leaves differed from those of WT only because of the presence of open loops (Fig. 6.3C,H,M,Q). And the vein networks of the remaining ~75% of E2331>>GN;*gn-13* leaves differed from those of WT because of the additional presence of vein fragments (Fig. 6.3D,I,N,Q).

Finally, *gn-13* defects in PIN1::PIN1:YFP expression and vein network formation were completely rescued in ~10% of E861>>GN;*gn-13* leaves and ~20% E100>>GN;*gn-13* leaves (Fig. 6.3B,G,L,Q). The vein networks of ~20% of E861>>GN;*gn-13* leaves and ~5% E100>>GN;*gn-13* leaves differed from those of WT only because of the presence of open loops (Fig. 6.3C,H,M,Q). And the vein networks of the remaining ~70% of E861>>GN;*gn-13* leaves and ~80% E100>>GN;*gn-13* leaves differed from those of WT because of the additional presence of vein fragments (Fig. 6.3D,I,N,Q).

6.3 DISCUSSION

To understand whether — and if so, where and when in leaf development — GN controls the production, the movement, or the interpretation of a signal with vein patterning function, we determined GN expression in leaf development; restricted that expression in specific tissues of

the strong *gn-13* mutant; and analyzed the effects of such tissue-specific *GN* expression on vein patterning, as reported by vein networks in mature leaves and PIN1 expression in developing leaves.

We found that GN is expressed in all the cells of the leaf throughout leaf development, though expression is stronger where new veins are forming. We also found that restricting *GN* expression to the nonvascular inner tissue of the leaf by the J0571 driver partially rescued *gn-13* defects in vein patterning. Those defects were rescued to a greater extent by *GN* expression in the leaf vascular tissue by the E2331 driver. However, E2331>>GN;*gn-13* leaves still had residual defects in vein continuity and connectivity. One account for the incomplete rescue of *gn-13* defects in vein patterning by either J0571>>GN or E2331>>GN is that *GN* expression is required in both leaf vascular tissue and nonvascular inner tissue. If so, *gn-13* defects in vein patterning should be completely rescued by ubiquitous *GN* expression. It is therefore surprising that *GN* expression by the E100 driver, which is homogeneously active in all the leaf tissues, was unable to rescue completely *gn-13* defects in vein patterning — though those defects were rescued to a greater extent by E100-driven *GN* expression than by E2331-driven *GN* expression.

We observed an incomplete rescue of *gn-13* defects in vein patterning similar to that resulting from E100-driven *GN* expression when *GN* is expressed by the E861 driver. The E861 driver is active in all the cells at early stages of leaf tissue development — though more so where new veins are forming — and at late stages of leaf tissue development is only active in newly formed veins. Therefore, the most parsimonious account for the similar inability of E100>>GN and E861>>GN to rescue completely *gn-13* defects in vein patterning is that (1) *GN* must be expressed in all the inner tissues of the leaf at both early and late stages of leaf tissue development and that (2) *GN* expression must be stronger where new veins are forming. E100>>GN satisfies only the former requirement, whereas E861>>GN satisfies only the latter one. In the future, it will be interesting to test the ability of *GN* expression by the combined activity of the E100 and E861 drivers to rescue *gn-13* defects in vein patterning.

Finally, we found that *GN* expression in the leaf epidermis by the E4259 driver is unable to rescue any of the vein patterning defects of *gn-13*. Therefore, *GN* expression in the leaf epidermis is insufficient for *GN*-dependent vein patterning. This conclusion is consistent with the observation that in the epidermis PIN-mediated auxin transport or MP-mediated auxin signaling — both of which depend on *GN* function (Mayer et al., 1993; Verna et al., 2019) — is insufficient for *PIN*- or *MP*-dependent vein patterning (Govindaraju et al., 2020; Krishna et al., 2021). Therefore, an influence of the leaf epidermis on vein patterning, if existing, would have to be mediated by pathways that are independent of *GN*, auxin transport, and auxin signaling.

In conclusion, our results suggest the *GN*-dependent production, propagation, or interpretation of vein patterning signal in the leaf inner tissues. Though for that function *GN* expression is required in all the inner tissues of the leaf throughout leaf development, stronger *GN* expression seems to be required where new veins are forming. By contrast, our results suggest that if a signal with vein patterning function is produced in the leaf epidermis, that production is independent of *GN*.

6.4 MATERIALS & METHODS

6.4.1 Plants

Origin and nature of lines, and oligonucleotide sequences are in Tables 6.1 and 6.2. Seeds were sterilized, sowed, and germinated, and seedlings were grown as in (Linh and Scarpella, 2022a) (Chapter 2). Plants were grown at 24 °C under fluorescent light (~100 μmol m^{-2} s^{-1}) in a 16-h-light/8-h-dark cycle. Plants were transformed and representative lines were selected as in (Sawchuk et al., 2008). *gn-13* was genotyped as in (Amalraj et al., 2020; Verna et al., 2019) (Chapters 3 and 4).

Table 6.1. Origin and Nature of Lines

Line	*Origin/Nature*
gn-13	SALK_045024 (ABRC[1]); (Alonso et al., 2003; Verna et al., 2019); (Chapter 3)
GN::GN:YFP	Translational fusion of of *GN* (AT1G13980; -2127[2] to +5388; primers: "GNfwdKpnI" and "GNrevSalI", and "GN Fwd NotIn" and "GN Rev SacIn") to a Venus-encoding sequence (Nagai et al., 2002) (primers : "YFP Fwd SalI" and "YFP Rev NotI")
PIN1::PIN1:YFP	(Xu et al., 2006)
PIN1::PIN1:GFP	(Benkova et al., 2003)
E100	CS70007 (ABRC); (Amalraj et al., 2020; Huang et al., 2014); (Chapter 4)
E861	CS70055 (ABRC); (Amalraj et al., 2020; Krogan and Berleth, 2012); (Chapter 4)
E4259	CS24272 (ABRC); (Amalraj et al., 2020); (Chapter 4)
J0571	CS65892 (ABRC); (Wenzel et al., 2012)
E2331	CS65892 (ABRC); (Amalraj et al., 2020; Gillmor et al., 2010); (Chapter 4)
UAS::GN	Transcriptional fusion of six copies of the *UAS* sequence (Giniger et al., 1985) upstream of the -46

Line	Origin/Nature
	Cauliflower Mosaic Virus 35S promoter (Odell et al., 1985) to a *GN*-encoding sequence (AT1G13980; +1 to +4811; primers: "GN Fwd XbaI" and "GN Rev SacI")

[1] Arabidopsis Biological Resource Center

[2] Gene coordinates are relative to the adenine (position +1) of the start codon

Table 6.2. Oligonucleotide Sequences

Name	Sequence (5' to 3')
GNfwdKpnI	GAGCGGGGTACCTCTAGAGGTGTGTATGATAaTGA
GNrevSalI	TCCACGCGTCGACTCTAGAGGTGTGTATGATAATGA
YFP Fwd SalI	TTTGTCGACGTGAGCAAGGGCGAGGAGCTG
YFP Rev NotI	TTTGCGGCCGCTTACTTGTACAGCTCGTCCA
GN Fwd NotIn	AAAGCGGCCGCCCTTACAAGTGAGATCATTAGGT
GN Rev SacIn	GCGGAGCTCTCTAGAAATCGAAATCCGTCTCCC
GN Fwd XbaI	GCGTCTAGAATGGGTCGCCTAAAGTTGCATTC
GN Rev SacI	GCTGAGCTCTCACGAACCAGTTGTGTTTTCAG

6.4.2 Imaging

Developing leaves were mounted and imaged by confocal laser scanning microscopy as in (Linh and Scarpella, 2022a) (Chapter 2). YFP and GFP/autofluorescence were excited and detected as in Chapter 5. GFP was excited and detected as in (Linh and Scarpella, 2022a) (Chapter 2). Emission was collected from ~2.5–5.0-µm-thick optical slices. Mature leaves were fixed, cleared, and mounted in 1 : 2 : 8 water : glycerol : chloral hydrate as in Chapter 5. Mounted leaves were imaged by dark-field-illumination microscopy as in (Odat et al., 2014). In the Fiji distribution (Schindelin et al., 2012) of ImageJ (Rueden et al., 2017; Schindelin et al., 2015; Schneider et al., 2012), grayscaled RGB color images were turned into 8-bit images; when necessary, 8-bit images were combined into stacks, and stacks were projected at maximum intensity; look-up-tables were applied to images; and image brightness and contrast were adjusted by linear stretching of the histogram.

Chapter 7: Control of Vein Patterning by Tissue-Specific Regulation of Plasmodesmata Aperture

7.1 INTRODUCTION

In both plants and animals, the long-distance transport of water, nutrients, and signals has been made possible by the evolution of tissue networks. Therefore, how tissue networks form is a key question in biology. In animals, those networks form by cell migration and direct interaction of proteins protruding from the plasma membranes (reviewed, for example, in (Betz et al., 2016; Hogan and Schulte-Merker, 2017)). Neither of those processes can take place in plants because of cell walls that keep cells apart and in place. Therefore, tissue networks such as the vein networks of leaves form differently in plants.

Though the molecular details of the underlying mechanisms remain unclear, available evidence suggests that leaf vein networks form by the coordinated action of three pathways. First, the cell-to-cell, polar transport of the plant hormone auxin, mediated by exporters of the PIN-FORMED (PIN) family (Mattsson et al., 1999; Petrasek et al., 2006; Sawchuk et al., 2013; Sieburth, 1999; Verna et al., 2015; Verna et al., 2019; Wisniewska et al., 2006) (Chapter 3). Second, the cellular transduction of the auxin signal, which ends with the activation of transcription factors of the AUXIN RESPONSE FACTOR (ARF) family (Alonso-Peral et al., 2006; Candela et al., 1999; Esteve-Bruna et al., 2013; Hardtke and Berleth, 1998; Powers and Strader, 2019; Przemeck et al., 1996; Strader et al., 2008; Verna et al., 2019). Third, the movement of auxin or an auxin-dependent signal through the plasmodesmata (PDs) intercellular channels (Chapter 5).

Members of the PIN and ARF families with nonredundant functions in vein patterning are expressed in all the cells at early stages of leaf tissue development (Bayer et al., 2009; Benkova et al., 2003; Donner et al., 2009; Govindaraju et al., 2020; Heisler et al., 2005; Krishna

et al., 2021; Krogan et al., 2012; Marcos and Berleth, 2014; Reinhardt et al., 2003; Scarpella et al., 2006; Verna et al., 2015; Verna et al., 2019; Wenzel et al., 2007) (Chapters 3 and 5). Over time, epidermal expression of those members of the PIN and ARF families becomes gradually restricted to the basalmost cells, and inner tissue expression becomes gradually restricted to the newly formed veins. Nevertheless, only expression of those members of the PIN and ARF families in developing veins is required for vein patterning: expression in epidermis and nonvascular inner tissue is dispensable for it (Govindaraju et al., 2020; Krishna et al., 2021).

Like expression of members of the PIN and ARF families with nonredundant functions in vein patterning, PD permeability is high in all the cells at early stages of leaf tissue development (Chapter 5). Over time, the permeability of PDs between newly formed veins and surrounding nonvascular tissues lowers but that of PDs between vein cells remains high. Interference with regulation of PD aperture and derived permeability leads to vein patterning defects, suggesting that the changes in PD permeability that occur during leaf development are relevant for vein patterning. However, it is unclear whether for vein patterning high PD permeability is required in all or only some of the tissues of the developing leaf.

Here we address this question by reducing PD aperture and derived permeability in specific tissues and by analyzing the effects of such tissue-specific reduction of PD aperture on vein patterning. We find that for vein patterning wide PD aperture is required in newly formed veins and in all the inner cells in areas of the leaf where new veins are forming. By contrast, for vein patterning wide PD aperture is dispensable in the epidermis and in the nonvascular inner tissue surrounding newly formed veins. Finally, our results suggest that the epidermis is a sink for signals that are produced in inner cells and move there through PDs to promote vein formation.

7.2 RESULTS

The permeability of plasmodesmata (PDs) is high in all the tissues of the developing Arabidopsis leaf where new veins are forming (Chapter 5). Moreover, Arabidopsis mutations that reduce PD aperture and permeability lead to vein patterning defects. However, it is unclear whether for vein patterning wide PD aperture is required in all the tissues of the developing leaf. To address this question, we leveraged Arabidopsis ET>>XVE>>cals3m plants, which allow tissue-specific reduction of PD aperture (Fig. 7.1A) (Vatén et al., 2011).

In ET>>XVE>>cals3m plants, tissue-specific GAL4:VP16 drivers activate expression of a transcriptional fusion of the *UAS* promoter to the sequence encoding the XVE chimeric transcription factor (Vatén et al., 2011). The XVE chimeric transcription factor derives from the fusion of the DNA-binding domain of the bacterial repressor LexA (X), the activating domain of the *Herpes simplex* Viral Protein 16 (V), and the regulatory region of the human estrogen receptor (E) (Zuo et al., 2000). In the presence of 17-β-estradiol (17βE), XVE will translocate into the nucleus, where it will activate expression of a transcriptional fusion of the *LexA* operator to the *cals3m* gene. The *cals3m* gene is a synthetic, gain-of-function mutant allele of the Arabidopsis *CALLOSE SYNTHASE3* gene, whose product localizes to PDs and catalyzes the reduction of their aperture (Vatén et al., 2011).

We expressed XVE>>cals3m by the E4259, J0571, E2331, and E861 tissue-specific GAL4:VP16 drivers (Amalraj et al., 2020; Wenzel et al., 2012) (Chapter 4), and by the combination of the J0571 and E2331 drivers (J0571+E2331 hereafter). We first asked whether those tissue-specific drivers retained their tissue-specific activity in 17βE-grown ET>>XVE>>cals3m backgrounds. To address this question, we imaged tissue-specific driver activity, as reported by GAL4:VP16-driven erGFP expression, in first leaves of control and 17βE-grown ET>>XVE>>cals3m backgrounds 4 days after germination (DAG).
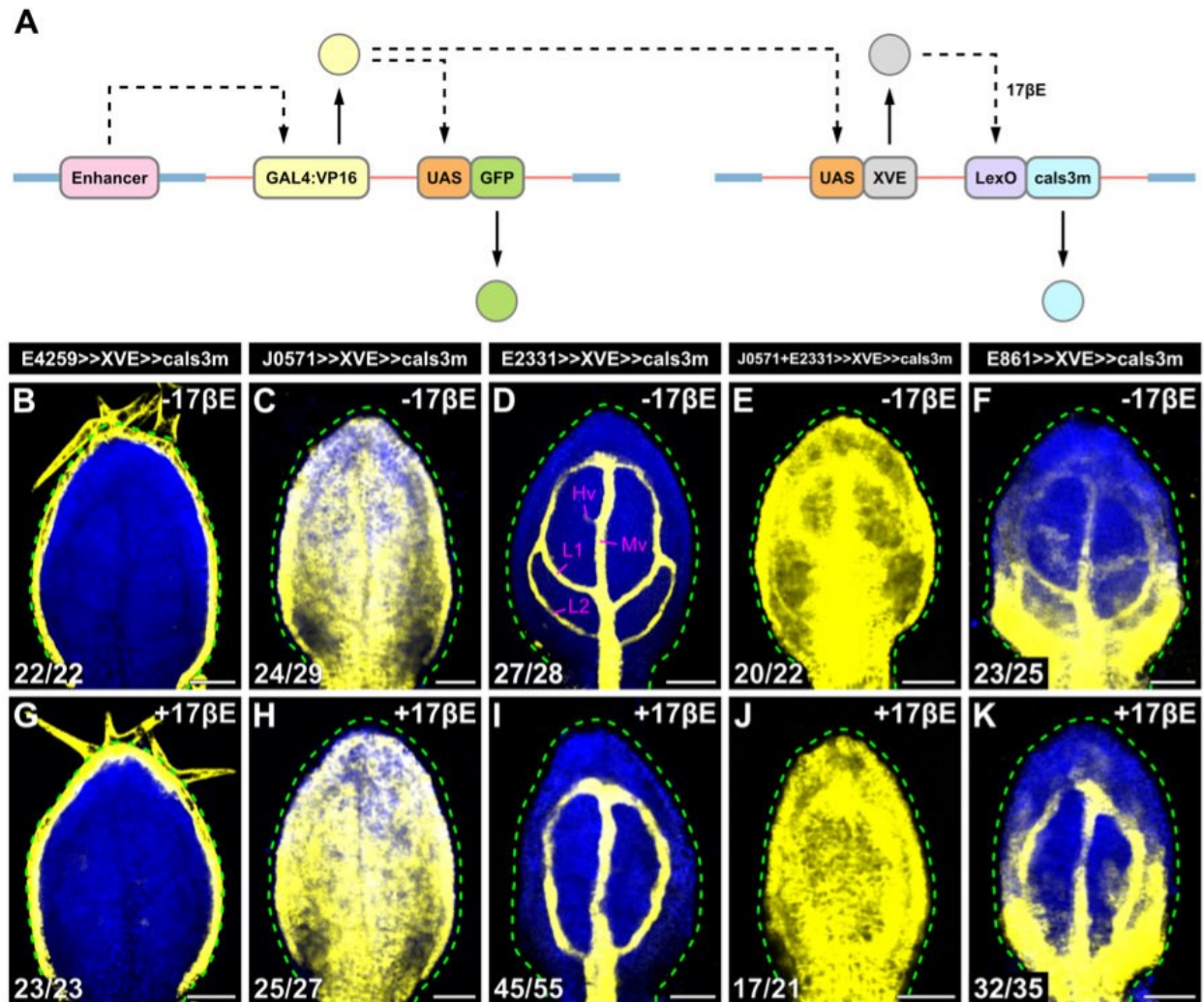
Figure 7.1. Activity of Tissue-Specific Drivers in ET>>XVE>>cals3m Leaves

(A) The ET>>XVE>>cals3m system. Cell- or tissue-specific enhancers in the Arabidopsis genome (blue line) activate transcription (dashed arrow) of a codon-usage-optimized translational fusion between the sequence encoding the GAL4 DNA-binding domain and the sequence encoding the activating domain of the *Herpes simplex* Viral Protein 16 (GAL4:VP16) in a T-DNA construct (red line) that is randomly inserted in the Arabidopsis genome (Berger et al., 1998; Haseloff, 1999). Translation of the *GAL4:VP16* fusion gene (solid arrow) leads to cell- or tissue-specific activation of transcription of a GAL4:VP16-responsive, *UAS*-driven, endoplasmic-reticulum-localized, improved *GFP* gene (*mGFP5*) (Haseloff et al., 1997; Siemering et al., 1996).

Crosses between lines with cell- or tissue-specific expression of GAL4:VP16 and lines where the sequence encoding the XVE chimeric transcription factor — which derives from the fusion of the DNA-binding domain of the bacterial repressor LexA, the VP16 activating domain, and the regulatory region of the human estrogen receptor (Zuo et al., 2000) — is driven by the *UAS* promoter lead to activation of *XVE* transcription in specific cells or tissues. In the presence of 17-β-estradiol (17βE), XVE will translocate into the nucleus, where it will activate expression of an XVE-responsive, *LexA* operat–r (*LexO*) - driven *cals3m* gene, which is a synthetic, gain-of-function allele of the *CALLOSE SYNTHASE 3* gene, whose product localizes to PDs and catalyzes their aperture reduction (Vatén et al., 2011). (B–K) Confocal laser scanning microscopy. First leaves 4 days after germination. Front view, median plane. Yellow, erGFP expression; blue, autofluorescence. Dashed line, leaf outline. HV, minor vein; L1, first loop; L2, second loop; MV, midvein. Top center: genotype. Top right: treatment. Bottom left: reproducibility index (number of samples with the displayed features / number of analyzed samples). Bars: (B–K) 50 μm.

In both control and 17βE-grown E4259>>XVE>>cals3m, E4259>>erGFP was expressed in the epidermis (Fig. 7.1B,G). In both control and 17βE-grown J0571>>XVE>>cals3m, J0571>>erGFP was expressed in the nonvascular inner tissue (Fig. 7.1C,H). In control E2331>>XVE>>cals3m, E2331>>erGFP expression was restricted to the midvein, first and second loops, and minor veins (Fig. 7.1F). E2331>>erGFP expression was also restricted to the veins in 17βE-grown E2331>>XVE>>cals3m, but no second loops or minor veins had formed in 17βE-grown E2331>>XVE>>cals3m, and first loops connected to the midvein more basally in 17βE-grown than in control E2331>>XVE>>cals3m (Fig. 7.1I). In both control and 17βE-grown J0571+E2331>>XVE>>cals3m, J0571+E2331>>erGFP was expressed in all the inner tissues (Fig. 7.1E,J). Finally, in both control and 17βE-grown E861>>XVE>>cals3m, E861>>erGFP expression was restricted to the midvein, first loops, and minor veins in the top half of the leaf, and was expressed in nearly all the cells in the bottom half of the leaf, even though expression was stronger where new veins were forming (Fig. 7.1F,K). However, in 17βE-grown E861>>XVE>>cals3m, E861>>erGFP expression in first loops was more heterogeneous and first loops connected to the midvein more basally than in control E861>>XVE>>cals3m (Fig. 7.1J,K).

We conclude that tissue-specific drivers retain their tissue-specific activity in both control and 17βE-grown ET>>XVE>>cals3m backgrounds.

We next asked in which tissues of the developing leaf wide PD aperture were required for vein patterning. To address this question, we imaged vein networks in mature first-leaves of control and 17βE-grown ET>>XVE>>cals3m backgrounds.

The vein pattern of mature leaves of control ET>>XVE>>cals3m backgrounds was no different from that of WT: (1) a narrow I-shaped midvein ran the length of the leaf; (2) lateral veins branched from the midvein and joined distal veins to form closed loops; (3) minor veins branched from midvein and loops, and either ended freely or joined other veins; and (4) minor

veins and loops curved near the leaf margin, lending a scalloped outline to the vein network (Fig. 7.2A,B,E,H,K).

The vein pattern of 17βE-grown E4259>>XVE>>cals3m leaves was no different from that of control E4259>>XVE>>cals3m leaves (Fig. 7.2A,B,N). However, the cardinality index — a proxy for the number of veins (Verna et al., 2015) — of 17βE-grown E4259>>XVE>>cals3m leaves was higher than that of control E4259>>XVE>>cals3m leaves (Fig. 7.2A,B,O), suggesting that 17βE-grown E4259>>XVE>>cals3m leaves have more veins than control E4259>>XVE>>cals3m leaves. The leaves of 17βE-grown J0571>>XVE>>cals3m were no different from those of control J0571>>XVE>>cals3m (Fig. 7.2C,D,N,O). Loops connected to the midvein more basally in leaves of 17βE-grown than in control E2331>>XVE>>cals3m leaves (Fig. 7.2E–G,N). In ~40% of 17βE-grown E2331>>XVE>>cals3m leaves loops were closed, but in nearly half of 17βE-grown E2331>>XVE>>cals3m leaves, loops were "open", i.e. they contacted the midvein or other loops at only one of their two ends (Fig. 7.2F,N). Finally, in ~10% of the leaves of 17βE-grown E2331>>XVE>>cals3m, veins were occasionally replaced by "vein fragments" — i.e. stretches of vascular elements that fail to contact other stretches of vascular elements at either one of their two ends (Fig. 7.2G,N). Vein pattern defects of 17βE-grown E861>>XVE>>cals3m and J0571+E2331>>XVE>>cals3m were no different from each other and were qualitatively similar to, but quantitatively stronger than, those of 17βE-grown E2331>>XVE>>cals3m: Only 20% of the 17βE-grown E861>>XVE>>cals3m and J0571+E2331>>XVE>>cals3m leaves had closed loops, and in ~30% of the 17βE-grown E861>>XVE>>cals3m and J0571+E2331>>XVE>>cals3m leaves veins were occasionally replaced by vein fragments (Fig. 7.2H–N).

Figure 7.2. Vein Patterns of Control and 17-β-Estradiol-Grown ET>>XVE>>cals3m Leaves

(A–M) Dark-field illumination of mature first leaves illustrating phenotype classes (top right). Class 0: closed vein-network outline (A,B,E,H,K); class a1: narrow leaf and closed vein-network outline (C,D); class a2: closed vein-network outline and loops connecting more basally to the midvein (F); class a3: narrow leaf and open vein-network outline (not shown); class a4: open vein-network outline and loops connecting more basally to the midvein (G); class a5: narrow leaf, open vein-network outline, and loops connecting more basally to the midvein (I,L); class a6: vein fragments (J,M). Arrowheads: open loops; asterisks: vein fragments. Top center: genotype. Top right: treatment. (N) Percentages of leaves in phenotype classes. Difference between 17βE-grown and control E2331>>XVE>>cals3m, between 17βE-grown and control

E861>>XVE>>cals3m, between 17βE-grown and control J0571+E2331>>XVE>>cals3m, between 17βE-grown E861>>XVE>>cals3m and 17βE-grown E2331>>XVE>>cals3m, and between 17βE-grown E861>>XVE>>cals3m and 17βE-grown J0571+E2331>>XVE>>cals3m was significant at $P<0.001$ (***) by Kruskal-Wallis and Mann-Whitney test with Bonferroni correction. Sample population sizes: control E4259>>XVE>>cals3m, 43; 17βE-grown E4259>>XVE>>cals3m, 47; control J0571>>XVE>>cals3m, 30; 17βE-grown J0571>>XVE>>cals3m, 30; control E2331>>XVE>>cals3m, 30; 17βE-grown E2331>>XVE>>cals3m, 48; control E861>>XVE>>cals3m, 30; 17βE-grown E861>>XVE>>cals3m, 45; control J0571+E2331>>XVE>>cals3m, 30; 17βE-grown J0571+E2331>>XVE>>cals3m, 45. (O) Cardinality index (mean ± SE) as defined (Verna et al., 2015) in and Materials & Methods. Difference between 17βE-grown and control E4259>>XVE>>cals3m was significant at $P<0.001$ (***) by F-test and t-test. Bars: (A–M) 1 mm.

7.3 DISCUSSION

To understand in which tissues of the developing leaf wide PD aperture were required for vein patterning, we expressed by tissue-specific drivers the *cals3m* gain-of-function mutant allele, which catalyzes dominant reduction of PD aperture (Vatén et al., 2011). We then analyzed the effects of such tissue-specific reduction of PD aperture on vein pattern formation, as reported by vein networks of mature leaves.

We found that vein-specific reduction of PD aperture through *cals3m* expression by the E2331 vascular driver led to vein pattern defects, suggesting that wide PD aperture in vein cells is required for vein patterning. This conclusion is consistent with the observation that PD permeability between vein cells remains high even when PD permeability between veins and surrounding nonvascular tissues has already lowered (Chapter 5).

We also found that *cals3m* expression by the E861 or J0571+E2331 driver led to vein pattern defects that were no different from each other and were qualitatively similar to, but quantitatively stronger than, those induced by E2331-driven *cals3m* expression. The E861 and J0571+E2331 drivers are both active in newly formed veins and in all the inner cells of the leaf where new veins are forming (Fig. 7.1) (Amalraj et al., 2020; Wenzel et al., 2012) (Chapter 4). By contrast, only E861 is also active in the epidermis of the areas of the leaf where new veins are forming, and only J0571+E2331 is also active in the nonvascular inner tissue surrounding newly formed veins. Therefore, that *cals3m* expression by the E861 or J0571+E2331 driver led to similar vein pattern defects suggests that wide PD aperture in newly formed veins and in all the inner cells of the leaf where new veins are forming is required for vein patterning. It also suggests that wide PD aperture in the epidermis of the areas of the leaf where new veins are forming and in the nonvascular inner tissue surrounding newly formed veins is dispensable for vein patterning. These conclusions are consistent with the observation that PD permeability is high in areas of the leaf where new veins are forming and remains high between vein cells even

when PD permeability between veins and surrounding nonvascular tissues has already lowered (Chapter 5).

That wide PD aperture in the epidermis of the areas of the leaf where new veins are forming is dispensable for vein patterning is also suggested by the observation that epidermal reduction of PD aperture through *cals3m* expression by the E4259 epidermal driver failed to induce vein pattern defects. However, that E4259-driven *cals3m* expression led to the formation of more veins suggests that the epidermis is a source of signals that move through PDs into inner cells and there inhibit vein formation. Alternatively, the epidermis is a sink for signals that are produced in inner cells and there move through PDs to promote vein formation. Though we cannot rule out the former possibility, only the latter one is consistent with findings suggesting the PD-enabled movement in leaf inner cells of an auxin-dependent signal that promotes vein formation (Chapter 5).

E4259-driven *cals3m* expression is expected to reduce the aperture not only of the PDs between epidermal cells but of those between the epidermis and the underlying inner cell layer. It might therefore be surprising that only *cals3m* expression in the epidermis led to formation of more veins and not *cals3m* expression in the nonvascular inner tissue by the J0571 driver, in all the inner tissues by the J0571+E2331 driver, or in all the cells in areas of the leaf where new veins are forming by the E861 driver. And indeed, it would be difficult to reconcile those observations if the epidermis were a source of signals that move through PDs into inner cells and there inhibit vein formation. However, that seeming inconsistency could be accounted for if the epidermis were a sink for signals that are produced in inner cells and there move through PDs to promote vein formation. If that were so, only when *cals3m* were to be expressed by the E4259 epidermal driver would a signal that is produced in inner cells be able to accumulate there and move through PDs and promote vein formation. In all the other cases — expression of *cals3m* expression by the J0571, E861, or J0571+E2331 driver — the additional reduction of PD aperture in inner cells would prevent such inductive movement.

In conclusion, for vein patterning wide PD aperture is required in newly formed veins and in all the inner cells in areas of the leaf where new veins are forming. By contrast, for vein patterning wide PD aperture is dispensable in the epidermis and in the nonvascular inner tissue surrounding newly formed veins. Finally, our results suggest that the epidermis is a sink for signals that are produced in inner cells and move there through PDs to promote vein formation.

7.4 MATERIALS & METHODS

7.4.1 Plants

Origin and nature of lines are in Table 7.1. Seeds were sterilized and sowed as in (Linh and Scarpella, 2022a) (Chapter 2). 17-β-estradiol was dissolved in dimethyl sulfoxide and stored at -20 °C for up to a month. Dissolved 17-β-estradiol was added (20 μM final concentration) to growth medium just before sowing. Stratified seeds were germinated and seedlings were grown at 22 °C under continuous light (~50–100 μmol m^{-2} s^{-1}). Plants were grown at 24 °C under fluorescent light (~100 μmol m^{-2} s^{-1}) in a 16-h-light/8-h-dark cycle. Plants were transformed and representative lines were selected as in (Sawchuk et al., 2008).

7.4.2 Imaging

Developing leaves were mounted and imaged by confocal laser scanning microscopy as in (Linh and Scarpella, 2022a) (Chapter 2). GFP and autofluorescence were excited and detected as in Chapter 5. Emission was collected from ~2.5–5.0-μm-thick optical slices. Mature leaves were fixed, cleared, and mounted in 1 : 2 : 8 water : glycerol : chloral hydrate as in Chapter 5. Mounted leaves were imaged by dark-field-illumination microscopy as in (Odat et al., 2014). In the Fiji distribution (Schindelin et al., 2012) of ImageJ (Rueden et al., 2017; Schindelin et al., 2015; Schneider et al., 2012), grayscaled RGB color images were turned into 8-bit images; when necessary, 8-bit images were combined into stacks, and stacks were projected at maximum

Table 7.1. Origin and Nature of Lines

Line	Origin/Nature
E4259	CS24272 (ABRC[1]); (Amalraj et al., 2020); (Chapter 4)
J0571	CS65892 (ABRC); (Wenzel et al., 2012)
E2331	CS65892 (ABRC); (Amalraj et al., 2020; Gillmor et al., 2010); (Chapter 4)
E861	CS70055 (ABRC); (Amalraj et al., 2020; Krogan and Berleth, 2012); (Chapter 4)
UAS::XVE-LexO::cals3m	(Sevilem et al., 2013); transformed into Col-0

[1] Arabidopsis Biological Resource Center

intensity; look-up-tables were applied to images; and image brightness and contrast were adjusted by linear stretching of the histogram.

7.4.3 Vein Network Analysis

The cardinality index was calculated as in (Verna et al., 2015). Briefly, the number of "touch points" (TPs, where a TP is the point where a vein end contacts another vein or a vein fragment), "end points" (EPs, where an EP is the point where an "open" vein — a vein that contacts another vein only at one end — terminates free of contact with another vein or a vein fragment), "break points" (KPs, where a KP is each of the two points where a vein fragment terminates free of contact with veins or other vein fragments), and "exit points" (XPs, where an XP is the point where a vein exits leaf blade and enters leaf petiole) in dark-field images of cleared mature leaves was calculated with the Cell Counter plugin in the Fiji distribution of ImageJ. Because a vein network can be understood as an undirected graph in which TPs, EPs, KPs, and XPs are vertices, and veins and vein fragments are edges, and because each vein is incident to two TPs, a TP and an XP, a TP and an EP, or an XP and an EP, the cardinality index — a measure of the size (i.e., the number of edges) of a graph — is a proxy for the number of veins and is calculated as $[(-Ps + XPs - Eps)/2] + EPs$, or $(TPs + XPs + EPs)/2$.

Chapter 8: General Discussion

8.1 CONCLUSION SUMMARY

Abundant evidence suggests that auxin controls coordination of cell polarity and the formation of veins that derives from such coordination (reviewed in Chapter 1 — parts of which were published in (Lavania et al., 2021; Linh et al., 2018; Ravichandran et al., 2020)). How auxin coordinates cell polarity to induce vein formation is poorly understood, and the goal of my Ph.D. thesis was to address that limitation.

For nearly 25 years the GN guanine-nucleotide exchange factor for ADP-ribosylation-factor GTPases has been thought to coordinate the cellular localization of PIN1 and possibly other PIN proteins; the resulting cell-to-cell, polar transport of auxin would propagate cell polarity across tissues and control developmental processes such as vein formation (reviewed in Chapter 1 and, for example, in (Berleth et al., 2000; Lavania et al., 2021; Linh et al., 2018; Nakamura et al., 2012; Ravichandran et al., 2020; Richter et al., 2010)). In Chapter 3 — most of which was published in (Verna et al., 2019) — I tested that hypothesis by a combination of molecular genetics, chemical interference, and cellular imaging, whose protocols I detailed in Chapter 2 (Linh and Scarpella, 2022a) (Chapter 2) and used throughout my thesis.

Contrary to predictions of the hypothesis, in Chapter 3 — and in (Verna et al., 2019) — I found that auxin-induced vein formation occurs in the absence of polar auxin transport, that the residual auxin-transport-independent vein-patterning activity relies on auxin signaling, and that a *GN*-dependent cell polarizing signal acts upstream of both auxin signaling and polar auxin transport in vein patterning. However, interference with both auxin signaling and polar auxin transport only phenocopied intermediate *gn* mutants, suggesting that additional *GN*-dependent pathways are involved in vein patterning. Because experimental evidence suggests that auxin can move through plasmodesmata (recently reviewed in (Band, 2021; Paterlini, 2020)), in Chapter 5 I asked whether movement of auxin or an auxin-dependent signal through

253

plasmodesmata is one of the missing *GN*-dependent vein-patterning pathways. To image

plasmodesma permeability, I leveraged the ability of a cytoplasmic YFP to diffuse through

plasmodesmata whose aperture is larger than the size of YFP. To transactivate YFP expression

and to image vascular systems in the different genetic backgrounds and upon the different

chemical treatments in Chapter 5, I used a vascular GAL4/GFP line I had contributed to

characterize in Chapter 4 — which was published in (Amalraj et al., 2020) (Chapter 4).

Chapter 5 showed that simultaneous interference with auxin signaling, polar auxin

transport, and movement of an auxin signal through plasmodesmata recapitulates vein

patterning defects of strong *gn* mutants. Therefore, my results suggest that veins are patterned

by the coordinated action of three *GN*-dependent pathways: auxin signaling, polar auxin

transport, and movement of auxin or an auxin-dependent signal through plasmodesmata.

However, it was still unknown whether — and if so, where and when in leaf development — *GN*

controlled the production, the movement, or the interpretation of an auxin signal with vein

patterning function. In Chapter 6, I addressed that question by determining GN expression in

leaf development, by restricting that expression to specific tissues in a strong *gn* mutant, and by

analyzing the effects of such tissue-specific *GN* expression on vein patterning. To restrict *GN*

expression to specific tissues I used a GAL4/*UAS* transactivation approach and tissue-specific

GAL4:VP16 drivers I had contributed to characterize in Chapter 4 — which was published in

(Amalraj et al., 2020) (Chapter 4).

Chapter 6 showed that GN is expressed in all the cells of the leaf throughout leaf

development, though expression was stronger where new veins were forming. Furthermore, my

results suggest that *GN* controls the production, propagation, or interpretation of a vein

patterning signal in the leaf inner tissues. For that function, *GN* expression was required in all

the inner tissues of the leaf throughout leaf development, but stronger *GN* expression seemed to

be required where new veins were forming. By contrast, if a signal with vein patterning function

were produced in the leaf epidermis, my results suggest that the production of such a signal would be independent of *GN*.

Like GN expression (Chapter 6), plasmodesma permeability was high in all the cells at early stages of leaf tissue development (Chapter 5). Over time, the permeability of plasmodesmata between newly formed veins and surrounding nonvascular tissues lowered but that of plasmodesmata between vein cells remained high. Interference with regulation of plasmodesma aperture and derived permeability led to vein patterning defects, suggesting that the changes in plasmodesma permeability that occur during leaf development are relevant for vein patterning. However, it was still unclear whether for vein patterning high plasmodesma permeability were required in all or only some of the tissues of the developing leaf. In Chapter 7, I addressed that question by reducing plasmodesma aperture and derived permeability in specific tissues and by analyzing the effects of such tissue-specific reduction of plasmodesma aperture on vein patterning. To reduce plasmodesma aperture in specific tissues I used a GAL4/*UAS* transactivation approach and tissue-specific GAL4:VP16 drivers I had contributed to characterize in Chapter 4 — which was published in (Amalraj et al., 2020) (Chapter 4).

Chapter 7 showed that for vein patterning wide plasmodesma aperture is required in newly formed veins and in all the inner cells in areas of the leaf where new veins are forming. By contrast, for vein patterning wide plasmodesma aperture was dispensable in the epidermis and in the nonvascular inner tissue surrounding newly formed veins. Furthermore, my results suggest that the epidermis is a sink for signals that are produced in inner cells and move there through plasmodesmata to promote vein formation. Therefore, available evidence (Govindaraju et al., 2020; Krishna et al., 2021) and my results in Chapter 7 together suggest that — contrary to widespread belief (reviewed in Chapter 1 and, for example, in (Bennett et al., 2014; Cieslak et al., 2021; Lavania et al., 2021; Linh et al., 2018; Prusinkiewicz and Runions, 2012; Runions et al., 2014)) — the epidermis is not a source of auxin signals that diffuse or are transported into the inner tissues to induce vein formation.

In the Discussion section of the respective chapters, I provided an account of how I reached those conclusions from the experimental evidence, how those conclusions could be integrated with one another and with those of studies by others to advance our understanding of vein patterning, and what the implications of such conclusions are for aspects of plant development beyond the formation of vein. Below, I instead wish to propose and discuss the hypothesis that auxin is not produced in the epidermis, or its production in the epidermis is inconsequential for vein patterning, and that it's instead auxin production in the inner tissues that's relevant for vein patterning. This hypothesis should be understood as an attempt to develop a conceptual framework to guide future experimentation and not as an exhaustive mechanistic account.

8.2 BACKGROUND

Specification of tissue stripes is a fundamental building block of biological patterning, from the recursive formation of veins in plant leaves to that of ribs and vertebrae in our bodies. Therefore, how multicellular organisms specify tissue stripes is a central question in biology.

In animals, where this question has been investigated extensively, tissue stripes are specified by organizer tissues whose position does not overlap with that of the stripes the organizers specify (e.g.,(Bellusci et al., 1997; Latinkic et al., 1998; Sato and Saigo, 2000; Yakoby et al., 2008)). Likewise, in plants, the leaf epidermis has long been thought to specify veins in the leaf inner tissue, mainly because genes whose function is required for vein patterning are expressed in the epidermis of the leaf in addition to the leaf inner tissues (Govindaraju et al., 2020; Krishna et al., 2021; Krogan et al., 2012; Scarpella et al., 2006; Verna et al., 2015; Verna et al., 2019; Wenzel et al., 2007).

For the past 20 years, the organizing activity of the epidermis had been thought to derive from the polar, cell-to-cell transport of the plant hormone auxin in the epidermis (Bayer et al., 2009; Benková et al., 2003; Hay et al., 2006; Heisler et al., 2005; Reinhardt et al., 2003;

Scarpella et al., 2006; Wenzel et al., 2007). Indeed, PIN1 polarity in the epidermis suggests auxin transport converging toward peak levels of auxin signaling in the epidermis — "convergence points" — from which PIN1 polarity suggests auxin transport into the inner tissues. However, recent work has shown that it isn't so (Govindaraju et al., 2020). *PIN1* expression in the epidermis is neither sufficient nor required for vein patterning. Instead, it turns out it's *PIN1* expression in the inner tissue that's both sufficient and required for vein patterning.

The possibility that auxin is imported from the epidermis into the inner tissues by auxin importers expressed in the inner cell layer immediately below the epidermis ("subepidermal layer") can be excluded for two reasons. (1) Mutants lacking the function of all auxin importers have no vein patterning defects and are unable to enhance vein pattern defects induced by auxin export inhibition (Verna et al., 2019). (2) Auxin importers can only import auxin into a cell from the intercellular space — i.e. the cell wall — but to reach the intercellular space between the epidermis and the subepidermal layer, auxin has to be exported from epidermal cells by exporters expressed in epidermal cells. Auxin is indeed a weak acid that at the intracellular pH is negatively charged and therefore cannot easily diffuse out of the plasma membrane (Raven, 1975; Rubery and Sheldrake, 1974). As such, auxin diffusion out of the cell is unfavored over diffusion into the cell by almost two orders of magnitude (Runions et al., 2014).

One other possibility to account for the existence of convergence points is that auxin is locally produced at such locations, giving rise to local peaks of auxin signaling, and that it's these peaks of auxin signaling that direct PIN1 polarity toward themselves and that somehow induce vein formation in the inner tissue (Bayer et al., 2009; Bhatia et al., 2016; Jönsson et al., 2006; Smith et al., 2006). However, epidermal auxin signaling turns out to be neither required nor sufficient for vein patterning (Krishna et al., 2021). Instead, it's auxin signaling in the inner tissues that turns out to be both sufficient and required for vein patterning.

Yet another possibility to account for the existence of convergence points is that auxin is locally produced at convergence point locations and moves into the inner tissue through plasmodesmata. However, reducing the aperture of plasmodesmata in the epidermis has no effect on vein patterning, whereas reducing the aperture of plasmodesmata in the inner tissues leads to vein patterning defects (Chapter 7).

8.3 HYPOTHESIS

I hypothesize that auxin is not produced in the epidermis, or its production in the epidermis is inconsequential for vein patterning, and that it's auxin production in the inner tissues that's relevant for vein patterning.

8.4 HYPOTHESIS TESTING

To test the hypothesis, I propose to analyze the expression of genes whose function is limiting to auxin production and to determine whether it's auxin production in the epidermis or in the inner tissues that's relevant for vein patterning.

8.4.1 Analyzing the Expression of Genes Whose Function is Limiting to Auxin Production

I will analyze expression during leaf development of the 11 *YUCCA* (*YUC*) genes, whose function is the limiting step in auxin production (Zhao, 2018). To do so, I will generate translational fusion of *YUC* genes to 3xYFP — including >10 kb of upstream sequences, introns, and >5 kb of downstream sequences — by means of improved recombineering (Brumos et al., 2020).

If auxin is not produced in the epidermis, I expect that none of the YFP fusions will be expressed in the epidermis. By contrast, expression of one or more of those fusions in the epidermis will suggest that auxin is produced in the epidermis. I can envision two mutually exclusive possibilities. (1) Some of the *YUC* genes that are expressed in the leaf are only

expressed in the epidermis (YUC_e hereafter) and some others are only expressed in the inner tissues (YUC_i hereafter) — i.e. YUC genes are mutually exclusively expressed in either epidermis or inner tissues. (2) All the YUC genes that are expressed in the leaf are expressed in both epidermis and inner tissues (YUC_l hereafter). Below, I will treat separately those two possibilities. Of course those two possibilities are only opposite extremes along a spectrum, and one could envision varied combinations of those two possibilities — i.e. some YUC genes are only expressed in the epidermis, some others are only expressed in the inner tissues, and the remaining ones are expressed in both tissues. However, for simplicity, below I will only discuss the two extremes along that spectrum of possibilities.

8.4.2 Determining Whether Auxin Production in The Epidermis or in the Inner Tissue is Relevant for Vein Patterning

8.4.2.1 Some YUC *genes are only expressed in the epidermis and others are only expressed in the inner tissues*

To test whether auxin production in the epidermis is relevant for vein patterning, I will analyze mature leaves of a mutant that lacks function in all the YUC_e genes. If that yuc_e mutant survives embryogenesis and produces leaves, I will analyze the vein patterns in those mature leaves. Should those vein patterns be abnormal, I will conclude that production of auxin in the epidermis is relevant for vein patterning. Should those vein patterns instead be normal, I will preliminarily conclude that production of auxin in the epidermis is inconsequential to vein patterning. Indeed, in that case it's possible that some YUC_i genes are expressed in the epidermis of the yuc_e mutant, thereby compensating for the lack of YUC_e function.

To test whether any of the YUC_i genes are expressed in the epidermis of the yuc_e mutant, I will transform or cross translational fusions to YFP of the YUC_i genes into the yuc_e mutant to generate YUC$_i$::YUC$_i$:YFP;yuc_e backgrounds. Should none of the fusions be expressed in the

epidermis, I will conclude that production of auxin in the epidermis is inconsequential to vein patterning. Should some of the fusions be expressed in the epidermis, I will first generate a mutant in all the *YUC* genes that are expressed in the leaf (yuc_e;yuc_i) and then transform it with constructs or cross it with lines in which expression of the YUC_i genes is driven by an inner-tissue-specific promoter such as the *PIN6* promoter (Sawchuk et al., 2013) to generate, for example, PIN6::YUC_i;yuc_e;yuc_i backgrounds. Alternatively, I will express the YUC_i genes by the *UAS* promoter, which is inactive in leaves (Engineer et al., 2005; Haseloff, 1999; Li et al., 2019; Linh and Scarpella, 2022b) (Chapter 5), and drive UAS::YUC_i expression with an inner-tissue-specific enhancer such as KS047 (Sawchuk et al., 2007) to generate, for example, KS047>>YUC_i;yuc_e;yuc_i backgrounds. I will then analyze the vein pattern in the mature leaves of the PIN6::YUC_i;yuc_e;yuc_i or KS047>>YUC_i;yuc_e;yuc_i background. Should those vein patterns be abnormal, I will conclude that production of auxin in the epidermis is relevant for vein patterning. Should those vein patterns instead be normal, I will conclude that production of auxin in the epidermis is inconsequential to vein patterning.

If the yuc_e mutant does not survive embryogenesis, I will first identify which YUC_e gene provides the most nonredundant functions in vein patterning. Available evidence suggests that in medium-size gene families (i.e. ~10 members) only one gene provides the most nonredundant functions in specific processes (e.g., (Huang et al., 2009; Prigge et al., 2020; Sawchuk et al., 2013; Stamatiou, 2007)). Typically, these genes can be easily identified from analysis of single mutants because those genes are the only ones whose single mutants lead to any or the most severe defects in the investigated process. In my case, I will analyze vein patterns in mature leaves of yuc_e single mutants to identify the one YUC_e gene with the most nonredundant functions in vein patterning, i.e. the YUC_e gene whose single mutant is the only one with vein pattern defects or is the one with the most severe vein pattern defects. I will refer to that YUC_e gene as *nrYUC_e*, for nonredundant *YUC_e*.

I will create a version of the *nrYUC$_e$* gene whose expression can be induced in the epidermis. For example, I will use the XVE system (Zuo et al., 2000) to generate lines (XVE>>nrYUC$_e$) in which the expression of the *nrYUC$_e$* gene is induced in the presence of 17-β-estradiol. To limit such inducible expression to the epidermis, I will use *nrYUC$_e$*'s own promoter or an epidermal promoter (e.g., *ATML1*; (Govindaraju et al., 2020; Lu et al., 1996; Sessions et al., 1999)) to generate the nrYUC$_e$::XVE>>nrYUC$_e$ or ATML1::XVE>>nrYUC$_e$ construct, respectively. Alternatively, I will express XVE>>nrYUC$_e$ by the *UAS* promoter, which is inactive in leaves (Engineer et al., 2005; Haseloff, 1999; Li et al., 2019; Linh and Scarpella, 2022b) (Chapter 5), and drive its expression with an epidermal enhancer (e.g., E4259; (Amalraj et al., 2020)) (Chapter 4) to generate the E4259>>XVE>>nrYUC$_e$ background. I will cross or transform the resulting inducible version of the *nrYUC$_e$* gene (hereafter XVE>>nrYUC$_e$) into the *yuc$_e$* mutant to generate the XVE>>nrYUC$_e$;*yuc$_e$* background. I will spray flowers and fruits of XVE>>nrYUC$_e$;*yuc$_e$* with — or dip flowers and fruits of that background into — the inducer (e.g., 17-β-estradiol in the case of a fusion to XVE) to induce epidermal expression of the *nrYUC$_e$* gene during embryogenesis, thereby allowing the *yuc$_e$* mutant to survive embryogenesis. I will withdraw induction post-embryonically and analyze the vein patterns in the resulting mature leaves. Should those vein patterns be abnormal, I will conclude that production of auxin in the epidermis is relevant for vein patterning. Should those vein patterns instead be normal, I will preliminarily conclude that production of auxin in the epidermis is inconsequential to vein patterning. Indeed, in that case it's possible that some *YUC$_i$* genes are expressed in the epidermis of the XVE>>nrYUC$_e$;*yuc$_e$* background, thereby compensating for the lack of *YUC$_e$* function.

To test whether any of the *YUC$_i$* genes are expressed in the epidermis of the XVE>>nrYUC$_e$;*yuc$_e$* background, I will transform or cross translational fusions to YFP of the *YUC$_i$* genes (YUC$_i$::YUC$_i$:YFP) into the XVE>>nrYUC$_e$;*yuc$_e$* background to generate YUC$_i$::YUC$_i$:YFP;XVE>>nrYUC$_e$;*yuc$_e$* backgrounds. Should none of the fusions be expressed in

the epidermis, I will conclude that production of auxin in the epidermis is inconsequential to vein patterning. Should some of the fusions be expressed in the epidermis, I will generate in the XVE>>nrYUC$_e$ background a mutant in all the *YUC* genes that are expressed in the leaf (XVE>>nrYUC$_e$;*yuc$_e$*;*yuc$_i$*), and transform it with constructs or cross it with lines in which expression of the *YUC$_i$* genes is driven by an inner-tissue-specific promoter such as the *PIN6* promoter (Sawchuk et al., 2013) to generate, for example, PIN6::YUC$_i$;XVE>>nrYUC$_e$;*yuc$_e$*;*yuc$_i$* backgrounds. Alternatively, I will express the *YUC$_i$* genes by the *UAS* promoter, which is inactive in leaves ((Engineer et al., 2005; Haseloff, 1999; Li et al., 2019; Linh and Scarpella, 2022b) (Chapter 5), and drive its expression with an inner-tissue-specific enhancer such as KS047 (Sawchuk et al., 2007) to generate KS047>>YUC$_i$ backgrounds. I will then cross these backgrounds into the XVE>>nrYUC$_e$;*yuc$_e$*;*yuc$_i$* background to generate KS047>>YUC$_i$;XVE>>nrYUC$_e$;*yuc$_e$*;*yuc$_i$* backgrounds. I will analyze the vein patterns in mature leaves of the PIN6::YUC$_i$;XVE>>nrYUC$_e$;*yuc$_e$*;*yuc$_i$* or KS047>>YUC$_i$;XVE>>nrYUC$_e$;*yuc$_e$*;*yuc$_i$* background. Should those vein patterns be abnormal, I will conclude that production of auxin in the epidermis is relevant for vein patterning. Should those vein patterns instead be normal, I will conclude that production of auxin in the epidermis is inconsequential to vein patterning.

To test whether auxin production in the inner tissues is relevant for vein patterning, I will repeat for *YUC$_i$* genes the experiments described above for *YUC$_e$* genes.

8.4.2.2 All YUC *genes are expressed in both epidermis and inner tissues*

To test whether auxin production in the epidermis is relevant for vein patterning, I will analyze mature leaves of a *yuc$_l$* multiple mutant that lacks epidermal expression of all the *YUC$_l$* genes. To do so, I will first generate a mutant in all the *YUC$_l$* genes and then transform it with constructs or cross it with lines in which expression of the *YUC$_l$* genes is driven by an inner-tissue-specific promoter such as the *PIN6* promoter (Sawchuk et al., 2013) to generate, for example, PIN6::YUC$_l$;*yuc$_l$* backgrounds. Alternatively, I will express the *YUC$_l$* genes by the *UAS* promoter,

which is inactive in leaves (Engineer et al., 2005; Haseloff, 1999; Li et al., 2019; Linh and Scarpella, 2022b) (Chapter 5), and drive UAS::YUC$_l$ expression with an inner-tissue-specific enhancer such as KS047 (Sawchuk et al., 2007) to generate, for example, KS047>>UAS::YUC$_l$;*yuc$_l$* backgrounds. If the PIN6::YUC$_l$;*yuc$_l$* or KS047>>UAS::YUC$_l$;*yuc$_l$* background survives embryogenesis and produces leaves, I will analyze the vein patterns in its mature leaves. Should those vein patterns be abnormal, I will conclude that production of auxin in the epidermis is relevant for vein patterning. Should those vein patterns instead be normal, I will conclude that production of auxin in the epidermis is inconsequential to vein patterning.

If neither the PIN6::YUC$_l$;*yuc$_l$* nor KS047>>UAS::YUC$_l$;*yuc$_l$* background survives embryogenesis, I will apply the same approach described above for the identification of the *nrYUC$_e$* gene and will identify which *YUC$_l$* gene provides nonredundant functions in vein patterning (*nrYUC$_l$*, for nonredundant *YUC$_l$*, hereafter). I will create a version of the *nrYUC$_l$* gene whose expression can be induced in the epidermis. For example, I will use the XVE system (Zuo et al., 2000) to generate lines (XVE>>nrYUC$_l$) in which the expression of the *nrYUC$_l$* gene is induced in the presence of 17-β-estradiol. To limit such inducible expression to the epidermis, I will use an epidermal promoter (e.g., *ATML1*; (Govindaraju et al., 2020; Lu et al., 1996; Sessions et al., 1999)) to generate the ATML1::XVE>>nrYUC$_l$ construct. Alternatively, I will express XVE>>nrYUC$_l$ by the *UAS* promoter, which is inactive in leaves (Engineer et al., 2005; Haseloff, 1999; Li et al., 2019; Linh and Scarpella, 2022b) (Chapter 5), and drive its expression with an epidermal enhancer line (e.g., E4259; (Amalraj et al., 2020) (Chapter 4) to generate the E4259>>UAS::XVE>>nrYUC$_l$ background. I will cross or transform the resulting inducible version of *nrYUC$_l$* (hereafter XVE>>nrYUC$_l$) into the PIN6::YUC$_l$;*yuc$_l$* or KS047>>UAS::YUC$_l$;*yuc$_l$* background to generate the XVE>>nrYUC$_l$;PIN6::YUC$_l$;*yuc$_l$* or XVE>>nrYUC$_l$;KS047>>UAS::YUC$_l$;*yuc$_l$* background, respectively. I will spray flowers and fruits of the XVE>>nrYUC$_l$;PIN6::YUC$_l$;*yuc$_l$* or XVE>>nrYUC$_l$;KS047>>UAS::YUC$_l$;*yuc$_l$* background with — or dip flowers and fruits of either background into — the inducer (e.g., 17-β-

estradiol in the case of a fusion to XVE) to induce epidermal expression of the *nrYUC$_l$* gene during embryogenesis, thereby allowing the PIN6::YUC$_l$;*yuc$_l$* or KS047>>UAS::YUC$_l$;*yuc$_l$* background to survive embryogenesis. I will withdraw induction post-embryonically and analyze the vein patterns in the resulting mature leaves. Should those vein patterns be abnormal, I will conclude that production of auxin in the epidermis is relevant for vein patterning. Should those vein patterns instead be normal, I will conclude that production of auxin in the epidermis is inconsequential to vein patterning.

To test whether auxin production in the inner tissues is relevant for vein patterning, I will repeat the experiments described above for a *yuc$_l$* multiple mutant that lacks the inner-tissue-specific expression of all the *YUC$_l$* genes.

8.5. OUTLOOK

The hypothesis I proposed above should not be understood as an exhaustive mechanistic account but as an attempt to develop a conceptual framework to guide future experimentation. Even though the hypothesis makes testable predictions, because of the complexity of vein patterning, it may be difficult to evaluate intuitively the results of the experimental tests of those predictions; a mathematical formulation of the hypothesis — one that can be simulated computationally — may be required. Iterative cycles of simulations and experimentation will take us closer to understanding how the plant vascular system forms and how the mechanisms by which the vascular system forms in plants compare with those by which the vascular system forms in animals — a key question to address if we are to understand how multicellular organisms develop and function.

Works Cited

Abas, L., Kolb, M., Stadlmann, J., Janacek, D. P., Lukic, K., Schwechheimer, C., Sazanov, L. A., Mach, L., Friml, J. and Hammes, U. Z. (2021). Naphthylphthalamic acid associates with and inhibits PIN auxin transporters. *Proc Natl Acad Sci U S A* **118**, e2020857118.

Abley, K., Sauret-Gueto, S., Maree, A. F. and Coen, E. (2016). Formation of polarity convergences underlying shoot outgrowths. *Elife* **5**, e18165.

Adamowski, M. and Friml, J. (2015). PIN-dependent auxin transport: action, regulation, and evolution. *Plant Cell* **27**, 20–32.

Aida, M., Beis, D., Heidstra, R., Willemsen, V., Blilou, I., Galinha, C., Nussaume, L., Noh, Y. S., Amasino, R. and Scheres, B. (2004). The PLETHORA genes mediate patterning of the Arabidopsis root stem cell niche. *Cell* **119**, 109–120.

Alim, K. and Frey, E. (2010). Quantitative predictions on auxin-induced polar distribution of PIN proteins during vein formation in leaves. *The European Physical Journal E* **33**, 165–173.

Aloni, R. (2001). Foliar and Axial Aspects of Vascular Differentiation: Hypotheses and Evidence. *Journal of Plant Growth Regulation* **20**, 22–34.

Aloni, R., Schwalm, K., Langhans, M. and Ullrich, C. I. (2003). Gradual shifts in sites of free-auxin production during leaf-primordium development and their role in vascular differentiation and leaf morphogenesis in Arabidopsis. *Planta* **216**, 841–853.

Alonso, J. M., Stepanova, A. N., Leisse, T. J., Kim, C. J., Chen, H., Shinn, P., Stevenson, D. K., Zimmerman, J., Barajas, P., Cheuk, R., et al. (2003). Genome-wide insertional mutagenesis of Arabidopsis thaliana. *Science (1979)* **301**, 653–657.

Alonso-Peral, M. M., Candela, H., del Pozo, J. C., Martínez-Laborda, A., Ponce, M. R., Micol, J. L., Martinez-Laborda, A., Ponce, M. R., Micol, J. L., Martínez-

Laborda, A., et al. (2006). The HVE/CAND1 gene is required for the early patterning of leaf venation in Arabidopsis. *Development* **133**, 3755–3766.

Alvarez, J. P., Furumizu, C., Efroni, I., Eshed, Y. and Bowman, J. L. (2016). Active suppression of a leaf meristem orchestrates determinate leaf growth. *Elife* **5**, e15023.

Amalraj, B., Govindaraju, P., Krishna, A., Lavania, D., Linh, N. M., Ravichandran, S. J. and Scarpella, E. (2020a). GAL4/GFP enhancer-trap lines for identification and manipulation of cells and tissues in developing Arabidopsis leaves. *Developmental Dynamics* **249**, 1127–1146.

Ash, A., Ellis, B., Hickey, L. J., Johnson, K., Wilf, P. and Wing, S. (1999). *Manual of leaf architecture*. Washington, DC: Leaf Architecture Working Group. Smithsonian Institution.

Avery Jr., G. S. (1935). Differential Distribution of a Phytohormone in the Developing Leaf of Nicotiana, and Its Relation to Polarized Growth. *Bulletin of the Torrey Botanical Club* **62**, 313–330.

Balcerowicz, M., Ranjan, A., Rupprecht, L., Fiene, G. and Hoecker, U. (2014). Auxin represses stomatal development in dark-grown seedlings via Aux/IAA proteins. *Development* **141**, 3165–3176.

Band, L. R. (2021). Auxin fluxes through plasmodesmata. *New Phytol* **231**, 1686–1692.

Barbosa, I. C. R., Hammes, U. Z. and Schwechheimer, C. (2018). Activation and Polarity Control of PIN-FORMED Auxin Transporters by Phosphorylation. *Trends Plant Sci* **23**, 523–538.

Bayer, E. M., Smith, R. S., Mandel, T., Nakayama, N., Sauer, M., Prusinkiewicz, P. and Kuhlemeier, C. (2009a). Integration of transport-based models for phyllotaxis and midvein formation. *Genes and Development* **23**, 373–384.

Beerling, D. J. and Fleming, A. J. (2007). Zimmermann's telome theory of megaphyll leaf evolution: a molecular and cellular critique. *Current Opinion in Plant Biology* **10**, 4–12.

Bellusci, S., Grindley, J., Emoto, H., Itoh, N. and Hogan, B. L. M. (1997). Fibroblast Growth Factor 10 (FGF10) and branching morphogenesis in the embryonic mouse lung. *Development* **124**, 4867–4878.

Benayoun, J., Aloni, R. and Sachs, T. (1975). Regeneration Around Wounds and the Control of Vascular Differentiation. *Annals of Botany* **39**, 447–454.

Benitez-Alfonso, Y., Cilia, M., San Roman, A., Thomas, C., Maule, A., Hearn, S. and Jackson, D. (2009). Control of Arabidopsis meristem development by thioredoxin-dependent regulation of intercellular transport. *Proc Natl Acad Sci U S A* **106**, 3615–3620.

Benitez-Alfonso, Y., Faulkner, C., Pendle, A., Miyashima, S., Helariutta, Y. and Maule, A. (2013). Symplastic intercellular connectivity regulates lateral root patterning. *Dev Cell* **26**, 136–147.

Benková, E., Michniewicz, M., Sauer, M., Teichmann, T., Seifertová, D., Jürgens, G. and Friml, J. (2003). Local, efflux-dependent auxin gradients as a common module for plant organ formation. *Cell* **115**, 591–602.

Bennett, S. R. M. M., Alvarez, J., Bossinger, G. and Smyth, D. R. (1995). Morphogenesis in pinoid mutants of Arabidopsis thaliana. *The Plant Journal* **8**, 505–520.

Bennett, T., Hines, G. and Leyser, O. (2014). Canalization: What the flux? *Trends in Genetics* **30**, 41–48.

Berger, F., Linstead, P., Dolan, L. and Haseloff, J. (1998). Stomata patterning on the hypocotyl of Arabidopsis thaliana is controlled by genes involved in the control of root epidermis patterning. *Dev Biol* **194**, 226–234.

Berleth, T. and Jurgens, G. (1993). The Role of the Monopteros Gene in Organizing the Basal Body Region of the Arabidopsis Embryo. *Development* **118**, 575–587.

Berleth, T., Mattsson, J. and Hardtke, C. S. (2000). Vascular continuity and auxin signals. *Trends in Plant Science* **5**, 387–393.

Betz, C., Lenard, A., Belting, H. G. and Affolter, M. (2016). Cell behaviors and dynamics during angiogenesis. *Development (Cambridge)* **143**, 2249–2260.

Bhatia, N., Bozorg, B., Larsson, A., Ohno, C., Jönsson, H. and Heisler, M. G. (2016). Auxin Acts through MONOPTEROS to Regulate Plant Cell Polarity and Pattern Phyllotaxis. *Current Biology* **26**, 3202–3208.

Bhatia, N., Åhl, H., Jönsson, H. and Heisler, M. G. (2019). Quantitative analysis of auxin sensing in leaf primordia argues against proposed role in regulating leaf dorsoventrality. *Elife* **8**, e39298.

Bilsborough, G. D., Runions, A., Barkoulas, M., Jenkins, H. W., Hasson, A., Galinha, C., Laufs, P., Hay, A., Prusinkiewicz, P. and Tsiantis, M. (2011). Model for the regulation of Arabidopsis thaliana leaf margin development. *Proc Natl Acad Sci U S A* **108**, 3424–3429.

Born, M. and Wolf, E. (2019). *Principles of optics*. 7th ed. Cambridge: Cambridge University Press.

Boulin, T., Etchberger, J. F. and Hobert, O. (2006). Reporter gene fusions. *WormBook* 1–23.

Brand, A. H. and Perrimon, N. (1993). Targeted gene expression as a means of altering cell fates and generating dominant phenotypes. *Development* **118**, 401–415.

Braybrook, S. A. and Peaucelle, A. (2013). Mechano-chemical aspects of organ formation in Arabidopsis thaliana: the relationship between auxin and pectin. *PLoS One* **8**, e57813.

Brumos, J., Zhao, C., Gong, Y., Soriano, D., Patel, A. P., Perez-Amador, M. A., Stepanova, A. N. and Alonso, J. M. (2020). An Improved Recombineering Toolset for Plants. *Plant Cell* **32**, 100–122.

Brunoud, G., Wells, D. M., Oliva, M., Larrieu, A., Mirabet, V., Burrow, A. H., Beeckman, T., Kepinski, S., Traas, J., Bennett, M. J., et al. (2012). A novel sensor

to map auxin response and distribution at high spatio-temporal resolution. *Nature* **482**, 103–106.

Bryan, W. H. and Newcomb, K. H. (1954). Stimulation of pectin methylesterase activity of cultured tobacco pith by indoleacetic acid. *Physiologia Plantarum* **7**, 290–297.

Bundy, M. G., Kosentka, P. Z., Willet, A. H., Zhang, L., Miller, E. and Shpak, E. D. (2016). A Mutation in the Catalytic Subunit of the Glycosylphosphatidylinositol Transamidase Disrupts Growth, Fertility, and Stomata Formation. *Plant Physiol* **171**, 974–985.

Burke, R. and Basler, K. (1996). Dpp receptors are autonomously required for cell proliferation in the entire developing Drosophila wing. *Development* **122**, 2261–2269.

Busch, M., Mayer, U. and Jurgens, G. (1996). Molecular analysis of the Arabidopsis pattern formation of gene GNOM: gene structure and intragenic complementation. *Molecular & General Genetics* **250**, 681–691.

Caggiano, M. P., Yu, X., Bhatia, N., Larsson, A., Ram, H., Ohno, C. K., Sappl, P., Meyerowitz, E. M., Jönsson, H. and Heisler, M. G. (2017). Cell type boundaries organize plant development. *Elife* **6**, e27421.

Caggiano, M. P., Yu, X., Ohno, C., Sappl, P. and Heisler, M. G. (2021). Live Imaging of Arabidopsis Leaf and Vegetative Meristem Development. In *Methods in Molecular Biology: Arabidopsis Protocols*, pp. 295–302. New York, NY: Springer US.

Calhoun, C., Crist, D., Knee, E., Miller, J., Nagy, E. and Somers, D. E. (2021). Handling Arabidopsis and Other Brassicaceae: Growth, Preservation of Seeds, Transformation, and Genetic Crosses. In *Arabidopsis protocols* (ed. Sanchez-Serrano, J. J. and Salinas, J.), pp. 3–23. New York, NY: Humana Press.

Calleja, M., Moreno, E., Pelaz, S. and Morata, G. (1996). Visualization of gene expression in living adult Drosophila. *Science (1979)* **274**, 252–255.

Cande, W. Z. and Ray, P. iM (1976). Nature of cell-to-cell transfer of auxin in polar transport. *Planta* **129**, 43–52.

Candela, H., Martínez-Laborda, A. and Micol, J. L. (1999). Venation pattern formation in Arabidopsis thaliana vegetative leaves. *Developmental Biology* **205**, 205–216.

Carland, F. M. and Nelson, T. (2004). Cotyledon vascular pattern2-mediated inositol (1,4,5) triphosphate signal transduction is essential for closed venation patterns of Arabidopsis foliar organs. *Plant Cell* **16**, 1263–1275.

Carland, F. and Nelson, T. (2009). CVP2- and CVL1-mediated phosphoinositide signaling as a regulator of the ARF GAP SFC/VAN3 in establishment of foliar vein patterns. *Plant J* **59**, 895–907.

Carland, F. M., Berg, B. L., FitzGerald, J. N., Jinamornphongs, S., Nelson, T. and Keith, B. (1999). Genetic regulation of vascular tissue patterning in Arabidopsis. *Plant Cell* **11**, 2123–2137.

Carraro, N., Forestan, C., Canova, S., Traas, J. and Varotto, S. (2006). ZmPIN1a and ZmPIN1b encode two novel putative candidates for polar auxin transport and plant architecture determination of maize. *Plant Physiol* **142**, 254–264.

Chalfie, M., Tu, Y., Euskirchen, G., Ward, W. W. and Prasher, D. C. (1994). Green fluorescent protein as a marker for gene expression. *Science (1979)* **263**, 802–805.

Chen, M. H. and Citovsky, V. (2003). Systemic movement of a tobamovirus requires host cell pectin methylesterase. *Plant J* **35**, 386–392.

Chen, M. H., Sheng, J., Hind, G., Handa, A. K. and Citovsky, V. (2000). Interaction between the tobacco mosaic virus movement protein and host cell pectin methylesterases is required for viral cell-to-cell movement. *EMBO J* **19**, 913–920.

Chen, X. Y., Liu, L., Lee, E., Han, X., Rim, Y., Chu, H., Kim, S. W., Sack, F. and Kim, J. Y. (2009). The Arabidopsis callose synthase gene GSL8 is required for cytokinesis and cell patterning. *Plant Physiol* **150**, 105–113.

Cheng, Y., Dai, X. and Zhao, Y. (2007). Auxin synthesized by the YUCCA flavin monooxygenases is essential for embryogenesis and leaf formation in Arabidopsis. *Plant Cell* **19**, 2430–2439.

Cieslak, M., Runions, A. and Prusinkiewicz, P. (2015). Auxin-driven patterning with unidirectional fluxes. *J Exp Bot* **66**, 5083–5102.

Cieslak, M., Owens, A. and Prusinkiewicz, P. (2021). Computational Models of Auxin-Driven Patterning in Shoots. *Cold Spring Harb Perspect Biol* **14**, a040097.

Ckurshumova, W., Koizumi, K., Chatfield, S. P., Sanchez-Buelna, S. U., Gangaeva, A. E., McKenzie, R. and Berleth, T. (2009). Tissue-specific GAL4 expression patterns as a resource enabling targeted gene expression, cell type-specific transcript profiling and gene function characterization in the Arabidopsis vascular system. *Plant Cell Physiol* **50**, 141–150.

Coen, E., Rolland-Lagan, A. G., Matthews, M., Bangham, J. A. and Prusinkiewicz, P. (2004). The genetics of geometry. *Proc Natl Acad Sci U S A* **101**, 4728–4735.

Colarusso, P. and Spring, K. R. (2003). Imaging at low light levels with cooled and intensified charge-coupled device cameras. *Methods Enzymol* **360**, 383–394.

Cook, S. D. (2019). An Historical Review of Phenylacetic Acid. *Plant Cell Physiol* **60**, 243–254.

Corson, F., Adda-Bedia, M. and Boudaoud, A. (2009). In silico leaf venation networks: growth and reorganization driven by mechanical forces. *J Theor Biol* **259**, 440–448.

Couder, Y., Pauchard, L., Allain, C., Adda-Bedia, M. and Douady, S. (2002). The leaf venation as formed in a tensorial field. *The European Physical Journal B* **28**, 135–138.

Cromey, D. W. (2010). Avoiding twisted pixels: ethical guidelines for the appropriate use and manipulation of scientific digital images. *Sci Eng Ethics* **16**, 639–667.

de Rybel, B., Adibi, M., Breda, A. S., Wendrich, J. R., Smit, M. E., Novák, O., Yamaguchi, N., Yoshida, S., van Isterdael, G., Palovaara, J., et al. (2014). Plant

development. Integration of growth and patterning during vascular tissue formation in Arabidopsis. *Science (1979)* **345**, 1255215.

de Storme, N., de Schrijver, J., van Criekinge, W., Wewer, V., Dörmann, P. and Geelen, D. (2013). GLUCAN SYNTHASE-LIKE8 and STEROL METHYLTRANSFERASE2 are required for ploidy consistency of the sexual reproduction system in Arabidopsis. *Plant Cell* **25**, 387–403.

Dengler, N. and Kang, J. (2001). Vascular patterning and leaf shape. *Current Opinion in Plant Biology* **4**, 50–56.

Deyholos, M. K., Cordner, G., Beebe, D. and Sieburth, L. E. (2000). The SCARFACE gene is required for cotyledon and leaf vein patterning. *Development* **127**, 3205–3213.

Dharmasiri, S., Dharmasiri, N., Hellmann, H. and Estelle, M. (2003). The RUB/Nedd8 conjugation pathway is required for early development in Arabidopsis. *Embo J* **22**, 1762–1770.

Dharmasiri, N., Dharmasiri, S., Weijers, D., Lechner, E., Yamada, M., Hobbie, L., Ehrismann, J. S., Jurgens, G., Estelle, M., Jürgens, G., et al. (2005). Plant Development Is Regulated by a Family of Auxin Receptor F Box Proteins. *Developmental Cell* **9**, 109–119.

Dharmasiri, N., Dharmasiri, S., Weijers, D., Karunarathna, N., Jurgens, G. and Estelle, M. (2007). AXL and AXR1 have redundant functions in RUB conjugation and growth and development in Arabidopsis. *The Plant Journal* **52**, 114–123.

Dimitrov, P. and Zucker, S. W. (2006). A constant production hypothesis guides leaf venation patterning. *Proc Natl Acad Sci U S A* **103**, 9363–9368.

Dobbie, I. M., Lowndes, N. F., Sullivan, K. F., Wilson, L. and Matsudaira, P. (2008). Autofluorescent Proteins. In *Fluorescent proteins* (ed. Sullivan, K. F.), pp. 1–22. London: Academic Press.

Donnelly, P. M., Bonetta, D., Tsukaya, H., Dengler, R. E. and Dengler, N. G. (1999). Cell cycling and cell enlargement in developing leaves of Arabidopsis. *Developmental Biology* **215**, 407–419.

Donner, T. J., Sherr, I. and Scarpella, E. (2009). Regulation of preprocambial cell state acquisition by auxin signaling in Arabidopsis leaves. *Development* **136**, 3235–3246.

Dorokhov, Y. L., Komarova, T. v, Petrunia, I. v, Frolova, O. Y., Pozdyshev, D. v and Gleba, Y. Y. (2012). Airborne signals from a wounded leaf facilitate viral spreading and induce antibacterial resistance in neighboring plants. *PLoS Pathog* **8**, e1002640.

Elefant, F. and Palter, K. B. (1999). Tissue-specific expression of dominant negative mutant Drosophila HSC70 causes developmental defects and lethality. *Mol Biol Cell* **10**, 2101–2117.

Engineer, C. B., Fitzsimmons, K. C., Schmuke, J. J., Dotson, S. B. and Kranz, R. G. (2005). Development and evaluation of a Gal4-mediated LUC/GFP/GUS enhancer trap system in Arabidopsis. *BMC Plant Biology* **5**, 1–15.

Esau, K. (1943). Origin and development of primary vascular tissues in seed plants. *Botanical Review* **9**, 125–206.

Esau, K. (1965). *Plant anatomy*. 2nd ed. New York ; London: John Wiley.

Esteve-Bruna, D., Pérez-Pérez, J. M., Ponce, M. R., Micol, J. L., Perez-Perez, J. M., Ponce, M. R. and Micol, J. L. (2013). incurvata13, a novel allele of AUXIN RESISTANT6, reveals a specific role for auxin and the SCF complex in Arabidopsis embryogenesis, vascular specification, and leaf flatness. *Plant Physiol* **161**, 1303–1320.

Fairon-Demaret, M. and Li, C.-S. (1993). Lorophyton goense gen. et sp. nov. from the Lower Givetian of Belgium and a discussion of the Middle Devonian Cladoxylopsida. *Review of Palaeobotany and Palynology* **77**, 1–22.

Faulkner, C., Petutschnig, E., Benitez-Alfonso, Y., Beck, M., Robatzek, S., Lipka, V. and Maule, A. J. (2013). LYM2-dependent chitin perception limits molecular flux via plasmodesmata. *Proc Natl Acad Sci U S A* **110**, 9166–9170.

Fendrych, M., Leung, J. and Friml, J. (2016). TIR1/AFB-Aux/IAA auxin perception mediates rapid cell wall acidification and growth of Arabidopsis hypocotyls. *Elife* **5**, e19048.

Feugier, F. G. and Iwasa, Y. (2006). How canalization can make loops: a new model of reticulated leaf vascular pattern formation. *J Theor Biol* **243**, 235–244.

Feugier, F. G., Mochizuki, A. and Iwasa, Y. (2005). Self-organization of the vascular system in plant leaves: Inter-dependent dynamics of auxin flux and carrier proteins. *Journal of Theoretical Biology* **236**, 366–375.

Fischer, U., Ikeda, Y., Ljung, K., Serralbo, O., Singh, M., Heidstra, R., Palme, K., Scheres, B. and Grebe, M. (2006). Vectorial Information for Arabidopsis Planar Polarity Is Mediated by Combined AUX1, EIN2, and GNOM Activity. *Current Biology* **16**, 2143–2149.

Fujita, H. and Mochizuki, A. (2006a). The origin of the diversity of leaf venation pattern. *Developmental Dynamics* **235**, 2710–2721.

Fujita, H. and Mochizuki, A. (2006b). Pattern formation of leaf veins by the positive feedback regulation between auxin flow and auxin efflux carrier. *Journal of Theoretical Biology* **241**, 541–551.

Fukaki, H., Nakao, Y., Okushima, Y., Theologis, A. and Tasaka, M. (2005). Tissue-specific expression of stabilized SOLITARY-ROOT/IAA14 alters lateral root development in Arabidopsis. *Plant J* **44**, 382–395.

Gallei, M., Luschnig, C. and Friml, J. (2020). Auxin signalling in growth: Schrödinger's cat out of the bag. *Curr Opin Plant Biol* **53**, 43–49.

Galweiler, L., Guan, C., Muller, A., Wisman, E., Mendgen, K., Yephremov, A. and Palme, K. (1998). Regulation of polar auxin transport by AtPIN1 in Arabidopsis vascular tissue. *Science (1979)* **282**, 2226–2230.

Gao, C., Liu, X. X., de Storme, N., Jensen, K. H., Xu, Q., Yang, J., Liu, X. X., Chen, S., Martens, H. J., Schulz, A., et al. (2020). Directionality of Plasmodesmata-Mediated Transport in Arabidopsis Leaves Supports Auxin Channeling. *Curr. Biol.* **30**, 1970-1977,e1-e4.

Gardiner, J., Donner, T. J. and Scarpella, E. (2011). Simultaneous activation of SHR and ATHB8 expression defines switch to preprocambial cell state in Arabidopsis leaf development. *Dev Dyn* **240**, 261–270.

Gardner, M. J., Baker, A. J., Assie, J. M., Poethig, R. S., Haseloff, J. P. and Webb, A. A. (2009). GAL4 GFP enhancer trap lines for analysis of stomatal guard cell development and gene expression. *J Exp Bot* **60**, 213–226.

Garrett, J. J., Meents, M. J., Blackshaw, M. T., Blackshaw, L. C., Hou, H., Styranko, D. M., Kohalmi, S. E. and Schultz, E. A. (2012). A novel, semi-dominant allele of MONOPTEROS provides insight into leaf initiation and vein pattern formation. *Planta* **236**, 297–312.

Geldner, N., Richter, S., Vieten, A., Marquardt, S., Torres-Ruiz, R. A., Mayer, U., Jurgens, G. and Jürgens, G. (2004). Partial loss-of-function alleles reveal a role for GNOM in auxin transport-related, post-embryonic development of Arabidopsis. *Development* **131**, 389–400.

George, S., Venkataraman, G. and Parida, A. (2010). A chloroplast-localized and auxin-induced glutathione S-transferase from phreatophyte Prosopis juliflora confer drought tolerance on tobacco. *J Plant Physiol* **167**, 311–318.

Gifford, E. M. and Foster, A. S. (1989). *Morphology and evolution of vascular plants*. 3rd ed. New York: W.H. Freeman and Co.

Gillmor, C. S., Park, M. Y., Smith, M. R., Pepitone, R., Kerstetter, R. A. and Poethig, R. S. (2010). The MED12-MED13 module of Mediator regulates the timing of embryo patterning in Arabidopsis. *Development* **137**, 113–122.

Giniger, E., Varnum, S. M. and Ptashne, M. (1985). Specific DNA binding of GAL4, a positive regulatory protein of yeast. *Cell* **40**, 767–774.

Godel-Jedrychowska, K., Kulinska-Lukaszek, K., Horstman, A., Soriano, M., Li, M., Malota, K., Boutilier, K. and Kurczynska, E. U. (2020). Symplasmic isolation marks cell fate changes during somatic embryogenesis. *J Exp Bot* **71**, 2612–2628.

Goodrich, L. v. and Strutt, D. (2011). Principles of planar polarity in animal development. *Development* **138**, 1877–1892.

Gooh, K., Ueda, M., Aruga, K., Park, J., Arata, H., Higashiyama, T. and Kurihara, D. (2015). Live-cell imaging and optical manipulation of Arabidopsis early embryogenesis. *Dev Cell* **34**, 242–251.

Gordon, S. P., Heisler, M. G., Reddy, G. V., Ohno, C., Das, P. and Meyerowitz, E. M. (2007). Pattern formation during de novo assembly of the Arabidopsis shoot meristem. *Development* **134**, 3539–3548.

Govindaraju, P., Verna, C., Zhu, T. and Scarpella, E. (2020). Vein Patterning by Tissue-Specific Auxin Transport. *Development* **147**, dev187666.

Groszmann, M., Gonzalez-Bayon, R., Greaves, I. K., Wang, L., Huen, A. K., Peacock, W. J. and Dennis, E. S. (2014). Intraspecific Arabidopsis hybrids show different patterns of heterosis despite the close relatedness of the parental genomes. *Plant Physiol* **166**, 265–280.

Guenot, B., Bayer, E., Kierzkowski, D., Smith, R. S., Mandel, T., Zadnikova, P., Benkova, E. and Kuhlemeier, C. (2012). PIN1-Independent Leaf Initiation in Arabidopsis. *Plant Physiol* **159**, 1501–1510.

Guitton, A. E., Page, D. R., Chambrier, P., Lionnet, C., Faure, J. E., Grossniklaus, U. and Berger, F. (2004). Identification of new members of Fertilisation Independent Seed Polycomb Group pathway involved in the control of seed development in Arabidopsis thaliana. *Development* **131**, 2971–2981.

Gunning, B. E. S. (1978). Age-related and origin-related control of the numbers of plasmodesmata in cell walls of developing Azolla roots. *Planta* **143**, 181–190.

Gunthorpe, D., Beatty, K. E. and Taylor, M. v (1999). Different levels, but not different isoforms, of the Drosophila transcription factor DMEF2 affect distinct aspects of muscle differentiation. *Dev Biol* **215**, 130–145.

Guseman, J. M., Lee, J. S., Bogenschutz, N. L., Peterson, K. M., Virata, R. E., Xie, B., Kanaoka, M. M., Hong, Z. and Torii, K. U. (2010). Dysregulation of cell-to-cell connectivity and stomatal patterning by loss-of-function mutation in Arabidopsis chorus (glucan synthase-like 8). *Development* **137**, 1731–1741.

Hadfi, K., Speth, V. and Neuhaus, G. (1998). Auxin-induced developmental patterns in Brassica juncea embryos. *Development* **125**, 879–887.

Hajný, J., Prát, T., Rydza, N., Rodriguez, L., Tan, S., Verstraeten, I., Domjan, D., Mazur, E., Smakowska-Luzan, E., Smet, W., et al. (2020). Receptor kinase module targets PIN-dependent auxin transport during canalization. *Science (1979)* **370**, 550–557.

Hamann, T., Mayer, U. and Jurgens, G. (1999). The auxin-insensitive bodenlos mutation affects primary root formation and apical-basal patterning in the Arabidopsis embryo. *Development* **126**, 1387–1395.

Hamann, T., Benkova, E., Baurle, I., Kientz, M. and Jurgens, G. (2002). The Arabidopsis BODENLOS gene encodes an auxin response protein inhibiting MONOPTEROS-mediated embryo patterning. *Genes & Development* **16**, 1610–1615.

Hamant, O., Heisler, M. G., Jonsson, H., Krupinski, P., Uyttewaal, M., Bokov, P., Corson, F., Sahlin, P., Boudaoud, A., Meyerowitz, E. M., et al. (2008). Developmental patterning by mechanical signals in Arabidopsis. *Science (1979)* **322**, 1650–1655.

Han, X., Hyun, T. K., Zhang, M., Kumar, R., Koh, E. J., Kang, B. H., Lucas, W. J. and Kim, J. Y. (2014). Auxin-callose-mediated plasmodesmal gating is essential for tropic auxin gradient formation and signaling. *Dev Cell* **28**, 132–146.

Hardtke, C. S. and Berleth, T. (1998). The Arabidopsis gene MONOPTEROS encodes a transcription factor mediating embryo axis formation and vascular development. *Embo J* **17**, 1405–1411.

Hardtke, C. S., Ckurshumova, W., Vidaurre, D. P., Singh, S. A., Stamatiou, G., Tiwari, S. B., Hagen, G., Guilfoyle, T. J. and Berleth, T. (2004). Overlapping and non-redundant functions of the Arabidopsis auxin response factors MONOPTEROS and NONPHOTOTROPIC HYPOCOTYL 4. *Development* **131**, 1089–1100.

Haseloff, J. (1999). Chapter 9: GFP Variants for Multispectral Imaging of Living Cells. In *Green Fluorescent Proteins* (ed. Sullivan, K. F.) and Kay, S. A. B. T.-M. in C. B.), pp. 139–151. Academic Press.

Haseloff, J., Siemering, K. R., Prasher, D. C. and Hodge, S. (1997). Removal of a cryptic intron and subcellular localization of green fluorescent protein are required to mark transgenic Arabidopsis plants brightly. *Proc Natl Acad Sci U S A* **94**, 2122–2127.

Hay, A., Jackson, D., Ori, N. and Hake, S. (2003). Analysis of the Competence to Respond to KNOTTED1 Activity in Arabidopsis Leaves Using a Steroid Induction System. *Plant Physiology* **131**, 1671–1680.

Hay, A., Barkoulas, M. and Tsiantis, M. (2006). ASYMMETRIC LEAVES1 and auxin activities converge to repress BREVIPEDICELLUS expression and promote leaf development in Arabidopsis. *Development* **133**, 3955–3961.

Heisler, M. G., Ohno, C., Das, P., Sieber, P., Reddy, G. v., Long, J. A. and Meyerowitz, E. M. (2005). Patterns of Auxin Transport and Gene Expression during Primordium Development Revealed by Live Imaging of the Arabidopsis Inflorescence Meristem. *Current Biology* **15**, 1899–1911.

Heisler, M. G., Hamant, O., Krupinski, P., Uyttewaal, M., Ohno, C., Jonsson, H., Traas, J., Meyerowitz, E. M., Jönsson, H., Heisler, M. G., et al. (2010). Alignment between PIN1 polarity and microtubule orientation in the shoot apical meristem reveals a tight coupling between morphogenesis and auxin transport. *PLoS Biol* **8**, e1000516.

Hellmann, H., Hobbie, L., Chapman, A., Dharmasiri, S., Dharmasiri, N., del Pozo, C., Reinhardt, D. and Estelle, M. (2003). Arabidopsis AXR6 encodes CUL1 implicating SCF E3 ligases in auxin regulation of embryogenesis. *Embo J* **22**, 3314–3325.

Herbst, D. (1971). Disjunct Foliar Veins in Hawaiian Euphorbias. *Science (1979)* **171**, 1247–1248.

Herbst, D. (1972). Ontogeny of Foliar Venation in Euphorbia forbesii. *American Journal of Botany* **59**, 843–850.

Herud-Sikimić, O., Stiel, A. C., Kolb, M., Shanmugaratnam, S., Berendzen, K. W., Feldhaus, C., Höcker, B. and Jürgens, G. (2021). A biosensor for the direct visualization of auxin. *Nature* **592**, 768–772.

Hobbie, L., McGovern, M., Hurwitz, L. R., Pierro, A., Liu, N. Y., Bandyopadhyay, A. and Estelle, M. (2000). The axr6 mutants of Arabidopsis thaliana define a gene involved in auxin response and early development. *Development* **127**, 23–32.

Hogan, B. M. and Schulte-Merker, S. (2017). How to Plumb a Pisces: Understanding Vascular Development and Disease Using Zebrafish Embryos. *Developmental Cell* **42**, 567–583.

Hou, H., Erickson, J., Meservy, J. and Schultz, E. A. (2010). FORKED1 encodes a PH domain protein that is required for PIN1 localization in developing leaf veins. *Plant J*.

Huang, L., Chen, X. Y., Rim, Y., Han, X., Cho, W. K., Kim, S. W. and Kim, J. Y. (2009). Arabidopsis glucan synthase-like 10 functions in male gametogenesis. *Journal of Plant Physiology* **166**, 344–352.

Huang, T., Harrar, Y., Lin, C., Reinhart, B., Newell, N. R., Talavera-Rauh, F., Hokin, S. A., Kathryn Barton, M. and Kerstetter, R. A. (2014). Arabidopsis KANADI1 acts as a transcriptional repressor by interacting with a specific cis-element and regulates auxin biosynthesis, transport, and signaling in opposition to HD-ZIPIII factors. *Plant Cell* **26**, 246–262.

Iglesias, V. A. and Meins Jr, F. (2000). Movement of plant viruses is delayed in a β-1, 3-glucanase-deficient mutant showing a reduced plasmodesmatal size exclusion limit and enhanced callose deposition. *The Plant Journal* **21**, 157–166.

Imlau, A., Truernit, E. and Sauer, N. (1999). Cell-to-cell and long-distance trafficking of the green fluorescent protein in the phloem and symplastic unloading of the protein into sink tissues. *Plant Cell* **11**, 309–322.

Irani, N. G., di Rubbo, S., Mylle, E., van den Begin, J., Schneider-Pizoń, J., Hniliková, J., Šíša, M., Buyst, D., Vilarrasa-Blasi, J. and Szatmári, A.-M. (2012). Fluorescent castasterone reveals BRI1 signaling from the plasma membrane. *Nat Chem Biol* **8**, 583.

Jacobs, W. P. (1952). The role of auxin in differentiation of xylem around a wound . *American Journal of Botany* **39**, 301–309.

Jásik, J., Bokor, B., Stuchlík, S., Mičieta, K., Turňa, J. and Schmelzer, E. (2016). Effects of Auxins on PIN-FORMED2 (PIN2) Dynamics Are Not Mediated by Inhibiting PIN2 Endocytosis. *Plant Physiology* **172**, 1019–1031.

Jayasinghege, C. P. A., Ozga, J. A., Nadeau, C. D., Kaur, H. and Reinecke, D. M. (2019). TIR1 auxin receptors are implicated in the differential response to 4-Cl-IAA and IAA in developing pea fruit. *J Exp Bot* **70**, 1239–1253.

Johnston, R., Leiboff, S. and Scanlon, M. J. (2015). Ontogeny of the sheathing leaf base in maize (Zea mays). *New Phytol* **205**, 306–315.

Jönsson, H., Heisler, M. G., Shapiro, B. E., Meyerowitz, E. M. and Mjolsness, E. (2006). An auxin-driven polarized transport model for phyllotaxis. *Proc Natl Acad Sci U S A* **103**, 1633–1638.

Jost, L. (1942). Über Gefässbrücken. *Zeitsch. Bot.* **38**, 161–215.

Kang, J. and Dengler, N. (2002). Cell cycling frequency and expression of the homeobox gene ATHB-8 during leaf vein development in Arabidopsis. *Planta* **216**, 212–219.

Kang, J. and Dengler, N. (2004). Vein pattern development in adult leaves of Arabidopsis thaliana. *International Journal of Plant Sciences* **165**, 231–242.

Katekar, G. F. and Geissler, A. E. (1980). Auxin Transport Inhibitors: IV. Evidence of a common mode of action for a proposed class of auxin transport inhibitors: the phytotropins. *Plant Physiol* **66**, 1190–1195.

Kawanabe, T., Ishikura, S., Miyaji, N., Sasaki, T., Wu, L. M., Itabashi, E., Takada, S., Shimizu, M., Takasaki-Yasuda, T. and Osabe, K. (2016). Role of DNA methylation in hybrid vigor in Arabidopsis thaliana. *Proceedings of the National Academy of Sciences* **113**, E6704–E6711.

Kierzkowski, D., Lenhard, M., Smith, R. and Kuhlemeier, C. (2013). Interaction between meristem tissue layers controls phyllotaxis. *Dev Cell* **26**, 616–628.

Kierzkowski, D., Runions, A., Vuolo, F., Strauss, S., Lymbouridou, R., Routier-Kierzkowska, A. L., Wilson-Sánchez, D., Jenke, H., Galinha, C., Mosca, G., et al. (2019). A Growth-Based Framework for Leaf Shape Development and Diversity. *Cell* **177**, 1405-1418.e17.

Kim, I., Hempel, F. D., Sha, K., Pfluger, J. and Zambryski, P. C. (2002). Identification of a developmental transition in plasmodesmatal function during embryogenesis in Arabidopsis thaliana. *Development* **129**, 1261–1272.

Kim, I., Kobayashi, K., Cho, E. and Zambryski, P. C. (2005a). Subdomains for transport via plasmodesmata corresponding to the apical-basal axis are established during Arabidopsis embryogenesis. *Proc Natl Acad Sci U S A* **102**, 11945–11950.

Kim, I., Cho, E., Crawford, K., Hempel, F. D. and Zambryski, P. C. (2005b). Cell-to-cell movement of GFP during embryogenesis and early seedling development in Arabidopsis. *Proc Natl Acad Sci U S A* **102**, 2227–2231.

Kinsman, E. A. and Pyke, K. A. (1998). Bundle sheath cells and cell-specific plastid development in Arabidopsis leaves. *Development* **125**, 1815–1822.

Kleinboelting, N., Huep, G., Kloetgen, A., Viehoever, P. and Weisshaar, B. (2012). GABI-Kat SimpleSearch: new features of the Arabidopsis thaliana T-DNA mutant database. *Nucleic Acids Res* **40**, D1211-5.

Kleine-Vehn, J., Dhonukshe, P., Sauer, M., Brewer, P. B., Wisniewska, J., Paciorek, T., Benkova, E. and Friml, J. (2008). ARF GEF-dependent transcytosis and polar delivery of PIN auxin carriers in Arabidopsis. *Curr Biol* **18**, 526–531.

Kleine-Vehn, J., Wabnik, K., Martinière, A., Łangowski, Ł., Willig, K., Naramoto, S., Leitner, J., Tanaka, H., Jakobs, S., Robert, S., et al. (2011). Recycling, clustering, and endocytosis jointly maintain PIN auxin carrier polarity at the plasma membrane. *Mol Syst Biol* **7**, 540.

Kobayashi, K., Otegui, M. S., Krishnakumar, S., Mindrinos, M. and Zambryski, P. (2007). INCREASED SIZE EXCLUSION LIMIT 2 encodes a putative DEVH box RNA helicase involved in plasmodesmata function during Arabidopsis embryogenesis. *Plant Cell* **19**, 1885–1897.

Koizumi, K., Sugiyama, M. and Fukuda, H. (2000). A series of novel mutants of Arabidopsis thaliana that are defective in the formation of continuous vascular network: calling the auxin signal flow canalization hypothesis into question. *Development* **127**, 3197–3204.

Koizumi, K., Naramoto, S., Sawa, S., Yahara, N., Ueda, T., Nakano, A., Sugiyama, M. and Fukuda, H. (2005). VAN3 ARF-GAP-mediated vesicle transport is involved in leaf vascular network formation. *Development* **132**, 1699–1711.

Kong, D., Karve, R., Willet, A., Chen, M. K., Oden, J. and Shpak, E. D. (2012). Regulation of plasmodesmatal permeability and stomatal patterning by the glycosyltransferase-like protein KOBITO1. *Plant Physiol* **159**, 156–168.

Koornneef, M. and Meinke, D. (2010). The development of Arabidopsis as a model plant. *The Plant Journal* **61**, 909–921.

Kramer, E. M. (2009). Auxin-regulated cell polarity: an inside job? *Trends in Plant Science* **14**, 242–247.

Kraus, E. J., Brown, N. A. and Hamner, K. C. (1936). Histological Reactions of Bean Plants to Indoleacetic Acid. *Botanical Gazette* **98**, 370–420.

Krishna, A., Gardiner, J., Donner, T. J. and Scarpella, E. (2021). Control of vein-forming, striped gene expression by auxin signaling. *BMC Biology* **19**, 213.

Krogan, N. T. and Berleth, T. (2012). A dominant mutation reveals asymmetry in MP/ARF5 function along the adaxial-abaxial axis of shoot lateral organs. *Plant Signal Behav* **7**, 940–943.

Krogan, N. T., Ckurshumova, W., Marcos, D., Caragea, A. E. and Berleth, T. (2012). Deletion of MP/ARF5 domains III and IV reveals a requirement for Aux/IAA regulation in Arabidopsis leaf vascular patterning. *New Phytologist* **194**, 391–401.

Kubo, M., Udagawa, M., Nishikubo, N., Horiguchi, G., Yamaguchi, M., Ito, J., Mimura, T., Fukuda, H. and Demura, T. (2005). Transcription switches for protoxylem and metaxylem vessel formation. *Genes Dev* **19**, 1855–1860.

Kuchen, E. E., Fox, S., de Reuille, P. B., Kennaway, R., Bensmihen, S., Avondo, J., Calder, G. M., Southam, P., Robinson, S., Bangham, A., et al. (2012). Generation

of leaf shape through early patterns of growth and tissue polarity. *Science (1979)* **335**, 1092–1096.

Kurihara, D., Mizuta, Y., Sato, Y. and Higashiyama, T. (2015). ClearSee: a rapid optical clearing reagent for whole-plant fluorescence imaging. *Development* **142**, 4168–4179.

Laguna, M. F., Bohn, S. and Jagla, E. A. (2008). The role of elastic stresses on leaf venation morphogenesis. *PLoS Comput Biol.*

Laplaze, L., Parizot, B., Baker, A., Ricaud, L., Martinière, A., Auguy, F., Franche, C., Nussaume, L., Bogusz, D. and Haseloff, J. (2005). GAL4-GFP enhancer trap lines for genetic manipulation of lateral root development in Arabidopsis thaliana. *J Exp Bot* **56**, 2433–2442.

Larkin, J. C., Young, N., Prigge, M. and Marks, M. D. (1996). The control of trichome spacing and number in Arabidopsis. *Development* **122**, 997–1005.

Latinkic, B. V., Umbhauer, M., Neal, K. A., Lerchner, W., Smith, J. C. and Cunliffe, V. (1998). Erratum: The Xenopus Brachyury promoter is activated by FGF and low concentrations of activin and suppressed by high concentrations of activin and by paired-type homeodomain proteins (Genes and Development (1997) 11 (3265-3276)). *Genes and Development* **12**, 1240.

Lau, S., de Smet, I., Kolb, M., Meinhardt, H. and Jurgens, G. (2011). Auxin triggers a genetic switch. *Nat Cell Biol* **13**, 611–615.

Lavania, D., Linh, N. M. and Scarpella, E. (2021). Of Cells, Strands, and Networks: Auxin and the Patterned Formation of the Vascular System. *Cold Spring Harb Perspect Biol* **13**, a039958.

Lavy, M. and Estelle, M. (2016). Mechanisms of auxin signaling. *Development* **143**, 3226–3229.

Le, J., Liu, X. G., Yang, K. Z., Chen, X. L., Zou, J. J., Wang, H. Z., Wang, M., Vanneste, S., Morita, M., Tasaka, M., et al. (2014). Auxin transport and activity regulate stomatal patterning and development. *Nat Commun* **5**, 3090.

Lee, M. H., Kim, B., Song, S. K., Heo, J. O., Yu, N. I., Lee, S. A., Kim, M., Kim, D. G., Sohn, S. O., Lim, C. E., et al. (2008). Large-scale analysis of the GRAS gene family in Arabidopsis thaliana. *Plant Mol Biol* **67**, 659–670.

Lee, B. H., Johnston, R., Yang, Y., Gallavotti, A., Kojima, M., Travençolo, B. A., Costa, L. F., Sakakibara, H. and Jackson, D. (2009). Studies of aberrant phyllotaxy1 mutants of maize indicate complex interactions between auxin and cytokinin signaling in the shoot apical meristem. *Plant Physiol* **150**, 205–216.

Lee, S. W., Feugier, F. G. and Morishita, Y. (2014). Canalization-based vein formation in a growing leaf. *J Theor Biol* **353**, 104–120.

Lersten, N. (1965). Histogenesis of Leaf Venation in Trifolium wormskioldii (Leguminosea). *American Journal of Botany* **52**, 767–774.

Levin, M. (2007). Gap junctional communication in morphogenesis. *Prog Biophys Mol Biol* **94**, 186–206.

Levin, M. (2021). Bioelectric signaling: Reprogrammable circuits underlying embryogenesis, regeneration, and cancer. *Cell* **184**, 1971–1989.

Levy, A., Erlanger, M., Rosenthal, M. and Epel, B. L. (2007). A plasmodesmata-associated beta-1,3-glucanase in Arabidopsis. *Plant J* **49**, 669–682.

Leyser, O. (2018). Auxin signaling. *Plant Physiology* **176**, 465–479.

Li, N., Yuan, D. and Huang, L. J. (2019). Development of a Gateway-compatible two-component expression vector system for plants. *Transgenic Research* **28**, 561–572.

Liao, C. Y., Smet, W., Brunoud, G., Yoshida, S., Vernoux, T. and Weijers, D. (2015). Reporters for sensitive and quantitative measurement of auxin response. *Nat Methods* **12**, 207–10, 2 p following 210.

Linh, N. M. and Scarpella, E. (2022a). Confocal Imaging of Developing Leaves. *Curr Protoc* **2**, e349.

Linh, N. M. and Scarpella, E. (2022b). Leaf vein patterning is regulated by the aperture of plasmodesmata intercellular channels. *PloS Biol* **20**, e3001781.

Linh, N. M., Verna, C. and Scarpella, E. (2018). Coordination of cell polarity and the patterning of leaf vein networks. *Current Opinion in Plant Biology* **41**, 116–124.

Lionetti, V., Raiola, A., Cervone, F. and Bellincampi, D. (2014). Transgenic expression of pectin methylesterase inhibitors limits tobamovirus spread in tobacco and Arabidopsis. *Mol Plant Pathol* **15**, 265–274.

Liu, Y., Xu, M., Liang, N., Zheng, Y., Yu, Q. and Wu, S. (2017). Symplastic communication spatially directs local auxin biosynthesis to maintain root stem cell niche in Arabidopsis. *Proc Natl Acad Sci U S A* **114**, 4005–4010.

Lu, P., Porat, R., Nadeau, J. A. and O'Neill, S. D. (1996). Identification of a Meristem L1 Layer-Specific Gene in Arabidopsis That Is Expressed during Embryonic Pattern Formation and Defines a New Class of Homeobox Genes. *Plant Cell* **8**, 2155–2168.

Luschnig, C. and Vert, G. (2014). The dynamics of plant plasma membrane proteins: PINs and beyond. *Development* **141**, 2924–2938.

Mähönen, A. P., Bishopp, A., Higuchi, M., Nieminen, K. M., Kinoshita, K., Törmäkangas, K., Ikeda, Y., Oka, A., Kakimoto, T., Helariutta, Y., et al. (2006). Cytokinin signaling and its inhibitor AHP6 regulate cell fate during vascular development. *Science (1979)* **311**, 94–98.

Mansfield, S. G. and Briarty, L. G. (1991). Early embryogenesis in Arabidopsis thaliana. II. The developing embryo. *Canadian Journal of Botany* **69**, 461–476.

Marcos, D. and Berleth, T. (2014). Dynamic auxin transport patterns preceding vein formation revealed by live-imaging of Arabidopsis leaf primordia. *Front Plant Sci* **5**, 235.

Marhava, P., Bassukas, A. E. L., Zourelidou, M., Kolb, M., Moret, B., Fastner, A., Schulze, W. X., Cattaneo, P., Hammes, U. Z., Schwechheimer, C., et al. (2018). A molecular rheostat adjusts auxin flux to promote root protophloem differentiation. *Nature* **558**, 297–300.

Martin, C. and Blatt, M. (2013). Manipulation and misconduct in the handling of image data. *Plant Cell* **25(9)**, 3147–3148.

Masucci, J. D. and Schiefelbein, J. W. (1994). The rhd6 Mutation of Arabidopsis thaliana Alters Root-Hair Initiation through an Auxin- and Ethylene-Associated Process. *Plant Physiol* **106**, 1335–1346.

Mathews, J. and Levin, M. (2017). Gap junctional signaling in pattern regulation: Physiological network connectivity instructs growth and form. *Dev Neurobiol* **77**, 643–673.

Matthes, M. and Torres-Ruiz, R. A. (2016). Boronic acid treatment phenocopies monopteros by affecting PIN1 membrane stability and polar auxin transport in Arabidopsis thaliana embryos. *Development (Cambridge)* **143**, 4053–4062.

Mattsson, J., Sung, Z. R. and Berleth, T. (1999). Responses of plant vascular systems to auxin transport inhibition. *Development* **126**, 2979–2991.

Mattsson, J., Ckurshumova, W. and Berleth, T. (2003). Auxin signaling in Arabidopsis leaf vascular development. *Plant Physiol* **131**, 1327–1339.

Mayer, U., Buttner, G. and Jurgens, G. (1993). Apical-basal pattern formation in the Arabidopsis embryo: studies on the role of the gnom gene. *Development* **117**, 149–162.

Mazur, E., Benková, E. and Friml, J. (2016). Vascular cambium regeneration and vessel formation in wounded inflorescence stems of Arabidopsis. *Sci Rep* **6**, 33754.

Mazur, E., Kulik, I., Hajný, J. and Friml, J. (2020). Auxin Canalization and Vascular Tissue Formation by TIR1/AFB-Mediated Auxin Signaling in Arabidopsis. *New Phytol.* **226(5)**, 1375–1383.

McGuire, S., Roman, G. and Davies, R. L. (2004). Gene expression systems in Drosophila: a synthesis of time and space. *Trends in Genetics* **20**, 384–391.

Mellor, N. L., Voß, U., Janes, G., Bennett, M. J., Wells, D. M. and Band, L. R. (2020). Auxin fluxes through plasmodesmata modify root-tip auxin distribution. *Development* **147**, dev181669.

Mitchison, G. J. (1980a). The Dynamics of Auxin Transport. *Proceedings of the Royal Society of London. Series B, Biological Sciences* **209**, 489–511.

Mitchison, G. J. (1980b). Model for Vein Formation in Higher-Plants. *Proceedings of the Royal Society of London Series B-Biological Sciences* **207**, 79–109.

Mitchison, G. J. (1981). The Polar Transport of Auxin and Vein Patterns in Plants. *Philosophical Transactions of the Royal Society of London Series B-Biological Sciences* **295**, 461–471.

Morgan, D. G. and Söding, H. (1958). Über die Wirkungsweise von Phthalsäuremono-α-Naphthylamid (PNA) auf das Wachstum der Haferkoleoptile. *Planta* **52**, 235–249.

Moriwaki, T., Miyazawa, Y., Fujii, N. and Takahashi, H. (2014). GNOM regulates root hydrotropism and phototropism independently of PIN-mediated auxin transport. *Plant Sci* **215–216**, 141–149.

Morvan, O., Quentin, M., Jauneau, A., Mareck, A. and Morvan, C. (1998). Immunogold localization of pectin methylesterases in the cortical tissues of flax hypocotyl. *Protoplasma* **202**, 175–184.

Nagai, T., Ibata, K., Park, E. S., Kubota, M., Mikoshiba, K. and Miyawaki, A. (2002). A variant of yellow fluorescent protein with fast and efficient maturation for cell-biological applications. *Nat Biotechnol* **20**, 87–90.

Nagel, A. C., Maier, D. and Preiss, A. (2002). Green fluorescent protein as a convenient and versatile marker for studies on functional genomics in Drosophila. *Development Genes and Evolution* **212**, 93–98.

Nakamura, M., Kiefer, C. S. and Grebe, M. (2012). Planar polarity, tissue polarity and planar morphogenesis in plants. *Current Opinion in Plant Biology* **15**, 593–600.

Nakata, M. T., Tameshige, T., Takahara, M., Mitsuda, N. and Okada, K. (2018). The functional balance between the *WUSCHEL-RELATED HOMEOBOX1* gene and the phytohormone auxin is a key factor for cell proliferation in Arabidopsis seedlings. *Plant Biotechnology* **35**, 141–154.

Nakayama, N., Smith, R. S., Mandel, T., Robinson, S., Kimura, S., Boudaoud, A. and Kuhlemeier, C. (2012). Mechanical regulation of auxin-mediated growth. *Curr Biol* **22**, 1468–1476.

Naramoto, S., Sawa, S., Koizumi, K., Uemura, T., Ueda, T., Friml, J., Nakano, A. and Fukuda, H. (2009). Phosphoinositide-dependent regulation of VAN3 ARF-GAP localization and activity essential for vascular tissue continuity in plants. *Development* **136**, 1529–1538.

Naramoto, S., Kleine-Vehn, J., Robert, S., Fujimoto, M., Dainobu, T., Paciorek, T., Ueda, T., Nakano, A., van Montagu, M. C. E. E., Fukuda, H., et al. (2010). ADP-ribosylation factor machinery mediates endocytosis in plant cells. *Proc Natl Acad Sci U S A* **107**, 21890–21895.

Naramoto, S., Otegui, M. S., Kutsuna, N., de Rycke, R., Dainobu, T., Karampelias, M., Fujimoto, M., Feraru, E., Miki, D., Fukuda, H., et al. (2014). Insights into the localization and function of the membrane trafficking regulator GNOM ARF-GEF at the Golgi apparatus in Arabidopsis. *Plant Cell* **26**, 3062–3076.

Narasimhan, M., Gallei, M., Tan, S., Johnson, A., Verstraeten, I., Li, L., Rodriguez, L., Han, H., Himschoot, E., Wang, R., et al. (2021). Systematic analysis of specific and nonspecific auxin effects on endocytosis and trafficking. *Plant Physiol.*

Nelson, T. and Dengler, N. (1997). Leaf vascular pattern formation. *Plant Cell* **9**, 1121–1135.

Nielsen, M. E., Feechan, A., Böhlenius, H., Ueda, T. and Thordal-Christensen, H. (2012). Arabidopsis ARF-GTP exchange factor, GNOM, mediates transport required for innate immunity and focal accumulation of syntaxin PEN1. *Proc Natl Acad Sci U S A* **109**, 11443–11448.

North, A. J. (2006). Seeing is believing? A beginners' guide to practical pitfalls in image acquisition. *J Cell Biol* **172**, 9–18.

O'Connor, D. L., Runions, A., Sluis, A., Bragg, J., Vogel, J. P., Prusinkiewicz, P. and Hake, S. (2014). A division in PIN-mediated auxin patterning during organ initiation in grasses. *PLoS Comput Biol* **10**, e1003447.

O'Connor, D. L., Elton, S., Ticchiarelli, F., Hsia, M. M., Vogel, J. P. and Leyser, O. (2017). Cross-species functional diversity within the PIN auxin efflux protein family. *Elife* **6**,.

Odat, O., Gardiner, J., Sawchuk, M. G., Verna, C., Donner, T. J. and Scarpella, E. (2014). Characterization of an allelic series in the MONOPTEROS gene of Arabidopsis. *Genesis* **52**, 127–133.

Odell, J. T., Nagy, F. and Chua, N. H. (1985). Identification of DNA sequences required for activity of the cauliflower mosaic virus 35S promoter. *Nature* **313**, 810–812.

Okada, K., Ueda, J., Komaki, M. K., Bell, C. J. and Shimura, Y. (1991). Requirement of the Auxin Polar Transport System in Early Stages of Arabidopsis Floral Bud Formation. *Plant Cell* **3**, 677–684.

Oparka, K. J. and Prior, D. A. M. (1992). Direct evidence for pressure-generated closure of plasmodesmata. *The Plant Journal* **2**, 741–750.

Oparka, K. J., Roberts, A. G., Boevink, P., Santa Cruz, S., Roberts, I., Pradel, K. S., Imlau, A., Kotlizky, G., Sauer, N. and Epel, B. (1999). Simple, but not branched, plasmodesmata allow the nonspecific trafficking of proteins in developing tobacco leaves. *Cell* **97**, 743–754.

Palevitz, B. A. and Hepler, P. K. (1985). Changes in dye coupling of stomatal cells of Allium and Commelina demonstrated by microinjection of Lucifer yellow. *Planta* **164**, 473–479.

Paponov, I. A., Friz, T., Budnyk, V., Teale, W. D., Wüst, F., Paponov, M., Al-Babili, S. and Palme, K. (2019). Natural auxin does not inhibit Brefeldin A induced PIN1 and PIN2 internalization in root cells. *Frontiers in Plant Science* **10**, 574.

Parizot, B., de Rybel, B. and Beeckman, T. (2010). VisuaLRTC: a new view on lateral root initiation by combining specific transcriptome data sets. *Plant Physiol* **153**, 34–40.

Park, K., Knoblauch, J., Oparka, K. and Jensen, K. H. (2019). Controlling intercellular flow through mechanosensitive plasmodesmata nanopores. *Nat Commun* **10**, 3564.

Paterlini, A. (2020). Uncharted routes: exploring the relevance of auxin movement via plasmodesmata. *Biol Open* **9**, 1–11.

Patton, D. A., Franzmann, L. H. and Meinke, D. W. (1991). Mapping Genes Essential for Embryo Development in Arabidopsis-Thaliana. *Molecular & General Genetics* **227**, 337–347.

Pautot, V., Dockx, J., Hamant, O., Kronenberger, J., Grandjean, O., Jublot, D. and Traas, J. (2001). KNAT2: evidence for a link between knotted-like genes and carpel development. *Plant Cell* **13**, 1719–1734.

Pawley, J. B. (1995). Handbook of Biological Confocal Microscopy. xiii, 232.

Peaucelle, A., Braybrook, S. A., le Guillou, L., Bron, E., Kuhlemeier, C. and Höfte, H. (2011). Pectin-induced changes in cell wall mechanics underlie organ initiation in Arabidopsis. *Curr Biol* **21**, 1720–1726.

Peterson, R. T., Link, B. A., Dowling, J. E. and Schreiber, S. L. (2000). Small molecule developmental screens reveal the logic and timing of vertebrate development. *Proc Natl Acad Sci U S A* **97**, 12965–12969.

Petrasek, J., Mravec, J., Bouchard, R., Blakeslee, J. J., Abas, M., Seifertova, D., Wisniewska, J., Tadele, Z., Kubes, M., Covanova, M., et al. (2006). PIN proteins perform a rate-limiting function in cellular auxin efflux. *Science (1979)* **312**, 914–918.

Petrásek, J., Friml, J., Petrasek, J., Friml, J., Petrášek, J. and Friml, J. (2009). Auxin transport routes in plant development. *Development* **136**, 2675–2688.

Picard, D., Salser, S. J. and Yamamoto, K. R. (1988). A movable and regulable inactivation function within the steroid binding domain of the glucocorticoid receptor. *Cell* **54**, 1073–1080.

Posakony, L. G., Raftery, L. A. and Gelbart, W. M. (1991). Wing formation in Drosophilamelanogasterequires decapentaplegicgenefunction along the anterior-posterior compartment boundary. *Mech Dev* **33**, 69–82.

Powers, S. K. and Strader, L. C. (2019). Regulation of auxin transcriptional responses. *Dev Dyn.* **249(4)**, 483-495.

Prabhakaran Mariyamma, N., Clarke, K. J., Yu, H., Wilton, E. E., van Dyk, J., Hou, H. and Schultz, E. A. (2018). Members of the Arabidopsis FORKED1-LIKE gene family act to localize PIN1 in developing veins. *Journal of Experimental Botany* **69**, 4773–4790.

Pray, T. R. (1955). Foliar venation of Angiosperms. IV. Histogenesis of the venation of Hosta. *American Journal of Botany* **42**, 698–706.

Prigge, M. J., Platre, M., Kadakia, N., Zhang, Y., Greenham, K., Szutu, W., Pandey, B. K., Bhosale, R. A., Bennett, M. J., Busch, W., et al. (2020). Genetic analysis of the arabidopsis TIR1/AFB auxin receptors reveals both overlapping and specialized functions. *Elife* **9**, 1–28.

Prusinkiewicz, P. and Runions, A. (2012). Computational models of plant development and form. *New Phytol* **193**, 549–569.

Przemeck, G. K., Mattsson, J., Hardtke, C. S., Sung, Z. R. and Berleth, T. (1996). Studies on the role of the Arabidopsis gene MONOPTEROS in vascular development and plant cell axialization. *Planta* **200**, 229–237.

Pyke, K. A., Marrison, J. L. and Leech, R. M. (1991). Temporal and Spatial Development of the Cells of the Expanding 1st Leaf of Arabidopsis-Thaliana (L) Heynh. *Journal of Experimental Botany* **42**, 1407–1416.

Radoeva, T., ten Hove, C. A., Saiga, S. and Weijers, D. (2016). Molecular Characterization of Arabidopsis GAL4/*UAS* Enhancer Trap Lines Identifies Novel Cell-Type-Specific Promoters. *Plant Physiol* **171**, 1169–1181.

Ramos Báez, R. and Nemhauser, J. L. (2021). Expansion and innovation in auxin signaling: where do we grow from here? *Development* **148**, dev187120.

Raven, J. A. (1975). Transport of indoleacetic acid in plant cells in relation to pH and electrical potential gradients, and its significance for polar IAA transport. *New Phytologist* **74**, 163–172.

Ravichandran, S. J., Linh, N. M. and Scarpella, E. (2020). The canalization hypothesis - challenges and alternatives. *New Phytologist* **227**, 1051–1059.

Reddy, S., Jin, P., Trimarchi, J., Caruccio, P., Phillis, R. and Murphey, R. K. (1997). Mutant molecular motors disrupt neural circuits in Drosophila. *J Neurobiol* **33**, 711–723.

Reddy, G. V., Heisler, M. G., Ehrhardt, D. W. and Meyerowitz, E. M. (2004). Real-time lineage analysis reveals oriented cell divisions associated with morphogenesis at the shoot apex of Arabidopsis thaliana. *Development* **131**, 4225–4237.

Reinhardt, D., Mandel, T. and Kuhlemeier, C. (2000). Auxin regulates the initiation and radial position of plant lateral organs. *Plant Cell* **12**, 507–518.

Reinhardt, D., Pesce, E. R., Stieger, P., Mandel, T., Baltensperger, K., Bennett, M., Traas, J., Friml, J. and Kuhlemeier, C. (2003). Regulation of phyllotaxis by polar auxin transport. *Nature* **426**, 255–260.

Richter, S., Anders, N., Wolters, H., Beckmann, H., Thomann, A., Heinrich, R., Schrader, J., Singh, M. K., Geldner, N., Mayer, U., et al. (2010). Role of the GNOM gene in Arabidopsis apical-basal patterning--From mutant phenotype to cellular mechanism of protein action. *Eur J Cell Biol* **89**, 138–144.

Rinne, P. L., Welling, A., Vahala, J., Ripel, L., Ruonala, R., Kangasjärvi, J. and van der Schoot, C. (2011). Chilling of dormant buds hyperinduces FLOWERING LOCUS T and recruits GA-inducible 1,3-beta-glucanases to reopen signal conduits and release dormancy in Populus. *Plant Cell* **23**, 130–146.

Rivero, L., Scholl, R., Holomuzki, N., Crist, D., Grotewold, E. and Brkljacic, J. (2014). Handling Arabidopsis Plants: Growth, Preservation of Seeds, Transformation, and Genetic Crosses. In *Arabidopsis protocols* (ed. Sanchez-Serrano, J. J.) and Salinas, J.), pp. 3–26. New York, NY: Humana Press.

Roberts, L. W. (1960). Experiments on Xylem Regeneration in Stem Wound Responses in Coleus. *Botanical Gazette* **121**, 201–208.

Roberts, A. G., Cruz, S. S., Roberts, I. M., Prior, D., Turgeon, R. and Oparka, K. J. (1997). Phloem Unloading in Sink Leaves of Nicotiana benthamiana: Comparison of a Fluorescent Solute with a Fluorescent Virus. *Plant Cell* **9**, 1381–1396.

Roberts, I. M., Boevink, P., Roberts, A. G., Sauer, N., Reichel, C. and Oparka, K. J. (2001). Dynamic changes in the frequency and architecture of plasmodesmata during the sink-source transition in tobacco leaves. *Protoplasma* **218**, 31–44.

Robinson, S., Barbier de Reuille, P., Chan, J., Bergmann, D., Prusinkiewicz, P. and Coen, E. (2011). Generation of spatial patterns through cell polarity switching. *Science (1979)* **333**, 1436–1440.

Rodriguez-Villalon, A., Gujas, B., Kang, Y. H., Breda, A. S., Cattaneo, P., Depuydt, S. and Hardtke, C. S. (2014). Molecular genetic framework for protophloem formation. *Proc Natl Acad Sci U S A* **111**, 11551–11556.

Rodriguez-Villalon, A., Gujas, B., van Wijk, R., Munnik, T. and Hardtke, C. S. (2015). Primary root protophloem differentiation requires balanced phosphatidylinositol-4,5-biphosphate levels and systemically affects root branching. *Development* **142**, 1437–1446.

Rolland-Lagan, A. G. and Prusinkiewicz, P. (2005). Reviewing models of auxin canalization in the context of leaf vein pattern formation in Arabidopsis. *Plant J* **44**, 854–865.

Rossner, M. and Yamada, K. M. (2004). What's in a picture? The temptation of image manipulation. *J Cell Biol* **166**, 11–15.

Roth-Nebelsick, A., Uhl, D., Mosbrugger, V. and Kerp, H. (2001). Evolution and function of leaf venation architecture: A review. *Annals of Botany* **87**, 553–566.

Ruan, Y. L., Llewellyn, D. J. and Furbank, R. T. (2001). The control of single-celled cotton fiber elongation by developmentally reversible gating of plasmodesmata and coordinated expression of sucrose and K+ transporters and expansin. *Plant Cell* **13**, 47–60.

Rubery, P. H. and Sheldrake, A. R. (1974). Carrier-Mediated Auxin Transport. *Planta* **118**, 101–121.

Rueden, C. T., Schindelin, J., Hiner, M. C., DeZonia, B. E., Walter, A. E., Arena, E. T. and Eliceiri, K. W. (2017). ImageJ2: ImageJ for the next generation of scientific image data. *BMC Bioinformatics* **18**, 529.

Ruiz Sola, M. A., Coiro, M., Crivelli, S., Zeeman, S. C., Schmidt Kjølner Hansen, S. and Truernit, E. (2017). OCTOPUS-LIKE 2, a novel player in Arabidopsis root and vascular development, reveals a key role for OCTOPUS family genes in root metaphloem sieve tube differentiation. *New Phytol* **216**, 1191–1204.

Runions, A., Fuhrer, M., Lane, B., Federl, P., Rolland-Lagan, A.-G. and Prusinkiewicz, P. (2005). Modeling and visualization of leaf venation patterns. *ACM Transactions on Graphics* **24**, 702–711.

Runions, A., Smith, R. S. and Prusinkiewicz, P. (2014). Computational Models of Auxin-Driven Development. In *Auxin and Its Role in Plant Development* (ed. Zažímalová, E.), Petrasek, J.), and Benková, E.), pp. 315–357. Vienna: Springer Vienna.

Russ, J. C. and Neal, F. B. (2016). *The image processing handbook*. Seventh ed. Boca Raton: CRC Press, Taylor & Francis Group.

Rutschow, H. L., Baskin, T. I. and Kramer, E. M. (2011). Regulation of solute flux through plasmodesmata in the root meristem. *Plant Physiol* **155**, 1817–1826.

Saatian, B., Austin, R. S., Tian, G., Chen, C., Nguyen, V., Kohalmi, S. E., Geelen, D. and Cui, Y. (2018). Analysis of a novel mutant allele of GSL8 reveals its key roles in cytokinesis and symplastic trafficking in Arabidopsis. *BMC Plant Biol* **18**, 295.

Sabatini, S., Beis, D., Wolkenfelt, H., Murfett, J., Guilfoyle, T., Malamy, J., Benfey, P., Leyser, O., Bechtold, N., Weisbeek, P., et al. (1999). An auxin-dependent distal organizer of pattern and polarity in the Arabidopsis root. *Cell* **99**, 463–472.

Sabatini, S., Heidstra, R., Wildwater, M. and Scheres, B. (2003). SCARECROW is involved in positioning the stem cell niche in the Arabidopsis root meristem. *Genes Dev* **17**, 354–358.

Sachs, T. (1968a). On determination of pattern of vascular tissues in peas. *Annals of Botany* **32**, 781–790.

Sachs, T. (1968b). The Role of the Root in the Induction of Xylem Differentiation in Peas. *Annals of Botany* **32**, 391–399.

Sachs, T. (1969). Polarity and the Induction of Organized Vascular Tissues. *Annals of Botany* **33**, 263–275.

Sachs, T. (1975). Control of Differentiation of Vascular Networks. *Annals of Botany* **39**, 197–204.

Sachs, T. (1981). The Control of the Patterned Differentiation of Vascular Tissues. *Advances in Botanical Research* **9**, 151–262.

Sachs, T. (1984). Axiality and polarity in vascular plants. In *Positional Controls in Plant Development* (ed. Barlow, P. W.), pp. 193–224. Cambridge: Cambridge University Press.

Sachs, T. (1989). The development of vascular networks during leaf development. *Current Topics in Plant Biochemistry and Physiology* **8**, 168–183.

Sachs, T. (1991). Cell polarity and tissue patterning in plants. *Development* **113**, 83–93.

Sachs, T. (2000). Integrating Cellular and Organismic Aspects of Vascular Differentiation. *Plant and Cell Physiology* **41**, 649–656.

Sachs, T. (2003). Collective specification of cellular development. *Bioessays* **25**, 897–903.

Sager, R. and Lee, J. Y. (2014). Plasmodesmata in integrated cell signalling: insights from development and environmental signals and stresses. *J Exp Bot* **65**, 6337–6358.

Sager, R., Wang, X., Hill, K., Yoo, B. C., Caplan, J., Nedo, A., Tran, T., Bennett, M. J. and Lee, J. Y. (2020). Auxin-dependent control of a plasmodesmal regulator creates a negative feedback loop modulating lateral root emergence. *Nat Commun* **11**, 364.

Sato, M. and Saigo, K. (2000). Involvement of pannier and u-shaped in regulation of Decapentaplegic-dependent wingless expression in developing Drosophila notum. *Mechanisms of Development* **93**, 127–138.

Sauer, M., Balla, J., Luschnig, C., Wisniewska, J., Reinohl, V., Friml, J. and Benkova, E. (2006). Canalization of auxin flow by Aux/IAA-ARF-dependent feedback regulation of PIN polarity. *Genes Dev* **20**, 2902–2911.

Savaldi-Goldstein, S., Baiga, T. J., Pojer, F., Dabi, T., Butterfield, C., Parry, G., Santner, A., Dharmasiri, N., Tao, Y., Estelle, M., et al. (2008). New auxin analogs with growth-promoting effects in intact plants reveal a chemical strategy to improve hormone delivery. *Proc Natl Acad Sci U S A* **105**, 15190–15195.

Sawa, S., Koizumi, K., Naramoto, S., Demura, T., Ueda, T., Nakano, A. and Fukuda, H. (2005). DRP1A is responsible for vascular continuity synergistically working with VAN3 in Arabidopsis. *Plant Physiol* **138**, 819–826.

Sawchuk, M. G., Head, P., Donner, T. J. and Scarpella, E. (2007). Time-lapse imaging of Arabidopsis leaf development shows dynamic patterns of procambium formation. *New Phytologist* **176**, 560–571.

Sawchuk, M. G., Donner, T. J., Head, P. and Scarpella, E. (2008). Unique and overlapping expression patterns among members of photosynthesis-associated nuclear gene families in Arabidopsis. *Plant Physiology* **148**, 1908–1924.

Sawchuk, M. G., Edgar, A. and Scarpella, E. (2013). Patterning of leaf vein networks by convergent auxin transport pathways. *PLoS Genet* **9**, e1003294.

Scacchi, E., Osmont, K. S., Beuchat, J., Salinas, P., Navarrete-Gómez, M., Trigueros, M., Ferrándiz, C. and Hardtke, C. S. (2009). Dynamic, auxin-responsive plasma membrane-to-nucleus movement of Arabidopsis BRX. *Development* **136**, 2059–2067.

Scacchi, E., Salinas, P., Gujas, B., Santuari, L., Krogan, N., Ragni, L., Berleth, T. and Hardtke, C. S. (2010). Spatio-temporal sequence of cross-regulatory events in root meristem growth. *Proc Natl Acad Sci U S A* **107**, 22734–22739.

Scarpella, E. (2017). The logic of plant vascular patterning. Polarity, continuity and plasticity in the formation of the veins and of their networks. *Curr Opin Genet Dev* **45**, 34–43.

Scarpella, E., Francis, P. and Berleth, T. (2004). Stage-specific markers define early steps of procambium development in Arabidopsis leaves and correlate termination of vein formation with mesophyll differentiation. *Development* **131**, 3445–3455.

Scarpella, E., Marcos, D., Friml, J. and Berleth, T. (2006). Control of leaf vascular patterning by polar auxin transport. *Genes and Development* **20**, 1015–1027.

Schena, M., Lloyd, A. M. and Davis, R. W. (1991). A steroid-inducible gene expression system for plant cells. *Proc Natl Acad Sci U S A* **88**, 10421–10425.

Scheres, B., Wolkenfelt, H., Willemsen, V., Terlouw, M., Lawson, E., Dean, C. and Weisbeek, P. (1994). Embryonic Origin of the Arabidopsis Primary Root and Root-Meristem Initials. *Development* **120**, 2475–2487.

Schindelin, J., Arganda-Carreras, I., Frise, E., Kaynig, V., Longair, M., Pietzsch, T., Preibisch, S., Rueden, C., Saalfeld, S., Schmid, B., et al. (2012). Fiji: an open-source platform for biological-image analysis. *Nat Methods* **9**, 676–682.

Schindelin, J., Rueden, C. T., Hiner, M. C. and Eliceiri, K. W. (2015). The ImageJ ecosystem: An open platform for biomedical image analysis. *Molecular Reproduction and Development* **82**, 518–529.

Schlereth, A., Moller, B., Liu, W., Kientz, M., Flipse, J., Rademacher, E. H., Schmid, M., Jurgens, G. and Weijers, D. (2010). MONOPTEROS controls embryonic root initiation by regulating a mobile transcription factor. *Nature* **464**, 913–916.

Schneider, C. A., Rasband, W. S. and Eliceiri, K. W. (2012). NIH Image to ImageJ: 25 years of image analysis. *Nat Methods* **9**, 671–675.

Seagull, R. W. (1983). Differences in the frequency and disposition of plasmodesmata resulting from root cell elongation. *Planta* **159**, 497–504.

Sessions, A., Weigel, D. and Yanofsky, M. F. (1999). The Arabidopsis thaliana MERISTEM LAYER 1 promoter specifies epidermal expression in meristems and young primordia. *Plant Journal* **20**, 259–263.

Sessions, A., Burke, E., Presting, G., Aux, G., McElver, J., Patton, D., Dietrich, B., Ho, P., Bacwaden, J., Ko, C., et al. (2002). A high-throughput Arabidopsis reverse genetics system. *Plant Cell* **14**, 2985–2994.

Sevilem, I., Miyashima, S. and Helariutta, Y. (2013). Cell-to-cell communication via plasmodesmata in vascular plants. *Cell Adh Migr* **7**, 27–32.

Shaw, S. L. (2006). Imaging the live plant cell. *Plant J* **45**, 573–598.

Shevell, D. E., Leu, W.-M. M., Gillmor, C. S. S., Xia, G., Feldmann, K. A. and Chua, N.-H. H. (1994). EMB30 is essential for normal cell division, cell expansion, and cell adhesion in Arabidopsis and encodes a protein that has similarity to Sec7. *Cell* **77**, 1051–1062.

Shevell, D. E., Kunkel, T. and Chua, N. H. (2000). Cell wall alterations in the arabidopsis emb30 mutant. *Plant Cell* **12**, 2047–2060.

Sieburth, L. E. (1999). Auxin is required for leaf vein pattern in Arabidopsis. *Plant Physiology* **121**, 1179–1190.

Sieburth, L. E., Muday, G. K., King, E. J., Benton, G., Kim, S., Metcalf, K. E., Meyers, L., Seamen, E. and van Norman, J. M. (2006). SCARFACE encodes an ARF-GAP that is required for normal auxin efflux and vein patterning in Arabidopsis. *Plant Cell* **18**, 1396–1411.

Siemering, K. R., Golbik, R., Sever, R. and Haseloff, J. (1996). Mutations that suppress the thermosensitivity of green fluorescent protein. *Curr Biol* **6**, 1653–1663.

Simon, S. and Petrášek, J. (2011). Why plants need more than one type of auxin. *Plant Sci* **180**, 454–460.

Simon, R., Igeño, M. I. and Coupland, G. (1996). Activation of floral meristem identity genes in Arabidopsis. *Nature* **384**, 59–62.

Sinnott, E. W. and Bloch, R. (1944). Visible expression of cytoplasmic pattern in the differentiation of xylem strands. *Proc Natl Acad Sci U S A* **30**, 388.

Sluder, G. and Wolf, D. E. (2007). Digital Microscopy, 3rd Edition. *Methods in Cell Biology* **81**, 608.

Smetana, O., Mäkilä, R., Lyu, M., Amiryousefi, A., Sánchez Rodríguez, F., Wu, M. F., Solé-Gil, A., Leal Gavarrón, M., Siligato, R., Miyashima, S., et al. (2019). High levels of auxin signalling define the stem-cell organizer of the vascular cambium. *Nature* **565**, 485–489.

Smit, M. E., Llavata-Peris, C. I., Roosjen, M., van Beijnum, H., Novikova, D., Levitsky, V., Sevilem, I., Roszak, P., Slane, D., Jürgens, G., et al. (2020). Specification and regulation of vascular tissue identity in the Arabidopsis embryo. *Development* **147**, dev186130.

Smith, R. S. and Bayer, E. M. (2009). Auxin transport-feedback models of patterning in plants. *Plant, Cell and Environment* **32**, 1258–1271.

Smith, R. S., Guyomarc'h, S., Mandel, T., Reinhardt, D., Kuhlemeier, C. and Prusinkiewicz, P. (2006). A plausible model of phyllotaxis. *Proc Natl Acad Sci U S A* **103**, 1301–1306.

Solereder, H. (1908). *Systematic Anatomy of the Dicotyledons*. Oxford: Clarendon Press.

Stadler, R., Lauterbach, C. and Sauer, N. (2005). Cell-to-cell movement of green fluorescent protein reveals post-phloem transport in the outer integument and identifies symplastic domains in Arabidopsis seeds and embryos. *Plant Physiol* **139**, 701–712.

Stahl, Y., Grabowski, S., Bleckmann, A., Kühnemuth, R., Weidtkamp-Peters, S., Pinto, K. G., Kirschner, G. K., Schmid, J. B., Wink, R. H., Hülsewede, A., et al. (2013). Moderation of Arabidopsis root stemness by CLAVATA1 and ARABIDOPSIS CRINKLY4 receptor kinase complexes. *Curr Biol* **23**, 362–371.

Stamatiou, G. (2007). The roles of auxin response factors in patterning processes during Arabidopsis development. Department of Cell and Systems Biology, Ph.D., i-xiv,1.

Steinmann, T., Geldner, N., Grebe, M., Mangold, S., Jackson, C. L. C. L., Paris, S., Gälweiler, L., Palme, K., Jürgens, G., Galweiler, L., et al. (1999). Coordinated polar localization of auxin efflux carrier PIN1 by GNOM ARF GEF. *Science (1979)* **286**, 316–318.

Stepanova, A. N., Robertson-Hoyt, J., Yun, J., Benavente, L. M., Xie, D.-Y., Dolezal, K., Schlereth, A., Jurgens, G. and Alonso, J. M. (2008). TAA1-Mediated Auxin

Biosynthesis Is Essential for Hormone Crosstalk and Plant Development. *Cell* **133**, 177–191.

Stewart, R. N. (1978). Ontogeny of the primary body in chimeral forms of higher plants. In *The Clonal Basis of Development*. (ed. Subtelny, S.) and Sussex, I. M.), pp. 131–160. New York: Academic Press.

Steynen, Q. J. and Schultz, E. A. (2003). The FORKED genes are essential for distal vein meeting in Arabidopsis. *Development* **130**, 4695–4708.

Stoma, S., Lucas, M., Chopard, J., Schaedel, M., Traas, J. and Godin, C. (2008). Flux-based transport enhancement as a plausible unifying mechanism for auxin transport in meristem development. *PLoS Comput Biol* **4**, e1000207.

Stonebloom, S., Burch-Smith, T., Kim, I., Meinke, D., Mindrinos, M. and Zambryski, P. (2009). Loss of the plant DEAD-box protein ISE1 leads to defective mitochondria and increased cell-to-cell transport via plasmodesmata. *Proc Natl Acad Sci U S A* **106**, 17229–17234.

Stonebloom, S., Brunkard, J. O., Cheung, A. C., Jiang, K., Feldman, L. and Zambryski, P. (2012). Redox states of plastids and mitochondria differentially regulate intercellular transport via plasmodesmata. *Plant Physiol* **158**, 190–199.

Strader, L. C., Monroe-Augustus, M. and Bartel, B. (2008). The IBR5 phosphatase promotes Arabidopsis auxin responses through a novel mechanism distinct from TIR1-mediated repressor degradation. *Bmc Plant Biology* **8**, 1–15.

Sullivan, K. E. (2008). Fluorescent Proteins. *Methods in Cell Biology* **85**, xx, 592.

Sussman, M. R. and Goldsmith, H. M. (1981). Auxin Uptake and Action of N-1-Naphthylphthalamic Acid in Corn Coleoptiles. *Planta* **151**, 15–25.

Takada, S. and Jürgens, G. (2007). Transcriptional regulation of epidermal cell fate in the Arabidopsis embryo. *Development* **134**, 1141–1150.

Tan, S., Zhang, X., Kong, W., Yang, X. L., Molnár, G., Vondráková, Z., Filepová, R., Petrášek, J., Friml, J. and Xue, H. W. (2020). The lipid code-dependent phosphoswitch PDK1-D6PK activates PIN-mediated auxin efflux in Arabidopsis. *Nat Plants* **6**, 556–569.

Teale, W. D., Pasternak, T., Dal Bosco, C., Dovzhenko, A., Kratzat, K., Bildl, W., Schwörer, M., Falk, T., Ruperti, B., Schaefer, J. v, et al. (2020). Flavonol-mediated stabilization of PIN efflux complexes regulates polar auxin transport. *EMBO J* **40**, e104416.

Telfer, A. and Poethig, R. S. (1994). Leaf development in Arabidopsis. In *Arabidopsis* (ed. Meyerowitz, E. M.) and Somerville, C. R.), pp. 379–401. New York: Cold Spring Harbor Press.

Thiele, K., Wanner, G., Kindzierski, V., Jürgens, G., Mayer, U., Pachl, F. and Assaad, F. F. (2009). The timely deposition of callose is essential for cytokinesis in Arabidopsis. *Plant J* **58**, 13–26.

Thimann, K. v and Skoog, F. (1934). On the Inhibition of Bud Development and other Functions of Growth Substance in Vicia Faba. *Proceedings of the Royal Society of London. Series B, Containing Papers of a Biological Character* **114**, 317–339.

Thomas, C. L., Schmidt, D., Bayer, E. M., Dreos, R. and Maule, A. J. (2009). Arabidopsis plant homeodomain finger proteins operate downstream of auxin accumulation in specifying the vasculature and primary root meristem. *Plant Journal* **59**, 426–436.

Thompson, N. P. and Jacobs, W. P. (1966). Polarity of IAA effect on sieve-tube and xylem regeneration in Coleus and tomato stems. *Plant Physiology* **41**, 673–682.

Tilney-Bassett, R. A. E. (1986). *Plant Chimeras*. London: Edward Arnold.

Tiwari, S. B., Hagen, G. and Guilfoyle, T. (2003). The roles of auxin response factor domains in auxin-responsive transcription. *Plant Cell* **15**, 533–543.

Töller, A., Brownfield, L., Neu, C., Twell, D. and Schulze-Lefert, P. (2008). Dual function of Arabidopsis glucan synthase-like genes GSL8 and GSL10 in male gametophyte development and plant growth. *The Plant journal* **54**, 911–923.

Torres-Ruiz, R. A. and Jurgens, G. (1994). Mutations in the FASS gene uncouple pattern formation and morphogenesis in Arabidopsis development. *Development* **120**, 2967–2978.

Troll, W. (1937). *Vergleichende Morphologie der höhren Pflanzen*. Berlin: Gebrüder Borntraeger.

Truernit, E., Bauby, H., Belcram, K., Barthélémy, J. and Palauqui, J. C. (2012). OCTOPUS, a polarly localised membrane-associated protein, regulates phloem differentiation entry in Arabidopsis thaliana. *Development* **139**, 1306–1315.

Ulmasov, T., Hagen, G. and Guilfoyle, T. J. (1997). ARF1, a transcription factor that binds to auxin response elements. *Science (1979)* **276**, 1865–1868.

Ulmasov, T., Hagen, G. and Guilfoyle, T. J. (1999). Dimerization and DNA binding of auxin response factors. *Plant Journal* **19**, 309–319.

Vaddepalli, P., Herrmann, A., Fulton, L., Oelschner, M., Hillmer, S., Stratil, T. F., Fastner, A., Hammes, U. Z., Ott, T., Robinson, D. G., et al. (2014). The C2-domain protein QUIRKY and the receptor-like kinase STRUBBELIG localize to plasmodesmata and mediate tissue morphogenesis in Arabidopsis thaliana. *Development* **141**, 4139–4148.

van den Berg, C., Willemsen, V., Hendriks, G., Weisbeek, P. and Scheres, B. (1997). Short-range control of cell differentiation in the Arabidopsis root meristem. *Nature* **390**, 287–289.

van Peer, A. F., Wang, F., van Driel, K. G., de Jong, J. F., van Donselaar, E. G., Müller, W. H., Boekhout, T., Lugones, L. G. and Wösten, H. A. (2010). The septal pore cap is an organelle that functions in vegetative growth and mushroom formation of the wood-rot fungus Schizophyllum commune. *Environ Microbiol* **12**, 833–844.

Vanneste, S., Coppens, F., Lee, E., Donner, T. J., Xie, Z., van Isterdael, G., Dhondt, S., de Winter, F., de Rybel, B., Vuylsteke, M., et al. (2011). Developmental regulation of CYCA2s contributes to tissue-specific proliferation in Arabidopsis. *EMBO J* **30**, 3430–3441.

Vatén, A., Dettmer, J., Wu, S., Stierhof, Y.-D. D., Miyashima, S., Yadav, S. R., Roberts, C. J., Campilho, A., Bulone, V., Lichtenberger, R., et al. (2011). Callose biosynthesis regulates symplastic trafficking during root development. *Dev Cell* **21**, 1144–1155.

Verna, C., Sawchuk, M. G., Linh, N. M. and Scarpella, E. (2015). Control of vein network topology by auxin transport. *BMC Biology* **13**, 1–16.

Verna, C., Ravichandran, S. J., Sawchuk, M. G., Linh, N. M. and Scarpella, E. (2019). Coordination of Tissue Cell Polarity by Auxin Transport and Signaling. *Elife* **8**, e51061.

von Ettinghausen, C. (1861). *Die Blatt-Skelette der Dikotyledonen* . Vienna: Kais. Kön. Hof- und Staatsdr.

Wabnik, K., Kleine-Vehn, J., Balla, J., Sauer, M., Naramoto, S., Reinohl, V., Merks, R. M. H., Govaerts, W., Friml, J., Reinöhl, V., et al. (2010). Emergence of tissue polarization from synergy of intracellular and extracellular auxin signaling. *Mol Syst Biol* **6**, 447.

Walker, M. L., Farcot, E., Traas, J. and Godin, C. (2013). The flux-based PIN allocation mechanism can generate either canalyzed or diffuse distribution patterns depending on geometry and boundary conditions. *PLoS One* **8**, e54802.

Wang, S. and Hazelrigg, T. (1994). Implications for bcd mRNA localization from spatial distribution of exu protein in Drosophila oogenesis. *Nature* **369**, 400–403.

Wang, S., Tiwari, S. B., Hagen, G. and Guilfoyle, T. J. (2005). AUXIN RESPONSE FACTOR7 restores the expression of auxin-responsive genes in mutant Arabidopsis leaf mesophyll protoplasts. *Plant Cell* **17**, 1979–1993.

Wang, J., Kucukoglu, M., Zhang, L., Chen, P., Decker, D., Nilsson, O., Jones, B., Sandberg, G. and Zheng, B. (2013). The Arabidopsis LRR-RLK, PXC1, is a regulator of secondary wall formation correlated with the TDIF-PXY/TDR-WOX4 signaling pathway. *BMC Plant Biol* **13**, 94.

Wang, L., Li, D., Yang, K., Guo, X., Bian, C., Nishimura, T., Le, J., Morita, M. T., Bergmann, D. C. and Dong, J. (2022). Connected function of PRAF/RLD and GNOM in membrane trafficking controls intrinsic cell polarity in plants. *Nat Commun* **13**, 7.

Wangermann, E. (1974). The pathway of transport of applied indolyl-acetic acid through internode segments. *New Phytologist* **73**, 623–636.

Weijers, D., van Hamburg, J. P., van Rijn, E., Hooykaas, P. J. and Offringa, R. (2003). Diphtheria toxin-mediated cell ablation reveals interregional communication during Arabidopsis seed development. *Plant Physiol* **133**, 1882–1892.

Weijers, D., Benkova, E., Jager, K. E., Schlereth, A., Hamann, T., Kientz, M., Wilmoth, J. C., Reed, J. W., Jurgens, G., Jäger, K. E., et al. (2005). Developmental specificity of auxin response by pairs of ARF and Aux/IAA transcriptional regulators. *Embo J* **24**, 1874–1885.

Weijers, D., Schlereth, A., Ehrismann, J. S., Schwank, G., Kientz, M. and Jurgens, G. (2006). Auxin triggers transient local signaling for cell specification in Arabidopsis embryogenesis. *Developmental Cell* **10**, 265–270.

Went, F. W. (1928). Wuchsstoff und Wachstum. *Recueil des travaux botaniques néerlandais* **25**, I-IV,1-116.

Wenzel, C. L., Schuetz, M., Yu, Q. and Mattsson, J. (2007). Dynamics of MONOPTEROS and PIN-FORMED1 expression during leaf vein pattern formation in Arabidopsis thaliana. *Plant J* **49**, 387–398.

Wenzel, C. L., Marrison, J., Mattsson, J., Haseloff, J. and Bougourd, S. M. (2012). Ectopic divisions in vascular and ground tissues of Arabidopsis thaliana result in distinct leaf venation defects. *J Exp Bot* **63**, 5351–5364.

Wille, A. C. and Lucas, W. J. (1984). Ultrastructural and histochemical studies on guard cells. *Planta* **160**, 129–142.

Willemsen, V. and Scheres, B. (2004). Mechanisms of Pattern Formation in Plant Embryogenesis. *Annu Rev Genet* **38**, 587–614.

Willemsen, V., Friml, J., Grebe, M., van den Toorn, A., Palme, K. and Scheres, B. (2003). Cell polarity and PIN protein positioning in Arabidopsis require STEROL METHYLTRANSFERASE1 function. *Plant Cell* **15**, 612–625.

Willmer, C. M. and Sexton, R. (1979). Stomata and plasmodesmata. *Protoplasma* **100**, 113–124.

Wilson, T. and Sheppard, C. (1984). *Theory and practice of scanning optical microscopy*. London: Academic Press.

Wisniewska, J., Xu, J., Seifartová, D., Brewer, P. B., Růžička, K., Blilou, L., Rouquié, D., Benková, E., Scheres, B., Friml, J., et al. (2006). Polar PIN localization directs auxin flow in plants. *Science (1979)* **312**, 883.

Wolpert, L. (2016). Positional information and pattern formation. In *Current topics in developmental biology 117*, pp. 597–608. Elsevier.

Wolters, H., Anders, N., Geldner, N., Gavidia, R. and Jürgens, G. (2011). Coordination of apical and basal embryo development revealed by tissue-specific GNOM functions. *Development* **138**, 117–126.

Wright, K. M., Roberts, A. G., Martens, H. J., Sauer, N. and Oparka, K. J. (2003). Structural and functional vein maturation in developing tobacco leaves in relation to AtSUC2 promoter activity. *Plant Physiol* **131**, 1555–1565.

Wu, S., O'Lexy, R., Xu, M., Sang, Y., Chen, X., Yu, Q. and Gallagher, K. L. (2016). Symplastic signaling instructs cell division, cell expansion, and cell polarity in the ground tissue of Arabidopsis thaliana roots. *Proc Natl Acad Sci U S A* **113**, 11621–11626.

Xavier da Silveira Dos Santos, A. and Liberali, P. (2019). From single cells to tissue self-organization. *FEBS J* **286**, 1495–1513.

Xiao, Y. and Offringa, R. (2020). PDK1 regulates auxin transport and Arabidopsis vascular development through AGC1 kinase PAX. *Nat Plants* **6**, 544–555.

Xu, J., Hofhuis, H., Heidstra, R., Sauer, M., Friml, J. and Scheres, B. (2006). A molecular framework for plant regeneration. *Science (1979)* **311**, 385–388.

Xu, M., Cho, E., Burch-Smith, T. M. and Zambryski, P. C. (2012). Plasmodesmata formation and cell-to-cell transport are reduced in decreased size exclusion limit 1 during embryogenesis in Arabidopsis. *Proceedings of the National Academy of Sciences* **109**, 5098–5103.

Yakoby, N., Lembong, J., Schüpbach, T. and Shvartsman, S. Y. (2008). Drosophila eggshell is patterned by sequential action of feedforward and feedback loops. *Development* **135**, 343–351.

Yamagishi, K., Nagata, N., Yee, K. M., Braybrook, S. A., Pelletier, J., Fujioka, S., Yoshida, S., Fischer, R. L., Goldberg, R. B. and Harada, J. J. (2005). TANMEI/EMB2757 encodes a WD repeat protein required for embryo development in Arabidopsis. *Plant Physiol* **139**, 163–173.

Yamaguchi, M., Goué, N., Igarashi, H., Ohtani, M., Nakano, Y., Mortimer, J. C., Nishikubo, N., Kubo, M., Katayama, Y., Kakegawa, K., et al. (2010). VASCULAR-RELATED NAC-DOMAIN6 and VASCULAR-RELATED NAC-DOMAIN7 effectively induce

transdifferentiation into xylem vessel elements under control of an induction system. *Plant Physiol* **153**, 906–914.

Yang, M. Y., Armstrong, J. D., Vilinsky, I., Strausfeld, N. J. and Kaiser, K. (1995). Subdivision of the Drosophila mushroom bodies by enhancer-trap expression patterns. *Neuron* **15**, 45–54.

Yoshida, S., Barbier de Reuille, P., Lane, B., Bassel, G. W., Prusinkiewicz, P., Smith, R. S. and Weijers, D. (2014). Genetic control of plant development by overriding a geometric division rule. *Dev Cell* **29**, 75–87.

Yoshida, S., van der Schuren, A., van Dop, M., van Galen, L., Saiga, S., Adibi, M., Möller, B., ten Hove, C. A., Marhavy, P., Smith, R., et al. (2019). A SOSEKI-based coordinate system interprets global polarity cues in Arabidopsis. *Nature Plants* **5**, 160–166.

Zhang, J. Y., He, S. B., Li, L. and Yang, H. Q. (2014). Auxin inhibits stomatal development through MONOPTEROS repression of a mobile peptide gene STOMAGEN in mesophyll. *Proc Natl Acad Sci U S A* **111**, E3015-23.

Zhang, Q., Wang, D., Lang, Z., He, L., Yang, L., Zeng, L., Li, Y., Zhao, C., Huang, H., Zhang, H., et al. (2016). Methylation interactions in Arabidopsis hybrids require RNA-directed DNA methylation and are influenced by genetic variation. *Proc Natl Acad Sci U S A* **113**, E4248-56.

Zhao, Y. (2018). Essential Roles of Local Auxin Biosynthesis in Plant Development and in Adaptation to Environmental Changes. *Annual Review of Plant Biology* **69**, 417–435.

Zhu, T., O'Quinn, R. L., Lucas, W. J. and Rost, T. L. (1998). Directional cell-to-cell communication in the Arabidopsis root apical meristem II. Dynamics of plasmodesmatal formation. *Protoplasma* **204**, 84–93.

Zourelidou, M., Absmanner, B., Weller, B., Barbosa, I. C. R., Willige, B. C., Fastner, A., Streit, V., Port, S. A., Colcombet, J., de la Fuente van Bentem, S.,

et al. (2014). Auxin efflux by PIN-FORMED proteins is activated by two different protein kinases, D6 PROTEIN KINASE and PINOID. *Elife* **3**, e02860.

Zuo, J., Niu, Q. W. and Chua, N. H. (2000). An estrogen receptor-based transactivator XVE mediates highly inducible gene expression in transgenic plants. *Plant Journal* **24**, 265–273.